MECHANICAL PROPERTIES OF SOME NITRIDED IRON ALLOYS

A dissertation submitted for the degree of

Doctor of Philosophy

of the University of Newcastle upon Tyne

by

David M. Jones

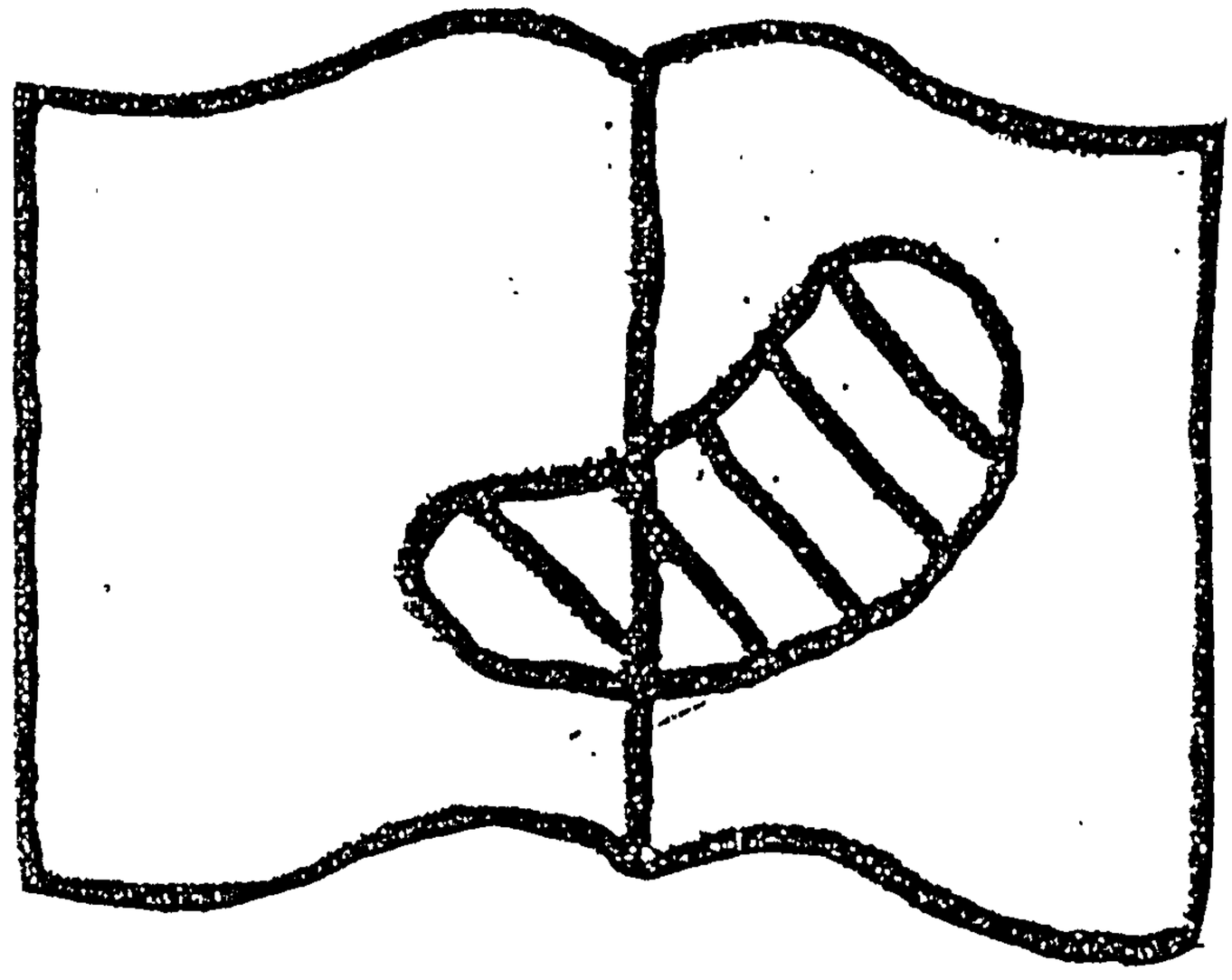
Department of Metallurgy and Engineering Materials

University of Newcastle upon Tyne

September 1976

Best Copy Available

Variable Print Quality



PREFACE

This dissertation describes original work which has not been submitted for a degree at any other University.

The investigations were carried out in the Department of Metallurgy and Engineering Materials of the University of Newcastle upon Tyne during the period October 1971 to October 1974 under the supervision of Professor K. H. Jack.

The thesis describes a study of the mechanical properties of some nitrided binary iron alloys and is part of a wider investigation being carried out at Newcastle on the effect of substitutional alloying elements on the behaviour of interstitial solutes in iron.

ACKNOWLEDGEMENTS

I wish to thank Professor K. H. Jack for advice, encouragement and general supervision of the work.

I also wish to express my gratitude to:

The Department of Metallurgy and Engineering Materials of the University of Newcastle upon Tyne for providing accommodation and research facilities;

The Science Research Council for the award of a maintenance grant;

Many colleagues in the Department of Metallurgy and Engineering Materials of the University of Newcastle upon Tyne for stimulating discussion and advice, in particular Dr. A. Stephenson;

Dr. J. H. Driver of the École Nationale Superieure Des Mines De Saint-Étienne for the field ion micrographs of Fe-Nb-N alloys;

Miss D. Warner for typing the script;

My wife for her help and encouragement.

David M. Jones

September 1976

ABSTRACT

When binary iron alloys containing strong nitride forming elements such as vanadium, niobium, titanium, molybdenum or chromium as the substitutional solute are nitrided under suitable conditions, a homogeneous dispersion of coherent, disc-shaped particles precipitates on the ferrite cube planes. Initially, the particles give rise to continuous streaking on electron diffraction patterns and, after subsequent heat treatment, overage to the equilibrium alloy nitride.

Although the internal friction Snoek peak of the nitrided alloys is extremely small and substitutional-interstitial interaction peaks are absent, relatively strong damping is observed at 150 - 230°C. Broad, assymmetric peaks occur indicating a distribution of relaxation times, the peak temperature being dependent on the associated microstructure. A qualitative interpretation for the origin of the peak is outlined based upon the movement of nitrogen atoms in the elastic strain fields surrounding the precipitated particles.

Nitrided alloys with as little as 0.1at.% substitutional solute produce large strength increases, the maximum strength being obtained at the smallest particle size. The yield strength is proportional to the square root of the volume fraction of precipitated phase and is strongly temperature dependent. When coherent particles are

precipitated deformation occurs by particle shearing and electron micrographs of the deformed microstructures show that slip is predominantly on $\{110\}_\alpha$ planes with dislocations having a Burgers vector of $a/2\langle 111\rangle$. The major part of the high initial strengthening is thought to derive from the energy required for dislocations to shear the coherent particles. A change to an Orowan type deformation mechanism occurs when the particles become incoherent.

CONTENTS

			page no.
		Preface	i
		Acknowledgements	ii
		Abstract	iii
		Contents	v
		Introduction	1
Chapter	I.	BACKGROUND INFORMATION	
	I.1	GP zone formation in ferrous alloys	5
	I.2	Constant activity nitrid ing	7
Chapter	II.	PREVIOUS INVESTIGATIONS	
	II.1	Iron-nitrogen alloys	9
	II.2	Fe-V and Fe-V-N alloys	10
	II.3	Fe-Nb and Fe-Nb-N alloys	11
	II.4	Quench-aged Fe-N and Fe-X-N alloys	12
	II.5	Homogeneous precipitation in Fe-X-N alloys	15
	II.6	Kinetics of nitriding	20
	II.7	Internal friction of Fe-N and Fe-X-N alloys	22
	II.8	Mechanical properties of Fe-X-N alloys	25
	II.9	Precipitation and strengthening in control cooled steels	28
	II.10	Secondary hardening steels	32
Chapter	III.	EXPERIMENTAL TECHNIQUES	
	III.1	The preparation of alloy samples	35
	III.2	Ammonia-hydrogen nitriding	35

CONTENTS

			page no.
Chapter	III.3	Nitriding Apparatus	39
	III.4	X-Ray methods	40
	III.5	Metallographic examination and hardness measurements	40
	III.6	Electron microscopy	41
	III.7	Nitrogen weighings and analysis	42
	III.8	Internal friction: theoretical aspects of damping	43
	III.9	Internal friction equipment	48
	III.10	Mechanical testing	50
Chapter	IV.	THE SCOPE OF THE PRESENT INVESTIGATION	52
Chapter	V.	INTERNAL FRICTION OF Fe-X-N ALLOYS	
	V.1	Introduction	55
	V.2	Experimental	59
	V.3	Microstructures of Fe-X-N alloys	60
	V.4	Internal friction of Fe-Mo-N alloys	64
	V.5	Internal friction of Fe-Cr-N alloys	70
	V.6	Internal friction of Fe-Ti-N alloys	73
	V.7	Activation energy for the high temperature damping	74
	V.8	The high temperature peaks	79
	V.9	Discussion	82
	V.10	Conclusions	92
Chapter	VI.	HOMOGENEOUS PRECIPITATION IN Fe-X-N ALLOYS	
	VI.1	Introduction	94
	VI.2	Homogeneous precipitation in Fe-V alloys	96
	VI.3	Hydrogen reduction of Fe-V alloys	104
	VI.4	Homogeneous precipitation in Fe-Nb alloys	107
	VI.5	High temperature ageing	110
	VI.6	Discussion	113
	VI.7	Conclusions	127

		page no.
Chapter VII.	MECHANICAL PROPERTIES OF Fe-X-N ALLOYS	
VII.1	Introduction	129
VII.2	Experimental	130
VII.3	Mechanical properties of Fe-V-N alloys	131
VII.4	Mechanical properties of Fe-Nb-N alloys	134
VII.5	The variation in yield strength with nitrogen content	137
VII.6	The effect of nitriding temperature on properties	139
VII.7	The influence of volume fraction on yield strength	141
VII.8	The variation in yield strengh with ageing time at 750°C	142
VII.9	Hydrogen reduction of Fe-0.15 at.% V	145
VII.10	High temperature properties	146
VII.11	Discussion	147
VII.12	Conclusions	158
Chapter VIII.	ELECTRON METALLOGRAPHY OF DEFORMED ALLOYS	
VIII.1	Introduction	160
VIII.2	Experimental	161
VIII.3	Fe-X-N alloys prior to peak strength	161
VIII.4	Fe-X-N alloys containing zones	162
VIII.5	Fe-X-N alloys containing precipitates	165
VIII.6	Burgers vector analysis	167
VIII.7	Discussion	168
VIII.8	Conclusions	174
Chapter IX.	STRENGTHENING MECHANISMS IN Fe-X-N ALLOYS	
IX.1	Introduction	176
IX.2	Strengthening by non-deformable particles	177
IX.3	Strengthening by deformable particles	179

			Page no.
Chapter IX.4		Application of theories to Fe-X-N alloys	184
	IX.5	Temperature dependence of the yield strength	189
	IX.6	Discussion	192
	IX.7	Conclusions	202
Chapter X		GENERAL CONCLUSIONS	203
References			206

INTRODUCTION

Nitriding has been used since 1923 as an effective surface hardening method to produce steels with improved fatigue and wear resistance. The high surface hardening is a result of the interaction of substitutional alloying elements with interstitial nitrogen. The commonly used materials are either Nitralloy steels containing aluminium, or chromium-molybdenum steels containing about 3 at.% Cr and 0.5 at.% Mo. High hardnesses can also be obtained by nitriding, under suitable conditions, binary iron alloys containing small amounts of a reasonably strong nitride forming element such as titanium, vanadium or niobium.

There have been many investigations into the effects of precipitation in alloy steels containing nitrogen, although the exact modes of the early stages of precipitation are not always clear. Additions of vanadium and niobium have been made to steels for many years in order to increase the yield strength. Both elements are well known for their secondary hardening capability and more recently, the precipitation of vanadium or niobium carbonitrides has been observed in isothermally transformed and controlled rolled steels. The development of high strength steels is based on increasing the resistance to motion of dislocations. In order to achieve the highest strengths it is necessary to produce a fine dispersion of nitrides

or carbides in ferrite, and it seems likely that this can be achieved most successfully by homogeneous precipitation. Obviously, a clearer understanding of the methods by which these materials are strengthened should be invaluable in the future development of higher strength materials.

Research into the effects of substitutional alloying elements on the behaviour of interstitial solutes in iron was started at Newcastle in order to obtain a more thorough understanding of the nucleation, growth and characterisation of phases precipitated from steels. Although the concentrations of interstitial and substitutional alloying elements in commercial ferrous materials are small, it is necessary to have a detailed knowledge of the phase relationships and thermodynamics of the whole of the appropriate multi-component systems.

Previous investigators found difficulty in studying the effects of precipitation in a complex matrix under conditions where the driving force for precipitation was continually changing as the solute content was depleted. These problems have been avoided by treating binary iron alloys in 'constant activity nitriding' gas atmospheres. Despite the fact that the initial research used nitrogen as the interstitial solute in ferrous alloys, subsequent research at Newcastle has shown that the general principles of 'constant activity nitriding' can be applied to other interstitial solutes, such as carbon, oxygen and hydrogen,

in a wide range of alloys.

The nitriding reaction is diffusion controlled and consequently the effects produced by substitutional alloy elements upon interstitial nitrogen change markedly with nitriding temperature. At temperatures above about 650°C substitutional solutes can move readily through the iron matrix and therefore, alloy nitrides are precipitated; the particular nitride or sequence of nitrides precipitated being predicted from the thermodynamics of the system. At temperatures below about 450°C substitutional solutes are almost immobile, but because they change the activity coefficient of nitrogen in iron, they affect the amount, size and rate of precipitation of iron nitrides from solid solution.

The most important aspect of the present research is in the range 450 - 650°C. At these temperatures substitutional atoms move only a few atomic distances in the same time that nitrogen atoms can move over considerably larger distances. In these circumstances a sequence of homogeneous transformations may occur prior to the formation of the equilibrium alloy nitride. Previous work at Newcastle has shown that the first stage of precipitation occurs by the formation of extremely small disc-shaped particles (substitutional-interstitial solute-atom clusters or GP zones) on the $\{100\}$ matrix planes.

The zones are produced isothermally at 400 - 650°C in iron which contains small amounts of substitutional alloy elements having a reasonably strong affinity for nitrogen, such as vanadium, niobium, titanium, molybdenum or chromium, by 'constant activity nitriding'. Once formed the zones are exceptionally hard and are very stable, persisting even after prolonged ageing at temperatures up to abcut 700°C. Both substitutional and interstitial solutes are required to produce this hardening, and the precipitation sequence goes thrcugh some, or all, of the stages recognised in the classical work on Al-Cu alloys:

GP zones - one or more metastable intermediate precipitates - equilibrium precipitate

Following these observations on the precipitation, kinetics and structural changes involved in the ternary nitrogen ferrites, an exploration of the internal friction and mechanical properties at the different stages of precipitation seemed advantageous.

Experimental techniques used in this investigation include controlled metal-gas equilibriation, X-ray diffraction, electron metallography, internal friction and mechanical testing, together with the standard metallographic techniques.

Chapter 1

BACKGROUND INFORMATION

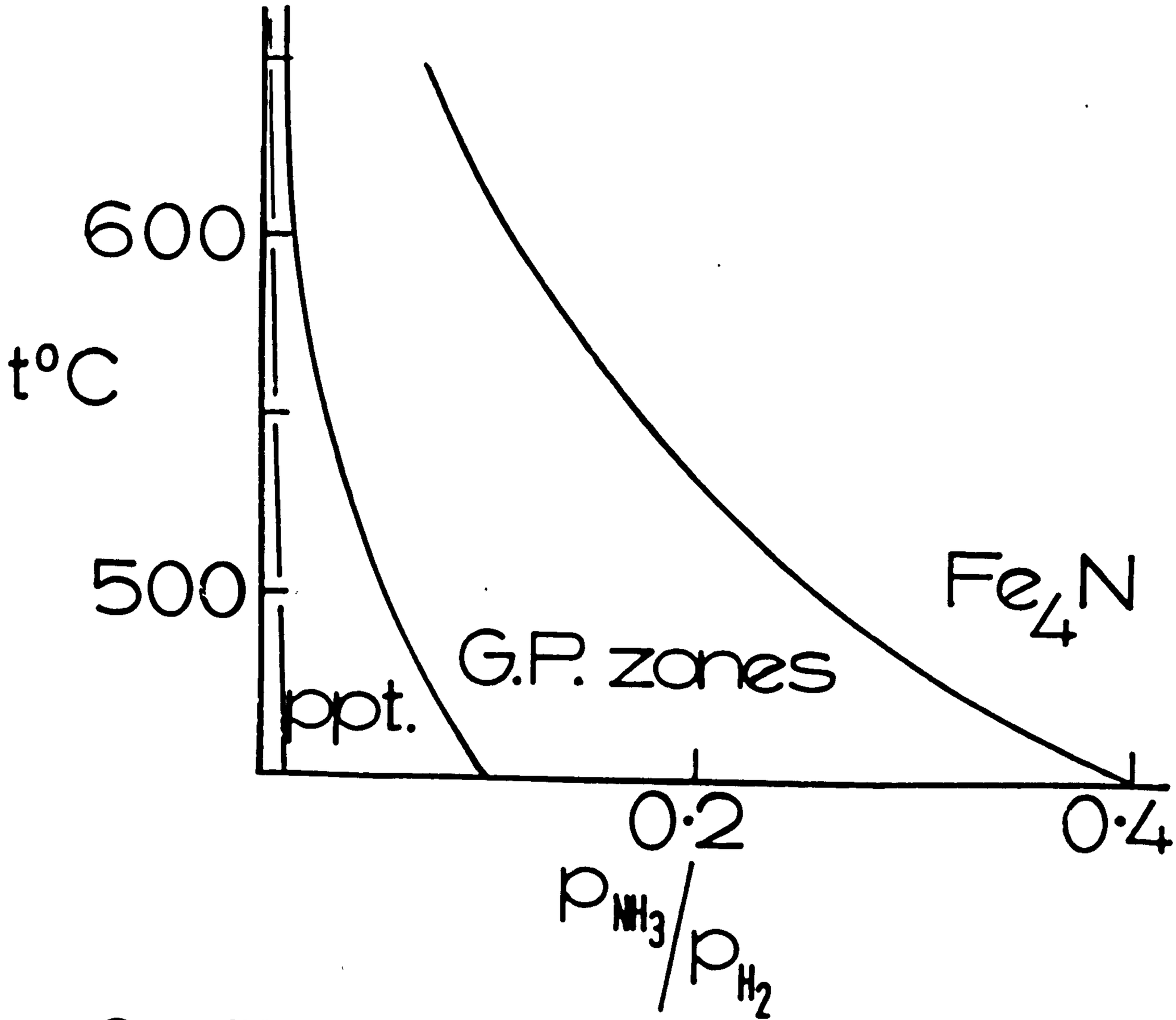
I.1 GP zone formation in ferrous alloys

In any system GP zones are metastable with respect to the equilibrium precipitate and so have a higher solubility (see Jack, 1973). The high supersaturation, which is the driving force to form zones, can only be obtained conventionally by cooling to low temperatures and here the solute atom diffusivity is too small to allow clustering unless there is an abnormally high concentration of quenched-in vacancies. These conditions are not met in b.c.c. metals and so GP zones are not usually obtained in dilute iron alloys. However, high supersaturations relative to the zone solvus can be produced isothermally at temperatures in the range 450 - 650°C by constant activity nitriding in controlled ammonia-hydrogen gas mixtures. This allows the formation of zones in much greater densities than can be produced by any quench ageing procedure. An example of the presence of a zone solvus is obtained in Fe-3at.%Mo alloys. A low nitrogen potential ($1NH_3:99H_2$) is insufficient to exceed the zone solvus and so under such conditions homogeneous precipitation does not occur; instead, the equilibrium nitride is slowly formed by heterogeneous nucleation. On the other hand, using a potential of $6NH_3:94H_2$ results in the homogeneous precipitation of small coherent particles.

The conditions necessary for zone formation are shown in figure I.1. The nitrogen potential must exceed that of the zone solvus, but must be insufficient to precipitate iron nitrides. There must also be an interaction between nitrogen and the substitutional solute atoms. The most effective solutes are those which increase the solubility of nitrogen prior to precipitation; that is, they decrease the activity coefficient of nitrogen in iron and have a high chemical affinity for nitrogen. Solutes which most suitably meet these requirements are titanium, vanadium and niobium, and so with these solutes only small atomic concentrations are required to form zones.

Another condition which must be satisfied is that the temperature should be high enough to allow the substitutional atoms to move over short distances, but must not be excessively high; otherwise large scale movement will allow the nucleation and growth of the equilibrium alloy nitride. Suitable temperatures are those in the range 450-650°C, but they depend to some extent on the particular alloy system. For example, zones have been produced at temperatures as low as 350°C in Fe - Ti -N alloys. Therefore, the flux of nitrogen relative to that of the metal atoms appears to be just as important as the substitutional-interstitial interaction.

Fig. I. 1



Conditions for Nitride Zone Formation

The importance of oxygen as an impurity in the precipitation sequence is also apparent. In some systems, oxygen may stabilise one structure at the expense of another. For example, in the Fe-Mo-N system f.c.c. γ-'Mo_2N' is really an oxynitride whereas the true binary nitride is c.p.h. ϵ-Mo_2N. Roberts (1970) has also shown that the phases precipitated in the Fe-Nb-N system are dependent upon the oxygen potential. Oxygen acts as a barrier to the transport of nitrogen, and by being absorbed at particle/matrix interfaces, it affects the morphology, size and dispersion of nitride precipitates (see Roberts, 1970). It seems possible, in view of these observations, that the oxygen potential of the gas atmosphere will influence the formation of GP zones in ferrous alloys.

I 2 Constant activity nitriding

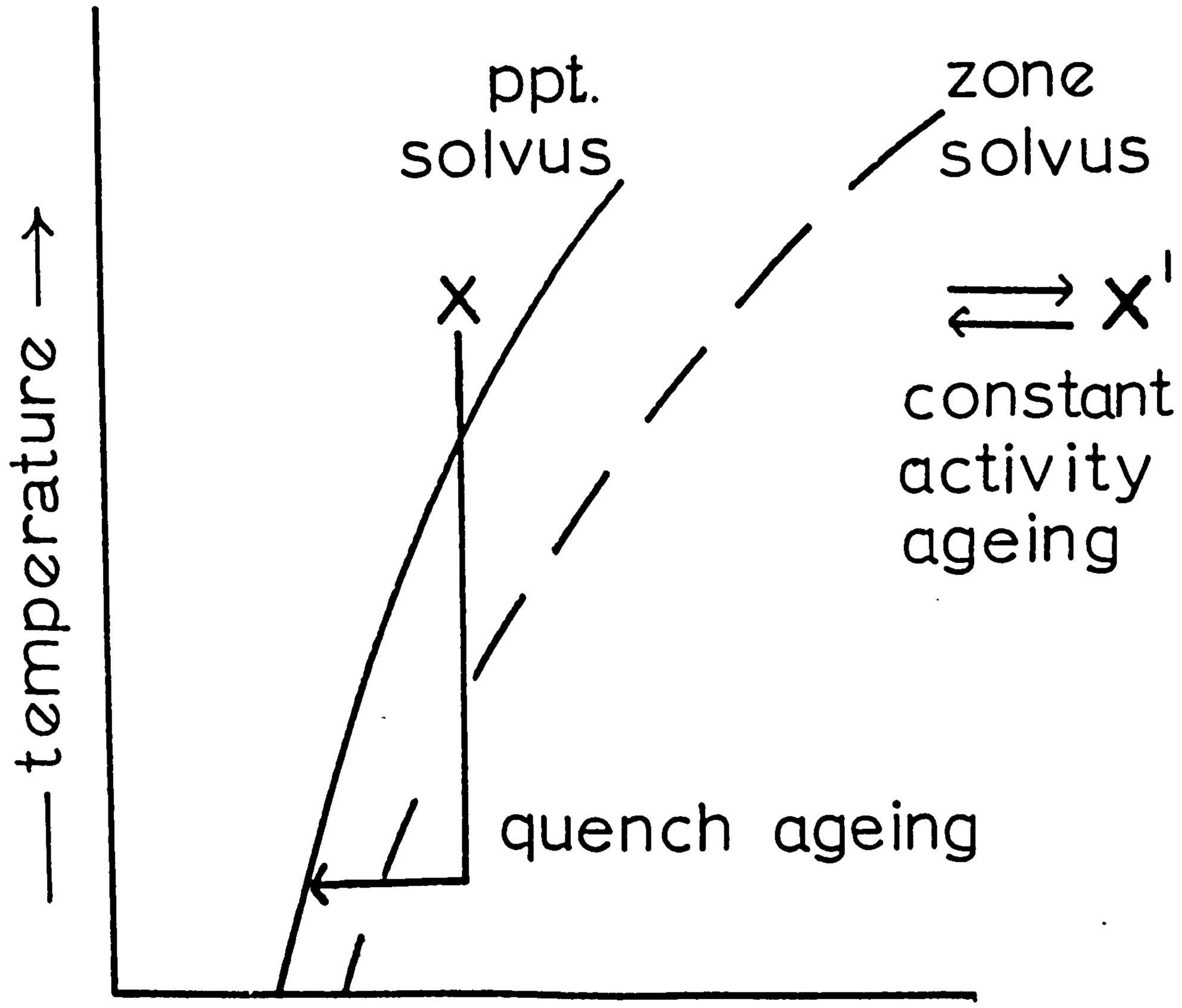
At normal nitriding temperatures interstitial nitrogen can move much more rapidly than substitutional solutes. The concentration of nitrogen dissolved in iron can be maintained very precisely by equilibriating the specimen with the appropriate pressure of molecular nitrogen or, more easily, with a given NH_3 : H_2 gas mixture. The nitrogen concentration is given by either:

$$\text{wt.\%N} = K' . p_{N_2} \qquad \ldots\ldots\ldots \text{(I).1}$$

$$\text{or} \quad \text{wt.\%N} = K'' . p_{NH_3}/p_{H_2}^{3/2} \qquad \ldots\ldots\ldots \text{(I).2}$$

but $K'' \gg K'$ so that very large pressures of molecular nitrogen are required to introduce the same concentration of nitrogen as obtained from a NH_3:H_2 gas mixture at one-atmosphere pressure. If nitrogen is removed from solution by precipitation, for example as an alloy nitride, it is immediately replenished from the gas atmosphere to the equilibrium value, and the process continues until the matrix is completely depleted of substitutional solute. When nitrogen combines with an alloying element it is precipitated at a rate controlled by the slowly diffusing substitutional solute and is replaced from the constant activity nitriding atmosphere at a rate determined by the rapidly diffusing interstitial solute. The decrease in driving force for precipitation, characteristic of quench-ageing, is avoided and precipitation occurs continuously. Figure I.2 compares the principles of quench-ageing with those required for GP zone formation by constant activity ageing.

Fig. I. 2



Principles of zone formation
by constant activity ageing

Chapter II

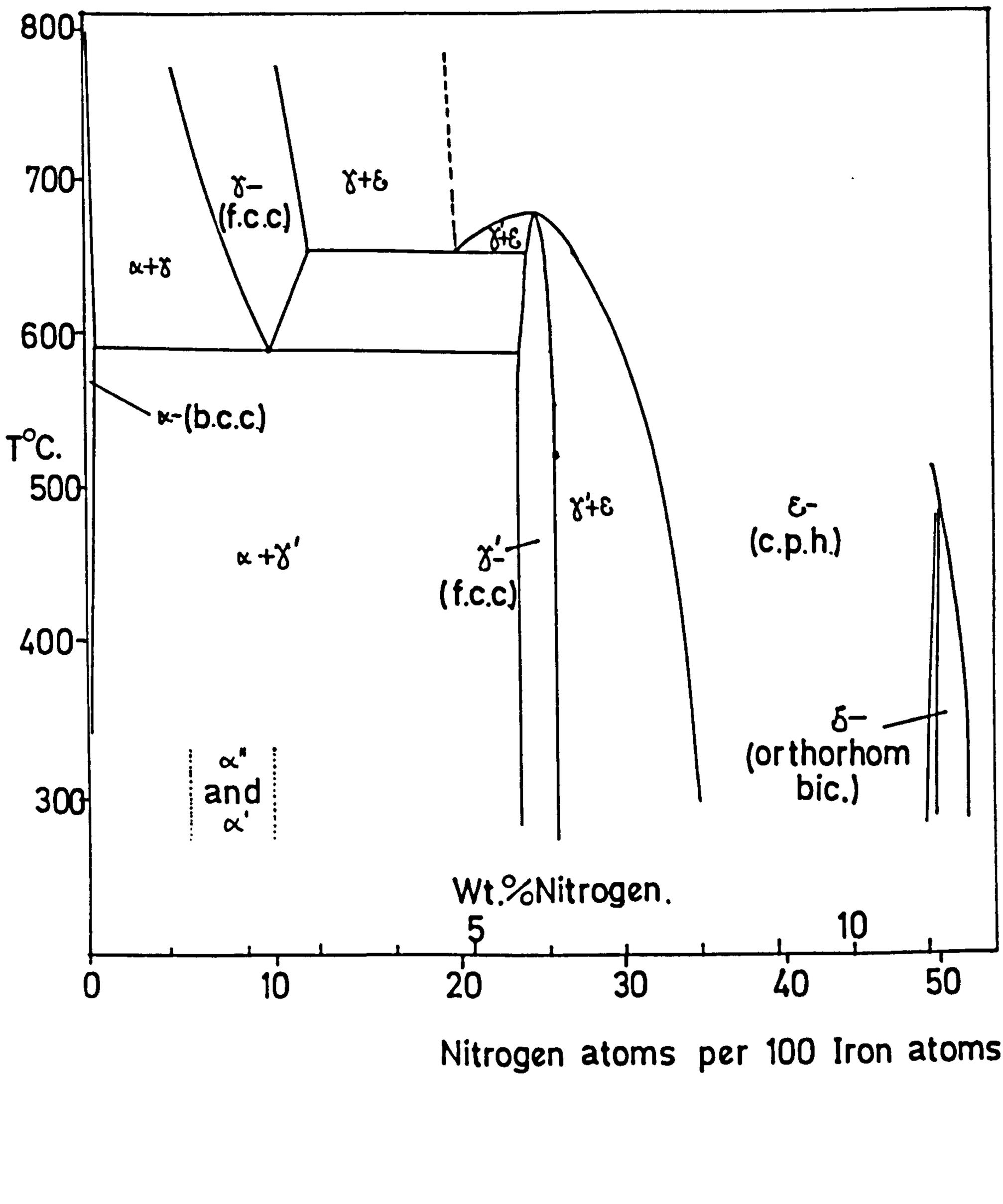
PREVIOUS INVESTIGATIONS

II.1 Iron-nitrogen alloys

In the iron-nitrogen system, shown in Figure II.1 (Jack, 1951 a), there are seven phases. Face-centred cubic nitrogen austenite is isostructural with carbon austenite and exists down to 590°C. At this temperature the nitrogen concentrations in γ and α iron are 9.4 and 0.4 at.% respectively. $\gamma' - Fe_4N$ has a face-centred cubic arrangement of iron atoms like austenite but the nitrogen atoms are fully ordered and occupy one-quarter of the available octohedral interstices. The ϵ -phase, which extends from about 20 to 33 at.%N, that is approximately Fe_4N to Fe_2N, has a close packed hexagonal arrangement of iron atoms. Orthorhombic $\zeta - Fe_2N$ is a distorted modification of ϵ formed by a change in the nitrogen-atom ordering.

Body-centred tetragonal nitrogen martensite (α') is isostructural with carbon-martensite and is obtained by quenching nitrogen-austenite. $\alpha'' - Fe_{16}N_2$ occurs as an intermediate precipitate during the tempering of nitrogen-martensite or upon ageing supersaturated nitrogen-ferrite. The solubilities of $\gamma' - Fe_4N$ and $\alpha'' - Fe_{16}N_2$ in body

Fig. II. 1



THE IRON-NITROGEN PHASE DIAGRAM.[After Jack, 1951].

centred cubic ferrite, together with that of molecular nitrogen at a pressure of one atmosphere, are shown in Figure II.2.

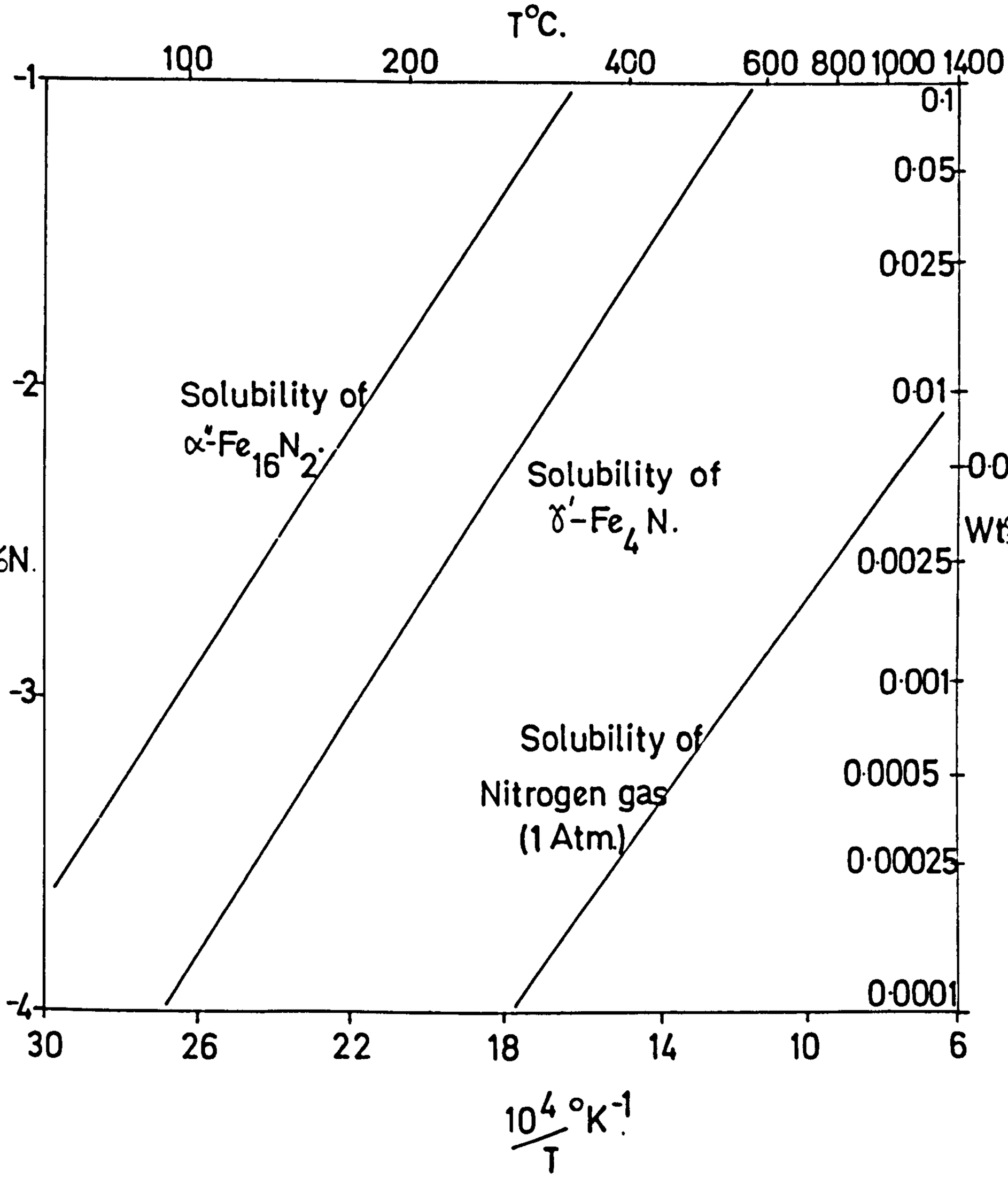
II.2 Fe-V and Fe-V-N alloys

The Fe-V equilibrium diagram is shown in Figure II.3(a) (after Hansen, 1958) and is based mainly upon the dilatometric work of Lucas & Fishel (1954) and thermal analysis by Wever & Jellinghaus (1930). It is supplemented by X-ray studies of Masteurs & Duwez (1952).

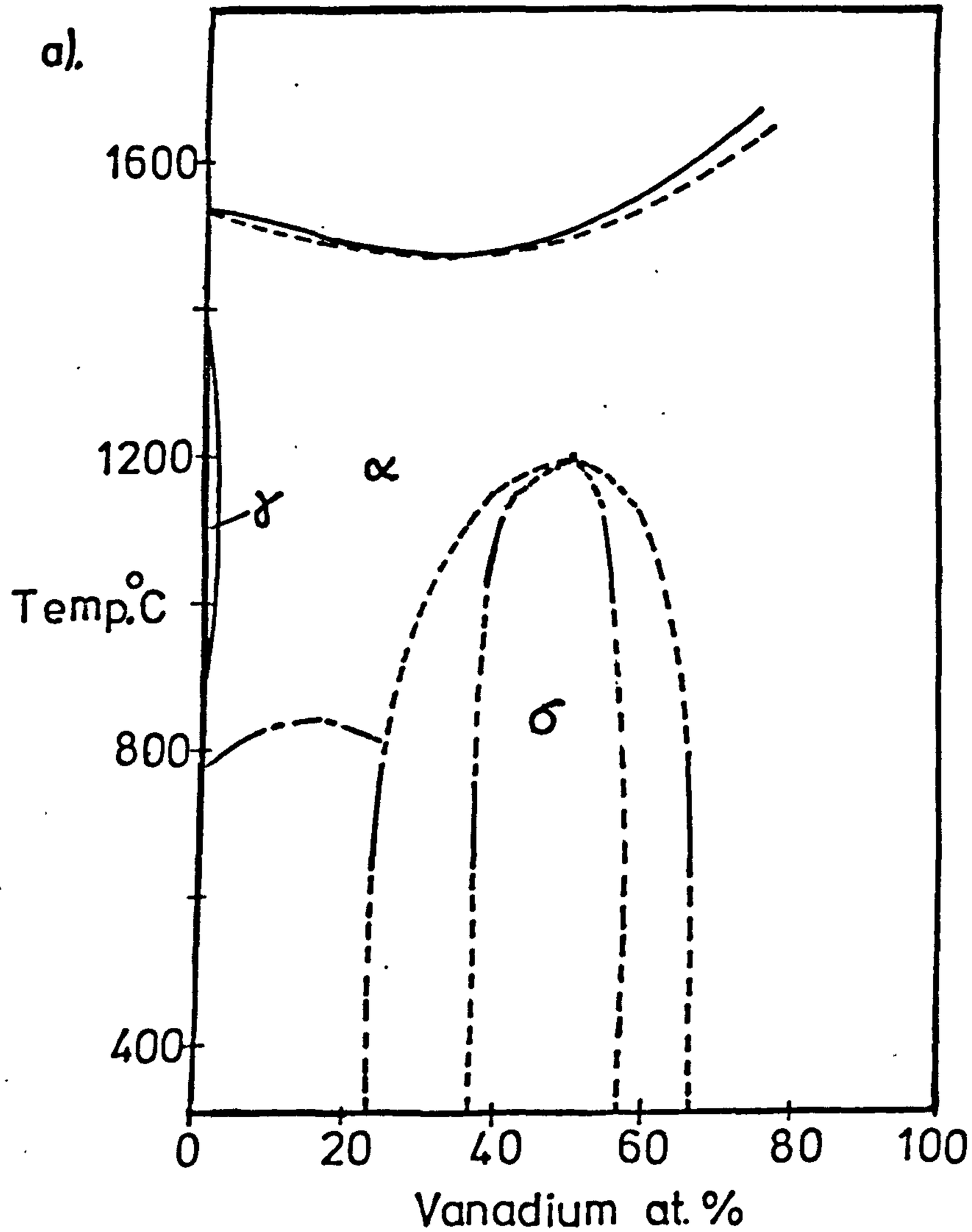
The solubility of VN in α-Fe and γ-Fe has been measured by Fountain & Chipman (1958) and by Frohberg & Graf (1960) using alloys of up to 0.5 wt.%V. The only nitride observed in the range 750 - 1250°C was f.c.c.VN. An extension of this work to C-Mn steels, by Irvine et al (1967), found that manganese slightly increased the solubility of VN. Phillips & Seybolt (1968) observed that ion-nitriding an Fe - 1.1 at%V alloy produced a high hardness due to a fine dispersion of discs, which were tentatively identified as VN, of approximately 1nm thick and 4 nm diameter precipitated on the ferrite cube planes.

Constant activity nitriding of Fe-V alloys containing up to 2.25 at.%V below 600°C was found to produce a homogeneous dispersion of disc shaped particles on $\{100\}_\alpha$ ferrite planes (Pope, 1972); but from the experimental

Fig. II. 2



THE SOLUBILITY OF NITROGEN AND IRON NITRIDES IN α-IRON.



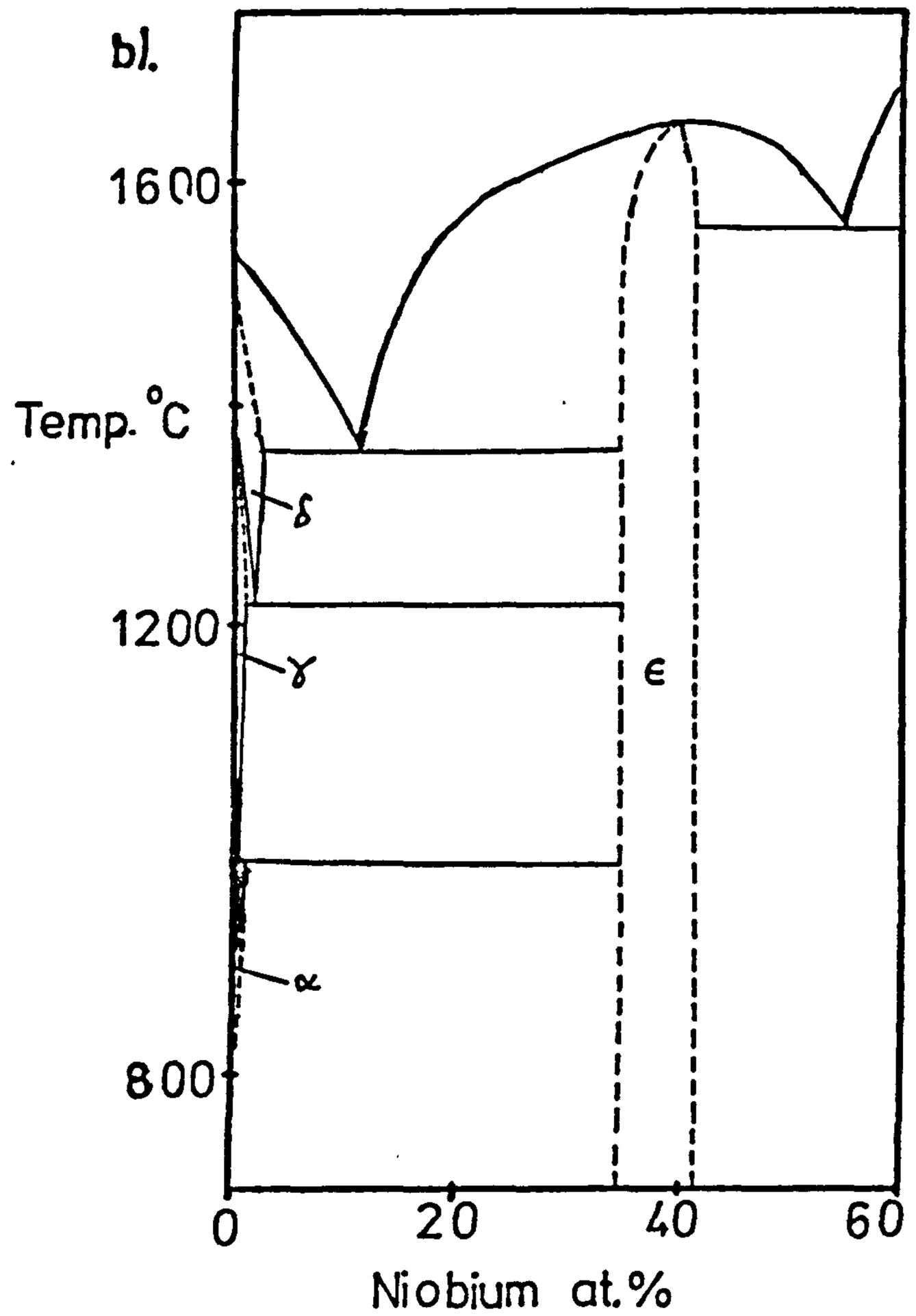


Fig. III.3

Iron – Vanadium and Iron-Niobium phase diagrams

evidence it was difficult to decide whether the first stage of homogeneous precipitation consisted of very fine platelets or of Fe-V-N disc-shaped clusters. If it was the former, then abnormally high concentrations of additional nitrogen were accommodated in the distorted ferrite lattice around the particles.

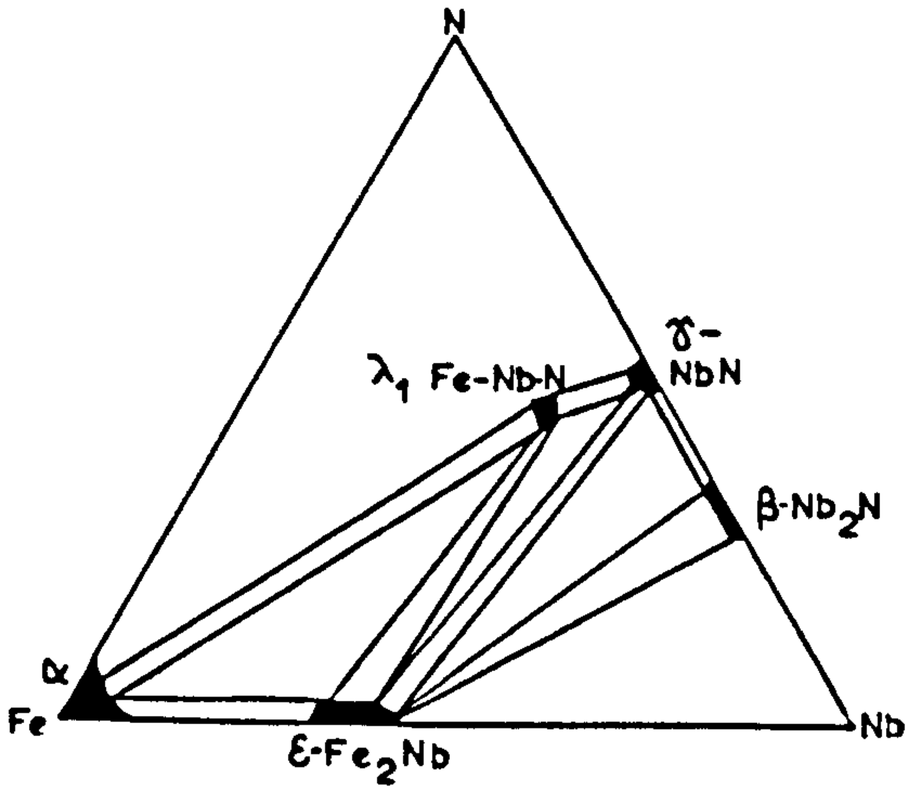
II.3 Fe-Nb and Fe-Nb-N alloys

The maximum solubility of niobium in ferrite in the range 450 - 800°C is only 0.3 - 0.6 at.%Nb, (see Figure II.3(b), after Hansen 1958). Alloys with a higher niobium content than this contain precipitated Laves phase (hexagonal Fe_2Nb with the $MgZn_2$ structure).

Little systemmatic work on precipitation from Fe-Nb-N alloys was done until Roberts (1970) found several different phases in ferritic Fe-Nb alloys nitrided at temperatures above 500°C under the conditions shown in Figure II.4. These included λ_1-$FeNb_4N_4$, λ_2-$FeNb_2N_2$, δ-NbN(O), ϵ-NbN(O)and γ-NbN.

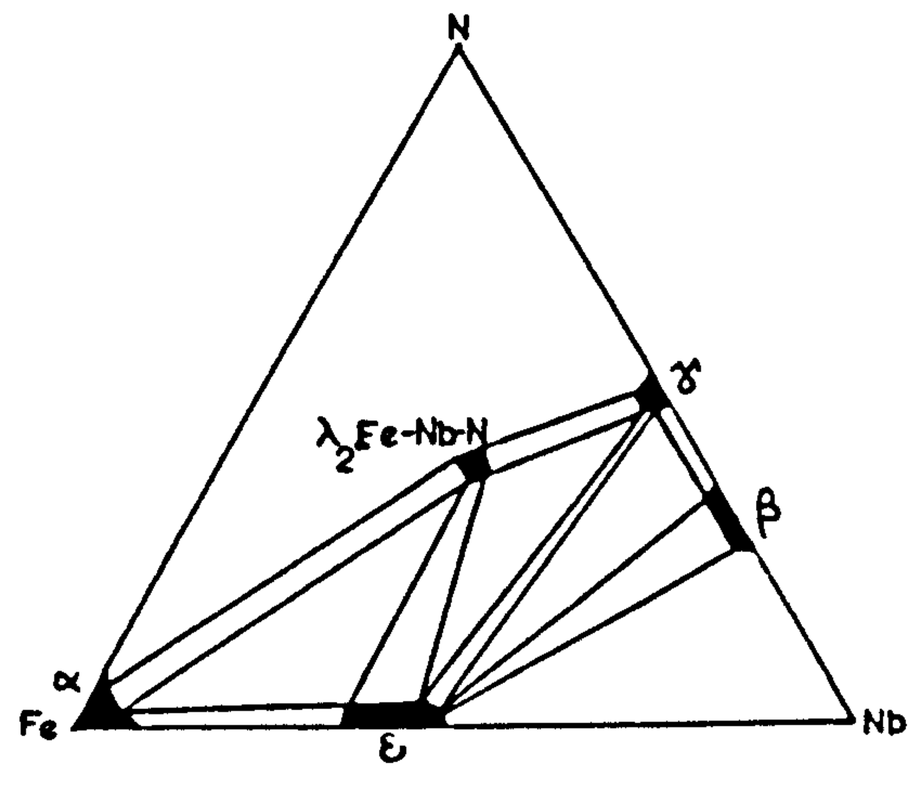
λ_1-$FeNb_4N_4$ exists over a wide range of homogeniety and has a hexagonal structure with typical unit-cell dimensions a, 5.192Å; c, 10.36Å; c/a, 1.977. The structure of λ_2-$FeNb_2N_2$ is undetermined and exists over only a small range of homogeniety. δ-NbN(O) has a lower oxygen content than ϵ-NbN(O)and transforms to the latter after

Fig. II. 4



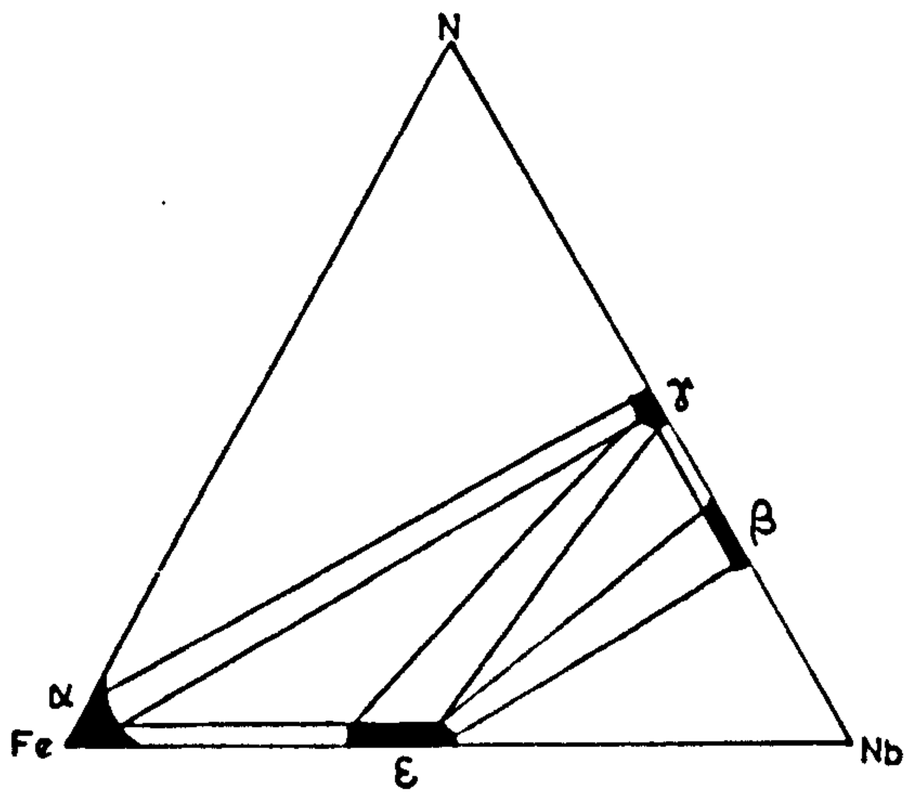
1. NH_3-H_2 [high pNH_3].

pN_2~ 5,000 Atm.



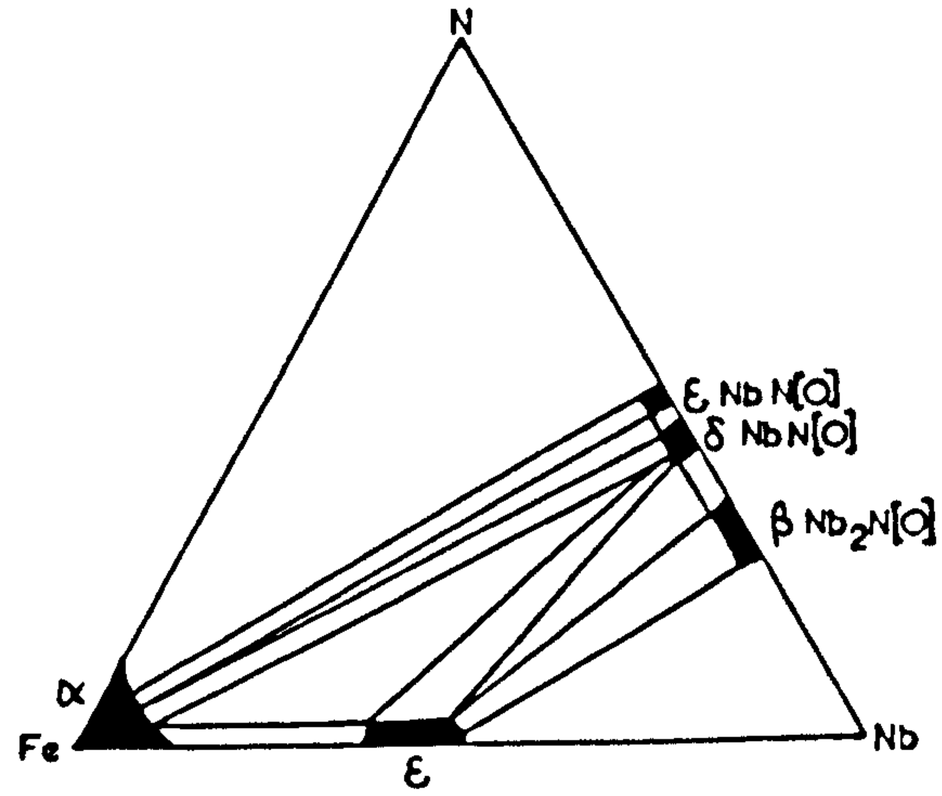
2. NH_3-H_2 [low pNH_3].

pN_2~2,500 Atm.



3. N_2-H_2 & P. Nitriding.

pN_2. 0·1–50 Atm.



4. As 3 with O_2 present.

PROPOSED TERNARY DIAGRAMS FOR Fe–Nb–N

ALLOYS AT VARIOUS NITROGEN PRESSURES.

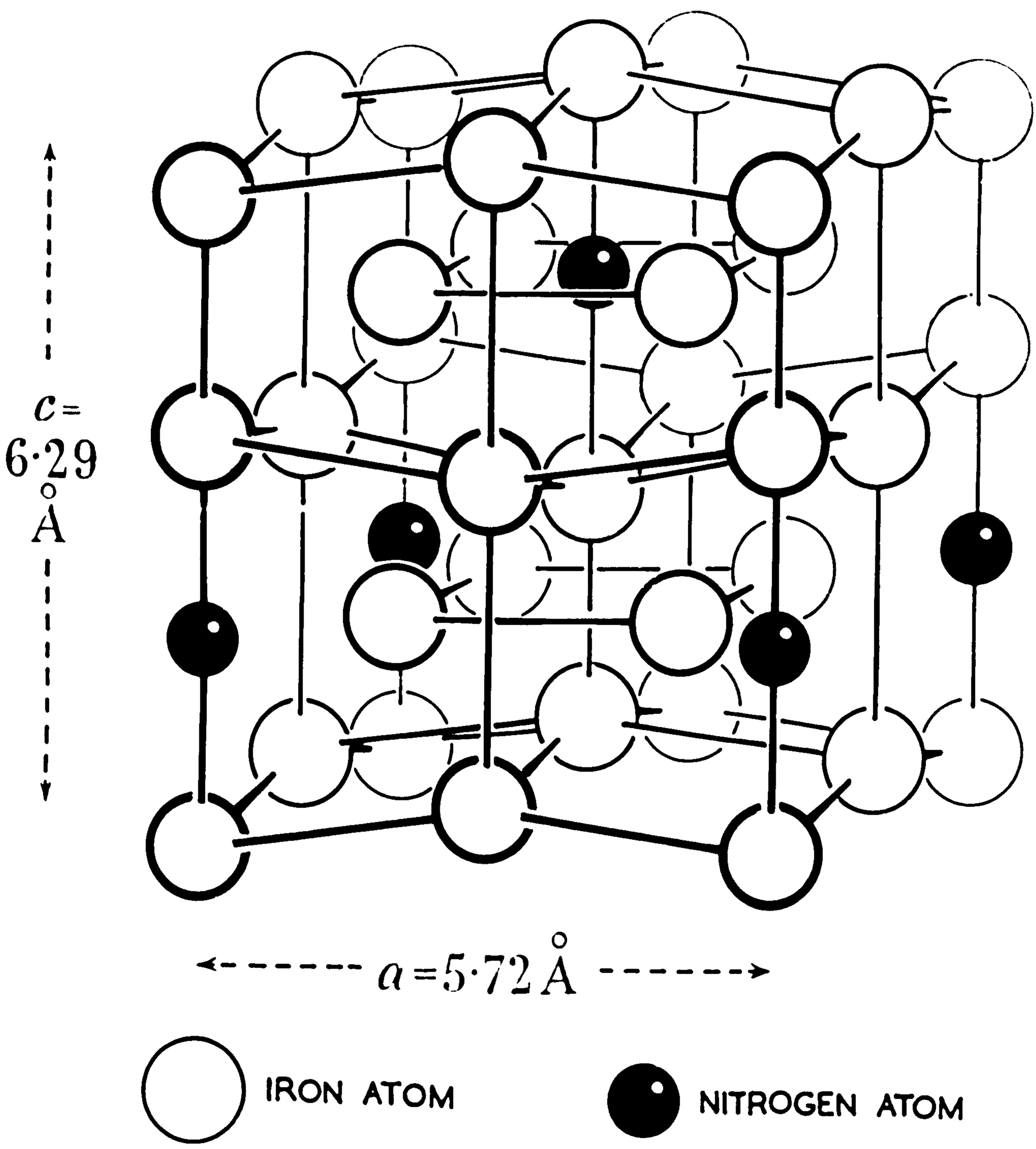
prolonged nitriding at temperatures above 700°C in NH_3:H_2 gas mixtures.

Mixed substitutional-interstitial solute-atom clusters are formed isothermally in Fe-Nb alloys during nitriding in NH_3:H_2 mixtures at 400 - 650°C (Roberts, 1970) and the sequence of homogeneous precipitation goes through similar stages to those found in the GP zone formation in Al-Cu alloys. The semi-coherent disc-shaped intermediate precipitate has a body centred tetragonal structure of the α''-$Fe_{16}N_2$ type containing some substitutional niobium atoms. After prolonged ageing at 600 - 800°C, transformation of ferrite to austenite occurs with the precipitation of γ—NbN.

II.4 Quench-aged Fe-N and Fe-X-N alloys

Dijkstra (1949) showed by internal friction and metallographic methods that at 250°C the precipitation of nitrogen from quench-aged nitrogen ferrite is a two stage process. Using X-ray techniques Jack & Maxwell (1952) showed that the initial precipitate was α'' $Fe_{16}N_2$; a phase characterised by Jack (1951 b) during the low-temperature tempering of nitrogen-martensite. The structure of Fe_{16} N_2 can be considered merely as eight unit cells of body-centred cubic iron strained anisotropically due to the presence of nitrogen (see Figure II.5). The nitrogen atoms occupy one

Fig. II. 5



twenty-fourth of the available interstices, but in such a manner as to expand the lattice in the c direction only. There is a consequent small contraction of the lattice in the a directions.

Electron microscope investigations (Booker, Norbury & Sutton, 1957; Keh & Wreidt, 1962; Hale & McLean, 1963) confirmed the orientation relationship proposed by Jack & Maxwell, that is:

$$(001)_{\alpha''} // (001)_{\alpha} , \quad [100]_{\alpha''} // [110]_{\alpha}$$

The phase readily precipitates as discs because of the excellent lattice "fit" in two directions, and the large degree of "misfit" in the third ($\approx 11\%$).

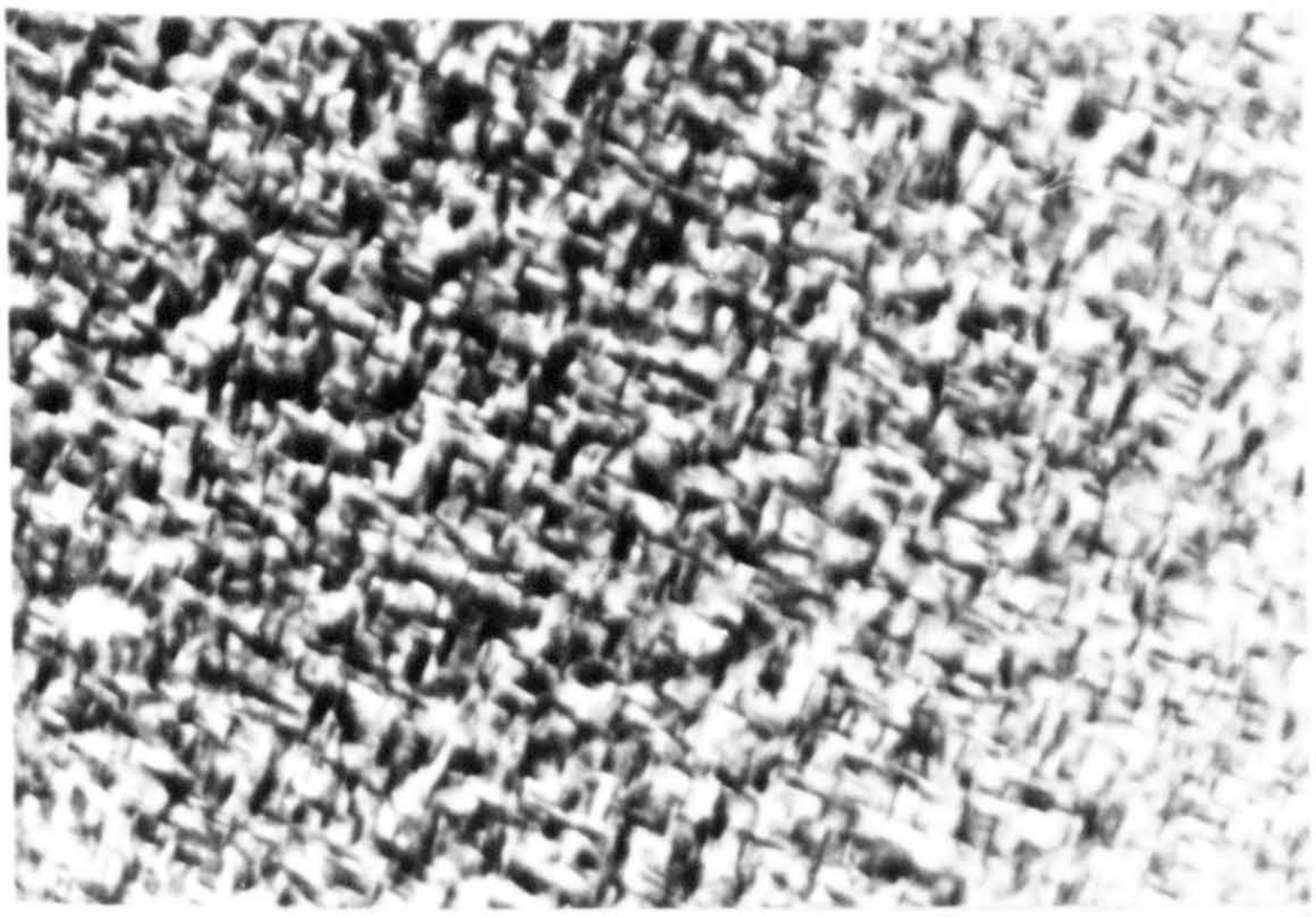
Recent work by Roberts (1970) shows that at high supersaturations and at low temperatures ($\approx 20^{\circ}C$) precipitation of α''-$Fe_{16}N_2$ is homogeneous and occurs via GP zone formation. As the temperature is increased and the supersaturation decreased, precipitation becomes heterogeneous (see Figure II.6).

The equilibrium phase, γ'-Fe_4N , precipitates at the expense of α''-$Fe_{16}N_2$ after longer ageing times. The orientation relationship between γ'-Fe_4N and α-Fe is shown by Mehl, Barrett & Jerabek (1934) and by Booker, Norbury & Sutton (1957) to be:

$$(112)_{\gamma'} // (210)_{\alpha} , \qquad [110]_{\gamma'} // [001]_{\alpha}$$

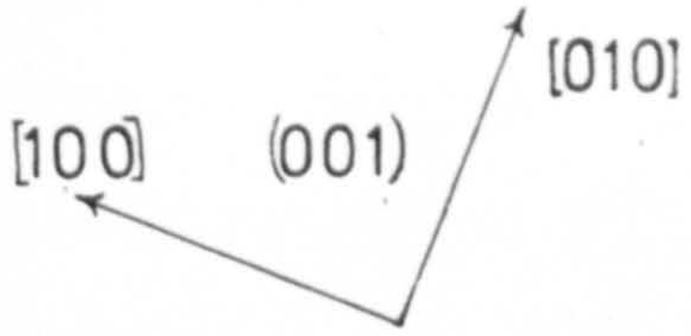
Fig. II. 6

Fig. II. 6



0·072%N. Aged 16h.21°C.

Homogeneous only

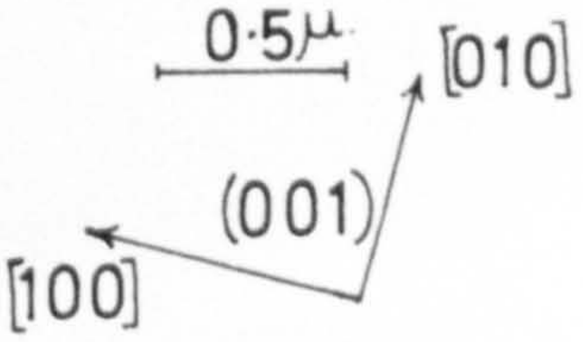


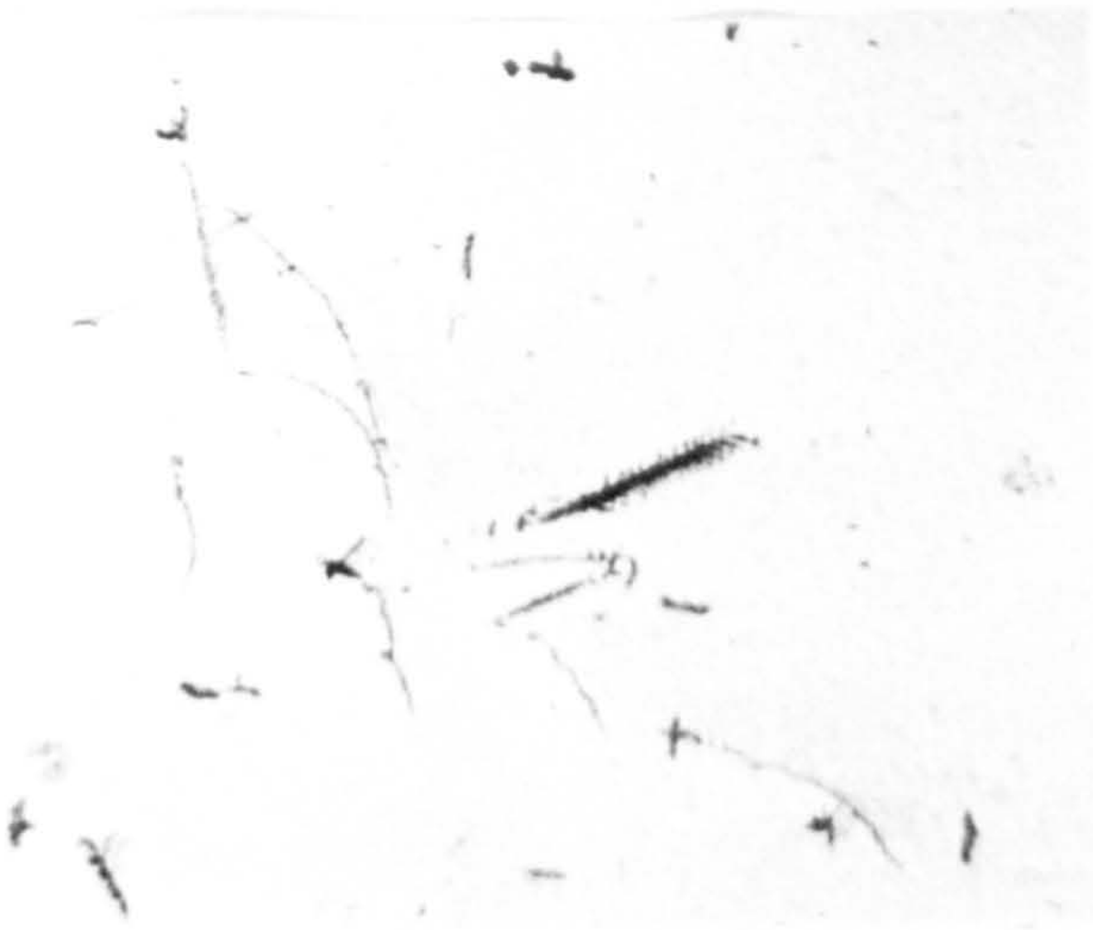


0·072%N. Aged 1h.55°C.

Homogeneous +

Heterogeneous





0·009%N. Aged 23h.45°C.

Heterogeneous only

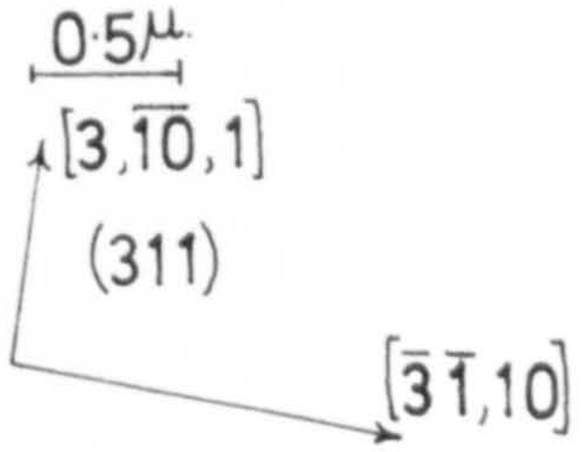


Fig PRECIPITATION MODES IN IRON-NITROGEN ALLOYS.

and γ' grows as plates so that $(112)_{\gamma'}$ is parallel to the plate surface.

Keh and Wreidt (1962) studied the precipitation of nitrides by electron metallography in quench-aged Fe-N alloys and found that the precipitated nitride, identified as $Fe_{16}N_2$, had $\{100\}_{\alpha}$ habit planes. Nucleation was observed to take place preferentially at dislocations and sub-boundaries, although some matrix precipitation was detected. From studies of the changes in mechanical properties and microstructures of deformed quench-aged Fe-N alloys, it was concluded that a transition in the deformation mechanism from particle cutting to an Orowan type mechanism occured. (Hale & McLean, 1963; Keh, 1963).

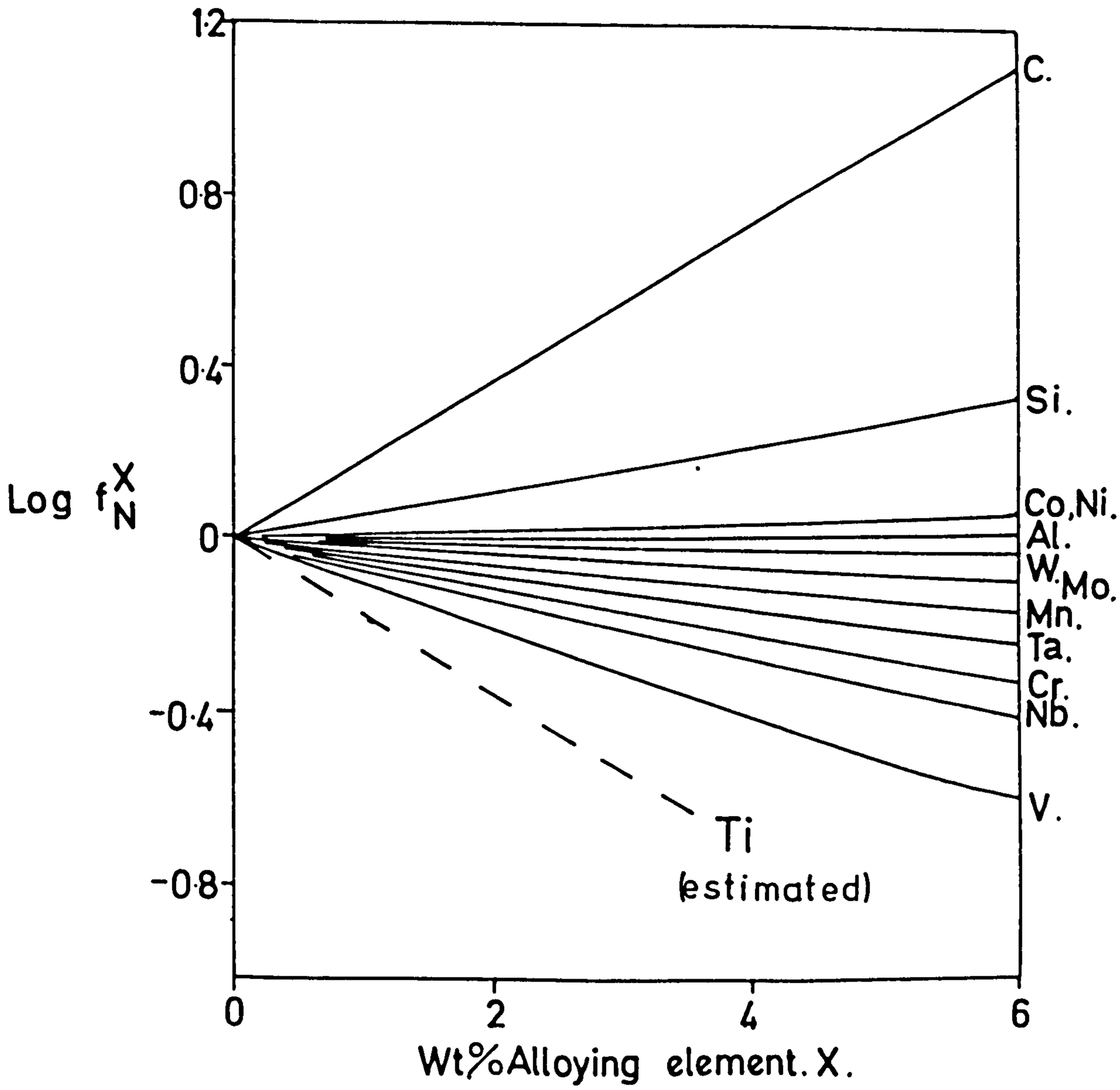
Even at temperatures where their diffusivities are negligible, the substitutional solutes still have a marked effect on the precipitation of iron nitrides from supersaturated ferrite. Most of the transition elements (X) decrease the activity coefficient of nitrogen (f_N^X) in iron but silicon and carbon increase it. Changes in precipitate size and distribution, with changes in the substitutional solute concentration in Fe-Mn-N (Pipkin, 1967), Fe-Mo-N (Speirs, 1969), Fe-Si-N (Roberts, 1970), Fe-Cr-N (Mortimer, 1971) and Fe-V-N alloys (Pope, 1972) are explained in terms of the effect of the substitutional solute upon the activity coefficient of nitrogen. The variation of nitrogen activity coefficient with an alloying element in liquid

iron is shown in Figure II.7, where the plot of log f_N^X against wt.%X is approximately linear. At lower temperatures, as solutions become less ideal, the effects become more marked.The amount and size of nitride precipitates are found to be larger, and the rate of precipitation slower, for elements which decrease f_N^X such as molybdenum, chromium, vanadium and other transition metal solutes. The reverse effect is true for Fe-Si alloys, since silicon increases f_N^X.

II.5 Homogeneous precipitation in Fe-X-N alloys

Speirs (1969) showed that constant activity nitriding of Fe-Mo alloys, containing from 1 to 3 at.%Mo in the temperature range 400 - 600°C, produces very hard material associated with the homogeneous nucleation of coherent particles on $\{100\}_\alpha$ matrix planes. These first formed particles were subsequently shown to be mixed substitutional - interstitial solute-atom clusters (Speirs et al 1970). Similar observations were made during the constant activity nitriding of ferrous alloys containing small amounts of a number of substitutional alloying elements, such as niobium (Roberts, 1970), chromium (Mortimer, 1971), vanadium (Pope, 1972), titanium (Jack, 1970) or tungsten (Stephenson, 1973). The precipitation produces marked hardness increments and, once formed, the particles are very stable. Both substitutional and interstitial solutes are essential to form clusters, and the homogeneous precipitation sequence leading to the precipitation of the equilibrium alloy nitride

Fig. II. 7



THE EFFECT OF ALLOYING ELEMENTS ON THE ACTIVITY COEFFICIENT OF NITROGEN IN IRON AT 1600°C.

[from Schenck et.al.(1958) &. Pehlke and Elliott (1960).]

goes through similar stages recognised in the classical work on Al-4wt.%Cu alloys:

i) disc-shaped clusters are formed on {100} matrix planes (GP zones);

ii) the formation of one or more intermediate metastable phases, which are coherent at first and then become incoherent;

iii) precipitation of the equilibrium precipitate.

Although this represents the general pattern of the precipitation sequence, each particular Fe-X-N system is different in detail.

In the Fe-Mo-N (Speirs, 1969), Fe-Nb-N (Roberts, 1970) and Fe-W-N (Stephenson, 1973) systems, the diffraction patterns of the first intermediate phase are all similar to that of α''- $Fe_{16}N_2$even though the equilibrium precipitates (η-Fe_3Mo_3N, γ -NbN and δ -WN respectively) are quite different. In Fe-Mo-N and Fe-Nb-N alloys each precipitation stage is clearly defined, whereas in Fe-W-N alloys stage two is the first to be recognised. In Fe-V-N (Pope, 1972), Fe-Cr-N (Mortimer, 1971) and Fe-Ti-N (Henderson, 1974) systems, dense, fine scale precipitation is also observed. However, from the experimental evidence obtained it is impossible to decide if the initial particles are clusters or small nitride precipitates. Subsequent ageing of these

particles produces incoherence normal to the plane of the disc along one of the cube directions of the matrix. The f.c.c. alloy nitrides form without any evidence for the presence of any intermediate precipitates, and are found to obey the Baker-Nutting (1959) orientation relationship:-

$$(001)_{XN} \;//\; (001)_{\alpha} \quad , \quad [110]_{XN} \;//\; [100]_{\alpha}$$

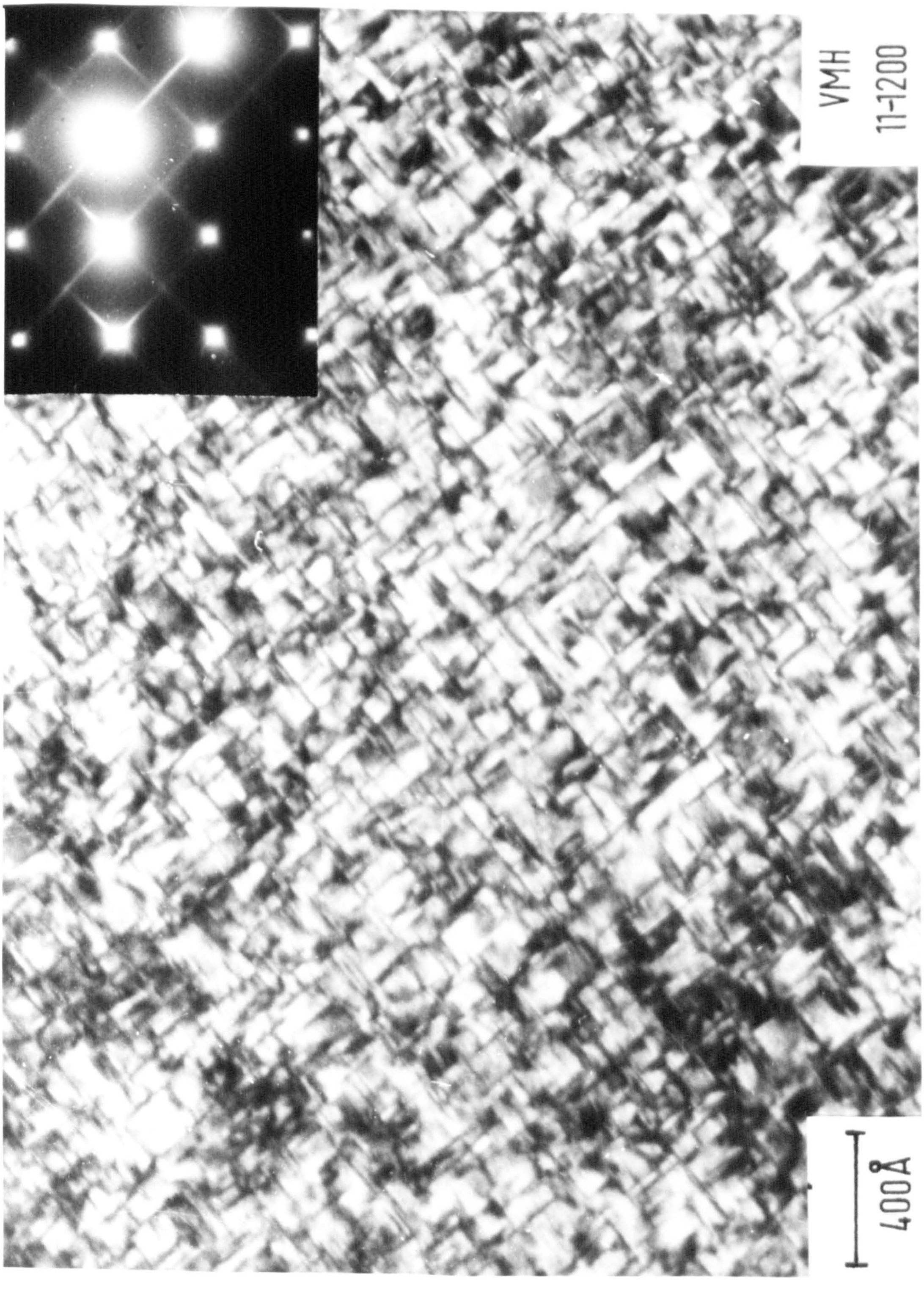
(XN is the particular f.c.c. alloy nitride such as VN)

The changes observed in the binary iron alloys nitrided above 450°C are very similar to the stages of homogeneous precipitation which occur in quench-aged Fe-N alloys. The effect of the substitutional solute is to stabilise the transformation structures to higher temperatures by 400 - 600°C compared with the Fe-N system.

In the early stages of precipitation, the thin disc-shaped clusters observed by Speirs (1969) (see Figure II.8) are microstructurally similar to the GP zones observed in Al-Cu alloys and to that of α''-$Fe_{16}N_2$ in quench-aged Fe-N alloys (see Figure II.6, after Roberts, 1970). The clusters produce continuous streaking on electron diffraction patterns in <100> matrix directions, a characteristic of thin plates on $\{100\}_{\alpha}$ planes. The micrograph of Figure II.8 is of a Fe-3at.%Mo alloy nitrided to peak hardness and shows a high density of disc-shaped clusters lying on matrix planes; the clusters have diameters of 10 - 15nm, typical interparticle spacings of 5 - 10nm, and they appear to be less than 2nm thick. Because the coherency strains

Fig. II. 8

Fig. II. 8



Fe-3at.%Mo nitrided to peak hardness

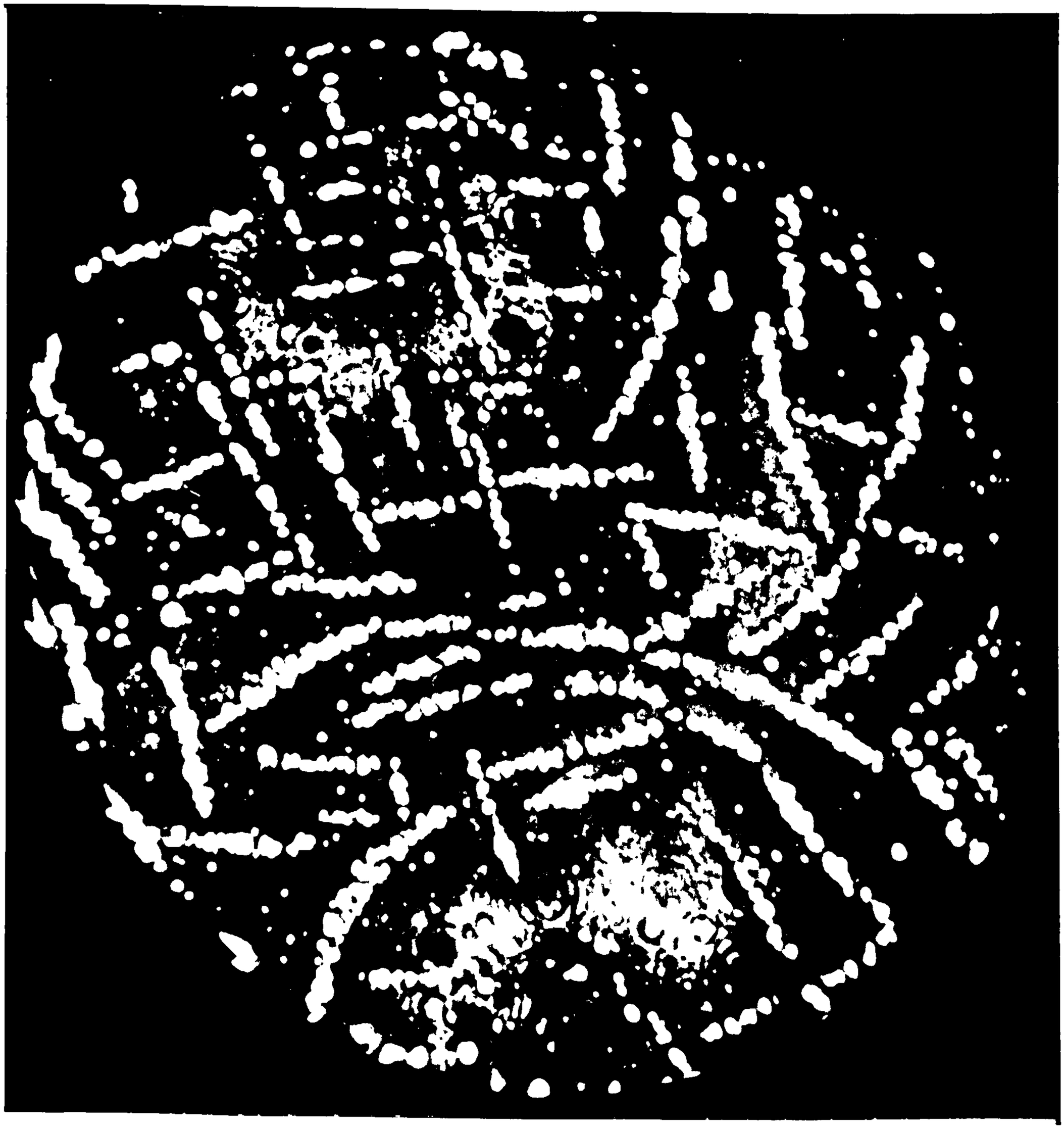
between the clusters overlap, the individual platelets are not resolvable. Similar micrographs are observed in other ternary Fe-X-N systems after constant activity nitriding under suitable conditions.

Homogeneous precipitation does not occur in all systems; for example, in Fe-Al-N alloys, finely dispersed AlN forms by continuous heterogeneous precipitation on dislocations propagated by the incoherent formation of earlier precipitates (Podgurski et al, 1969).

When clusters or precipitates are only two or three atom layers thick, their structures and compositions cannot be determined with certainty. The most direct evidence of clustering has been obtained by transmission electron microscopy and field-ion microscopy combined with atom probe analysis. A typical field-ion micrograph of constant activity nitrided Fe-3at%Mo is shown in Figure II.9 (after Driver & Papazian, 1973). The micrograph shows the disc-shaped, fully coherent clusters with a $\{100\}_\alpha$ habit plane. The clusters are only 0.6 - 1.2nm thick and have an apparent interplanar spacing of 0.27 ± 0.05nm. These observations were interpreted on the basis of the clusters having a body-centred tetragonal structure in which some iron atoms are partially or completely ordered on alternate $\{002\}_\alpha$ planes, i.e. with a α''-$Fe_{16}N_2$ type structure of composition near $Fe_{12}Mo_4N_2$.

Fig. II. 9

Fig II. 9.



Field ion micrograph of nitrided Fe-3at.%Mo

Further evidence of clustering has been obtained by hydrogen reduction experiments on a Fe-3at.%Mo alloy nitrided to peak hardness (Unthank, Driver & Jack, 1972). Hydrogen reduction at the nitriding temperature removed all except a trace of nitrogen, yet electron microscopy still showed disc-shaped clusters of molybdenum atoms, which gave continuous diffraction streaking in $\langle 100 \rangle_\alpha$ matrix directions. No such clustering occurred in Fe-3at.%Mo without the nitriding treatment, nor did it occur by decomposition of the equilibrium nitride precipitate. Therefore, the constant activity nitriding of Fe-Mo alloys produces metastable clusters, rather than stable molybdenum nitride precipitates.

Recent work by Krawitz & Sinclair (1974), based upon a principle assumed independently by Guinier (1938) and by Preston (1938), gives further evidence for mixed cluster formation.

The unit-cell dimensions of a solid solution are essentially invariant with respect to the distribution and arrangement of its solute atoms. A matrix containing clusters or GP zones is a solid solution in which non-random local atomic arrangements exist, but its unit-cell dimensions are the same as for a random solution having the same solute concentration. When precipitation occurs the lattice parameter changes to that of the depleted matrix. The increases in unit-cell dimensions observed after nitriding ferritic alloys are much larger than

those expected from alloy nitride precipitation. They are accounted for only if almost all the nitrogen remains in solid solution and occupies the octahedral interstices of the alloy-ferrite lattice. Unit-cell dimensions of the matrix thereby provide a sensitive method of determining whether nitrogen is in solution, randomly or as zones; or whether it is precipitated as a second phase.

Phillips and Seybolt (1968) ion nitrided at 550 - 600°C various binary iron alloys containing either 1% aluminium, chromium, manganese, silicon, titanium or vanadium as the substitutional solute. Electron metallography revealed fine particle formation and from electron diffraction patterns AlN, CrN and Si_3N_4 were positively identified, VN tentatively identified, whilst in the titanium alloy, clusters of less than 1.5nm were observed. Lambert and Greday (1970) studied the isothermal precipitation of VN in Fe-Mn-Si-V-N alloys aged in the range 425 - 1000°C for various times. Incoherent precipitation of f.c.c. VN was observed, the particles being aligned in rows and measuring from 3 - 10nm in diameter. The density of particles was from $1\text{-}2\times10^{16}/cm^3$ and some of them were found to obey the Baker-Nutting (1959) orientation relationship.

II.6 Kinetics of nitriding

When there is a strong interaction between nitrogen and a substitutional solute nitriding proceeds by the formation

of a hard subscale, the thickness of which progressively increases. This has been observed in nitrided Fe-Ti (Jack et al 1971), Fe-Cr with $\geqslant$ 2at.%Cr (Mortimer, 1971) and in Fe-V alloys (Pope, 1972). In the absence of iron nitride formation the subscale thickness (X) varies with time (t) according to:-

$$X^2 = \frac{2 \text{ at.\%N}}{r \text{ at.\%M}} \; D.t \qquad \ldots\ldots\ldots \text{(II).1}$$

which is derived from theories of diffusion accompanied by a phase change, and which has been applied to internal oxidation. r is the atomic ratio N/M in the phase formed by nitriding; at.%N is the atomic concentration of nitrogen in solution at the metal interface (determined by the NH_3:H_2 ratio of the nitriding gas atmosphere); at.%M is the atomic concentration of substitutional solute M, originally in solution; and D is the diffusivity of nitrogen.

In iron containing $<$2at.%Cr Mortimer (1971) showed that a hard subscale was not formed, but that the hardness increased almost uniformly over the cross-section. One possible interpretation was that the rate determining factor was the diffusion of chromium. Similar profiles were observed during nitriding Fe-3at.%Mo alloys (Jack et al, 1971), where the abnormally slow nitrogen penetration was suggested as being due either to surface reaction control, where nitrogen entry is retarded by an adsorbed impurity film (probably oxygen), or to the slow nucleation of clusters due to the relatively

weak Mo-N interaction. Recent work (Hayes & Grieveson, 1975) has shown that the condition of the metal surface plays an important role in determining the hardening behaviour of Fe-Mo alloys because by careful pre-treatment of samples, and at certain oxygen and nitrogen potentials, internal nitriding behaviour was observed.

II.7 Internal friction of Fe-N and Fe-X-N alloys

The study of internal friction produced by interstitials dissolved in b.c.c. metals has been the subject of many investigations. In nitrogen-ferrite, the stress induced ordering of nitrogen produces an internal friction peak at about 20°C for a testing frequency of 1 c.p.s. The physical origin of this peak was traced by Snoek (1941) to the local tetragonal symmetry of the interstitial positions in alpha iron.

When small amounts of a substitutional alloy element and nitrogen are dissolved in alpha iron, additional peaks (termed interaction peaks) are observed in addition to the Snoek damping. Previous related work (Dijkstra & Sladek, 1953; Fast & Meijering, 1953; Jamieson & Kennedy, 1966; Leak et al, 1955; Enrietto, 1962; Couper & Kennedy, 1967; Rawlings & Robinson, 1961) has produced evidence of peaks in the temperature ranges 10 - 95°C with manganese, chromium, molybdenum, silicon or vanadium acting as the substitutional solute in ternary Fe-X-N systems. All investigators agree that these

peaks are due to nitrogen jumps involving Fe-X sites, (the octahedral sites co-ordinated by one substitutional atom and five iron atoms). This arises because the effect of nitrogen in an octahedron containing a substitutional atom is different to that in an octahedron containing only iron atoms.

Fast & Meijering (1953) found by nitriding Fe-0.5at.%V wires at 950°C and quenching to room temperature that the interaction peak could not be described, as suggested by Dijkstra & Sladek (1953), by a single relaxation time. Also, they found that the interaction peak temperature increased from 80 to 88°C after prolonged heating at 950°C. Fast & Meijering (1953) attributed the peak to the movement of nitrogen atoms trapped in abnormal interstices around fine VN precipitates. They suggested that the shift in peak temperature was due to a coarsening of the precipitates and the consequent displacement of the binding energy distribution towards higher values. Fast (1961) subsequently explained the peak on the basis of nitrogen atoms jumping around single vanadium atoms which were made available by the dissociation of VN at 950°C. More recently, Jamieson & Kennedy (1966) have ascribed the peak to both mechanisms in order to explain the shift of the peak temperature.

In general, the interaction peaks cannot be interpreted in terms of a single relaxation time and consequently a number of relaxation processes are assumed to contribute to the

damping. Different researchers have produced a variety of theories. Perry, Malone & Boon (1966) suggest that the peak in the Fe-V-N system has three components whilst Ritchie & Rawlings (1967) analyse the equivalent peak in Fe-Cr-N and Fe-Mn-N alloys into either six or seven components depending upon the substitutional concentration. Similar work by Nacken & Kuhlmann (1966) resolved the Fe-Mn-N peak into seven components, whereas Enrietto (1962) and Couper & Kennedy (1967) resolve it into three peaks. A recent investigation into the interaction peak in Fe-V-N alloys using both internal friction and stress-relaxation methods (Welch & Carpenter, 1972) shows that the abnormal peak can be resolved into three separate Debye peaks and that the damping is consistent with the stress-induced diffusion of nitrogen around a VN 'defect'. The 'defect' model explains the peaks as being due to nitrogen atoms in the first and second nearest neighbour sites moving in octahedral - tetrahedral - octahedral sites, with one of the nitrogen atoms being tightly bound to vanadium and therefore, being unable to diffuse.

Damping at high temperatures has been observed in Fe-C and Fe-N cold worked specimens and is interpreted as being due to the interaction of interstitials with dislocations, the peak temperature varying from 160 - 200°C with the degree of cold work (Petarra & Beshers, 1967).

In martensites, Stark et al (1956) and Mura et al (1961) have interpreted the peak observed at about 220°C as being due to the motion of dislocations in the vicinity of either carbide and nitride precipitates or interstitial atmospheres.

The presence of an abnormal peak in the range 150 - 200°C has been observed by Köster & Horn (1966) in nitrided iron alloys containing from 0.5 - 4 at.%Mo or V. The damping was suggested to arise from a mechanism similar to that responsible for the deformation damping in Fe-N and Fe-C alloys. Szabó-Miszenti (1970) observed two abnormal peaks in the temperature ranges 115-165° and 220 - 240°C in nitrided dilute Fe-Ti alloys (0.18 - 0.70 at.%Ti) with peak temperatures and widths varying with composition and heat treatment. Both peaks were considered to be due to an interaction between interstitial nitrogen and substitutional titanium.

Pope (1972) has shown that constant activity nitriding of Fe-V alloys produces high temperature damping from 150 - 200°C. This damping is associated with a microstructure showing extensive strain due to the formation of coherent particles on the ferrite cube planes.

II.8 Mechanical properties of Fe-X-N alloys

Forrest & Hopkin (1963) first observed a marked

enhancement of the fatigue and creep resistance of Fe-C and Fe-N alloys when small amounts of manganese (< 1at.%) were present in solution. They observed a finely dispersed precipitate on dislocations in alloys containing 0.75at.%Mn and 0.09at.%N after creep testing at 450°C and suggested that the formation of this precipitate was the major factor in improving the creep resistance. Hopkin (1965) later suggested that the improved properties were not due to precipitation but to the formation of solute atmospheres associated with manganese atoms. Although a precipitate was formed at 450°C, there was much less observed at 650°C; yet the creep resistance was maintained at the higher temperature, suggesting that manganese atoms clustered around single nitrogen atoms and acted as barriers to dislocation movement.

After a study of the tensile properties of Fe-Mn-N alloys in the range 20 - 600°C, Baird and Jamieson (1966) also favoured the cluster theory proposed by Hopkin. Hopkin (1965) observed that the precipitate was formed at 450°C on the {100} ferrite planes, and concluded that it was a Fe-Mn nitride, $(Fe\ Mn)_{16}N_2$, isostructural with α''- $Fe_{16}N_2$. Subsequently, Pipkin (1967) made an investigation by X-ray methods of a similar sample aged at 450°C and found that η - Mn_3N_2 was the precipitated nitride.

In a recent investigation into the creep behaviour of Fe-Cr, Fe-Mn and Fe-Mo alloys containing nitrogen, Baird &

Jamieson (1972) observed increases in the initial creep strength; the largest increases being in Fe-Mo alloys. The high initial creep strength was ascribed as being due to solid solution strengthening by small groups of substitutional and interstitial atoms. Precipitation took place on dislocations and grain boundaries during creep and in systems where such precipitation was extensive, the main strengthening mechanism was found to change during creep to either precipitation hardening or precipitation on dislocations. Ishida & McLean (1967) studied the strong alloying effect of manganese and nitrogen on the creep rate. Nitride precipitates were observed by transmission electron microscopy. Consequently, it was suggested that the manganese and nitrogen atoms had combined to form 'clusters', causing solid solution strengthening of the steel.

In Chen's study (1965) of the dispersion strengthening of internally nitrided Fe-Ti alloys, the strengthening was attributed to the formation of non-deformable particles. Nitriding was carried out at 600 - 1000^{o}C in low NH_3:H_2 ratio gas mixtures or in molecular nitrogen, producing what were described as thin TiN plates, being coherent with the matrix when they were less than 40nm diameter.

Phillip & Seybolt (1968) and Seybolt (1969) investigated the behaviour of a number of binary iron alloys after 'ion-nitriding' at 550 - 600^{o}C. Transmission electron microscopy revealed particle formation of the appropriate alloy nitride (e.g. CrN) on the ferrite cube planes in all

alloys except those containing manganese or molybdenum. The precipitation was also accompanied by a large increase in hardness.

Roberts (1970) showed that a high hardness and yield strength are developed by the GP zone structure in nitrided Fe-Nb alloys. The hardness and yield strength decreased after ageing at 800°C with the formation of the α'' - $Fe_{16}N_2$ type intermediate precipitate, and still further when precipitation of γ - NbN occurred.

II.9 Precipitation and strengthening in control cooled steels

Considerable interest has been shown in the combined effects of vanadium and nitrogen in commercial steels. Epstein et al (1950) and Jones and Coombes (1953) showed that the addition of small amounts of vanadium to rimming steels rendered them unsusceptible to strain ageing without producing any deleterious side effects. Stephenson, Karchner & Stark (1964) studied the strengthening phenomena in semi killed low C-Mn steels to which additions of 0.15 at.%V and 0.056 at.%N had been made. They found that the increases in yield strength in hot rolled steels, due to the combined vanadium and nitrogen additions, resulted from precipitation hardening of extremely fine plates of vanadium nitride on the {100} ferrite planes. Plates of 10 - 40nm diameter and 2 - 9nm thick, some of them being coherent, were observed. Some

contribution to the increase in strength was also considered to be due to the precipitation hardening effect of vanadium carbide.

Morrison (1963) observed that small additions of niobium (≈ 0.01%) to C-Mn steels produced marked strengthening effects. Although no precipitate could be extracted, very small particles were observed by transmission electron microscopy which were thought to be either NbC or NbN. Gray et al (1965) observed precipitates in the form of 4 - 8nm diameter discs, from 1.5 to 3nm thick, in mild steels containing niobium. Gray & Yeo (1968) studied the precipitation of Nb(CN) in low alloy steels with the emphasis on precipitate row formation. The rows were readily visible in control cooled steels, but not always in the isothermally transformed samples, whilst the row spacing increased as the cooling rate decreased. The rate controlling step was found to be due to niobium diffusion.

Woodhead and Webster (1969) investigated the precipitation reactions in a vanadium bearing mild steel during isothermal transformation. Lines of precipitate formed on the γ/α interface in a similar manner to those in niobium steels. Similar studies by Sutton and Whiteman (1971) on Fe-V-C steels observed that several different morphologies of V_4C_3 were formed, and that the carbide distribution was so fine that considerable strengthening was obtained.

Particles of various shapes were observed by Lambert et al (1970) in iron alloys containing vanadium and nitrogen. After isothermal precipitation a high density of particles ($\approx$ 1-2x10^{16}/cm^3) of 3-10nm diameter were formed. It was also observed that the yield strength decreased with the length of holding time. Interphase precipitation has been studied in a 0.5 at%Ti steel by Freeman (1971). On transformation from γ to α iron, TiC was found to precipitate as small particles (3-10nm diameter) in the form of sheets, (8-65nm apart).

During a study on the effects of nickel and manganese on the precipitate strengthening of vanadium steels, Suzuki et al (1970) observed that the strengthening was due to V_4C_3 precipitation and the effects of coherency stresses. The steel containing only coherent particles had a remarkably high yield strength; the peak strength being associated with a high density of coherent V_4C_3 precipitates, (8-10nm diameter) and a high density of dislocations. Work by Schiller (1971) on normalised low alloy steels containing 1.5at.%Mn and 0.06at.%al, together with 0.1at.%V and 0.07at.%N found marked strengthening increments; however, it was considered to be due to grain refinement produced by the fine dispersion of vanadium nitride. Gladman et al (1971) showed that providing the matrix is simple, as in high strength low alloy and quench-aged steels, the strengthening by hard second phase particles in a ferrite matrix can be described by an Ashby-

Orowan (1964) relationship. Similar work by Gray & Yeo (1968) also advocates an Orowan type relationship for the small dispersed particles.

Baker (1973,a) examined the structures of Fe-C-N-V alloys containing various amounts of manganese by transmission electron microscopy. After rolling, particles of 17nm diameter with spacings of 20nm, were observed as interphase precipitates. However, in control cooled samples, particles of only 3nm diameter were observed as thin plates on $\{100\}_{\alpha}$.

Gray (1973) studied the effect of niobium on the transformation and precipitation processes in high-strength low alloy steels, and found that the yield strength was not proportional to interparticle spacing for particles in the size range 4-12nm. The yield strength increased down to the smallest particle size (1.5-2nm), where it was thought that particle cutting would be predominant. This phenomenon has been observed by Greday and Lamberigts (1972) at particle sizes of less than 5nm.

In an investigation into the grain refining effects of niobium, vanadium and titanium in low carbon steels, Irvine et al (1967) found that niobium and vanadium could produce additional strengthening above that due to the fine grain size. Some contrast effects indicative of coherency strains were observed in the vanadium steels, whereas in the titanium

steels more closely spaced precipitates of about 3nm diameter were found. In the niobium and vanadium steels, strength increments varied from 50-150N/mm^2, whereas very high increments of up to 300N/mm^2 were found in the titanium steels. Whilst determining the mechanical properties of structural steels containing vanadium or niobium, in respect of the state of precipitation induced by thermomechanical treatments, Lamberigts and Greday (1974) found that the peak hardness was obtained when coherent particles of 7nm diameter were precipitated.

II.10 Secondary hardening steels

Whilst studying the secondary hardening of steels containing vanadium or niobium, several investigators noted the appearance of what were probably coherent particles. These particles were described using various terminology. Kuo (1956) tempered steels containing vanadium, titanium and molybdenum for one hour at 500 - 600^{o}C and found that 'threads' of VC and TiC precipitates, which had a diameter of 3nm and a length of 20nm, caused an increase in hardness. Vanadium carbide started to form at 525^{o}C and the greatest degree of hardening was associated with the highest rate of precipitation. Smith and Nutting (1957) observed 'cloud-like' VC precipitates of less than 10nm diameter and suggested that vanadium enriched zones had been formed prior to the precipitation of VC. Some microstructural evidence supported this, since after tempering at 400^{o}C, small spots were

observed in the ferrite matrix. Seal and Honeycombe (1958) observed 'rods' or 'threads' of precipitate measuring 1.5 - 2.5nm wide and 5-20nm diameter. Prior to peak hardness being attained, V_4C_3 was identified as the precipitate present, and the hardening curves were explained by invoking the concept of a coherent precipitate.

Tekin and Kelly (1965) noted that the hardening of Fe-1%-V-C alloys after tempering was due to either V_4C_3 precipitation on dislocations, or to the homogeneous precipitation of coherent particles in the matrix on $\{100\}_\alpha$ planes. In similar alloys, Smith (1966), observed that the peak hardness coincided with the formation of coherent V_4C_3 precipitates of only a few unit cells thick and 10nm diameter. The decrease from peak hardness was accompanied by an increase in the size and a reduction in the number of the precipitates. During the tempering of carbon martensite containing some niobium, Tanino and Aoki (1968) attributed the secondary hardening to the formation of small coherent plates of f.c.c. niobium carbide. Using selected area diffraction techniques, the orientation relationship was found to be the same as the relationship established by Baker and Nutting (1959) for V_4C_3 precipitation in ferrite:

$$(001)_{NbC} \,//\, (001)_\alpha, \quad [010]_{NbC} \,//\, [110]_\alpha$$

After short tempering times at 500°C, considerable streaking was observed in $\langle 100 \rangle_\alpha$ directions. Streaking has also been observed in the secondary hardening of vanadium containing

steels, (Davenport et al, 1968). During a study of the relationship between the microstructure and mechanical properties after tempering a Mo-W-V steel, Simcoe et al (1968) found that 'filmy' patches of (V Mo W)C had formed in the range 530 - 615°C. A large increase in the yield strength was noticed, although not in the work hardening rate, inferring that the cutting of coherent particles had contributed to the strength. Baker (1973,b) determined that during the tempering of control cooled low carbon, vanadium steels containing nitrogen and various amounts of manganese, precipitation of V(CN) developed as thin plates on $\{100\}_\alpha$. Detailed qualitative estimates of the yield strength indicated that the Ashby-Orowan (1964) model for strengthening, as modified by Gladman (1971), did not account for all the additional strengthening. An alternative mechanism, such as particle cutting, was thought to have contributed to the strength of the particles.

Chapter III

EXPERIMENTAL TECHNIQUES

III.1 The preparation of alloy samples

High purity iron-base alloys were supplied in either plate or bar form by the British Iron and Steel Research Association and by the National Physical Laboratory. Analyses of the alloys used are listed in Table III.1

Internal friction and X-ray specimens were prepared by cold drawing to 0.60mm diameter wire. Material for tensile test specimens was prepared by hot rolling to 2mm thick plate, followed by cold rolling to 0.75mm; flat specimens, having a gauge length of 20mm and a cross-section of 5.0 by 0.75mm, were then stamped out from the rolled plate. Sheet specimens, 10mm square and 0.1mm thick, were prepared by cold rolling as the starting materials for electron microscopy.

Before nitriding, all specimens were abrasively cleaned, degreased and annealed in hydrogen at temperatures above 750°C.

III.2 Ammonia-hydrogen nitriding

The required nitrogen concentration was introduced into the specimens by treating them in an ammonia-hydrogen gas mixture of the appropriate nitrogen potential.

TABLE III 1.

ANALYSES OF ALLOYS

Cast Code	at.%substitutional solute	wt.%C
23 DAK 2	0.15 V	-
K 1294	0.52 V	0.004
K 1302	1.08 V	0.016
38 AF 3	1.20 Cr	0.003
K 990	2.0 Cr	0.01
K 1412	0.65 Ti	0.016
K 673	0.10 Nb	0.005
K 674	0.31 Nb	0.005
K 675	0.60 Nb	0.004
39 AF 3	1.70 Mo	0.002
39 AF 2	2.92 Mo	0.001

K codes are B.I.S.R.A. alloys
others N.P.L.

The nitrogen potential of an ammonia-hydrogen gas mixture is determined by the ratio of the concentrations of ammonia and hydrogen; Lehrer (1930), Brunhauer et al (1931) and Paranjpe et al (1950). The nitriding reaction is:

$$NH_3(g) = \underline{N}\ (\text{in Fe}) + \frac{3}{2} H_2(g) \quad .... \quad (III)1$$

and the equilibrium constant, K, at a given temperature is:

$$K = {}^{a}N. P_{H_2}^{3/2} / P_{NH_3} \quad .... \quad (III)2$$

where a_N is the activity of the nitrogen in iron and P_{NH_3} and P_{H_2} are the partial pressure of ammonia and hydrogen respectively. The nitrogen activity is therefore proportional to $P_{NH_3} / P_{H_2}^{3/2}$.

For example, in the iron-nitrogen system at 620°C the successive phases formed with increasing nitrogen content are α-solid solution, γ-solid solution and γ'-Fe_4N. When an iron specimen is exposed to an ammonia-hydrogen mixture of sufficient nitrogen potential to form Fe_4N, the activity of the combined nitrogen will vary in the following manner. There will be an increase from zero in the α (pure metal) to a value of $a_N^{\alpha\text{-max}}$ in the saturated nitrogen ferrite; this occurs when it has reached the limit of the terminal solid solution. The α-phase is then in equilibrium with the γ-phase of composition γ^{min}, so that the activity of nitrogen $a_N{}^{\gamma min}$ is equal to $a_N^{\alpha\text{-max}}$. As the total nitrogen content increases, the α-phase gradually disappears. When no α remains, the activity of nitrogen in

γ increases and the composition of γ changes. Eventually, the solubility limit in γ is reached and at this point $a_N^{\gamma\text{-max}}$ is equal to $a_N^{\gamma'\text{-min}}$. The γ' phase then forms at the expense of the γ phase until the activity of nitrogen in the γ' increases to the value in equilibrium with the nitriding gas.

In any single nitride phase the nitrogen activity varies regularly with composition. Consequently, as a_N is proportioned to $P_{NH_3}/P_{H_2}^{3/2}$, a gas mixture of given composition is in equilibrium with a nitride phase of fixed nitrogen content. Therefore, it is possible to prepare a nitride or an iron-nitrogen solid solution of any composition by precisely controlling the ammonia-hydrogen gas ratio.

In practice there are two complicating reactions which can occur:

a) the "cracking" of ammonia, by the reaction

$$NH_3(g) = \tfrac{1}{2} N_2(g) + 3/2\ H_2(g) \quad \ldots\ (III).3$$

and b) the thermal decomposition of the nitride phase,

$$\underline{N} = \tfrac{1}{2} N_2(g) \quad \ldots\ (III).4$$

which is virtually a non-reversible process for iron nitrides at one atmosphere pressure.

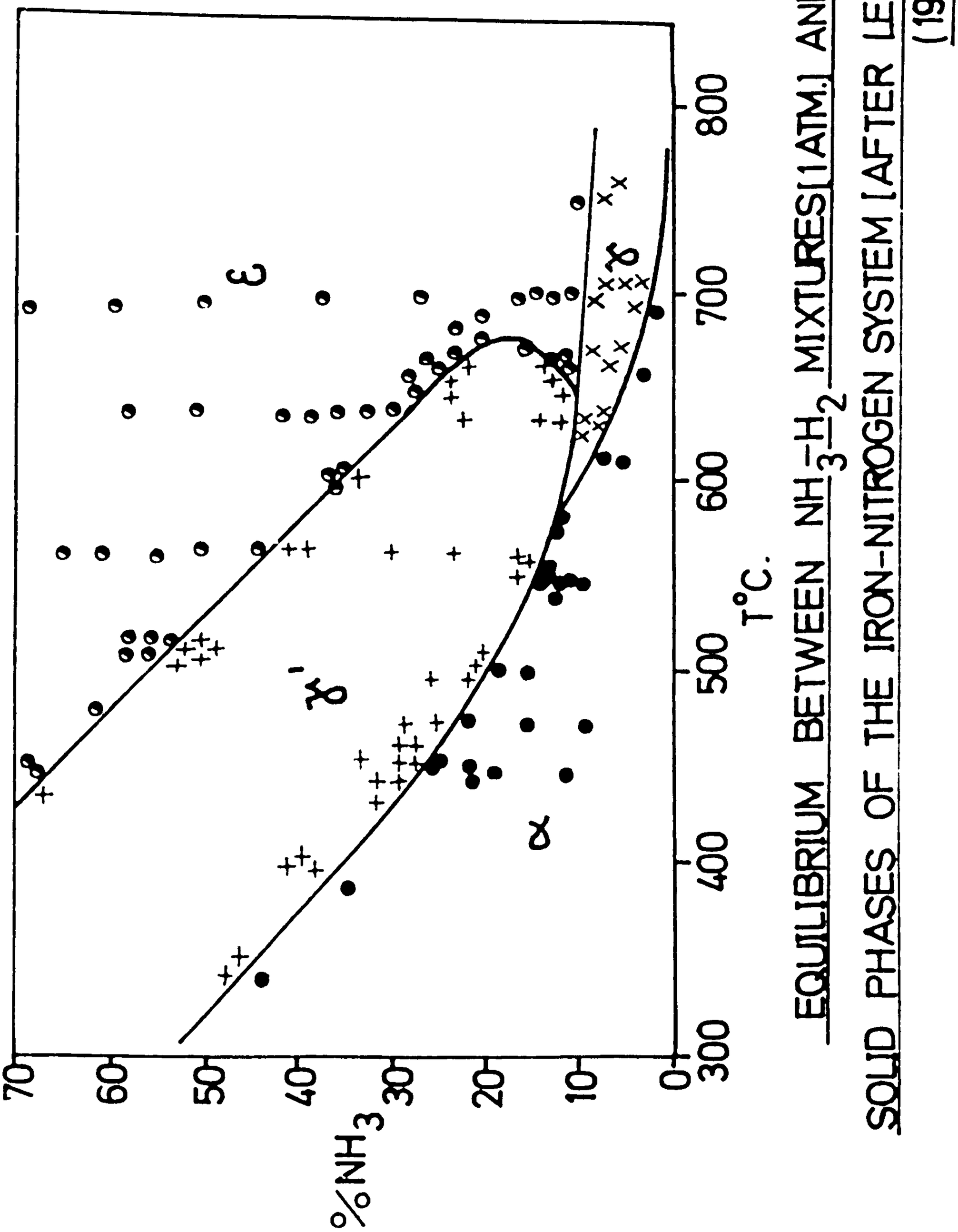
When the catalytic effect of the metal sample and the reaction tube upon the cracking of ammonia is constant, the degree to which the gas approaches its equilibrium $NH_3/N_2/H_2$ mixture is determined by the gas flow. Therefore, not only the composition of the gas, but also its rate of flow must be controlled if the required nitrogen potential is to be maintained. In addition to this, the nitriding potential of the gas must exceed the decomposition pressure of the nitride phase. Consequently, the nitriding action of ammonia depends upon the balance of three reactions which are affected by many variables. These variables include temperature, gas composition, the catalytic effect of the surfaces to which the gas is exposed, gas contamination and flow, the decomposition pressures of solid nitride phases and any previous treatment or impurities in the metal itself.

The nitrogen solubility in α-iron is sufficiently small (maximum $\approx$ 0.4 at %N at 590°C), that no appreciable error is introduced by assuming Henry's law, i.e. at constant temperature the partial pressure of nitrogen is proportional to its mole fraction. The equilibrium constant for the ammonia nitriding reaction (III).2 can be written as:

$$K' = \text{wt \% N} \cdot P_{NH_3}/P_{H_2}^{3/2} \qquad \ldots\ldots(III)5$$

The diagram compiled by Lehrer (1930) and shown in Figure III.1, was used to give a guide to the nitrogen potential and ammonia-hydrogen ratios reqired to produce given quantities of nitrogen in solution in iron.

Fig. III. 1


EQUILIBRIUM BETWEEN SOLID AND
NH3–H2 MIXTURES [1 ATM.] ACCORDING TO LEHRER (1930)].
THE IRON-NITROGEN SYSTEM [AFTER
EQUILIBRIUM BETWEEN
PHASES OF THE IRON-N
SOLID
T°C.
%NH3
300
400
500
600
700
800
0
10
20
30
40
50
60
70
α
γ
ε

III.3 Nitriding Apparatus

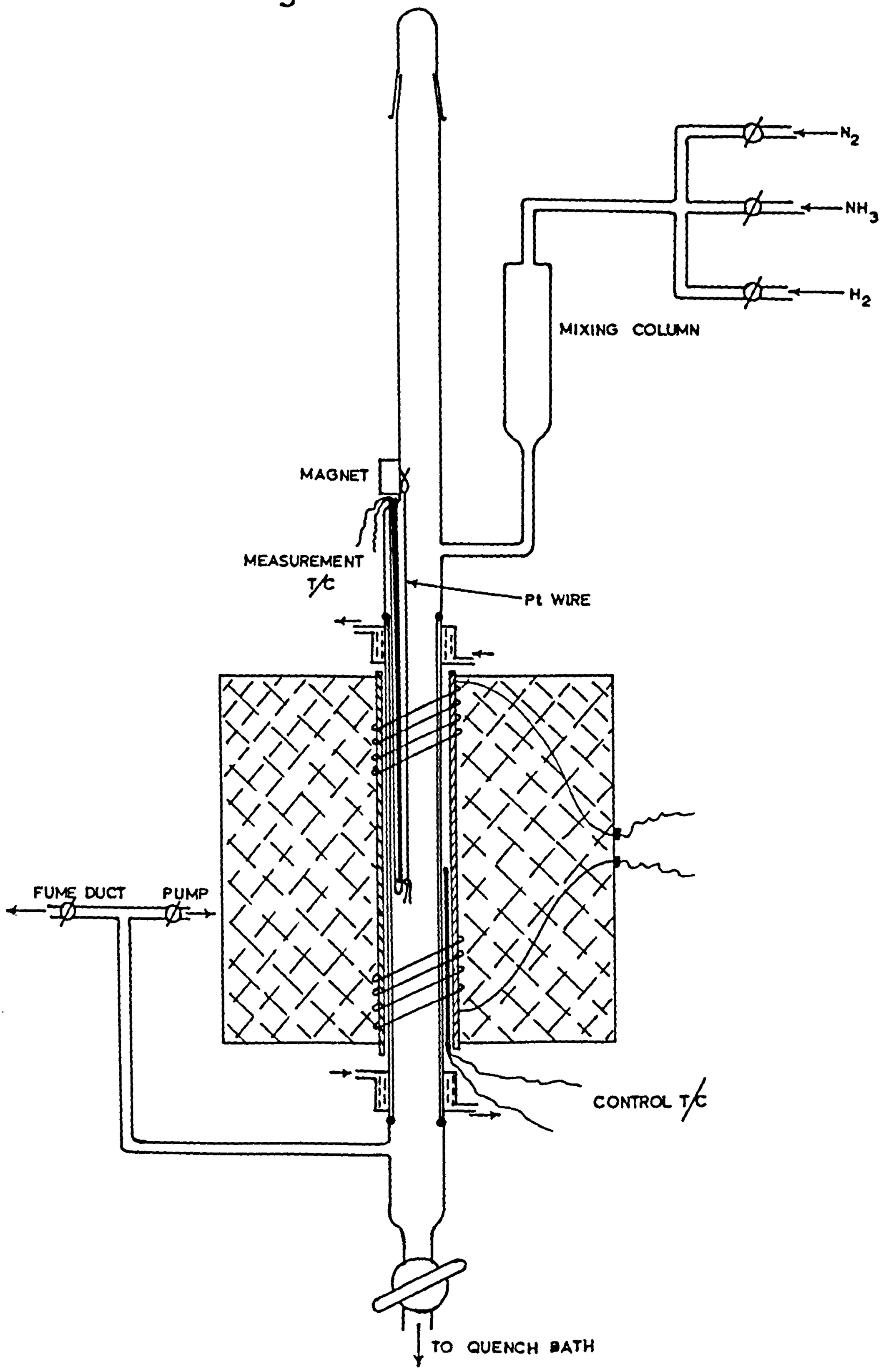
The nitriding apparatus is shown in figure III.2. Commercial hydrogen, ammonia and nitrogen were purified by standard methods as shown in figure III.3. The calcium oxide was freshly prepared by decomposition of small marble blocks at 950°C. The activated copper was pre-reduced in hydrogen for two days at 180°C and was maintained at 120°C during use. Gas flows were measured by capillary flowmeters (see Figure III.4) which were calibrated by a bubble displacement method.

The furnace temperature was controlled to $\pm$ 3°C by standard controllers using a Pt/Pt:Rh thermocouple near the furnace winding and the specimen temperature was recorded by using a sheathed thermocouple located within the reaction tube directly alongside the specimen. The pressure in the system was maintained slightly above atmospheric by a 1 - 2cm head of oil in an exit bubbler. Previous experience at Newcastle has shown that linear gas flow rates of $\geq$ 50 c.c. per minute give no detectable cracking ofammonia below about 650°C. Therefore, depending upon the size of the reaction tube used, total gas flow rates of 200 - 600 c.c. per minute were used in order to prevent cracking of the ammonia.

The procedure adopted in each nitriding run was as follows:

The specimens were suspended by a platinum wire in the

Fig. III. 2



THE VERTICAL NH_3-H_2 AND N_2-H_2 EQUILIBRATION APPARATUS.

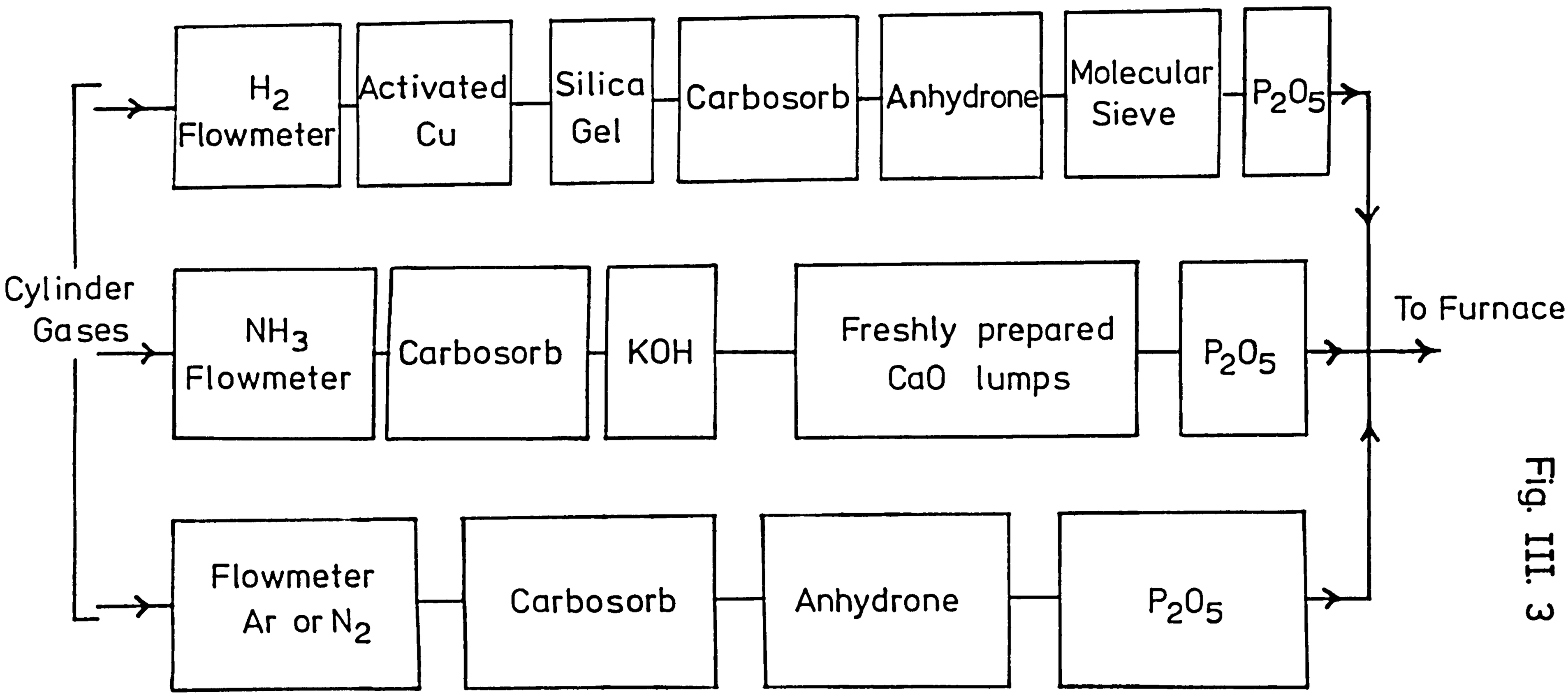
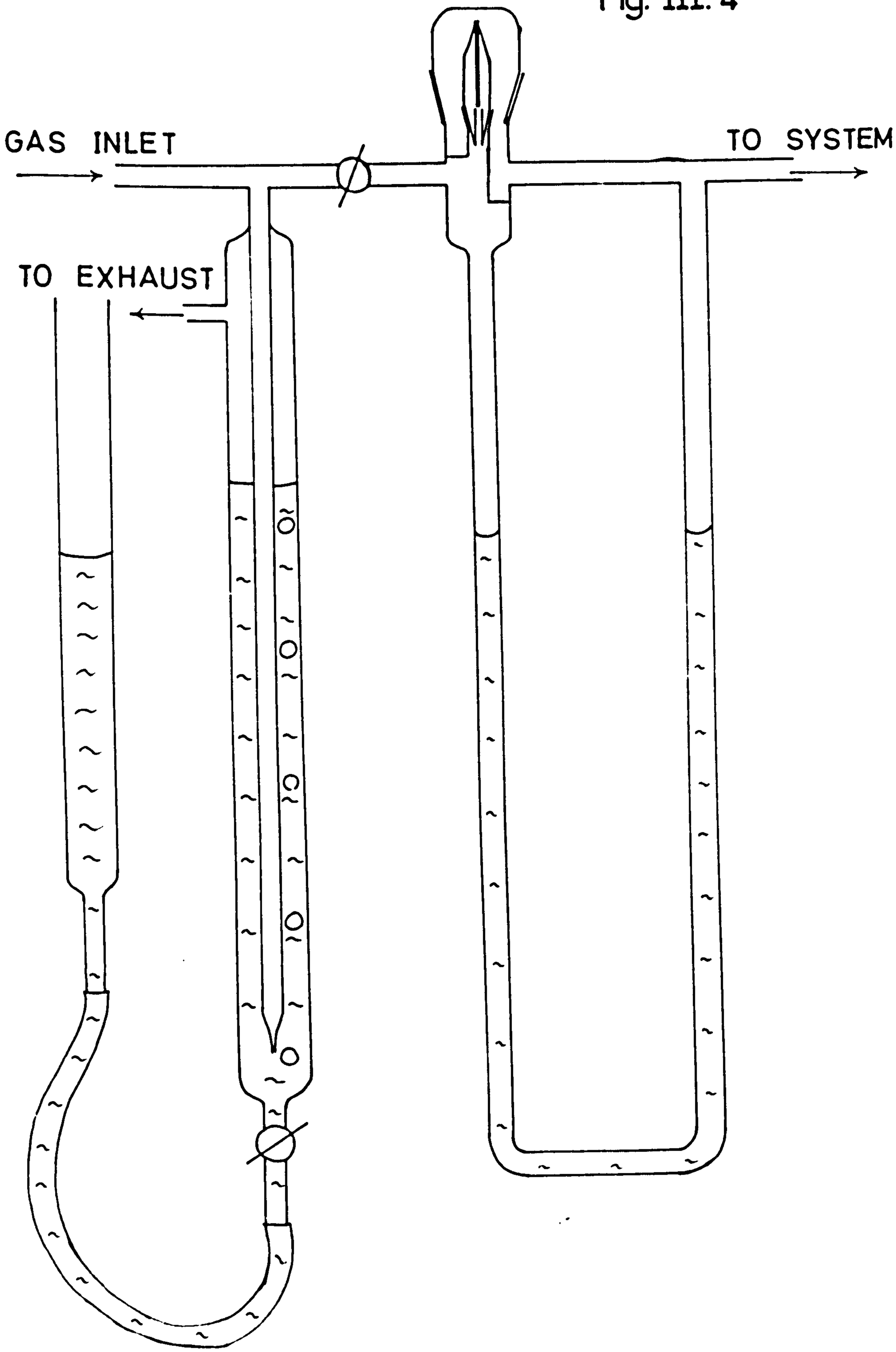


Fig. III. 3

Gas Flow System for NH_3-H_2 and N_2-H_2 Equilibrations.

Fig. III. 4



A CAPILLARY FLOWMETER [SCHEMATIC].

cold upper extension of the reaction tube which was then evacuated and flushed with nitrogen. The nitriding gases were then equilibriated at the required potential for one hour before the specimens were lowered into the reaction tube using a magnetic device. After nitriding, the specimens were either raised into the cold zone at the top of the furnace or, if a fast quench was required, they were released and dropped into an oil quench-bath. After purging with nitrogen the specimens were removed. All the specimens were weighed prior to and after nitriding.

III.4 X-Ray methods

X-Ray diffraction patterns were obtained with monochromatic X-radiation reflected from a lithium fluoride single crystal. Monochromatic radiation was used in order to reduce the background intensity during the long exposures that were often required to bring up the weak diffraction patterns of precipitated phases. The diffraction patterns were recorded photographically using 9 cm. and 19 cm. diameter Debye-Scherrer cameras. Iron filtered CoK_{α} was used with either a 19 cm. Unicam or a 114.83 mm Philips camera to measure the unit cell dimensions of nitrided specimens.

III.5 Metallographic examination and hardness measurements

Specimens were mounted in either a cold mounting compound in a 2 cm. diameter mould or in bakelite pressure cured at 140°C. After a preliminary reduction on an

abrasive wheel, the specimens were polished successively on 25,3,1 and 0.25 diamond wheels; a 2% 'nital' solution was found to be a suitable etchant. Optical microscopy was carried out using a Reichart projection microscope.

Grain size determination of the tensile test specimens was made by using a linear intercept method. Hardness measurements were made by using 20g or 50 g loads with the standard microhardness tester fitted to the Reichart microscope.

III.6 Electron microscopy

A Philips E M 300 microscope equipped with extensive tilting and rotation facilities was used for the examination of thin foil and carbon extraction replicas.

Thin foils were prepared using the window technique, from 0.1 mm thick sheet samples, by electropolishing in 68% acetic acid: 16% perchloric acid: 16% 2-butoxyethanol at $0^{\circ}C$ using a potential of 20 volts and a current density of 0.1 amps/cm^2. Foils were washed in methanol and stored under glycerol until required.

When thicker specimens were used (eg. 0.75 mm) they were first subjected to a preliminary chemical polish in a solution of 50% water: 45% 100 vols H_2O_2 = 5% - HF. The final electropolishing to produce thin foils was then achieved using the window technique.

Extraction replicas were prepared by electropolishing the specimens lightly and then etching them in nital for 30 - 40 secs. at 0°C. A thin film of carbon was deposited by evaporation and subsequently scored into 1mm squares. The replicas were removed in 2% nital and given a short electropolish. After washing in ethanol, the replicas were collected on copper grids.

III.7 Nitrogen weighings and analysis

In general, the nitrogen levels in nitrided alloys are so much higher than those in steels (up to 2.0 at %) that weight differences before and after nitriding give accurate nitrogen contents. Weighings to ± 0.0001 gm were made on an Oertling balance, the average of at least three weighings being taken as correct. By using batches of samples weighing up to 20gms in certain instances, good reproducibility to ± 0.005 at % N was obtained.

When necessary, nitrogen analysis was carried out using a standard semi-micro Kjeldhal method with the ammonia concentration determined calorimetrically using Nessler's reagent; ammonium chloride solution was used as standard.

III.8 Internal friction: theoretical aspects of damping

Internal friction may be defined as the ability of a vibrating solid, completely isolated from its surroundings, to convert mechanical energy into thermal energy. Departures from perfectly elastic behaviour, resulting in a phase difference between the applied stress and resultant strain at low stress levels, produce this effect.

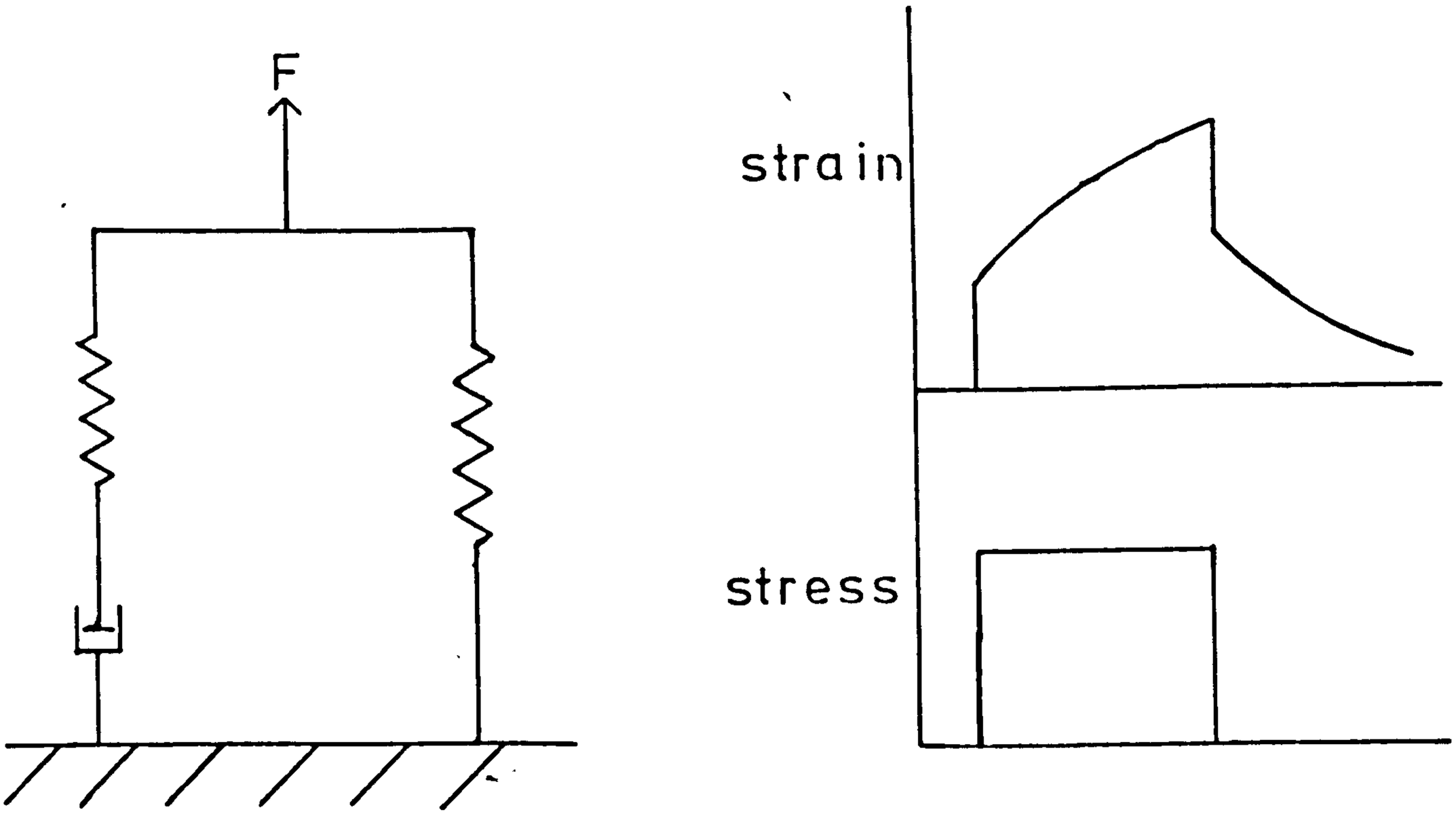
If Hooke's law regarding the elastic deformation of materials was completely obeyed, no damping of vibrations would be possible because time would not enter the stress/strain equation. For real materials the strain is not uniquely determined by stress, as it is also time dependent; The strain lags behind the stress by an amount δ. The behaviour of real materials can be satisfactorily described by using anelastic theory and a standard linear solid model for which Zener(1948) proposed the equation:

$$a_1\sigma + a_2\dot{\sigma} = b_1\epsilon + b_2\dot{\epsilon} \qquad \ldots\ (III).6$$

where stress and strain are linked with their first time derivatives. Materials obeying this equation are termed, 'standard linear solids', and their behaviour can be represented schematically as shown in Figure III.5: a_1, a_2, b_1 and b_2 are constants, σ is the stress and ϵ is strain.

Dividing throughout to obtain three new constants, equation (III).6 can be written as

Fig. III. 5



Mechanical model and behaviour
of a standard linear solid

$$\sigma + \tau_\epsilon \dot{\sigma} = M_R (\epsilon + \tau_\sigma \dot{\epsilon}) \quad \ldots\ldots \quad (III).7$$

where τ_ϵ is the relaxation time of stress under constant strain, τ_σ is the relaxation time of strain under constant stress and M_R is the relaxed modulus.

Solving equation (III).7 when t=0, i.e. $\epsilon=0$, $\dot{\epsilon}=0$ gives

$$\sigma = \sigma_o \exp -t/\tau_\epsilon \quad \ldots\ldots \quad (III).8$$

When a strain, ϵ_o , is applied at time t=0, the stress relaxes to its minimum value $M_R \epsilon_o$. Under these conditions the time dependence of stress under constant strain may be represented as:

$$\sigma(t) = M_R \epsilon_o + (\sigma_o - M_R \epsilon_o) \exp -t/\tau_\epsilon \quad \ldots\ldots \quad (III).9$$

Similarly the time dependence of strain under constant stress may be represented as:

$$\epsilon(t) = M_R^{-1} \sigma_o + (\epsilon_o - M_R^{-1} \sigma_o) \exp -t/\tau_\sigma \ldots\ldots \quad (III).10$$

This behaviour is illustrated in Figure III.5.

New constants, which have considerable physical significance may be derived from $\tau_\sigma, \tau_\epsilon$ and M_R. If in a time δt the stress receives a finite increment $\Delta\sigma$, then from equation (III).7,

$$\tau_\epsilon \Delta\sigma = M_R \tau_\sigma \Delta\epsilon \qquad \ldots\ldots \quad (III).11$$

The relationship $\Delta\sigma/\Delta\epsilon$ is the unrelaxed modulus , Mu, which correlates changes in stress and strain occurring so rapidly that no relaxation has time to take effect. The relaxed modulus, M_R, is the modulus for the condition when relaxation is complete; consequently $Mu > M_R$ and from equation III.11,

$$M_u = M_R \frac{\tau_\sigma}{\tau_\epsilon} \qquad \ldots\ldots \quad (III).12$$

Equations (III).9 and (III).10 represent the behaviour of a standard linear solid when it is under conditions of constant strain and constant stress respectively. Internal friction measurements are carried out under dynamic conditions of periodic stress and strain illustrated by the following equations:

$$\sigma = \sigma_0 \exp i\omega t \quad ; \qquad \epsilon = \epsilon_0 \exp i\omega t$$

from which

$$\frac{d\sigma(t)}{dt} = \sigma_0 i\omega \exp i\omega t \quad ; \qquad \frac{d\epsilon(t)}{dt} = \epsilon_0 i\omega \exp i\omega t$$

Putting these terms in (III).7,

$$\sigma_t + \tau_\epsilon \sigma_0 i\omega \exp i\omega t = M_R(\epsilon_t + \tau_\sigma \epsilon_0 i\omega \exp i\omega t) \ldots \quad (III).13$$

If t is small, which is true for internal friction measurements, then $\sigma_t = \sigma_0$, $\epsilon_t = \epsilon_0$ and $\exp^t \longrightarrow 1$. Consequently,

$$(1 + i\omega\tau_\epsilon)\sigma_o = M_R(1 + i\omega\tau_o)\epsilon_o \quad \ldots\ldots \quad (III).14$$

$$\text{and} \quad \sigma_o = \mathcal{M}\epsilon_o \quad \ldots\ldots \quad (III).15$$

where $\mathcal{M}$ is the complex modulus, $\frac{1 + i\omega\tau_\sigma}{1 + i\omega\tau_\epsilon} M_R$

Under conditions of alternating stress, the lag between stress and strain gives rise to damping. The phase angle, δ, by which the strain lags behind the stress is used as a measure of the internal friction and can be derived from the complex modulus:

$$\tan\delta = \frac{\text{imaginary part of } \mathcal{M}}{\text{real part of } \mathcal{M}}$$

$$= \frac{\omega(\tau_\sigma - \tau_\epsilon)}{1 + \omega^2(\tau_\sigma\tau_\epsilon)} \quad \ldots\ldots \quad (III).16$$

The phase difference is very small, and so $\tan\delta \approx \delta$. If the geometric mean of the relaxation times, $\bar{\tau}$, and the moduli, $\bar{M}$, are introduced, then

$$\delta = \frac{M_u - M_R}{\bar{M}} \cdot \frac{\omega\tau}{1 + (\omega\bar{\tau})^2} \quad \ldots\ldots \quad (III).17$$

The maximum value of δ occurs when $\omega\tau = 1$: therefore,

$$\delta_{max} \simeq \frac{M_u - M_R}{2\bar{M}} \quad \ldots\ldots \quad (III).18$$

By analogy with electrical circuit theory, δ is often expressed as Q^{-1} and using this notation,

$$Q^{-1} \simeq 2Q^{-1}_{max} \frac{\omega\tau}{1 + (\omega\tau)^2} \quad \ldots\ldots \quad (III).19$$

(τ is understood to represent the geometric mean of the relaxation times.)

If the damping of a specimen is measured over a sufficiently wide range of frequencies a peak will be observed at a particular frequency, and knowing that $\omega\tau=1$ at Q^{-1}_{max} the relaxation time can be calculated.

Experimentally it is not always easy to obtain a wide range of frequencies for testing purposes. However, a damping peak will be observed at constant frequency if the relaxation time of the specimen can be altered. Many relaxation phenomena are strongly temperature dependent, the relaxation time obeying an Arrhenius equation:

$$\tau = \tau_o \exp H/RT \qquad \ldots\ldots\ldots \quad (III).20$$

where H is the heat of activation for the relaxation. This relationship is of great importance in the experimental determination of internal friction. If the peak is to be measured by frequency variations, changes of several orders of magnitude are required and this is experimentally very difficult. However, (III).19 may now be written:

$$Q^{-1} = Q^{-1}_{max} \frac{2\omega\tau_o \exp(H/RT)}{1+\omega^2\tau_o^2 \exp(2H/RT)}$$

and since at constant w, Q^{-1}_{max} occurs at Tp and w =1,

$$Q^{-1} = Q^{-1}_{max} \operatorname{sech}\left[\frac{H}{R}\left(\frac{1}{T} - \frac{1}{T_p}\right)\right] \ldots\ldots\ldots \quad (III).21$$

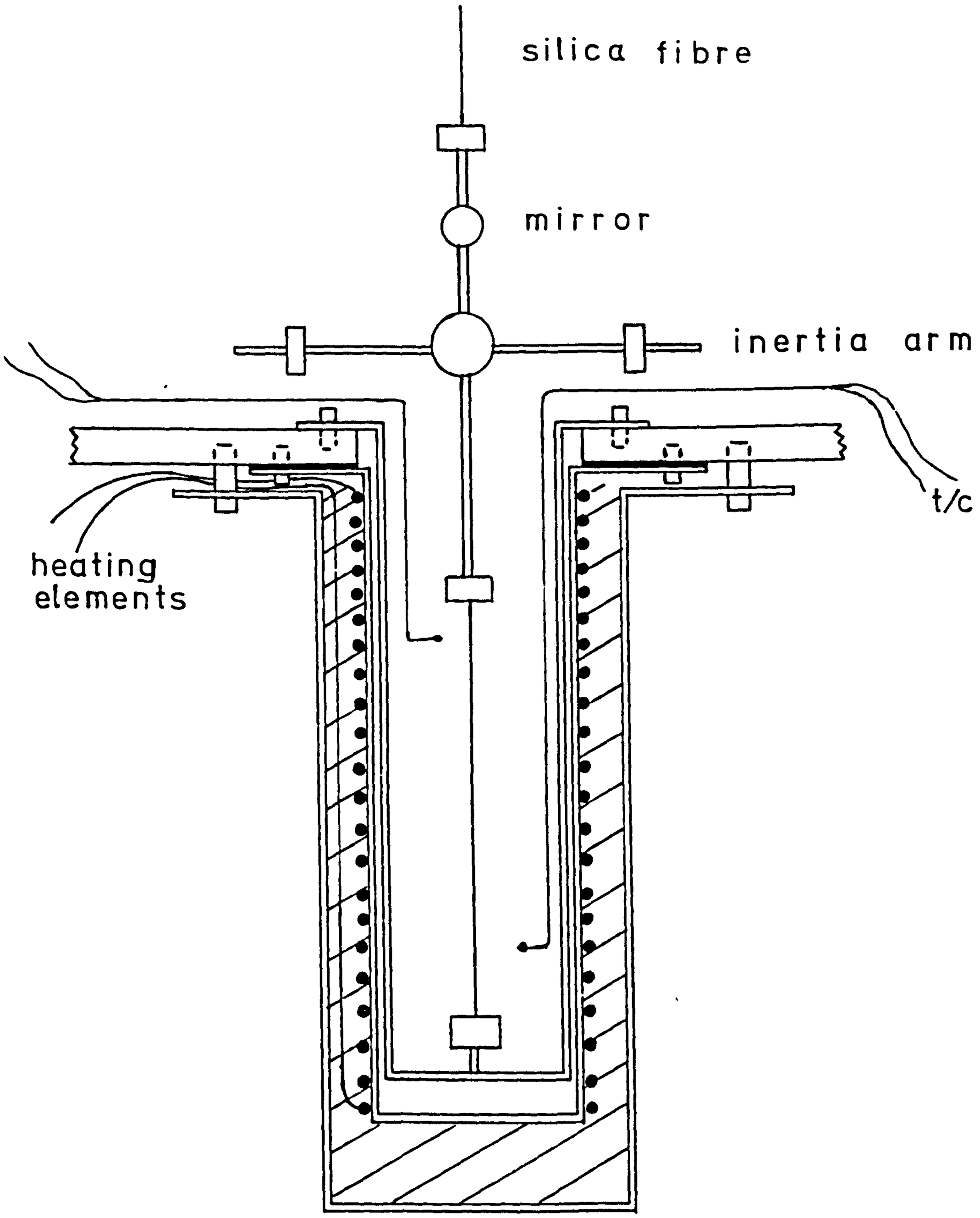
Tp is taken to be the peak temperature, and hence damping can be measured at constant frequency by varying the temperature. Equation (III).21 defines the ideal internal friction characteristics of a single relaxation process. One example of this is the stress induced ordering of interstitial atoms in a pure b.c.c. metal.

III.9 Internal friction equipment

Internal friction measurements as a function of temperature were made on 200mm long wire specimens in an inverted torsional pendulum assembly, (see Figure III.6), equipped with a non-inductively wound furnace. A torsionally rigid knife-edge balance arm and counterweight, used in conjunction with a fine silica fibre as the suspension element, enabled a small constant load to be maintained on the specimen. This suspension system, together with an operating vacuum of $2x10^{-5}$ torr, results in a very low level of background damping. Electromagnets acting upon the bar start the oscillation, the frequency of which can be adjusted in the range 0.2 - 1.6 c.p.s. by varying the inertia of the system.

Wire specimens that had been prepared in a vertical nitriding furnace and quenched into cooled oil were measured at appropriate temperature intervals in the range -20 to 300°C.

Fig. III. 6



INTERNAL FRICTION APPARATUS

The temperature was recorded by copper-constantan thermocouples placed near the top and bottom of the specimen. The temperature was maintained to $\pm 2^{o}C$ by varying the power supplied to three parallel heating coils using external rheostats. A constant heating rate of $1^{o}C$ per minute was followed by a period of thermal equilibrium under reduced power for two minutes in all tests.

The whole system was enclosed in a bell jar and evacuated down to $\leq 2x10^{-5}$ torr using rotary and diffusion pumps. The oscillation was started by the electromagnets acting upon the inertia bar. An automatic Sefram photodyne followed the rate of decay of a light beam reflected from a mirror mounted on the inertia bar assembly.

The logarithmic decrement, Δ, of the vibrational amplitude is related to the internal friction by

$$\frac{\Delta}{\pi} = Q^{-1} \qquad \ldots\ldots\ldots \quad (III).22$$

In metallic materials tested at low stresses, the damping is usually found to be independent of amplitude and so shear strains of $\geq 2x10^{-5}$ were used in this investigation. At these levels, the damping can be expressed as the natural logarithm of successive amplitudes of vibration:

$$\Delta = \log_e \frac{A_o}{A_n} \qquad \ldots\ldots\ldots \quad (III).23$$

and consequently from (III).22

$$Q^{-1} = \frac{1}{n\pi} \log_e \frac{A_o}{A_n} \qquad \ldots\ldots\ldots \quad (III)24$$

where Ao and An are the amplitudes of vibration after the first and the n^{th} oscillation. The internal friction was then evaluated using (III)24. Several values of Q^{-1} were obtained over successive values of n (usually 50 oscillations) and the average value was taken as correct; the frequency of oscillation was determined over a number of cycles using a stopwatch.

III.10 Mechanical testing

Tensile tests were made with an Instron type 1115 testing machine equipped with automatic chart control and stepped zero suppresion facilities. Flat tensile test specimens, having a 20mm guage length, were used together with nominal strain rates of 4.1×10^{-4} and 1.67×10^{-4}. Mean values of the limit of proportionality, 0.05% and 0.1%P.S., U.T.S. and work hardening rates were determined from at least two specimens for each treatment. The stepped zero suppression facilities were used to obtain maximum accuracy from the results.

High temperature tensile tests were made using the same instrument, with specimens of the same dimensions and with a vertical furnace arrangement having three windings controlled by three thyristor units. Thermocouples were arranged so that the upper and lower furnace zones were controlled by the

difference in e.m.f. produced by each of the two 'end-zone' thermocouples and the one in the centre; this enabled control to be within $\pm 2^{\circ}C$. The capsule containing the specimen, grips and pull rods was evacuated and filled with argon to give one atmosphere pressure at the testing temperature and the temperature of the specimen was recorded by a thermocouple placed directly alongside the specimen. The whole arrangement permits tensile testing up to $900^{\circ}C$.

Chapter IV

THE SCOPE OF THE PRESENT INVESTIGATION

Previous work at Newcastle by Speirs (1969), Roberts (1970), Mortimer (1971) and Pope (1972) on the precipitation of nitrogen from Fe-Mo-N, Fe-Nb-N, Fe-Cr-N and Fe-V-N alloys showed that the characterisation of precipitates under a wide range of equilibrium and non-equilibrium conditions was possible using gas equilibriation methods together with sensitive X-ray diffraction techniques. In particular, it was found that homogeneous precipitation occurred and that the precipitation sequence often involved several intermediate stages. It was proposed that a study should be made of the internal friction and mechanical properties of a selection of these alloys nitrided in NH_3:H_2 gas mixtures from 500 - 700°C.

Internal friction has proved to be an extremely powerful technique for the study of interstitial solid solutions and its applications in the present investigation are described in Chapter V. Abnormal, high temperature damping peaks are observed in the range 150 - 240°C and reasons for their occurrence are suggested. It was hoped to apply internal friction measurements to follow the continuous ordering process in ternary Fe-X-N alloys, and to determine the nitrogen solubility at the various precipitation stages.

Despite this being impossible, the internal friction characteristics associated with the previously unrecognised stages of homogeneous precipitation are described for several ternary Fe-X-N alloy systems.

An exploration of the mechanical properties of Fe-X-N alloys containing zones and precipitates seemed advantageous. Because of the large number of variables involved, most of the work is concentrated on dilute alloys in the Fe-V-N and Fe-Nb-N systems. Correlation of the properties with existing theories of dislocation-particle interactions was attempted in order to understand the strengthening mechanism in the nitrided alloys. The principal strengthening mechanism was identified by examining the effect of composition and heat treatment on the mechanical properties and microstructure. The structures of the nitrided alloys were studied by electron metallography before and after deformation in order to assist the interpretation of the mechanical properties.

There is increasing interest in using precipitation as a means of improving the strength and creep resistance of steels. Steels containing vanadium, niobium and nitrogen as micro-alloy additions are frequently being used when the precipitates are small and finely dispersed. Comparisons are made between the strengths of these materials and those in the present investigation.

Much of the earlier work at Newcastle was done with substitutional alloy contents above 0.5at.% in order to characterise the precipitation sequence and equilibrium precipitates. Because of this, further information was sought on the mechanisms of precipitation in alloys containing additions similar to those used in commercial materials. Consequently, precipitation in the more technologically important Fe-Nb-N and Fe-V-N alloys has been more thoroughly examined and is described in Chapter VI.

Chapter V

INTERNAL FRICTION OF Fe-X-N ALLOYS

V.1 Introduction

Internal friction measurements provide a convenient method for studying the behaviour of interstitial atoms in alpha iron. The effect produced by solid solutions of nitrogen in iron is well-known, and has been the subject of many investigations since Snoek (1941) first observed anomolous damping in iron-nitrogen and iron-carbon alloys. Snoek determined that the peak arose from the preferential ordering of interstitial atoms under the applied stress.

An interstitial atom in body-centred cubic iron occupies the octahedral interstices, thereby producing a tetragonal distortion of the lattice in the direction of the two closest iron atoms (i.e. along <100> directions). If the directions are designated x,y,z, the interstitial sites may also be termed x,y,z, according to the direction in which the maximum distortion is produced. In an unstressed specimen all octahedral sites are equivalent, and are randomly occupied, each containing one-third of the total interstitial content. If a tensile stress is applied, for example in the z direction, then a redistribution of interstitials will take place so that the z sites will contain

more than one-third of the total interstitial concentration. The movement of interstitials from x and y sites to z sites will be at a rate dependent on D, the diffusivity of the interstitial atoms in iron, and the application of the applied stress will produce a strain varying with time, resulting in anelasticity.

If the excess number of interstitials in the z sites is represented by n at time t, Fast (1971) has shown that:-

$$n = n_e\left[I - \exp -\frac{t}{\tau}\right] \qquad \ldots\ldots (V).1$$

where n_e is the maximum value of n. The magnitude of the strain produced by this ordering is proportional to n and consequently from (III).18 the internal friction maximum, $Q^{-1}max$, is proportional to the dissolved nitrogen according to:-

$$5.04\ Q^{-1}max = \text{at.\%N (Fast \& Verrijp, 1955)}$$

$$\text{or } 5.12\ Q^{-1}max = \text{at.\% (Rawlings \& Tambini, 1956)} \ldots (V).2$$

This proportionality has been successfully used to investigate the ageing of supersaturated nitrogen in ferrite and to determine the solubility of nitrogen in equilibrium with α''-$Fe_{16}N_2$ and γ' - Fe_4N in the range 10 - 600°C.

Using internal friction methods Dijkstra (1949) provided the first experimental evidence of a two stage precipitation sequence in quench-aged nitrogen ferrite. Figure V.1 shows

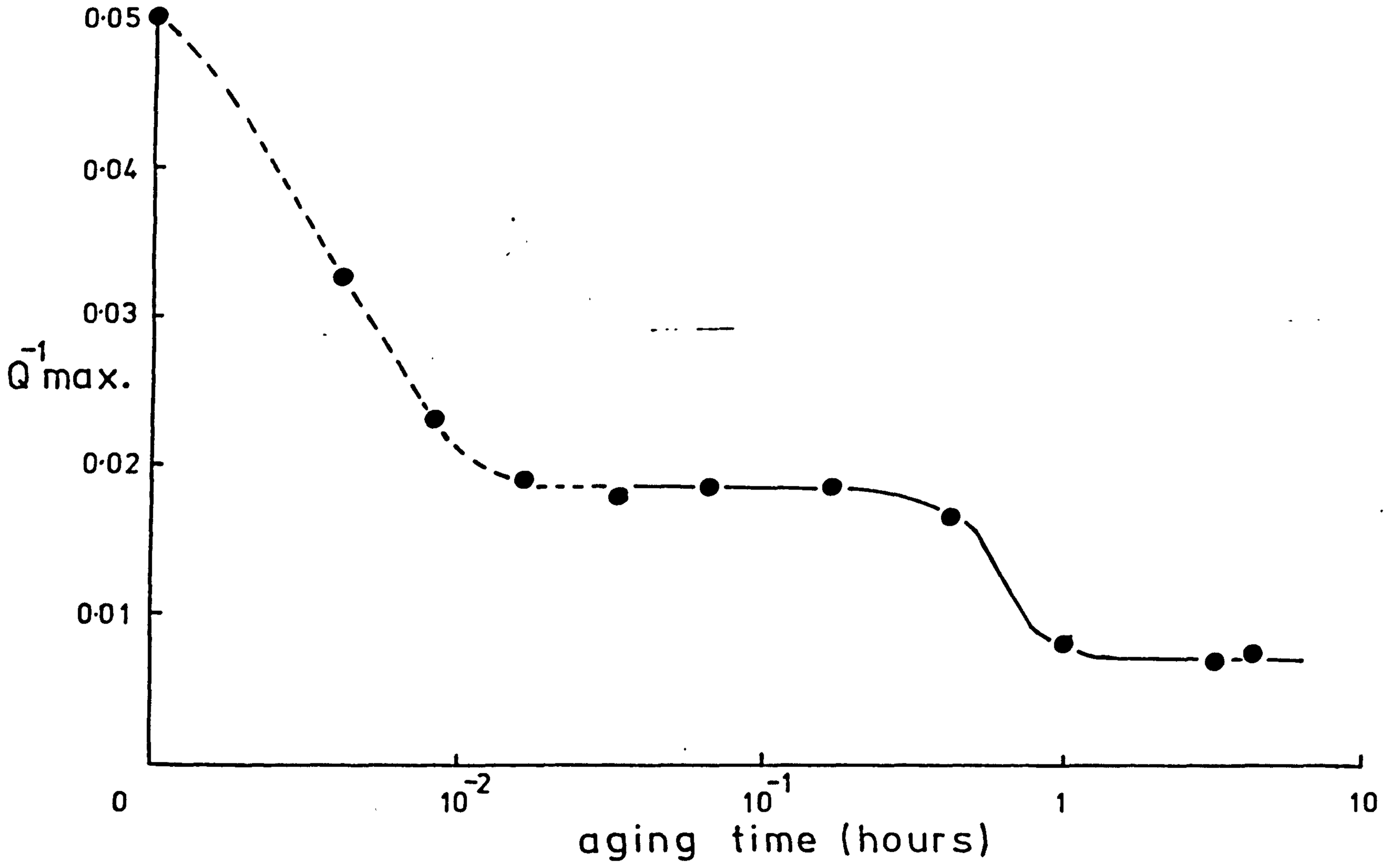


Fig. V.1

INTERNAL FRICTION V AGING TIME FOR Fe~0·05 wt.% N AGED AT 250 °C

[from Dijkstra, 1949]

the experimental data obtained for a Fe - 0.20at.%N alloy aged at 250°C. The plateaux correspond to the nitrogen solubilities in equilibrium with α''-$Fe_{16}N_2$ and γ'-Fe_4N respectively, and demonstrate the reduction in nitrogen solubility accompanying the change from the metastable $Fe_{16}N_2$ precipitate to the more stable Fe_4N. Dijkstra suggested that the solubility of Fe_4N was probably higher than the true equilibrium solubility because the tempering times used were too short to reach equilibrium. However, subsequent work by Fast & Verrijp (1955) has not confirmed this, and has shown that the equilibrium solubility is higher than that determined by Dijkstra, particularly near the eutectoid temperature.

When substitutional alloy elements such as manganese, molybdenum, chromium, vanadium or titanium are dissolved in iron they interact with interstitial nitrogen atoms, thereby complicating the internal friction measurements. Some of the nitrogen atoms become located in octahedra comprised of iron atoms plus one, or more, substitutional atoms and so the subsequent energy barrier which must be surmounted when the nitrogen atoms diffuse is modified. These alternative environments produce one or more secondary relaxation processes in addition to Snoek damping and are caused by the stress induced motion of nitrogen atoms in the vicinity of substitutional solute atoms. The additional peaks are termed substitutional-interstitial interaction peaks in this investigation.

In previous investigations 'random' substitutional-interstitial solid solutions have been produced by either nitriding alloy austenites at 950°C in N_2:H_2 gas mixtures and quenching; or by solution treating in vacuum at 950°C or 600°C and quenching after nitriding at lower temperatures in various gas mixtures. In the present investigation, pure Fe-X alloys (X-substitutional element) have been nitrided in carefully controlled NH_3:H_2 gas mixtures in the temperature range 500 - 650°C. Under these conditions dense, fine scale precipitation occurs and alloy nitride formation may be preceeded by substitutional-interstitial solute atom clustering on $\{100\}_\alpha$ planes. Overageing occurs to give the equilibrium alloy nitride through a precipitation sequence which may involve one or more intermediate stages.

Internal friction testing has been applied to various ternary Fe-X-N alloys in order to study the precipitation sequence and to determine the nitrogen solubility in equilibrium with the various stages of precipitation. For this reason, the systems chosen for investigation are those which behave differently in the mode of precipitation. For example, in the Fe-Mo-N system the initial clusters transform to the equilibrium precipitate via two intermediate metastable precipitates (Speirs et al 1970); whereas in Fe-Cr-N alloys no evidence of any intermediate precipitates was detected (Mortimer, 1971). In order to assist the interpretation of the internal friction data, particular reference is made to the microstructures associated with the damping character-

istics (see section V.3).

V.2 Experimental

Alloys received as hot-rolled 12mm diameter bar were cold drawn to 0.55mm diameter wire and sectioned into 200mm lengths. All specimens were annealed in pure hydrogen for 4 hours at 850°C to remove any traces of nitrogen, and to reduce the dislocation density. The wires were then nitrided in purified NH_3:H_2 gas mixtures in the range 500 - 650°C and subsequently quenched from the nitriding temperature into cooled oil.

A major problem with internal friction studies of nitrogen ferrite is the high rate of precipitation, even at room temperature. Dijkstra (1949) has shown that the internal friction of iron containing about 0.20at.%N decreases after ageing for one hour at room temperature, whilst Fast & Verrijp (1955) have shown that the precipitation rate is even faster in alloys containing 0.32at.%N. In the present investigation every step has been taken to prevent precipitation from occurring. After quenching, the specimens were transferred to a refrigerator maintained at -40°C. Prior to testing, the internal friction furnace was cooled to 10°C using a water cooling coil, or if necessary, to -60°C using liquid nitrogen. Damping measurements under conditions of increasing temperature were made in an inverted torsional pendulum assembly (see Chapter III.9). In certain instances, measurements were

re-taken after several heating and cooling cycles.

All measurements have been corrected for the background damping of the system, which is extremely low, the logarithmic decrement increasing slowly from 2.5×10^{-4} at 20°C to 3.2×10^{-4} at 300°C. No peaks were detected upon testing the as-annealed wires, indicating that any traces of carbon or nitrogen present in the received alloys had been removed during the hydrogen anneal.

V.3 Microstructures of Fe-X-N alloys

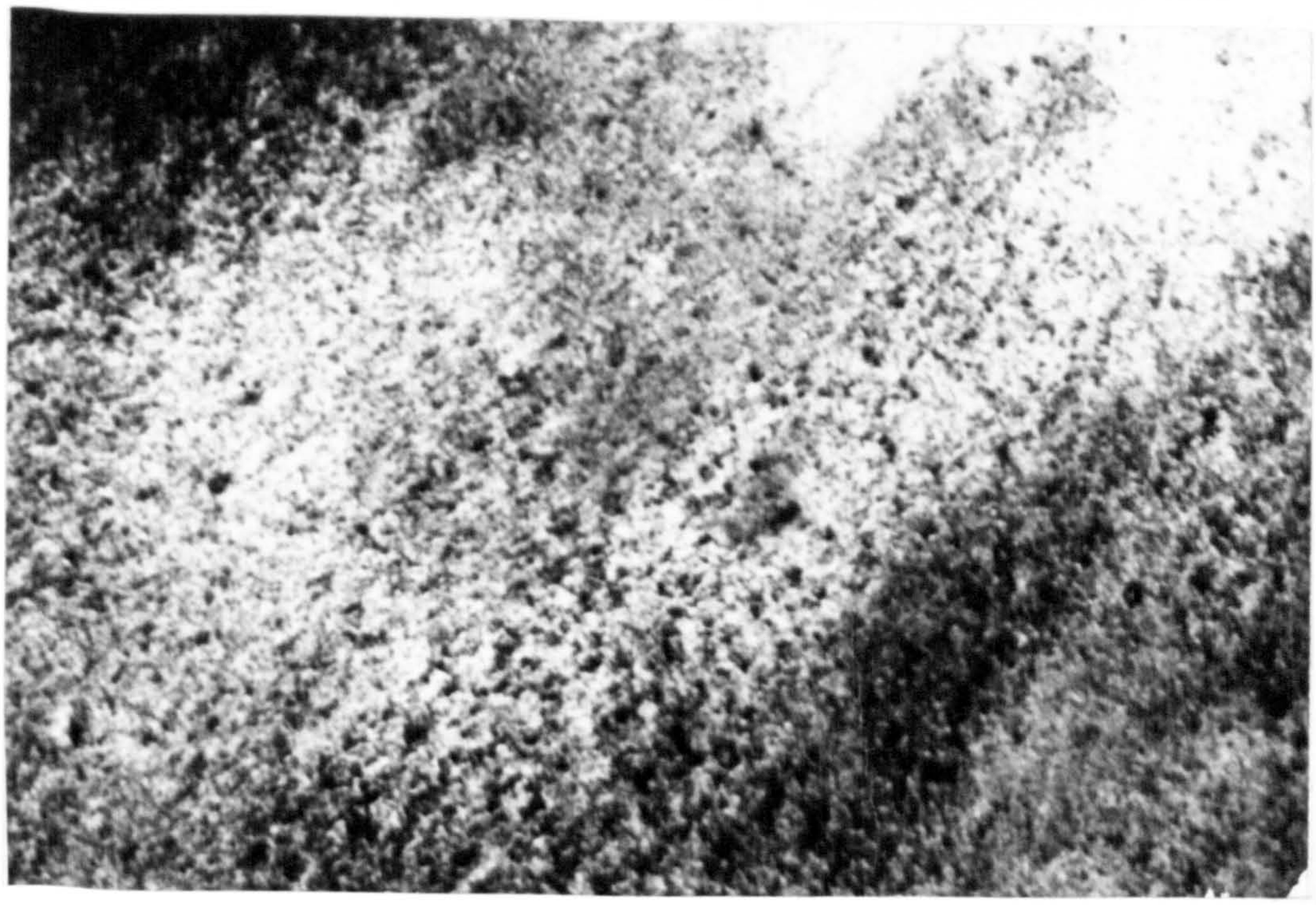
Nitriding alloys containing small concentrations of substitutional solutes such as molybdenum (Speirs et al, 1970), chromium (Mortimer, 1970), vanadium (Pope, 1972) or titanium (Henderson, 1974) show large increases in hardness and nitrogen concentrations which often exceed those necessary for the complete formation of the equilibrium alloy nitride (see Table V.1). Electron and field-ion micrographs show the presence of extremely thin disc-shaped clusters on the ferrite cube planes, which give continuous diffraction streaking in $\langle 100 \rangle_\alpha$ directions. Typical micrographs of a nitrided Fe- 3 at.%Mo alloy are shown in Figures II.8 and II.9. Similar micrographs are obtained after nitriding with other substitutional solutes under suitable conditions (see Figures V.2 and V.3). The observations are indistinguishable from those associated with GP zone formation in Al-4wt.%Cu and other f.c.c. alloys. Recent work by Krawitz & Sinclair (1974)

TABLE V.1

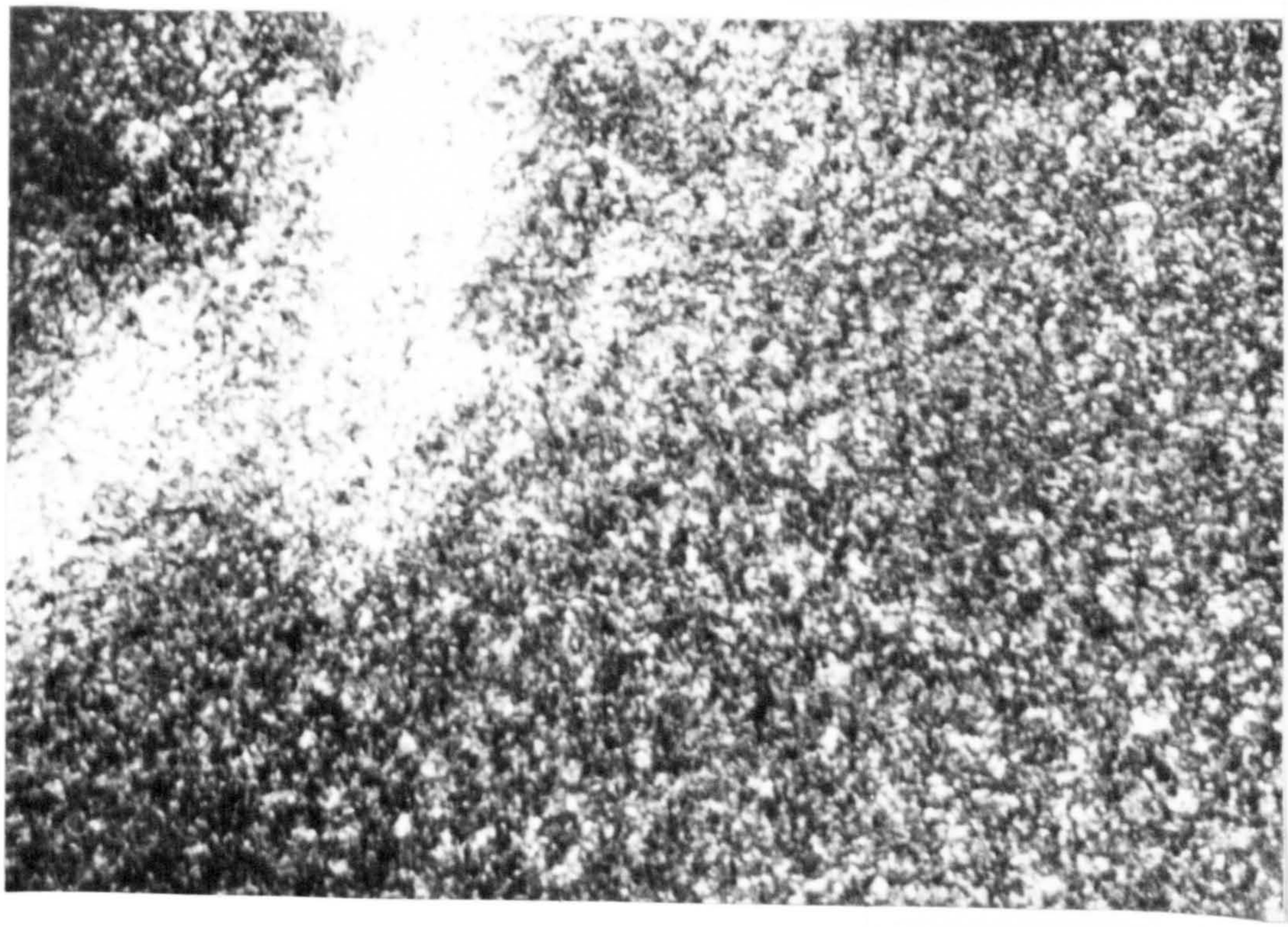
PREPARATION AND PROPERTIES OF Fe-X-N ALLOYS

alloy composition at.%	nitriding conditions			at.%N	N/X	hardness increase kg/mm^2	unit-cell dimension, Å	
	temp °C	ratio $NH_3:H_2$	time hours				calc.	obs.
2.92 Mo	580	7:93	30	2.48	0.85	780	2.891	2.890
1.2 Cr	475	19:81	240	1.18	0.91	450	2.875	2.874
1.2 Cr	575	10:90	35	1.46	1.12	400	2.877	2.868
0.65 Ti	580	4:96	24	0.92	1.42	400	2.873	2.873
0.65 Ti	580	8:92	48	1.20	1.85	450	2.875	2.875
1.08 V	570	3:97	94	1.16	1.07	600	2.875	2.874

Fig. V. 2



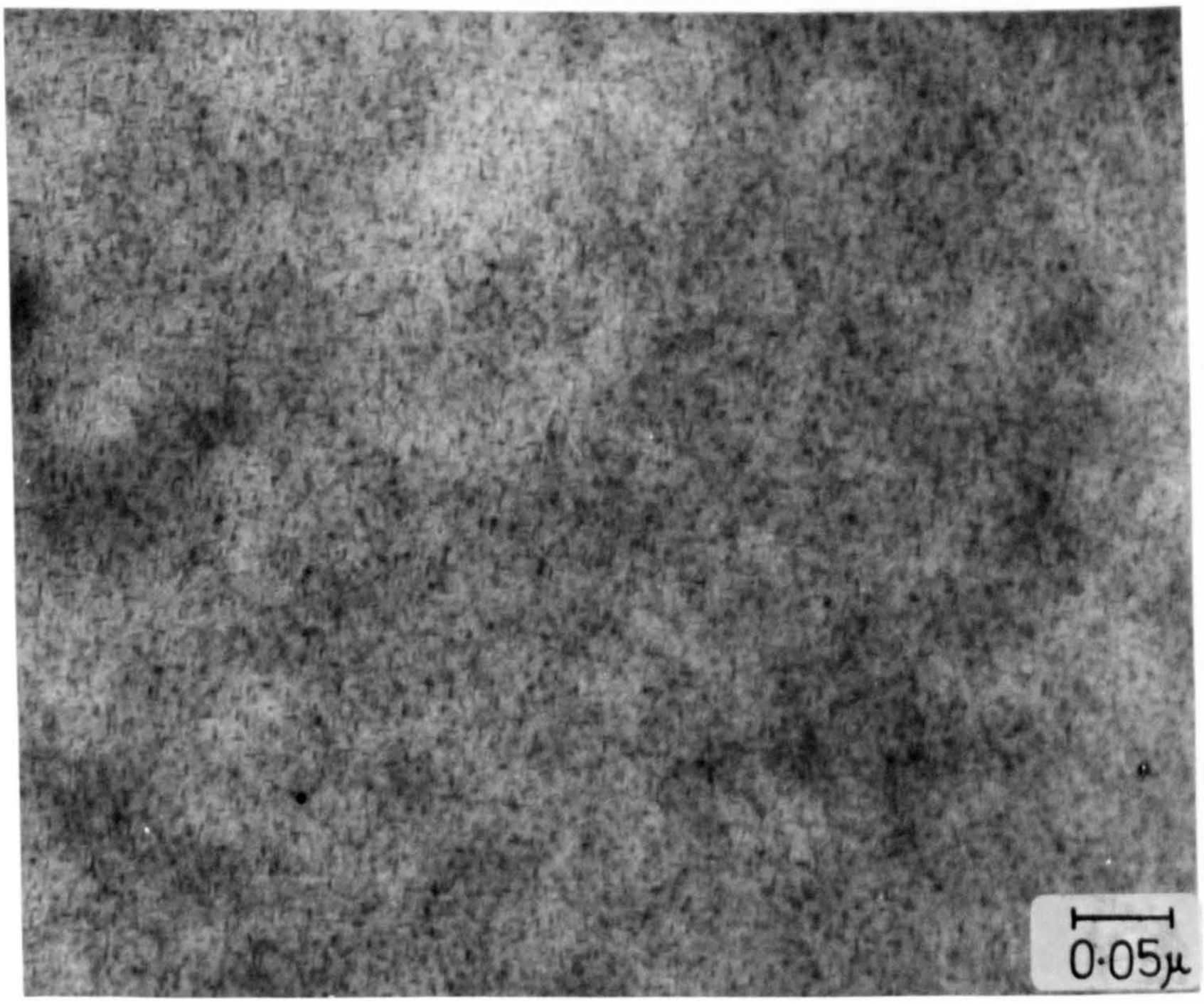
(a) Bright field



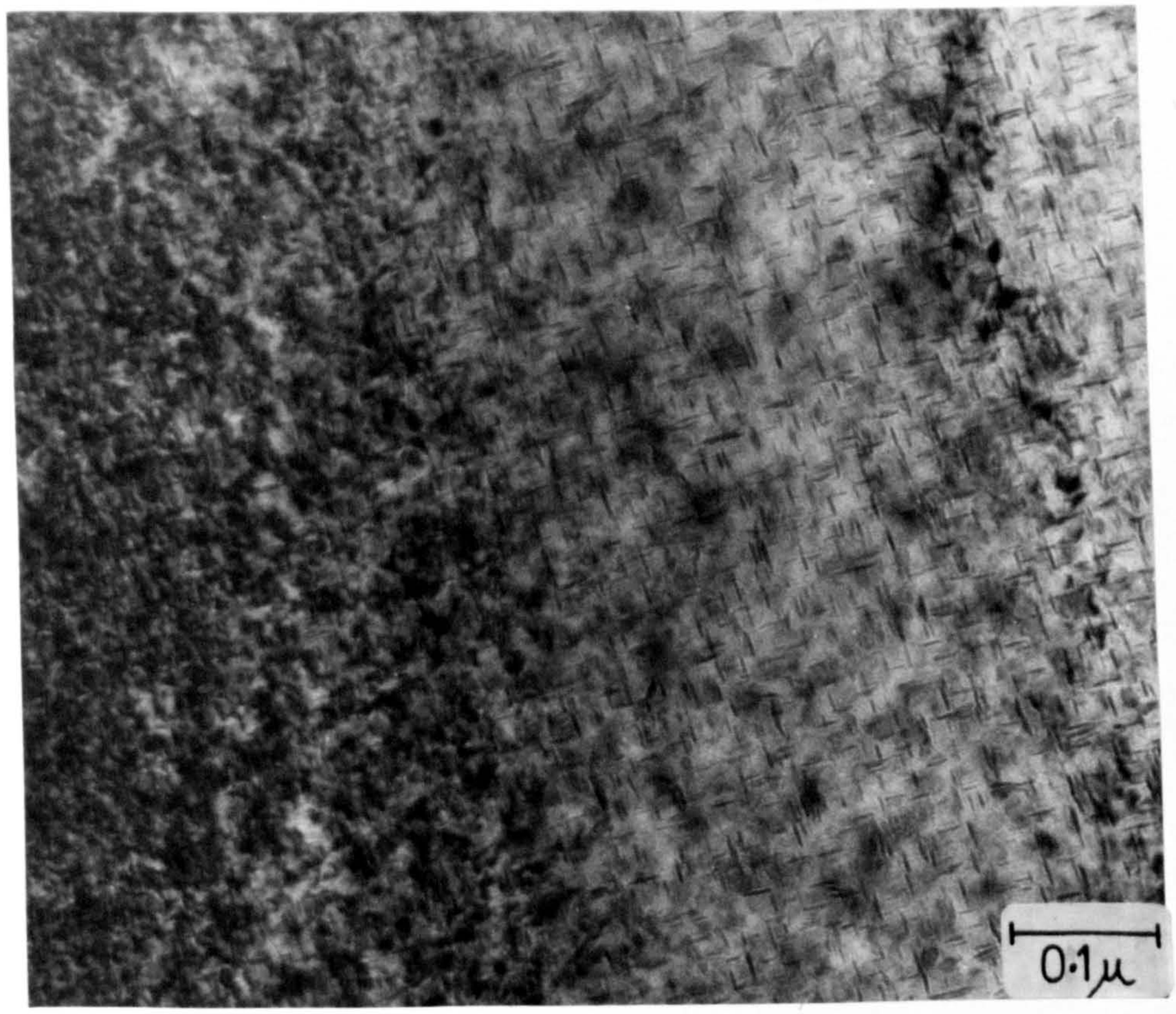
(b) Centred dark field using (200) reflection

Electron micrographs of Fe-065 at.% Ti nitrided in $5NH_3:95H_2$ at 575°C

Fig. V. 3



(a) Nitrided at 500°C in $13NH_3:87H_2$



(b) Nitrided at 575°C in $6NH_3:94H_2$

Electron micrographs of Fe-2·0at.%Cr

involving the determination of the ferrite matrix unit-cell dimensions before and after nitriding (see Table V.1) gives further evidence for the formation of mixed substitutional-interstitial solute-atom clusters. The increases in unit-cell dimensions obtained on nitriding are much greater than those expected from alloy nitride precipitation together with the nitrogen content in equilibrium with the ferrite matrix. However, they are accounted for if almost all the nitrogen remains in solid solution and occupies the octahedral interstices of the ferrite lattice.

The unit cell edge length of a substituted nitrogen ferrite (Fe-X-N) is given by:-

$$a_o = a_{Fe} + a_x + a_n \qquad \ldots\ldots\ldots \quad (V).3$$

where a_{Fe} is the unit-cell dimension of pure α-iron (2.8664 $\mathring{A}$) and a_n and a_x are the increases due to the solution of nitrogen and the substitutional solute respectively; a_x is known from the dimensions of the annealed un-nitrided alloys compared with that of a_{Fe}. For the calculation of a_N, extrapolation of data for nitrogen ferrite (Wreidt & Zwell, 1962) to the nitrogen concentrations encountered in the present work is of doubtful accuracy. More reliable values based upon the structures of α'-nitrogen martensite containing up to 9.2at.%N and of α''-$Fe_{16}N_2$ (Jack, 1951,(a) 1951,(b)), are:-

$$a_N = 0.007 \pm 0.0003 \ \mathring{A} \quad \text{per N atom per 100 metal atoms}$$

= 0.0285 ± 0.0015 Å per wt.%N in Fe. These figures, within the limits of experimental error, agree with the values of Wreidt & Zwell. This dilation of ferrite due to nitrogen in solid solution has been used in (V)3 to calculate the lattice parameters of the nitrided alloys given in Table V.1. The close agreement of the calculated and observed values clearly indicates that most of the solute atoms exist in solid solution and not as alloy nitride precipitates.

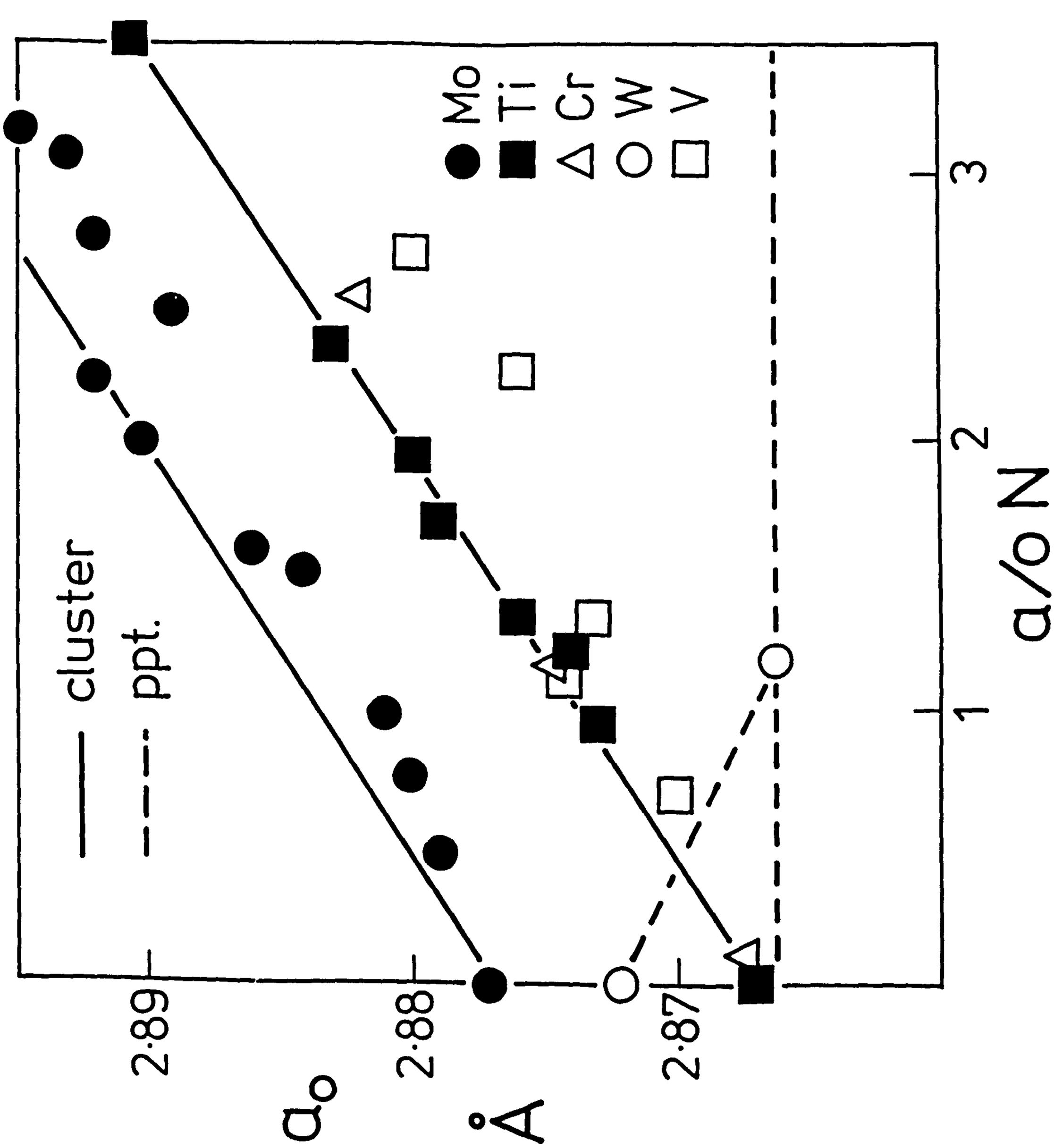
Fe-Cr alloys nitrided at 575°C are the exception; the observed lattice parameters are lower than those calculated for complete solid solution and indicate that nitride precipitation has occurred. The data for Fe-1.2at.%Cr nitrided in $10NH_3:90H_2$ at 575°C for 26 hours can be accounted for by complete precipitation of CrN together with the nitrogen in solution expected for pure α-iron in equilibrium with the nitriding atmosphere. However, the values obtained after nitriding at the lower temperature of 475°C agree with those expected when the chromium and nitrogen atoms are retained in solid solution as mixed substitutional-interstitial solute-atom clusters. This confirms the suggestion of Mortimer (1971) that clusters in Fe-Cr-N alloys are less stable than in other Fe-X-N systems.

Examples of the electron microstructure of a nitrided Fe-2at.%Cr alloy are shown in Figure V.3. After nitriding at 500°C in $13NH_3:87H_2$ small, coherent particles of 3-5nm diameter are observed (see Fig.V.3(a)) which give continuous streaking on electron diffraction patterns. However, nitriding to the

same nitrogen potential at 575°C results in particles of 14-25nm diameter being precipitated (see Fig.V.3(b)), which give intensity maxima on the streaks, indicating CrN to be present. The difference in microstructure shows the importance of nitriding temperature upon the size of the precipitated particles in Fe-Cr alloys.

The unit cell dimensions of a solid solution are essentially invariant with respect to the distribution of its solute atoms. A matrix containing clusters or GP zones is a solid solution in which non-random local atomic arrangements exist, but its dimensions are the same as a random solid solution having the same solute concentration. When precipitation occurs the lattice parameter changes to that of the depleted solid solution. For substitutional solutes the change in unit cell dimensions is small, but for interstitials the increase in a_o is, as shown above, about .007 Å per at.% interstitial solute in b.c.c. iron. Therefore, the unit cell dimensions of the matrix, even when measured to only 1 in 5,000 provide a very sensitive method of determining whether nitrogen is in solution, (randomly or as zones), or whether it is precipitated as a second phase. Figure V.4 shows that after nitriding Fe-X alloys under suitable conditions, the unit cell dimensions increase by the amount expected if all the absorbed nitrogen goes into solution; yet from the electron micrographs and the hardness of the material the solute-atom distribution cannot be random. By contrast, on nitriding Fe-W alloys there is a decrease in unit cell dimensions,

Fig. V. 4



Unit-cell dimensions of nitrided ferritic alloys

because the first formed clusters transform immediately to a metastable α''-type Fe-W-N intermediate precipitate (Stephenson, 1973).

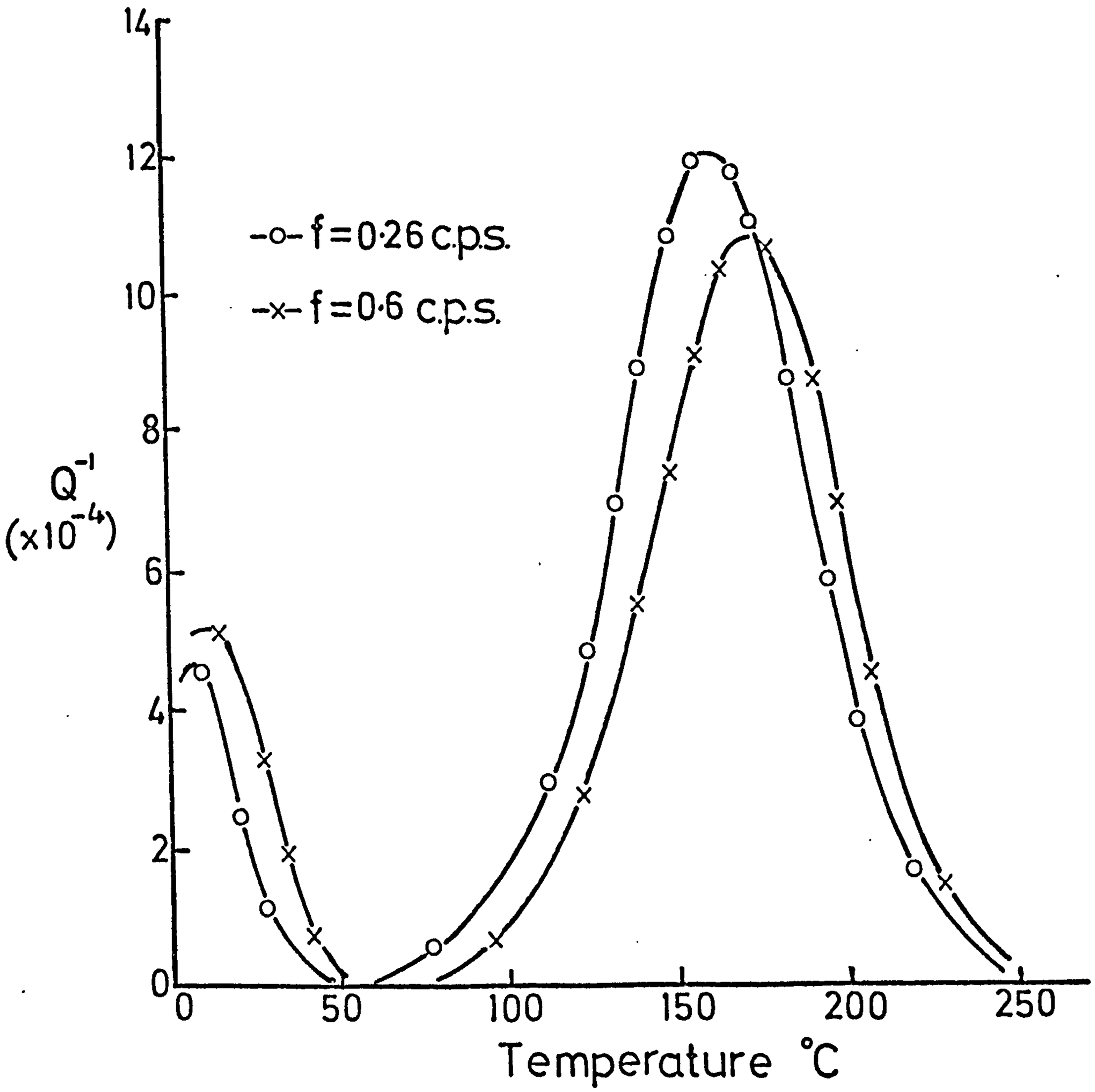
V.4 Internal friction of Fe-Mo-N alloys

Typical damping curves obtained after nitriding Fe-3.0 at.%Mo in $6NH_3:94H_2$ at 580°C for 24 hours are shown in Figure V.5, where Q^{-1} (corrected for background damping) is represented as a function of temperature. Under these nitriding conditions a GP zone structure is fully developed (see Figs. II.8 & II.9). The maximum nitrogen concentration obtained after nitriding is 2.5at.%N. Therefore, the damping is extremely low considering the amount of nitrogen present, implying that only a small proportion of the dissolved nitrogen moves under the applied stress.

Continued nitriding for 48 hours produces little change in nitrogen concentration, although optical microscopy shows that some grain boundary regions begin to transform by the discontinuous precipitation reaction. The effect of continued nitriding upon the internal friction characteristics is to cause both the peak height and temperature to increase slightly (see Figure V.6).

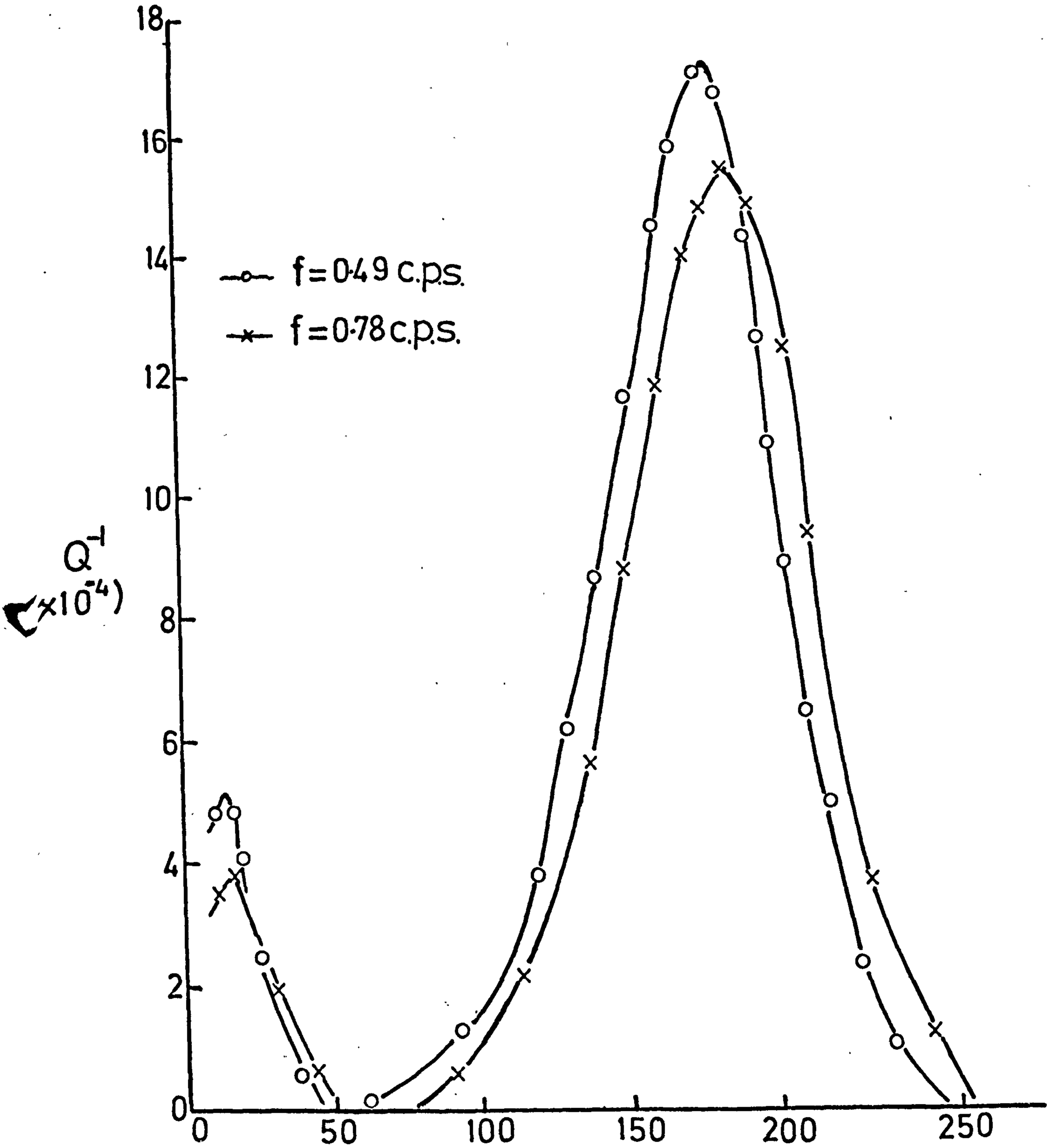
In Figures V.5 & V.6 the duplicate curves are obtained from wires prepared together and subsequently tested at different frequencies. Only very slight variations in peak

Fig. V. 5



Internal friction of Fe–3·0a.t.%Mo nitrided for 24hrs. at 580°C in $6NH_3$:$94H_2$.

Fig. V. 6



Internal friction of Fe–30 at.%Mo nitrided for 48hrs. at 580°C in $6NH_3 94H_2$.

heights are observed, confirming that the low level of damping is a consistent effect and is not due to rapid precipitation occurring whilst the specimens are retained prior to testing. The shifts in peak temperature occur because of the relationship

$$\tau = \tau_o \exp \Delta H / RT \qquad \ldots\ldots\ldots (V)4$$

which enables an average value of ΔH to be calculated (see section V.7).

The noticable features of the internal friction results are:-

i) the absence of a significant Snoek peak,

ii) the absence of a Mo-N interaction peak,

iii) the appearance of a damping peak in the range 150 - 180°C.

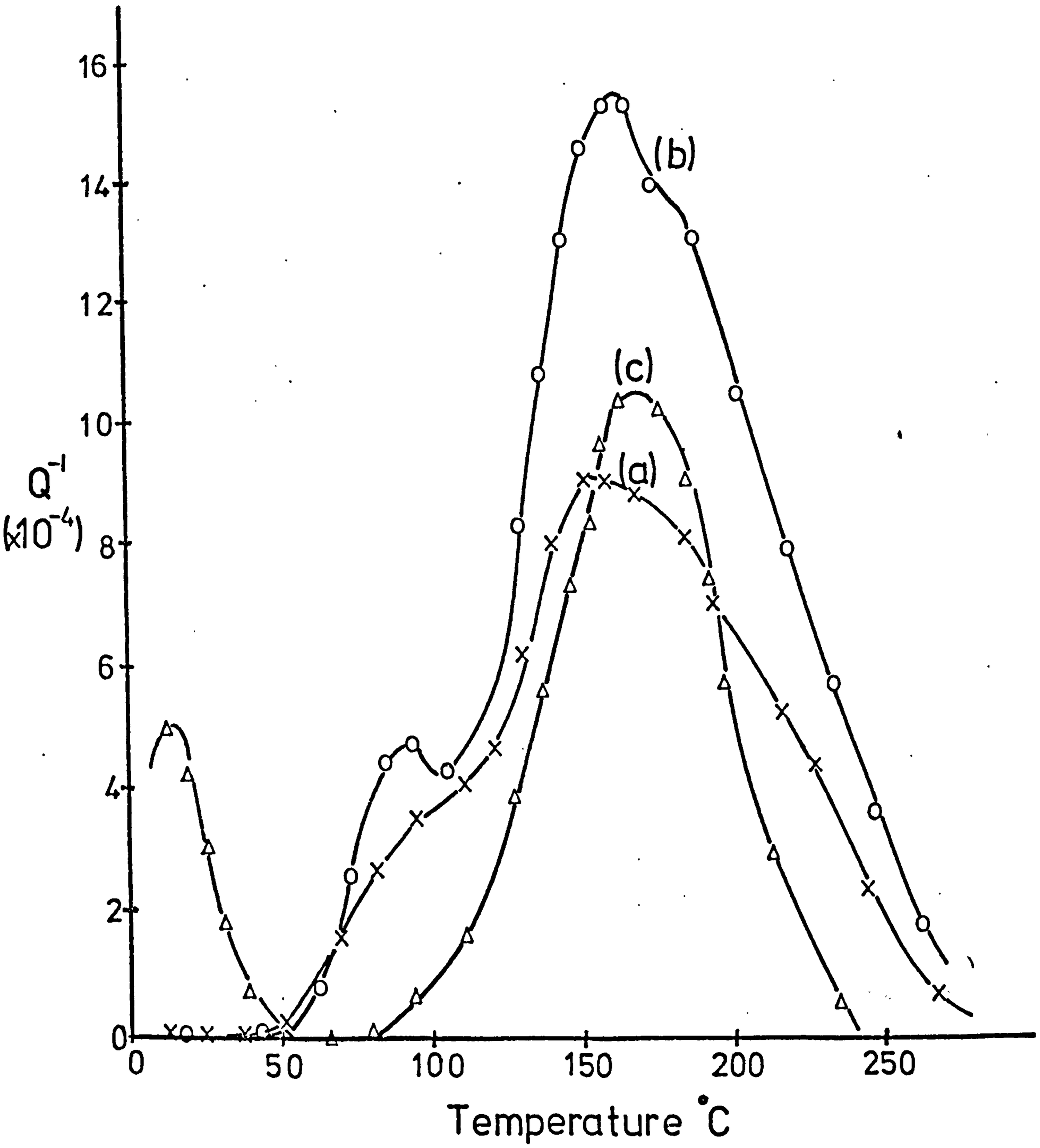
The absence of a significant Snoek peak and of the Mo-N interaction peak implies that either there is very little nitrogen in random solid solution; or, if there is, it cannot contribute to the damping within the normal temperature range. Electron microscope and field-ion microscope observations (Driver & Papazian, 1973) confirm the presence of mixed substitutional-interstitial solute-atom clusters in Fe-Mo alloys nitrided under similar conditions to those used in the preparation of the internal friction samples. Clusters of 10 - 15nm diameter, producing extensive coherency strains and having

interparticle spacings of 5 - 15nm, are observed (see Figs. II.8 & II.9). Because of the relatively small intercluster spacing only a few atomic jumps would be necessary for nitrogen atoms to reach the coherency strain fields. Therefore, it seems probable that the nitrogen in solid solution is located in the extensive strain fields surrounding the zones; this results in a low or non-existant Snoek peak.

The appearance of the high temperature damping peak implies that nitrogen atoms are present in alternative enviroments to normal Snoek sites. Prolonged nitriding causes both the peak height and temperature to increase slightly (see Figs. V.5 & V.6). The increase in peak height could be explained as being due to the slight coarsening of the structure which occurs, resulting in a larger intercluster spacing which would then leave more nitrogen free to contribute to the damping. The increase in peak temperature implies that an increase in the activation energy for the process contributing to the damping has occurred.

The internal friction characteristics of partially nitrided specimens, in which the GP zone structure is not fully developed, is particularly complex. Figure V.7 shows the changes occurring after nitriding for various times in a $6NH_3:94H_2$ gas mixture at 580°C. Initially, (see Fig.V.7(a)), damping is observed in the entire range 50 - 280°C, inferring

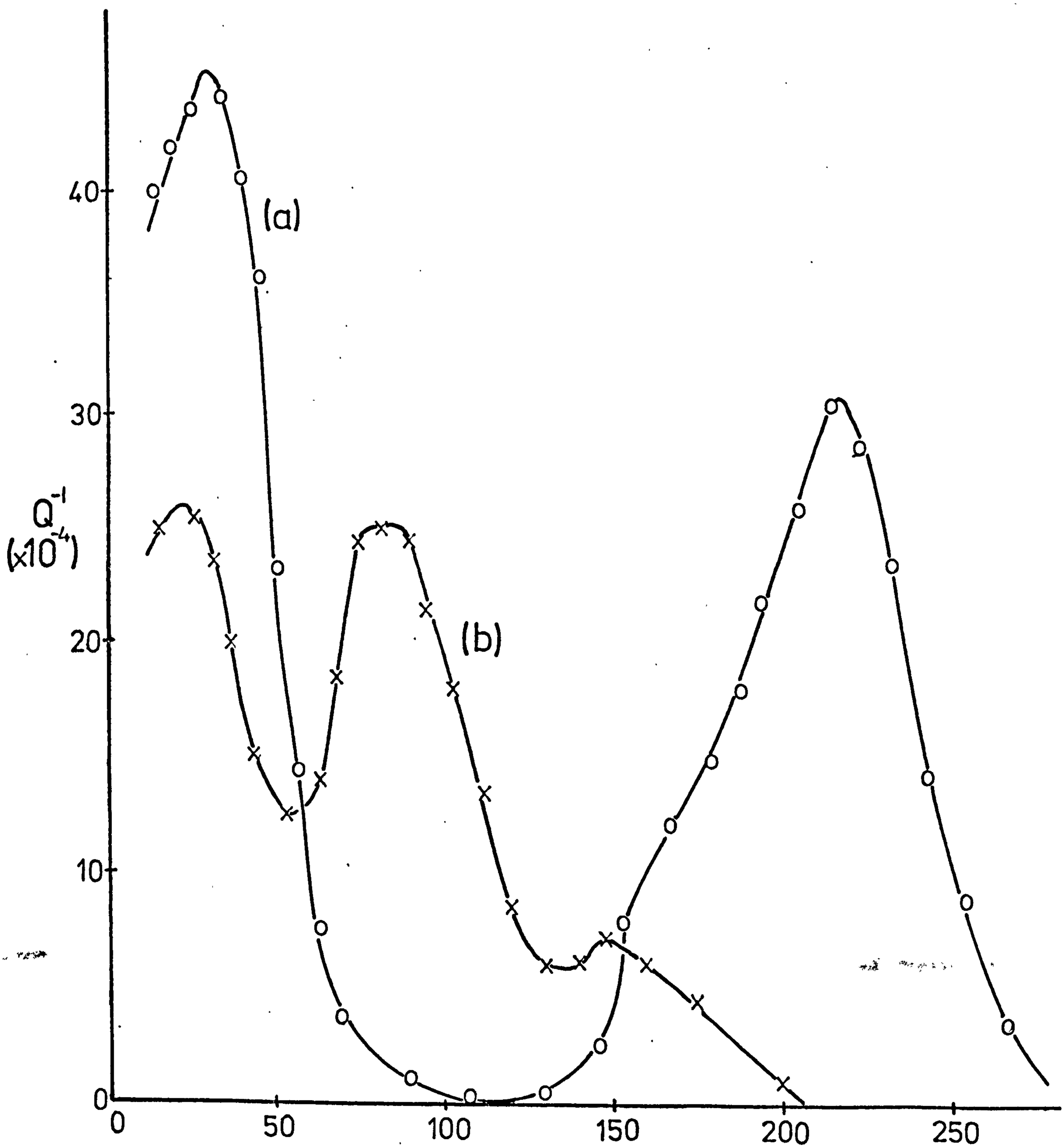
Fig. V. 7



Internal friction of Fe-3·0 at.%Mo nitrided at 580°C in $6NH_3:94H_2$ for (a)–x– 2hrs. (b)–o– 5hrs & (c)–Δ– 48hrs.

that a wide spectrum of nitrogen atom enviroments exists. During the short nitriding times used the specimens are increasing in hardness. Driver & Papazian (1973) have shown that in these early stages the zone density continuously increases with nitrogen concentration and therefore, with hardness. At any one time, little deviation in hardness is evident across the specimens and so it is reasonable to assume that the structure is uniform. When peak hardness, (and consequently zone density), is reached a distinct high temperature damping peak is observed (see Fig. 7(c)). Therefore, the complex damping effects observed after short nitriding times are associated with the embryonic stages of clustering. The complete absence of any Snoek damping is very significant, showing that as soon as nitrogen atoms enter the specimen, they are preferentially attracted to sites other than normal octahedral ones. The most likely sites would appear to be those associated with clusters or substitutional molybdenum atoms. The enhanced broadening of the internal friction peak which occurs within the range 60 - 120^{o}C could be explained in terms of a Mo-N interaction peak being superimposed on the high temperature peak. The position of this peak was determined in the absence of a high temperature peak by nitriding a Fe-1.7 at.%Mo alloy at a nitrogen potential below the zone solvus for homogeneous precipitation. By doing so, some nitrogen and molybdenum atoms are left in random solid solution and hence, upon testing, the Mo-N interaction peak is observed (see Fig. V.8(b)). At a testing frequency of 0.75 c.p.s. the peak is observed to occur at 82^{o}C. This compares favourably with the

Fig. V. 8



Internal friction of Fe–1·7 at% Mo nitrided for 24hrs. at 580°C in (a) $10NH_3:90H_2$ and (b) $6NH_3:94H_2$

value given by Dijkstra & Sladek (1953) of 75°C for a Fe-0.3 at.%Mo alloy tested at 1 c.p.s.

The likely presence of this peak in the partially nitrided Fe-3at.%Mo alloy confirms that some of the nitrogen atoms move into the vicinity of molybdenum atoms immediately upon entering the specimen as a prerequisite for cluster formation. The disappearance of this peak in the fully nitrided sample (see Fig.V.7(c)) is expected, since there are now no molybdenum atoms remaining in random solid solution. The enhanced broadening which occurs above 160°C is more difficult to explain, but since it disappears in the fully nitrided alloy it must also be associated with the initial stages of cluster formation.

Significant differences in damping behaviour are observed after nitriding a Fe-1.7at.%Mo alloy at two different nitrogen potentials (see Fig.V.8). A $6NH_3:94H_2$ gas mixture is insufficient to exceed the solvus for GP zone formation, thus leaving nitrogen and molybdenum atoms in random solid solution. The internal friction data clearly confirms this phenomenon showing both a Snoek and a Mo-N interaction peak, whilst only a very small high temperature peak is detectable. Raising the nitriding potential to $10NH_3:90H_2$ produces a significant change in microstructure, enabling relatively coarse zones to form which slowly transform to δ-MoN. Metallographic examination of this sample showed some evidence of grain boundary

transformation and X-ray examination indicated that some δ-MoN was precipitated. The internal friction associated with this structure is shown in Figure V.8(a), where the presence of a Snoek and a high temperature damping peak are observed.

Using these observations the internal friction characteristics of Fe-Mo-N alloys can be interpreted in a consistent manner. A peak at about 80°C only occurs when there are molybdenum atoms remaining in solid solution. The anomolous high temperature damping peak is associated with homogeneous precipitation, the peak moving to higher temperatures as the structure coarsens. Simultaneously, the Snoek peak height slowly increases, indicating that more nitrogen is present in normal Snoek sites. This can be explained as being due to the fact that as the particles coarsen a wider interparticle spacing results, leaving more unstrained lattice available for normal Snoek sites.

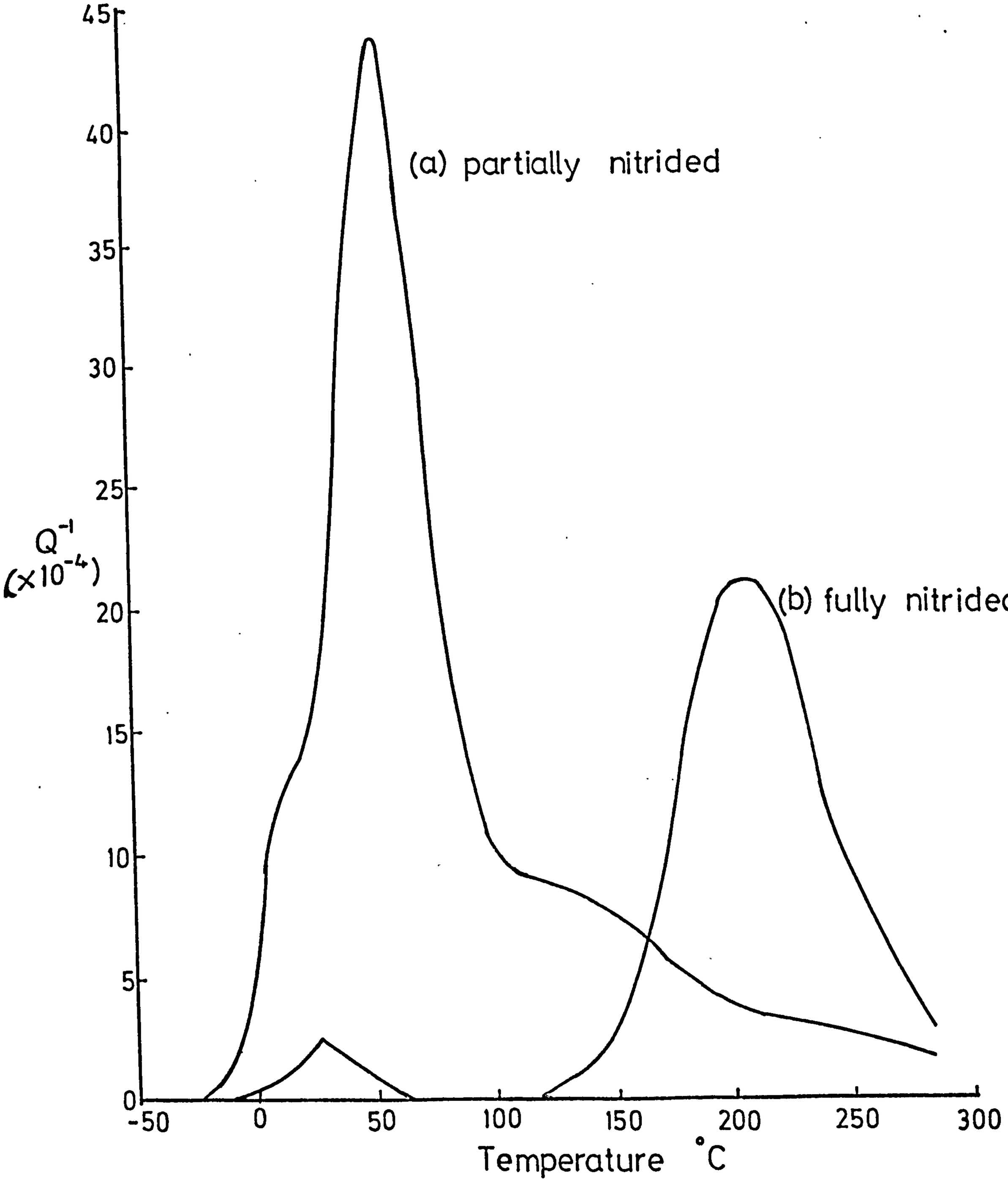
Hydrogen reduction experiments give some indication of the state of the combination of nitrogen. Thus, nitrogen in clusters is removed more quickly than nitrogen which is more strongly combined as alloy nitride precipitates; in Fe-Mo-N alloys the nitrogen can be removed completely, leaving only Fe-Mo clusters in the ferrite matrix (Unthank et al, 1972). During hydrogen reduction experiments the nitrogen

concentration diminishes rapidly at first, presumably as nitrogen is removed from solid solution and from low-energy sites in the strain fields surrounding the zones. After reduction for about 10 hours, the rate of nitrogen removal decreases as nitrogen is removed from the substitutional-interstitial zones and, eventually, after about 200 hours, almost no nitrogen remains. Internal friction measurements on samples subjected to such treatments give no evidence of any peaks even after short reduction times (10 hrs at 580°C). These observations confirm that it is the nitrogen atoms trapped in the strain fields around the particles that are responsible for the anomolous damping characteristics; the nitrogen atoms coalesced as particles being too strongly bound to contribute to the damping.

V.5 Internal friction of Fe-Cr-N alloys

The internal friction characteristics of Fe-1.2 at.%Cr and Fe-2.0at.%Cr alloys have been investigated at various stages of the precipitation sequence. Figure V.9(a) shows the damping characteristics obtained after partial nitriding. Damping is complex, as in partially nitrided Fe-3.0at.%Mo alloys, confirming that nitrogen atoms are present in a wide range of environments. The damping occurring in the range 0 - 100°C can be explained as being due to the presence of a composite Snoek and Cr-N interaction peak. Dijkstra & Sladek (1953) observed a similar composite peak at about 47°C in a Fe-0.5at.%Cr alloy containing nitrogen. In Figure V.9(a) the damping maxima is observed to be at 53°C. Therefore, the

Fig. V. 9



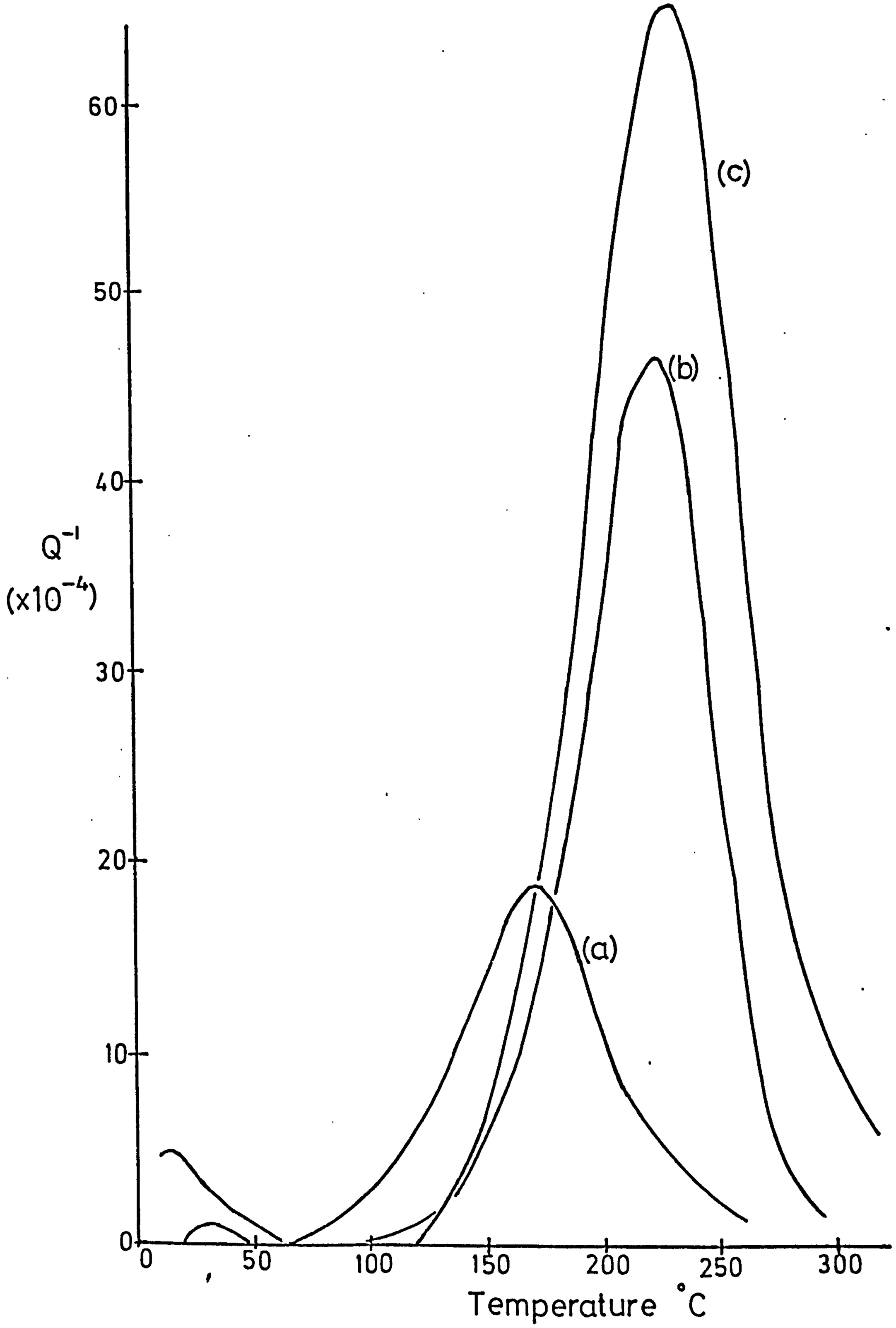
Internal friction of Fe-1·2 at.%Cr nitrided in 6:94 NH_3:H_2 at 575 °C (f=1·05 cps)

damping of the partially nitrided alloy can be interpreted as being due to nitrogen atoms moving into the vicinity of chromium atoms immediately upon entering the specimen.

Continued nitriding to peak hardness results in a distinct high temperature damping peak occurring at 210°C (Fig. V.9(b)). At peak hardness the microstructure consists of CrN plates of about 20nm diameter. From this result it is apparent that the anomolous damping observed in the partially nitrided alloy above 100°C is due to nitrogen atoms other than those associated with either Cr-N solid solution interactions or those trapped around CrN precipitates.

In a Fe-2.0at.%Cr alloy nitrided at 500°C for 20 hours in $13NH_3:87H_2$ damping is very similar to that observed in Fe-Mo-N alloys containing GP zones, with a high temperature damping peak occurring at approximately 170°C. Lattice parameter measurements of similar samples indicate the presence of solute-atom clusters and electron microscopy (see Fig.V.3 (a)) reveals small coherent particles of about 5nm diameter, which give continuous streaking on electron diffraction patterns. It is interesting to note that this sample is not fully nitrided, yet a distinct high temperature damping peak is observed, despite there being no damping at low temperatures (Fig.V.10).This behaviour is unlike partially nitrided Fe-1.2at.%Cr and Fe-Mo alloys where additional damping occurs, inferring that a different type of nitriding behaviour. exists.

Fig. V. 10



Internal friction of Fe-2·0 at.% Cr nitrided for

(a) 20hrs. at 500°C in $13NH_3:87H_2$.

(b) 24hrs. at 575 °C in $6NH_3:94H_2$.

(c) 70hrs. at 575 °C in $10NH_3:90H_2$.

Mortimer (1971), found that the nitriding of the Fe-1.2at.%Cr alloy differed from that of the higher chromium alloys in that a hard subscale was not observed and that the rate of nitriding was slower than expected from internal nitriding theory. The reason for this was interpreted as being due to the fact that only part of the nitrogen interacts with chromium upon entering the specimen; the remainder diffuses inwards, leaving unreacted chromium to combine with nitrogen at a later stage. This phenomenon produced 'dish' shaped hardness profiles; the rate controlling step was thought to be the diffusion of chromium over small distances around the nucleating and growing CrN particles. The present internal friction work supports this explanation because a composite Snoek and Cr-N interaction peak is observed in the partially nitrided Fe-1.2at.%Cr alloy; this shows that all of the nitrogen has not reacted with chromium upon entering the sample. By contrast, practically no unreacted nitrogen is detectable in the case hardened alloy.

Nitriding Fe-Cr alloys at 575^{o}C results in rapid over-ageing of the structure, although the nitride precipitates retain the disc-shaped morphology of clusters. High temperature damping is still associated with such a structure, although the peak now occurs at a higher temperature, 215 - 230^{o}C, depending upon the nitriding time and potential (see Fig.V.10). These damping observations confirm that the nitrogen atom environment responsible for the anomolous high temperature damping is the same when both solute-atom clusters and fine nitride precipitates are present. As the peak

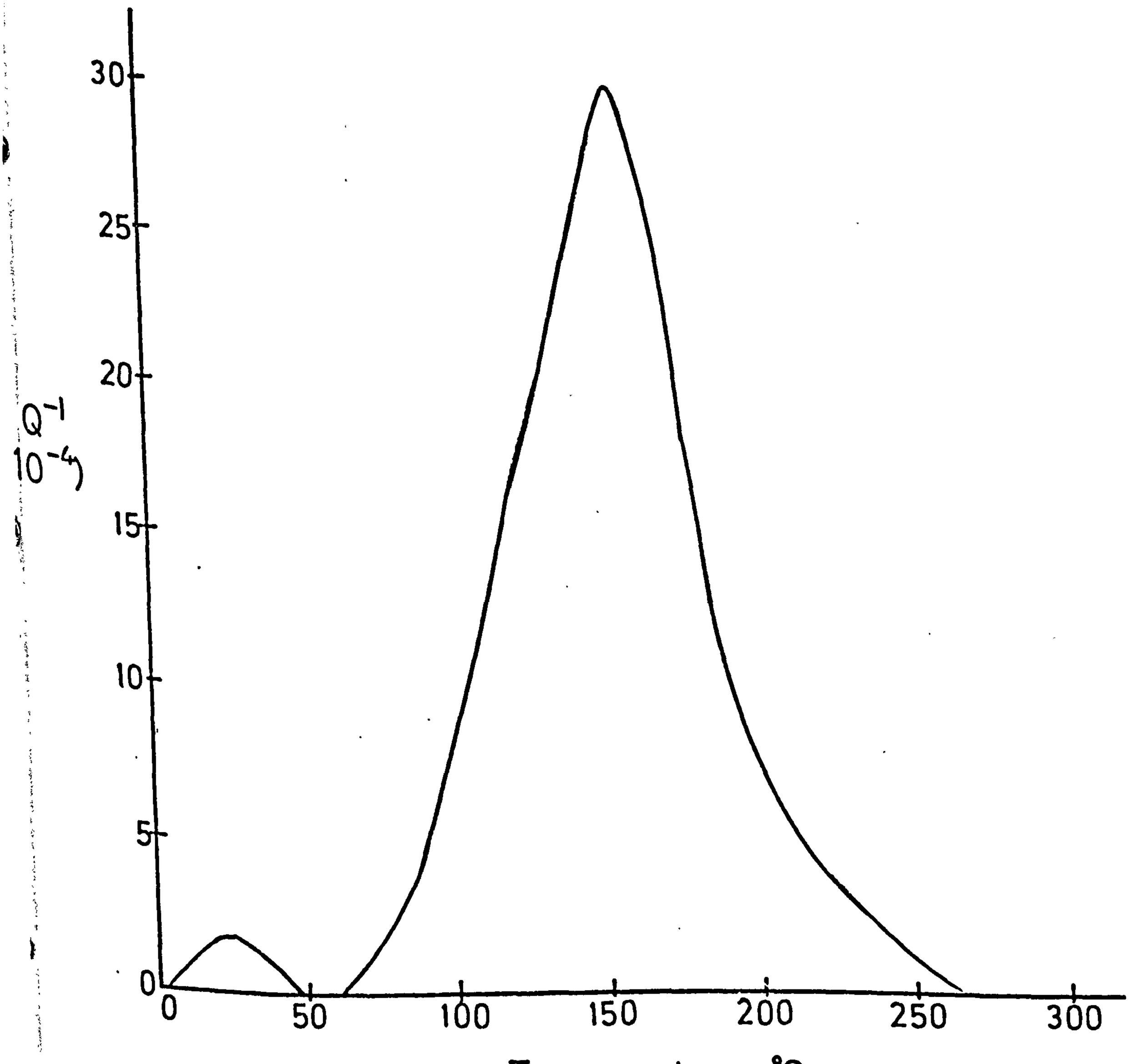
temperature increases from 170 to 225°C, there is a simultaneous increase in peak height from $18x10^{-4}$ to $43x10^{-4}$, although the nitriding potential used at 500°C and 575°C is the same. Therefore, more nitrogen is free to contribute to the damping when the abnormal peak temperature increases.

V.6 Internal friction of Fe-Ti-N alloys

The damping characteristics of a Fe-0.65at.%Ti alloy nitrided to saturation in $5NH_3:95H_2$ are shown in Figure V.11. A high temperature damping peak is observed at 150°C together with a small Snoek peak. The effects are similar to those observed in Fe-Mo and Fe-Cr alloys nitrided under conditions to produce a similar microstructure. Electron micrographs of the nitrided Fe-Ti alloy are shown in Figure V.2. It is possible to resolve some of the strain fields around very small coherent particles of about 2nm diameter. Pope(1972) observed that similar microstructures in Fe-V alloys produced an internal friction peak at 150°C. Therefore, from the results of this investigation and Pope's (1972) work, it is apparent that an internal friction peak occurs at from 150 to 170°C when a microstructure containing small coherent particles is produced.

Two damping peaks in the ranges 116 - 160°C and 220 - 242°C have been observed in nitrided Fe-Ti alloys by Szabó-Miszenti (1970). Peak temperatures and widths varied with heat treatment, and the peaks were ascribed to interstitial

Fig. V. 11



Internal friction of Fe-065 at%Ti nitrided for 24 hrs in 5:95 NH_3:H_2 at 575°C (f=1·0 cps)

nitrogen - substitutional titanium interactions. Heavily nitrided samples were observed to be very brittle, a characteristic of a structure containing a high volume fraction of fine particles. It is interesting to note that a peak at 150°C was observed in these samples. The present work suggests that this peak is in fact due to the movement of the less firmly bound nitrogen atoms around fine coherent particles.

V.7 Activation energy for the high temperature damping

Despite the anomolous high temperature peak being too broad to be ascribed to a single relaxation process, an average value of the activation energy, ΔH, can be calculated from (III).20 using the fact that the maximum damping occurs when $w\tau=1$. By testing at two frequencies, a shift in peak temperature occurs enabling ΔH to be calculated. From (III).20:-

$$1/\omega = \tau_0 \exp \Delta H / RT_p \qquad \ldots\ldots\ldots \quad (V)5$$

where Tp is the peak temperature. If T_1 and T_2 are the peak temperatures at two testing frequencies, w_1 and w_2, then solving for ΔH:-

$$\Delta H = 19.14 \frac{\log \omega_2/\omega_1}{1/T_1 - 1/T_2} \qquad \ldots\ldots\ldots \quad (V)6$$

This method has been applied to nitrided Fe-3at.%Mo alloys (see Figs. V.5 &V.6), from which ΔH is calculated to be 29 ± 5 and 26.5 ± 5 k cals respectively. The large errors

arise from the difficulty in defining the peak temperatures accurately. Similar calculations from the Fe-2.0at.%Cr alloy nitrided at 580°C, give ΔH values of 31±5 k cals. Measurements at other temperatures and especially at those over a wider frequency range would be necessary to find the value of ΔH with greater accuracy.

Wert & Marx (1953) have shown that for a given frequency, the temperature at which a relaxation peak is found increases as the activation energy increases. For many relaxation effects $\Delta H/Tp$ has approximately the same value, and an almost straight line relationship, passing through the origin, is obtained when ΔH is plotted as a function of Tp. Theoretical justification for this relationship has been obtained for a given model. Using the migration of interstitials in b.c.c. lattices as an example, the mean time of stay (τ) of an interstitial atom in a given position is determined by the condition,

$$1/\tau = nv\ (\exp \Delta S/R)(\exp - \Delta H/RT) \ldots\ldots\ldots (V).7$$

where R is the gas constant, v the interstitial atomic frequency, n is the number of elementary diffusion paths and ΔS and ΔH are the entropy and enthalpy of activation respectively. The exponential terms overwhelm any variation in v; therefore, by taking an average value of $v = 1.2 \times 10^{13}$ c.p.s. little error is involved.

τ is related to the relaxation time, τr, by:-

$$\tau = 3/2 \tau_r = 3/2 \left(1/2\pi f_m \right) \quad \ldots\ldots\ldots \quad (V).8$$

where fm is the frequency of the applied stress at the temperature at which the internal friction peak is observed. From this analysis it follows that

$$\Delta H = RT \ln \left(v/f_m \right) + T\Delta S \quad \ldots\ldots\ldots \quad (V).9$$

Thus, a linear relationship is found and it is observed that the entropy changes are approximately the same for all processes which obey the relationship. Further data by Stephenson (1965) on interstitial diffusion in b.c.c. metals has become available, showing that the best straight line relationship is obtained from,

$$H = 62.6Tp - 250 \text{ cal/mole} \pm 860 \text{ cal/mole} \quad \ldots\ldots (V).10$$

In the present work, peaks are observed in the range 150 - 230°C. Applying the relationship in (V).10 gives ΔH values of 27.5 - 32.5 k cals; which agree closely to the values calculated by the peak shift method.

Using the relationship found in (V).8 for τ and the experimentally determined value of ΔH, it is possible to calculate a value of τ_o ; from (III).20

$$\tau = \tau_o \exp \Delta H/RT$$

substituting for τ,

$$3/2\ (1/2\pi \cdot fm) = \tau_o \exp \Delta H/RT_p \quad \ldots\ldots\ldots \quad (V).11$$

For the peak in Fe-3at.%Mo this gives τo = 1.02×10^{-16} cps, whereas the Fe-2.0at.%Cr peak at 230°C gives $\tau o = 7.05 \times 10^{-15}$ cps. Both values are seen to be in close agreement with those derived by Fast and Verrijp (1954) for the diffusion of nitrogen in alpha-iron (2.06×10^{-15} cps). Therefore, it seems that the long relaxation times in the present work arise solely from the large activation energy.

The relatively high values for the activation energy are believed to be due to nitrogen atoms within the strain fields around the precipitated particles. The resultant interaction provides an additional barrier for lattice diffusion and explains why nitrogen diffusion is abnormal in Fe-X-N alloys.

Values for the diffusion rate of nitrogen in pure iron, within the range of peak temperatures found in the present work, can be calculated from

$$D = Do \exp -Q/RT \quad \ldots\ldots\ldots \quad (V).12$$

Using the values of Fast and Verrijp (1954) of 6.6×10^{-3} for Do and 18,600 k cals for Q, the diffusion rates of nitrogen at 150 and 230°C are 1.49×10^{-12} and 5.11×10^{-11} cm^2/sec respectively.

If the diffusion of nitrogen in a b.c.c. lattice is considered to be a random process, then the diffusion co-efficient

can be shown to be

$$D = \frac{\lambda^2}{6\tau} \qquad \ldots\ldots\ldots \quad (V).13$$

where λ is the jump length and τ is the mean time of stay at a given lattice site. λ is the distance between the nearest interstitial positions and is only half the lattice constant, a.

$$\text{Therefore,} \quad D = a^2/24\tau \qquad \ldots\ldots\ldots \quad (V).14$$

The mean time of stay, τ, is related to the relaxation time τ_r by

$$\tau = \frac{3\tau_r}{2} \qquad \ldots\ldots\ldots \quad (V).15$$

and the relaxation time by

$$\tau_r = \frac{1}{\omega} = \frac{f_m}{2\pi} \qquad \ldots\ldots\ldots \quad (V).16$$

Combining (V)14, (V)15 and (V)16, an expression can be obtained for D:

$$D = \pi a^2/18\ f_m \qquad \ldots\ldots\ldots \quad (V).17$$

and hence, the diffusion co-efficient at the temperature corresponding to the maximum internal friction can be calculated from the lattice spacing and periodic time of the

oscillations.

Using this expression, the value of D for the peaks found at 150 and 230°C is 1.43×10^{-16} cm^2/sec, which is considerably less than the values expected for nitrogen diffusion in pure iron. The above values should be used with caution since the peak is not a single relaxation process. Nevertheless, they represent an average value and give an idea of the slower rate of nitrogen diffusion in the nitrided alloys. The lower values explain the slow rate of decay of the high temperature peak and the consequent slow rate of iron nitride precipitation in Fe-X-N alloys containing zones or precipitates.

V.8 The high temperature peaks

High temperature damping peaks were first observed in constant-activity nitrided Fe-V alloys (Pope, 1972). This investigation has shown that similar peaks are observed in nitrided Fe-Mo, Fe-Cr and Fe-Ti alloys; whereas Middleton (1974) has also observed a similar peak in a nitrided Fe-Mn alloy.

Therefore, the peak appears to be a general feature associated with homogeneous precipitation in nitrogen ferrites. The changes in peak height and temperature appear to be related to changes in the microstructure, both increasing as the microstructure coarsens. The peak is thought to arise from the movement of nitrogen atoms in the strain fields surrounding

zones or precipitates; the nitrogen in the particles being too firmly held to contribute to the relaxation spectrum in the temperature ranges used.

The broadness of the peak suggests that it is, in fact, a composite peak due to the presence of a relaxation spectrum. The range of relaxation times is probably due to nitrogen atoms moving in the vicinity of particles of various sizes and stability. The ideal damping curve of a process occurring with a single relaxation time is given by:-

$$Q^{-1} = Q_{max}^{-1} \cdot \operatorname{sech}\left[\frac{\Delta H}{R}\left(\frac{1}{T} - \frac{1}{T_p}\right)\right] \quad \ldots \quad (V).18$$

which predicts that damping is symmetric about the reciprocal peak temperature and that the relationship

$$\Delta H = 5.268 \Big/ \Delta(1/T) \quad \ldots \quad (V).19$$

defines the activation energy in terms of the half-peak width $\Delta(1/T)$.

Comparison of the half-peak widths calculated from (V).19 with the corresponding experimentally observed values indicates whether or not damping occurs with a single relaxation time. ΔH can be measured by either observing the shift in peak temperature with frequency or by calculation using the method of Wert & Marx (1953). Data from both techniques is given in Table V.2. The peaks are seen to be considerably

TABLE V. 2

INTERNAL FRICTION OF Fe-X-N ALLOYS:HIGH-TEMPERATURE PEAKS

alloy composition at.%	nitriding conditions			ΔH kcal/mole		half peak width $K^{-1} \times 10^{-4}$	
	temp °C	ratio $NH_3:H_2$	time hours	calc. from (V).10	obs.	calc.	obs.
2.92 Mo	580	6:94	24	27.9	29.0	1.88	3.40
1.20 Cr	575	6:94	24	31.1	-	1.68	3.20
2.0 Cr	580	10:90	21	31.1	30.8	1.68	3.83
2.0 Cr	580	10:90	70	32.9	-	1.63	3.45
0.65 Ti	575	5:95	24	27.4	-	1.91	3.90
1.08 V	580	10:90	67	27.9	28.0	1.88	3.10

broader than predicted from (V).19, inferring that the high temperature damping is due to a relaxation spectrum. Observed data for the high temperature damping peak in Fe-Mo-N alloys, has been replotted as a function of (1/T) in Fig.V.12. Comparison is made to the damping expected from a single relaxation process having the same peak temperature and an activation energy of 30 k cals/mole, (see Fig.V.12(b)). The experimental damping is clearly broader than the ideal curve and is also noticably assymmetric.

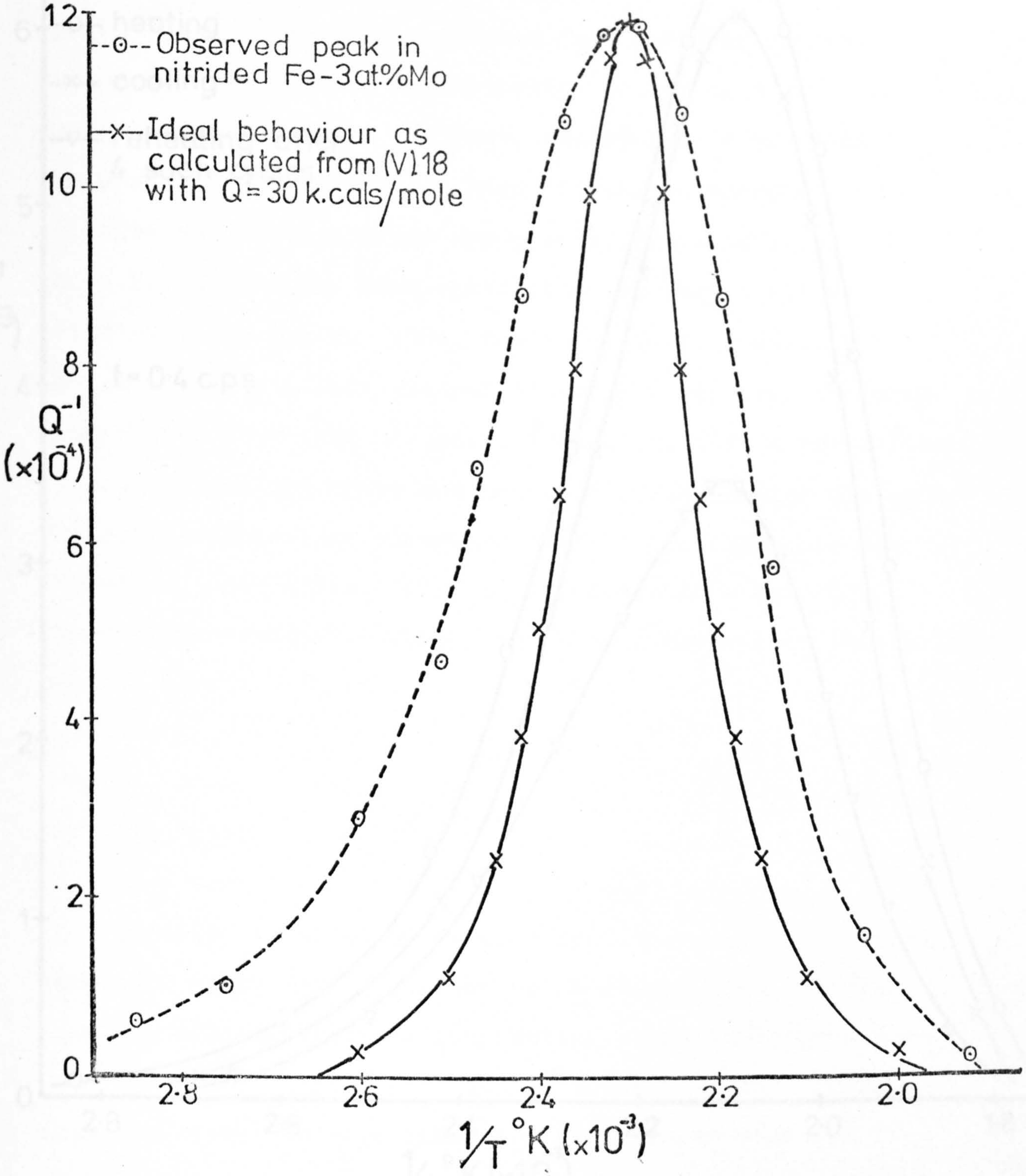
The presence of a broad damping peak occurs because of a distribution of relaxation times, τ, where

$$\tau = \tau_o \exp \frac{\Delta H}{RT} \qquad \ldots\ldots\ldots \quad (V).20$$

A distribution of relaxation times can, therefore, arise from a variation in τ_o (a pre-exponential constant), in ΔH, or possibly both. Certain broad peaks which exhibit a Guassian distribution of relaxation times (a lognormal distribution) have been described by a mathematical distribution function (Nowick & Berry, 1961). However, this analysis cannot be applied in the present investigation because the peaks are assymmetric, being broader on the low-temperature side.

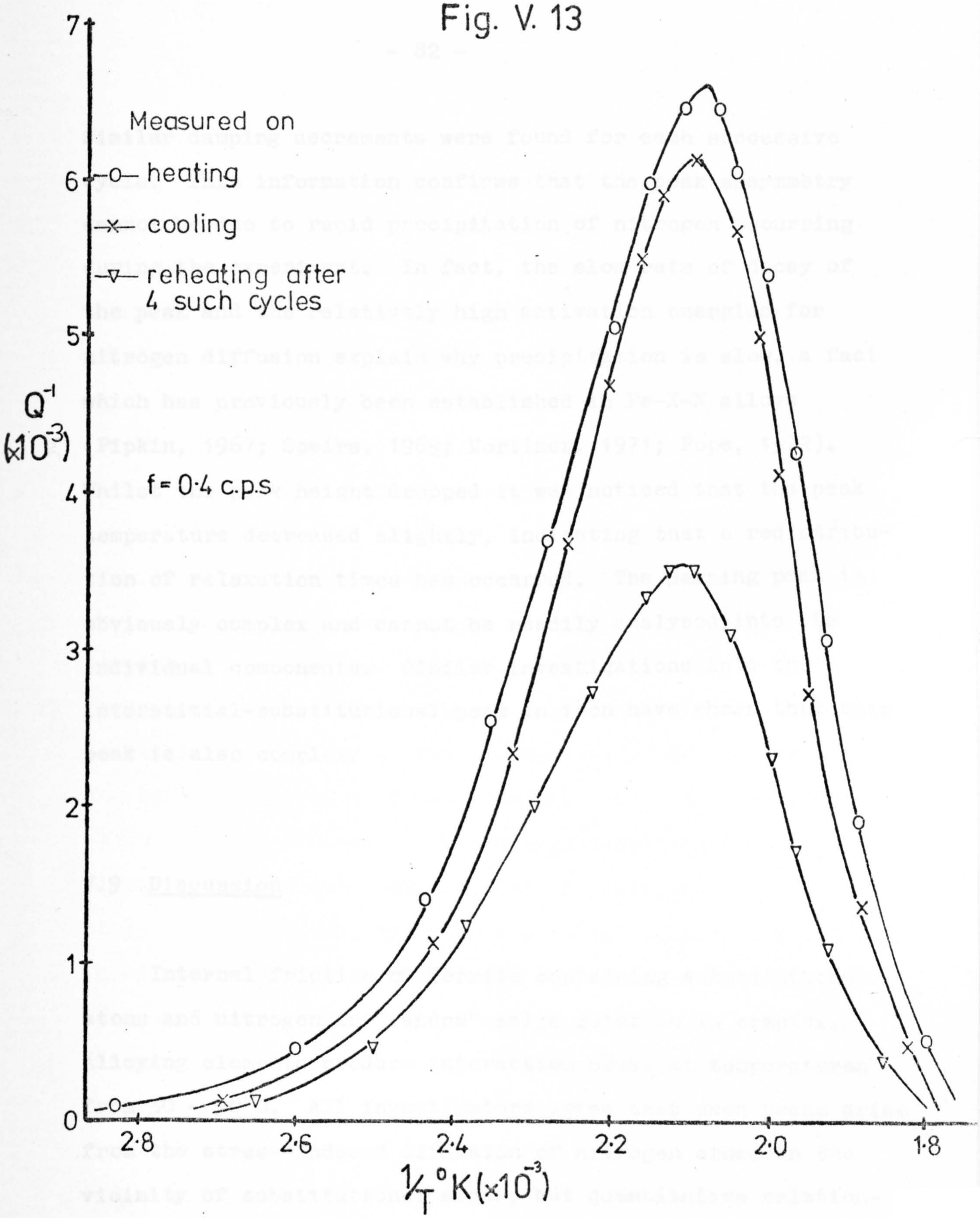
Upon measuring the damping curves after several heating (up to 300°C) and cooling cycles, the peak height was found to diminish slowly (see Fig.V.13). For example, after one such cycle the peak was observed to drop from 68×10^{-4} to 63×10^{-4}.

Fig V. 12



Comparison of the observed high temperature peak to the damping expected from a single relaxation process

Fig. V. 13



Stability of the high temperature peak

Similar damping decrements were found for each successive cycle. This information confirms that the peak assymmetry cannot be due to rapid precipitation of nitrogen occurring during the experiment. In fact, the slow rate of decay of the peak and the relatively high activation energies for nitrogen diffusion explain why precipitation is slow, a fact which has previously been established in Fe-X-N alloys (Pipkin, 1967; Speirs, 1969; Mortimer, 1971; Pope, 1972). Whilst the peak height dropped it was noticed that the peak temperature decreased slightly, indicating that a redistribution of relaxation times has occurred. The damping peak is obviously complex and cannot be readily analysed into its individual components. Similar investigations into the interstitial-substitutional peak in iron have shown that this peak is also complex.

V.9 Discussion

Internal friction of ferrite containing substitutional atoms and nitrogen in "random" solid solution is complex. Alloying elements produce interaction peaks at temperatures from 30 - 90°C. All investigators agree that such peaks arise from the stress-induced diffusion of nitrogen atoms in the vicinity of substitutional atoms, but quantitative relationships between peak heights and the associated nitrogen concentration have not been established. Such analyses would be extremely complicated because interaction peaks are composed

of several elementary peaks each occurring at different temperatures. Even if the composite peak is accurately analysed in terms of its components, the heights of the latter will not necessarily give a true assessment of the nitrogen contributing to the interaction peak, because the ratio of the number of nitrogen atoms associated with each component peak may vary with temperature. Consequently, the accurate determination of dissolved nitrogen in ternary alloys using damping measurements is difficult.

The internal friction of Fe-X-N alloys containing solute atom clusters is further complicated by the occurrence of damping at temperatures much higher than that expected from random substitutional-interstitial interactions. The damping is observed in nitrided Fe-V, Fe-Mo, Fe-Cr and Fe-Ti alloys and consequently part of the original aim of this investigation, the determination of nitrogen concentrations in equilibrium with the successive stages of precipitation, is impossible. Nevertheless, the unexpected high temperature damping is extremely significant and will be discussed further in the context of small precipitated particles and the associated matrix strain.

The temperature dependence of damping produced by a single relaxation process is defined by (III),21, which predicts that damping is symmetric about the reciprocal peak temperature. Data for the high temperature peak of the Fe-3at.%Mo alloy

nitrided at 580° in $6NH_3$:$94H_2$ was replotted as a function of reciprocal temperature (see Figure V.12). This shows that the damping is broad and assymmetric, confirming that the relaxation process occurs from a number of different relaxation times. Interaction peaks between substitutional atoms and nitrogen are of this form and numerous attempts have been made to analyse them in terms of their components. Perry, Malone and Boon (1966) have shown that the V-N interaction peak has at least three components, whilst Ritchie and Rawlings (1967) have analysed the Cr-N peak into four peaks, excluding the carbon and nitrogen Snoek peaks. The Fe-Mn-N system has received most attention and findings by Ritchie and Rawlings (1967) and by Nacken and Kuhlman (1966) have shown that seven peaks are necessary to describe the composite interaction peak in iron containing up to 2at.%Mn and 0.28at.%N. However, other research by Couper and Kennedy (1967) and by Enrietto (1962) analysed the peak by computer programme into three peaks.

Recently, Welch and Carpenter (1972) investigated the V-N interaction peak and found that the peak temperature increased as the nitrogen concentration increased. They also found the peak to be assymmetric and not a single Debye peak. By computer programme, they found the best correlation to consist of three Debye peaks, having temperatures of 75, 86 and 103°C. The activation energy for the average process was found to be 24.5 k cals with a τ_o value of 2×10^{-16} sec. They predicted the possibility of other peaks occurring at 135 and 165°C from stress relaxation methods, but found no

internal friction at these temperatures. The data was explained as being consistent with stress induced diffusion of nitrogen around a VN 'defect', in which a nitrogen atom is tightly bound to a vanadium atom. This nitrogen atom is supposedly in a tetrahedral site since Beshers (1965) showed that interstitial nitrogen energetically favours this site in the vanadium lattice. Damping is caused by diffusion of nitrogen in first and second nearest neighbour sites through octahedral - tetrahedral - octahedral diffusion paths. No Snoek or abnormal damping was observed until the nitrogen concentration exceeded a N:V ratio of 1:1, a fact which substantiates the earlier work of Fast and Meijering (1953) on Fe-V-N alloys. In the present investigation it is apparent that only the excess nitrogen causes the peak, there being no peaks after hydrogen reduction treatments.

All models have attempted to describe the composite interaction peak in terms of a relatively small number of elementary peaks and clearly the agreement between the observed and calculated data will increase with the number of component peaks. A different approach, which is applicable to symmetrically broadened peaks, has been described by Nowick & Berry (1961). They assumed that a Guassian distribution of relaxation times occurs and in principle this technique indicates whether the distribution of relaxation times arises from a distribution in τ_o or in activation energy. However, this approach cannot be applied in the present investigation because of the assymmetric damping peaks. Clearly the analysis

of composite peaks into their components is a complicated procedure of questionable reliability and so no attempt has been made to treat the high temperature damping peaks observed in Fe-X-N alloys containing zones or precipitates in this way.

There is growing evidence that solid solutions of interstitials are not random. For example, Keefer & Wert (1963) have shown that nitrogen and carbon atoms cluster around iron atoms and broaden the normal Snoek peak. The effects of high concentrations cannot be determined by measurements of the Snoek damping in iron since low solubilities exist. However, high interstitial concentrations especially of oxygen and nitrogen, are obtained in b.c.c. tantalum and niobium. Ké (1948) observed that the Snoek damping peaks in these alloys were too broad for a single relaxation process. Further work by Powers & Doyle (1956,1959) demonstrated that in Ta-O alloys the broadening was due to the superposition of two seperate peaks with different τ values, one due to O - O pairs and one to random atoms. In agreement with the studies of Zener (1948), it is usually assumed that the binding energy originates mainly from elastic interactions. When an interstitial atom is in an octahedron of a b.c.c. metal, the lattice is distorted in its vicinity. In some adjacent sites the shortest distance between two metal atoms is somewhat increased, the others decreased. The deformation energy caused by the introduction of a second interstitial atom in an already elongated site will be less than in an arbitrary non deformed

site. The difference between the two energies acts as a type of binding energy between the two interstitials, causing them to cluster. At higher concentrations it is likely that larger groups of atoms will be bound together.

In the present work relatively high concentrations of nitrogen are present. Although it is unlikely that nitrogen present in mixed substitutional-interstitial solute-atom clusters or nitride precipitates will contribute to Snoek damping, it is perhaps surprising that little damping is obtained from the nitrogen in equilibrium with the nitriding atmosphere. This absence is probably attributable to the segregation of nitrogen into the vicinity of the clusters or precipitates at low temperatures. In this context it is interesting to note that Stark et al (1956) found no Snoek peak in carbon martensite; also, a reduction in Snoek peak height is known to result from a decrease in grain size. Therefore, a general trend exists in that increasing the strained volume decreases the mobility of the interstitials. It appears that in these cases, the applied torsional stress is insufficient to overcome the internal strain and produce the periodic variations necessary for diffusion of interstitials at the normal Snoek temperature. It seems likely that the lattice strain associated with the solute atom clusters acts in a similar manner and prevents atomic motion at low temperatures. Indeed, as the inter-cluster spacing is increased by prolonged hydrogen reduction and renitriding cycles, or by using higher nitriding temperatures, small

Snoek peaks are observed. The increased spacing between clusters is expected to produce small regions of ferrite free from distortion, and it is the stress induced diffusion of nitrogen in these regions which produces Snoek damping. Such an explanation is equally applicable to a dispersion of fine nitride precipitates.

In addition to Snoek peaks produced by stress induced ordering of interstitials, damping has been noted at high temperatures in Fe-C and Fe-N alloys. Snoek (1941) first reported the cold work damping peak associated with the interaction between dislocations and nitrogen, and in further work Petarra & Beshers (1967) demonstrated that the peak temperature varied within the range 160 - 200°C depending upon the degree of cold work and nitrogen concentration. The existence of a high temperature damping peak at 220°C in carbon martensite has been demonstrated by Stark et al (1956) and by Mura et al (1961). It is generally agreed that the anelastic strain responsible for these peaks arises from the motion of dislocations under stress in the presence of carbide or nitride precipitates, or interstitial atmospheres. However, the explanation cannot satisfactorily account for high temperature damping observed in the present investigation because the dislocation density is certainly reduced by the hydrogen annealing treatment carried out prior to nitriding, and Snoek (1941) showed that the dislocation density of annealed materials does not produce a cold work peak.

In the present investigation, the source of anelastic strain responsible for the high temperature damping peak is probably the motion of a small proportion of the nitrogen atoms in the interstices furthest away from the coherent particles. It is probable that a range of activation energies exists corresponding to the varying matrix strain, but only atoms having activation energies at the lower end of the spectrum can move under the applied stress. Such a model predicts a composite damping peak, with an activation energy corresponding to the average value of the component relaxation processes.

It is well known that interstitial solutes are preferentially attracted to such lattice defects which prevail in the elastic strain fields around the coherent particles. The relatively high activation energy for damping is a result of this interaction, being higher than that in pure iron, but less than that for substitutional solutes in iron (Morrison & Leslie, 1973). Similar activation energies have been determined from strain ageing tests of vanadium and titanium strengthened low alloy steels, the higher value being indicative of a reduction in strain ageing (Rashid, 1976).

Previous research has shown that the cold work and martensite peaks in iron vary from 160 to 250°C, (Petarra and Beshers, 1967; Stark et al, 1956). Apparent activation energies for the peaks were calculated to be from 30 to 40 k cals/mole. Activation energies calculated for the peaks in the present investigation range from 24 to 31 k cals/mole. Therefore,

it appears that the peak observed in the present investigation is of similar origin to these other peaks.

The heights of the damping peaks in the present work show no apparent correlation with nitrogen concentration. Likewise, the cold work peak soon reaches a saturation value any excess nitrogen causing no additional damping. An interesting feature often noticed with the cold work peak was that at higher interstitial levels, the peak height started to rise again. This was thought to be due to nitride precipitation. The present work confirms that this is possible, since the peaks are within the same temperature range as that for coarse precipitates. When the precipitates lose coherency they generate structural dislocations, due to the lattice misfit, and could add to the dislocation peak.

Damping characteristics very similar to those in the present investigation have previously been reported by Köster and Horn (1966) in nitrided Fe-0.75wt.%V and Fe-Mo alloys. Abnormal peaks were observed in the temperature range 150 - 230°C and were attributed to martensite. However, electron metallography showed a fine dispersion of particles on $\{100\}_\alpha$. The preparative technique of nitriding in N_2/NH_3 gases at 590°C, would certainly produce small particles. Consequently, the observations made by Köster and Horn can be explained using the model developed in the present investigation. High temperature peaks have also been reported by Szabó - Miszenti (1970) in nitrided Fe-Ti alloys, and were interpreted as

Ti-N interaction peaks. However, a number or samples were noted to be extremely brittle, a characteristic of materials containing a high volume fraction of clusters, and so it is probable that at least one of the high temperature peaks arises from the mechanism proposed in the present investigation. Recent work by Baldi & Buzzichelli (1973) found a broad internal friction peak at about 170°C in Fe-Nb-N alloys. Both peaks were related to niobium atoms in solution since no extensive nitride precipitation was observed. However, peaks at as a high a temperature as this are not normally associated with substitutional-interstitial interaction peaks and it would appear that the peak is analogous to those observed in the present investigation. Peaks at from 150 - 220°C can be found in all Fe-X-N systems when homogeneous precipitation occurs and indeed may appear in a wide range of alloys. For example, Sagues & Gibala (1974) have observed broad peaks at about 150°C in Ta-Re-N alloys which were attributed to nitrogen atoms in the vicinity of ReN clusters. Therefore, internal friction peaks in the temperature range 150 to 220°C appear in any ternary alloy system containing substitutional and interstitial atoms which have a strong attraction for one another. The peak probably originates from the interstitial atoms moving in the strain fields around clustered or precipitated particles.

Kinetic studies have shown that nitrogen in hardened Fe-X-N alloys is very similar to that in pure iron; but the precipitation of iron nitrides from Fe-X-N alloys containing

clusters or precipitates is much slower than in pure ferrite. These observations suggest that the rate controlling stage in the precipitation reaction is not the diffusion of nitrogen through the ferrite lattice. Interpretation of the internal friction data tends to confirm this and infers that the removal of nitrogen from the vicinity of clusters or precipitates is the likely rate controlling factor.

V.10 Conclusions

a) The lack of Snoek damping and the occurrence of a high temperature damping peak in the range 150 - 230°C complicates the analysis of the internal friction observed in Fe-X-N alloys. Consequently, part of the original aim of the investigation, the determination of the equilibrium concentration of nitrogen at the successive stages of the precipitation sequence, is impossible to attain.

b) The precipitate dispersion is so fine that there are few undistorted octahedral sites in nitrided Fe-X-N alloys and so little or no Snoek relaxation occurs.

c) Damping at 150 - 230°C is found in nitrided Fe-Mo, Fe-Cr, Fe-V and Fe-Ti alloys and probably arises from the stress induced diffusion of nitrogen atoms at the periphery of solute-atom clusters or in the strained matrix adjacent to fine nitride precipitates.

d) Broad, assymmetric peaks occur, indicating a distribution of relaxation times. Peaks at about 150°C are associated with fine coherent particles of 5nm diameter. Coarsening of the structure successively moves the peak to

higher temperatures, until a peak at about 230°C is associated with precipitates of 20nm diameter. At this stage, the peak is very similar to that observed in martensite and cold worked structures.

e) The peak is of a different origin to the cold worked and martensite peaks previously found within the same temperature range in Fe-N and Fe-C alloys.

f) The internal friction of partially nitrided material is particularly complex. Substitutional-interstitial interaction peaks are observed together with the characteristic high temperature peak. However, additional damping is also present and is probably due to atomic arrangements intermediate between random solid solution and clusters.

g) Calculation of the activation energies from the peak shift method agree with the values proposed by the semi-empirical formula of Stephenson (1965). The relatively high activation energies are considered to be the consequence of interactions between interstitial nitrogen and the extensive strain fields around the precipitated particles.

h) Hydrogen reduction treatment removes all of the peaks, confirming that it is the excess nitrogen which causes the anomolous damping.

Chapter VI

HOMOGENEOUS PRECIPITATION IN Fe-X-N ALLOYS

VI.1 Introduction

Speirs (1969) observed that the constant activity nitriding of Fe-Mo alloys below 600°C produced very hard material associated with non-equilibrium precipitation. Electron metallography revealed the presence of small, coherent particles precipitated on the {100} ferrite planes and further work (Speirs et al, 1970) confirmed that the first formed particles were substitutional-interstitial solute-atom clusters. Upon subsequent ageing, the clusters follow a precipitation sequence similar to aged f.c.c. alloys such as Al-4wt.%Cu:

GP zones - one or more metactable intermediate precipitates - equilibrium precipitate

These observations provided the first evidence of mixed substitutional-interstitial solute-atom clusters in b.c.c. metals. Subsequently, Roberts (1970) found that a similar precipitation sequence occurred in Fe-Nb-N alloys, the intermediate precipitate possessing a body centred tetragonal structure. Pope (1972) observed that homogeneous precipitation in nitrided Fe-V alloys was preceeded by the formation of coherent discs on {100} ferrite planes, although from the experimental evidence it was difficult to decide if the initial particles were solute-atom clusters or coherent vanadium nitride platelets.

Upon subsequent ageing, only evidence of the equilibrium precipitate was obtained.

Previous work aimed at providing thermodynamic and precipitate identification data using alloys of 0.5-5.0 at % substitutional solute. When such alloys are constant activity nitrided, high volume fractions of clusters or precipitates are produced, causing the material to become very hard and tensile test specimens invariably fracture before yeilding. Such properties are of limited use except where a high surface hardness and wear or abrasion resistance are required.

The desire to channel the high specific strength of nitrided alloys to more practical applications led to a more detailed examination of dilute alloy ferrites, often containing as little as 0.1 at.% substitutional solute. Previous research neglected the homogeneous precipitation in such alloys and, therefore, further experimental data was required in order to enable a correlation of the mechanical properties with the associated microstructures to be made. Consequently, a study of the homogeneous precipitation in dilute Fe - V and Fe-Nb alloys was initiated, together with additional experiments on the effects of nitriding the higher alloys at low potentials, high tempratures and in the partially recovered state, in order to try and produce a more ductile structure.

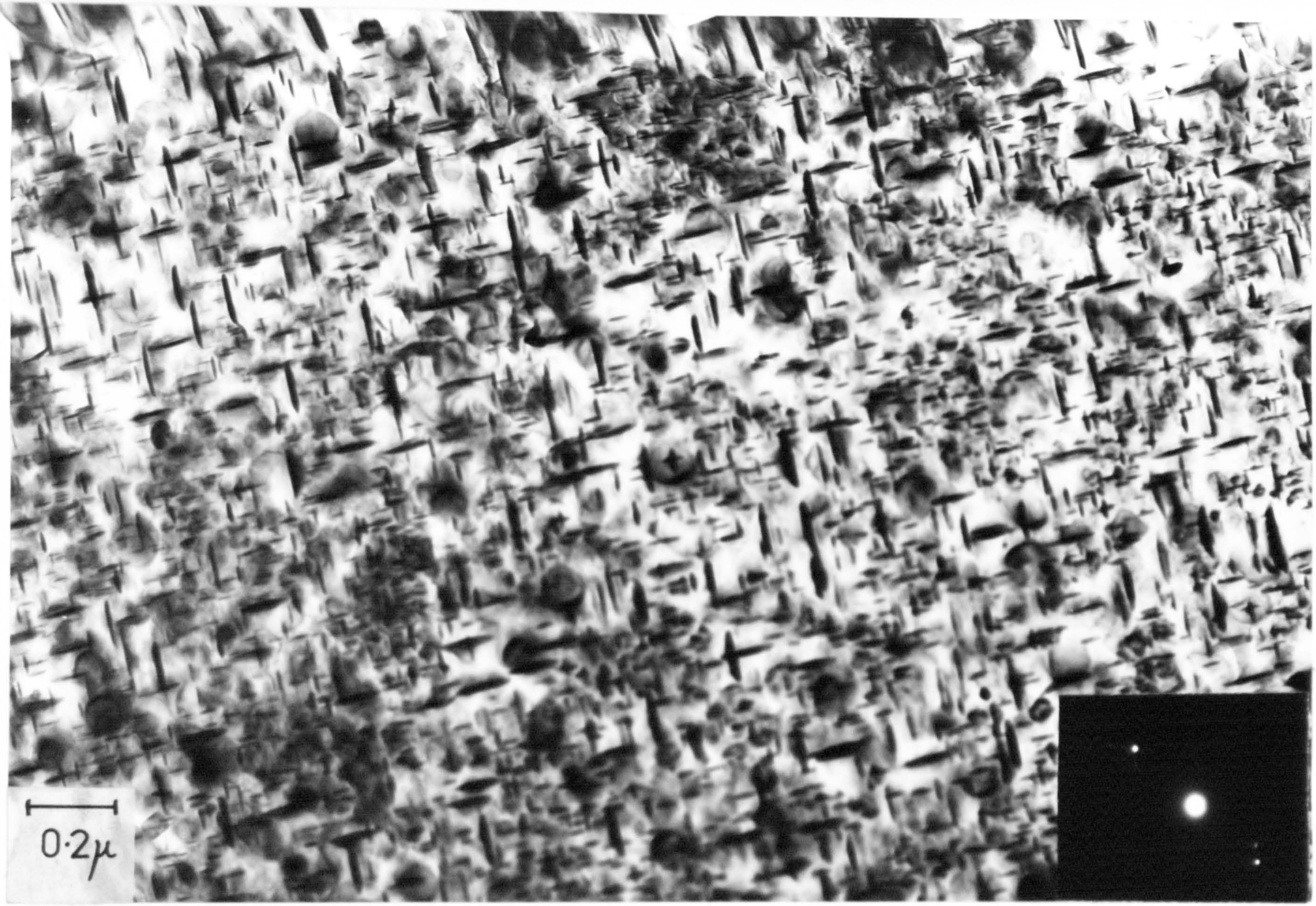
V1.2 Homogeneous precipitation in Fe-V alloys

Constant activity nitriding Fe-V alloys in the range 450 - 650 °C produces considerable hardness increments. With alloy contents ≥ 0.52 at.%V the structures are obscured by strain contrast; but the electron diffraction effects, continuous streaking in <100> directions, indicates the presence of disc-shaped clusters or thin precipitates on the ferrite cube planes (Pope 1972). Only by nitriding these alloys at higher temperatures and at low nitrogen potentials does the structure become resolvable.

Fig V1.1 shows a typical dispersion of platelets of 40-120 nm diameter obtained after nitriding a Fe-1.1 at.%V alloy at 700 °C in 0.6 NH_3 : 99.4H_2. The plates lie on $\{100\}_\alpha$ planes and from electron diffraction patterns they can be identified as vanadium nitride.

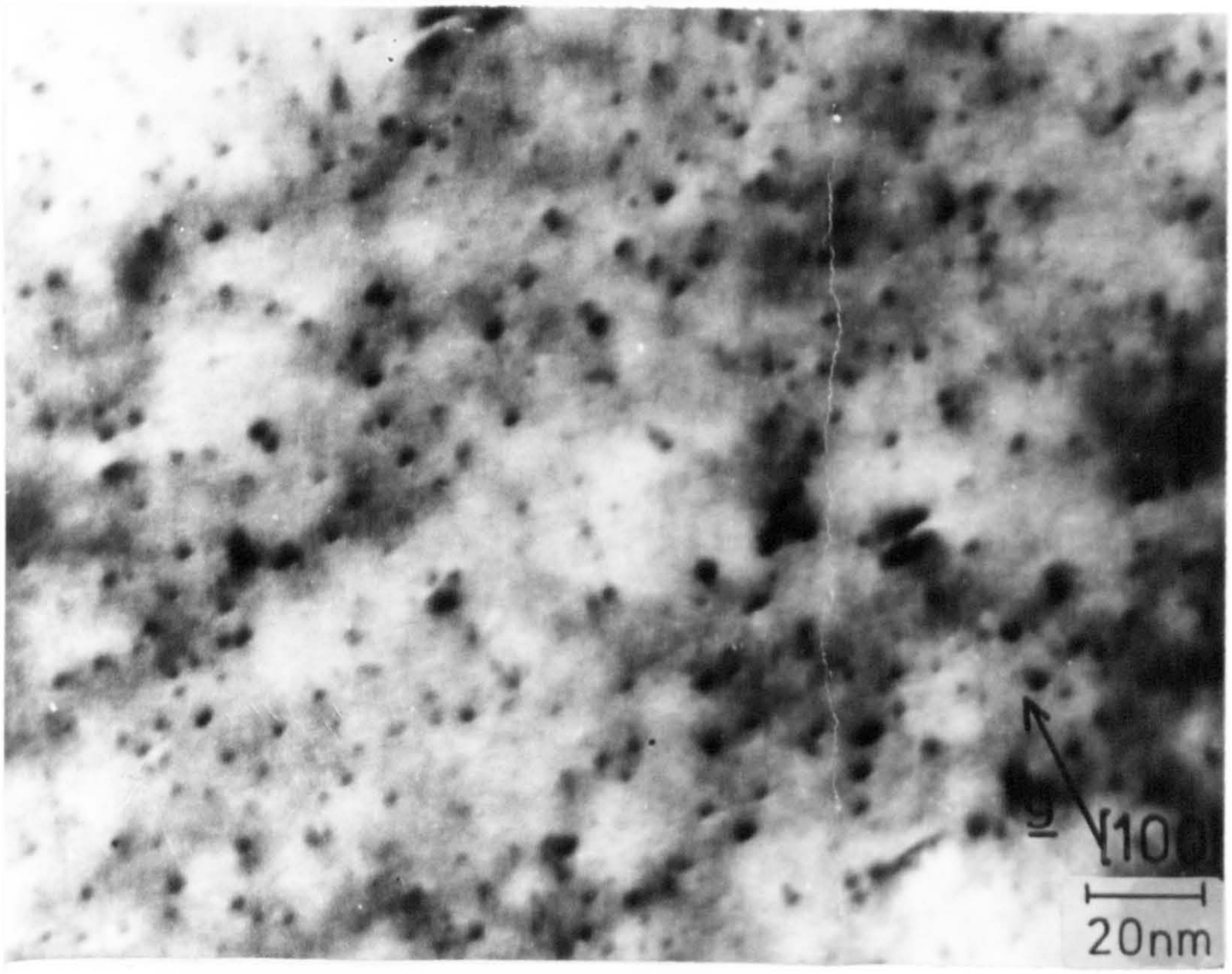
Nitriding a Fe-0.15 at.%V alloy produces microstructures which are readily resolvable in the electron microscope. A typical bright field micrograph of this alloy nitrided at 575 °C in 5 NH_3 : 95H_2 for 24 hours is shown in Fig V1.2a. Coherent particles of 1.5-5 nm diameter, with thickness of 0.5-2nm, are revealed by typical strain field contrast. The strained regions appear as dark lobes adjacent to the particles and are clearly visible when the thin foil is favourably orientated. Estimates of the particle-matrix misfit strain (ϵ) for particles similar to those in Fig V1.2 have been made by Stephenson (1974) using the method of Ashby & Brown (1963), and exceptionally high values of ϵ(20-40%) were obtained.

Fig. VI. 1

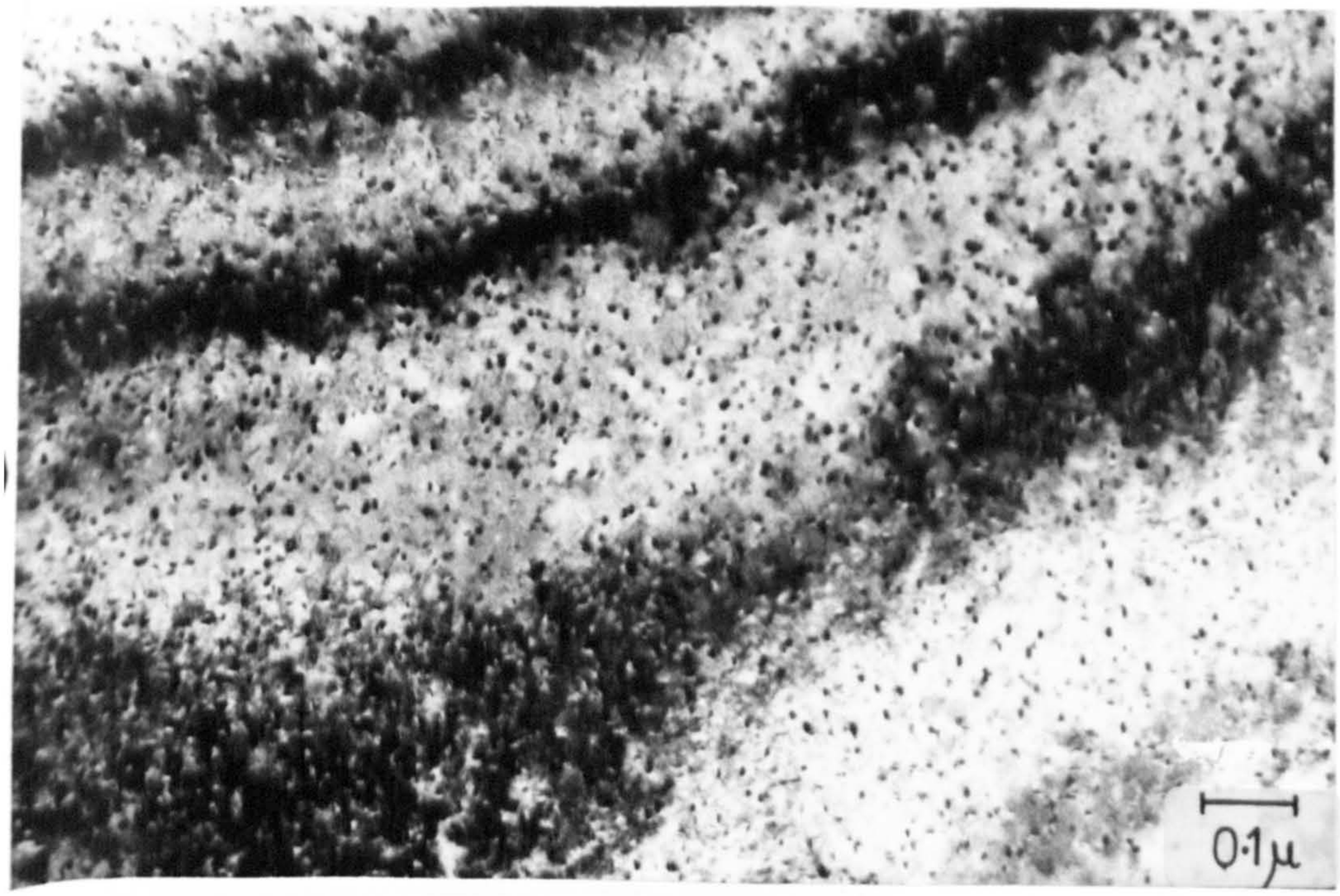


Fe- 1·1 at %V nitrided in 0·6NH_3:99·4H_2 at 700 C for 14 hrs.

Fig. VI. 2



(011)



(1̄13)



(a) nitrided in $5NH_3$: $95H_2$ at 575°C

(b) nitrided in $1NH_3$: $99H_2$ at 575°C

(c)SADP from area nitrided as in(a)

Electron microscopy of Fe-0·15 at.%V

The extent of the strain fields observed in this alloy explains why the structures of the higher vanadium alloys, nitrided under similar conditions, were irresolvable (see Pope, 1972); if higher volume fractions of particles are precipitated, the extersive strain fields will overlap and obscure any detail.

Diffraction patterns of the nitrided Fe-0.15at.%V alloy exhibit continuous streaking in $\langle 100 \rangle_\alpha$ directions. The origin of the streaking is discussed by Hirsch et al (1965) and can arise from two sources:

i) Thin precipitates or zones of different scattering power to the matrix.

ii) Matrix distortion produced by zones or precipitates. Therefore, the origin of streaking is consistent with the observation of thin platelets lying on $\{100\}_\alpha$ matrix planes.

The effect of nitriding at lower nitrogen potentials is to cause a slight coarsening of the microstructure. For example, particles of about 6nm diameter are obtained after nitriding in $1NH_3:99H_2$ at 575^oC (see Fig. VI.2(b)). This micrograph has a $\{311\}$ orientation and it can be seen that some of the particles show a reversal of contrast due to changes in diffraction conditions occurring across the bend contours of the foil.

The particles are visible as a result of matrix strain contrast arising from the elastic distortion of the matrix near the particle. This suggests that the fine platelets are coherent with the matrix, because both coherent GP zones and coherent precipitates produce similar images (Nicholson & Nutting 1958: Phillips & Livingstone 1963).
The lobes are the coherency strain fields

around the zones or precipitate, and not the particle itself, which is invisible.

Several other facets associated with the electron metallography of small, coherent particles are visible in Fig V1.2. The line of no contrast varies in direction from one contour to another, due to changes in diffraction conditions. Also,the complete reversal of contrast is visible in Figure V1.2(b) due to very small particles on either side of a thickness extinction contour. The appearance of unusually wide, assymmetrical images occurs from particles which are within about half an extinction distance of the foil surface. The sense of the assymmetry depends upon whether the particles are near the top or the bottom of the foil and is due to surface relaxation of the strain field.

Table V1.1 shows the nitrogen contents obtained after nitriding Fe-V alloys to saturation under various conditions. The N/V ratios have been calculated assuming that the ferrite is in equilibrium with the nitriding atmosphere and so excludes the matrix nitrogen. Some of the data for the higher alloys is taken from Pope (1972). The effect of nitriding the Fe-0.15 at.%V alloy in a constant potential (a_N = 0.046 at.%) at varying temperatures, is to increase the N/V ratio as the temperature increases; similary, increasing the nitrogen potential at constant temperature increases the N/V ratio.

TABLE VI.1

NITROGEN CONCENTRATIONS OF NITRIDED Fe-V ALLOYS

	nitriding conditions		at.% N		
at.%V	$\%NH_3$	temp °C	$[N]_\alpha$	N Total	N/V
0.15	2.7	550	0.046	0.108	0.41
0.15	1	575	0.020	0.10	0.53
0.15	2	575	0.046	0.156	0.73
0.15	3	575	0.068	0.20	0.88
0.15	5	575	0.122	0.31	1.25
0.15	1.5	650	0.046	0.172	0.84
0.52	10	575	0.26	1.01	1.44
1.08	10	575	0.26	1.65	1.29
1.08	0.6	700	0.046	1.08	0.96

These results can be explained in one of two possible ways: either,

i) the particle composition varies with nitriding conditions; or

ii) the particles are of fixed composition and the precipitate density increases with nitriding potential and temperature.

Hahn (1949) has shown that vanadium nitride has a range of stoichiometry extending from $VN_{0.71}$ to $VN_{1.0}$. Therefore, at the lowest nitriding potentials the N/V ratios are less than these expected for VN precipitation, whereas nitriding at 575°C in $5NH_3$:$95H_2$ produces a ratio of 1.25. Consequently, nitrogen in excess of that required to form equilibrium VN can be accommodated in the matrix. This phenomenon is typical of that found in the higher vanadium alloys nitrided at 450 - 650°C (see Pope, 1972) and is frequently associated with homogeneous precipitation in Fe-X-N alloys.

The excess nitrogen can be accounted for if a N/V ratio of >1 is present in the initial particles, or if it is accommodated in the extensive coherency strain fields around the rim of each particle. Previous work by Pope (1972) showed that in the higher vanadium alloys the extent of the strain fields was such that the structure was irresolvable. Also, matrix lattice parameter measurements were high, indicating the presence of exceptionally high nitrogen concentrations in the matrix. Therefore, the presence of excess nitrogen could support the arguement for the formation of solute atom clusters, possibly containing iron and having N/V ratios greater than one.

However, Podgurski & Knetchel (1969) have noted excess nitrogen in the Fe-Al-N system, where Al/N nucleates heterogeneously on dislocations, generating fresh dislocations, as the particles coarsen. They suggest that part of the excess nitrogen can be accommodated at these dislocations and that the remainder is associated with the particle-matrix interface. Consequently, the presence of excess nitrogen does not necessarily support the arguement for the formation of solute atom clusters, since it can be accommodated equally well in the coherency strain fields, as trapped in dislocations around inchorent precipitates.

Internal friction measurements (see chapterV) of Fe-X-N alloys confirms the absence of any nitrogen in normal Snoek sites when small, coherent particles are precipitated. However, anamolous high temperature peaks arise and can be explained in terms of the excess nitrogen being in higher energy sites, i.e. in strained areas of the matrix. Therefore, it appears that the excess nitrogen is trapped in the coherency strain fields around the first formed particles.

The size and coherence of the particles observed in the Fe-0.15 at.%V alloy could support the hypothesis that they are truly in solution, the large chemical interaction between vanadium and nitrogen in iron ensuring that the nitrogen potentials required for their formation are lower than in other Fe-X systems. However, measurements of the yield strength increments (see Chapter VII) show that at the higher nitriding potentials, the excess nitrogen only marginally contributes to the strengthening above that expected from nitrogen in random solid solution.

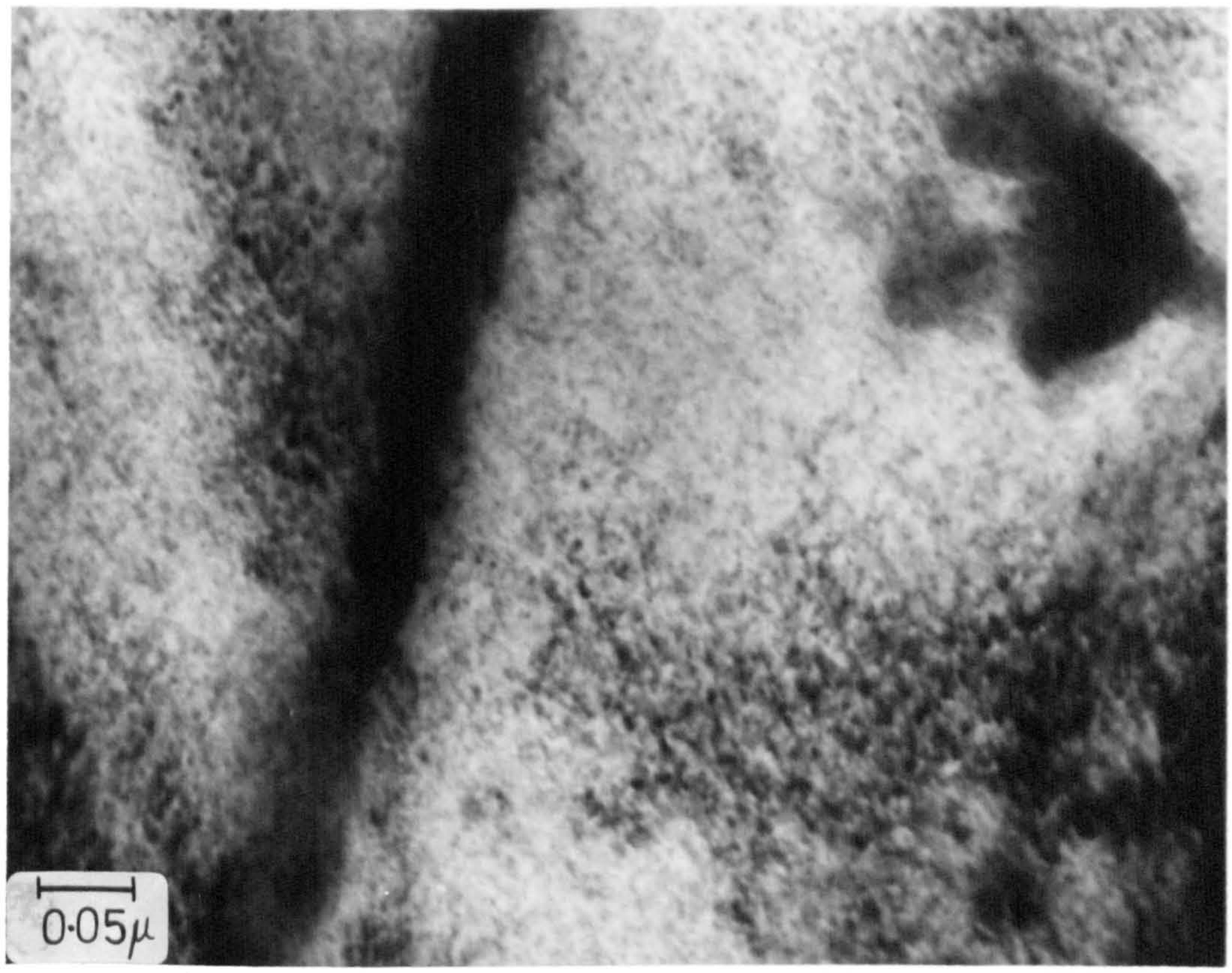
Therefore, it appears that both the initial structure and volume fraction of the precipitated phase remains constant provided complete precipitation of vanadium occurs. Only at the lowest nitriding potentials does a decrease in strength occur, and this would be consistent with the low N/V ratios observed at these potentials.

In any alloy system where homogeneous precipitation takes place, it is expected that a solvus exists below which precipitation ceases. In the Fe-0.15at.%V alloy this was found after nitriding in $1NH_3:99H_2$ at 550°C, since no hardening developed during normal times. Electron metallography of the samples confirmed the absence of any precipitation. Above this solvus a high density of zones are formed, although there is a range of potentials where the precipitation of vanadium is incomplete. From Table VI.1 it is apparent that the temperature plays a very important role in determining the solvus for homogeneous precipitation. At 550°C precipitation is more difficult, due to the lower diffusivity of the substitutional atoms.

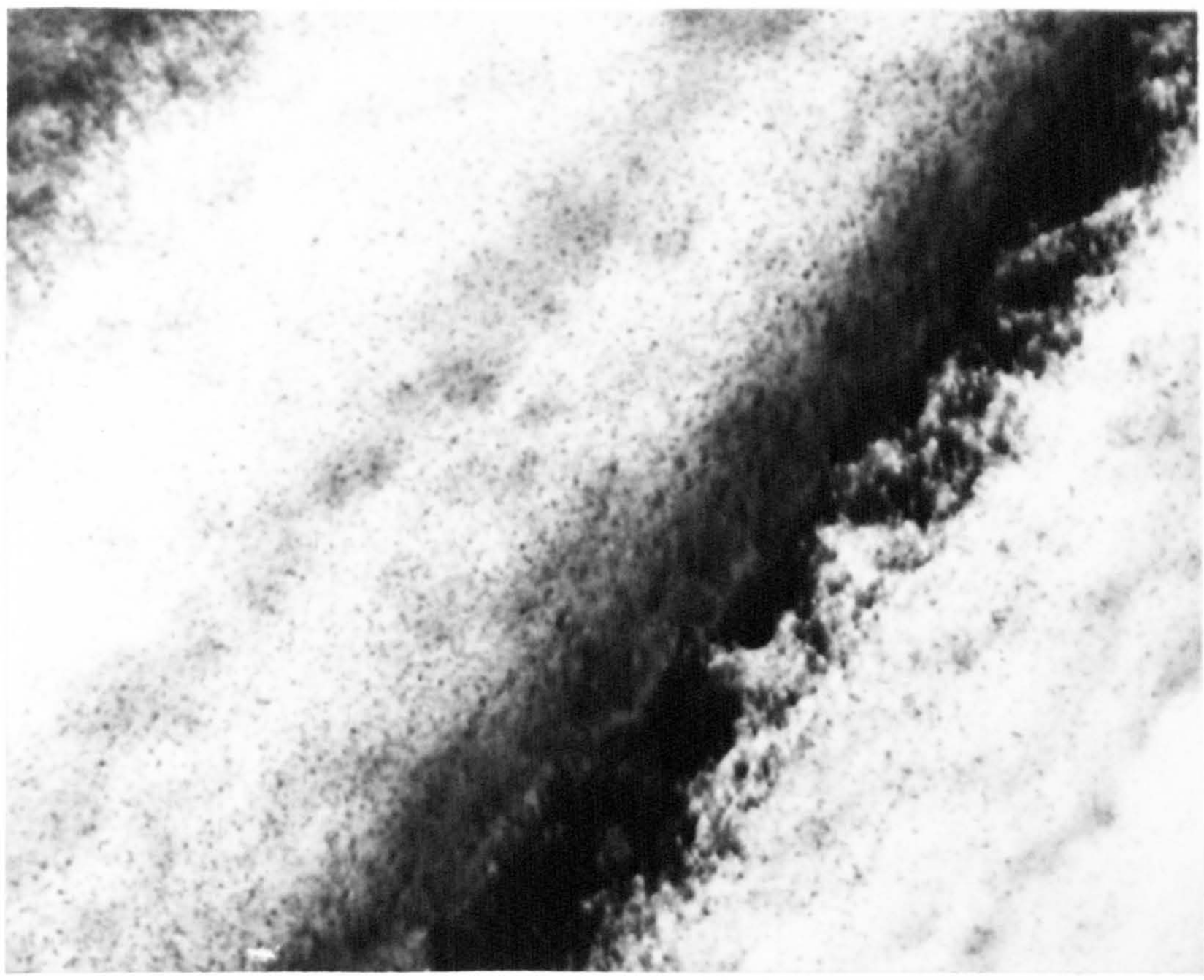
Providing that nitriding occurs above the zone solvus, the initial particles form after very short times. For example, after nitriding a thin foil (0.1mm thick) for only 0.5 hrs at 575°C in $5NH_3:95H_2$, clustering has commenced, the structure having a 'modulated' type of appearance (see Fig.VI.3(a)). Despite the short nitriding time, some very small particles of only 3nm diameter are detectable. Subsequent ageing of this structure in vacuo for 16hrs at 575°C causes the particles to become distinct, (see Fig.VI.3(b)). These observations confirm that provided the nitrogen is in the alloy, the particles continue to grow in an environment free of nitrogen, the initial clustered part-

Fig. VI. 3

(a)



(b)



a) Nitrided for 0·5 hrs in $5NH_3$:$95H_2$ at 575 °C

b) As a)+vacuum aged for 16 hrs at 575 °C

Electron micrographs showing the initial stages of precipitation in a nitrided Fe-0·15at% V alloy

icles being relatively unstable. Prolonged nitriding under identical conditions to those used for this experiment produces a microstructure similar to that shown in Fig. VI.2(a).

Estimates of the particle densities obtained after nitriding for 0.5 hrs and vacuum ageing, and those after nitriding after 24 hrs both yield values of $\approx 2 \times 10^{17}/cm^3$. Therefore, the prolonged nitriding does not increase the particle density. Consequently, the structure shown in Figure VI.3(a) must be the very earliest stage of homogeneous precipitation, consisting of a clustering of vanadium and nitrogen atoms. The result of further nitriding or vacuum ageing is the formation of discrete particles. It is relevant to note that no electron diffraction effects were associated with Fig. VI.3(a), whereas either continued nitriding or vacuum ageing causes continuous streaking in $\langle 100 \rangle_\alpha$ matrix directions. Measurements of the average particle diameter (see Table VI.2) show that increasing the nitrogen potential decreases the diameter, whereas increasing temperature leads to an increase in diameter. These observations are consistent with those expected from a system producing homogeneous precipitation by a nucleation and growth process. The particle size increases with temperature due to the greater mobility of the atoms; whereas the size decreases with increasing solute content at constant temperature due to the greater supersaturation leading to a finer critical nucleus size.

TABLE VI.2

VARIATION OF PARTICLE DIAMETER WITH NITRIDING CONDITIONS

alloy composition at.%	nitriding conditions		diameter nm.
	$\%NH_3$	temp ^oC	
0.15 V	1	575	6
0.15 V	2	575	5
0.15 V	5	575	4
0.15 V	10	575	3.5max
0.15 V	1	640	8

Estimations of the particle densities obtained after nitriding yield values of 10^{16}–$2\times10^{17}/cm^3$. These values are similar to those observed for GP zones in Al-Cu alloys (Nicholson & Nutting, 1959) and indeed, the densities in the Fe-V-N alloys may be even higher because the size of the particles is such that they are at the resolution limits of the electron microscope. In some of the micrographs, faint images of very small particles are just discernable.

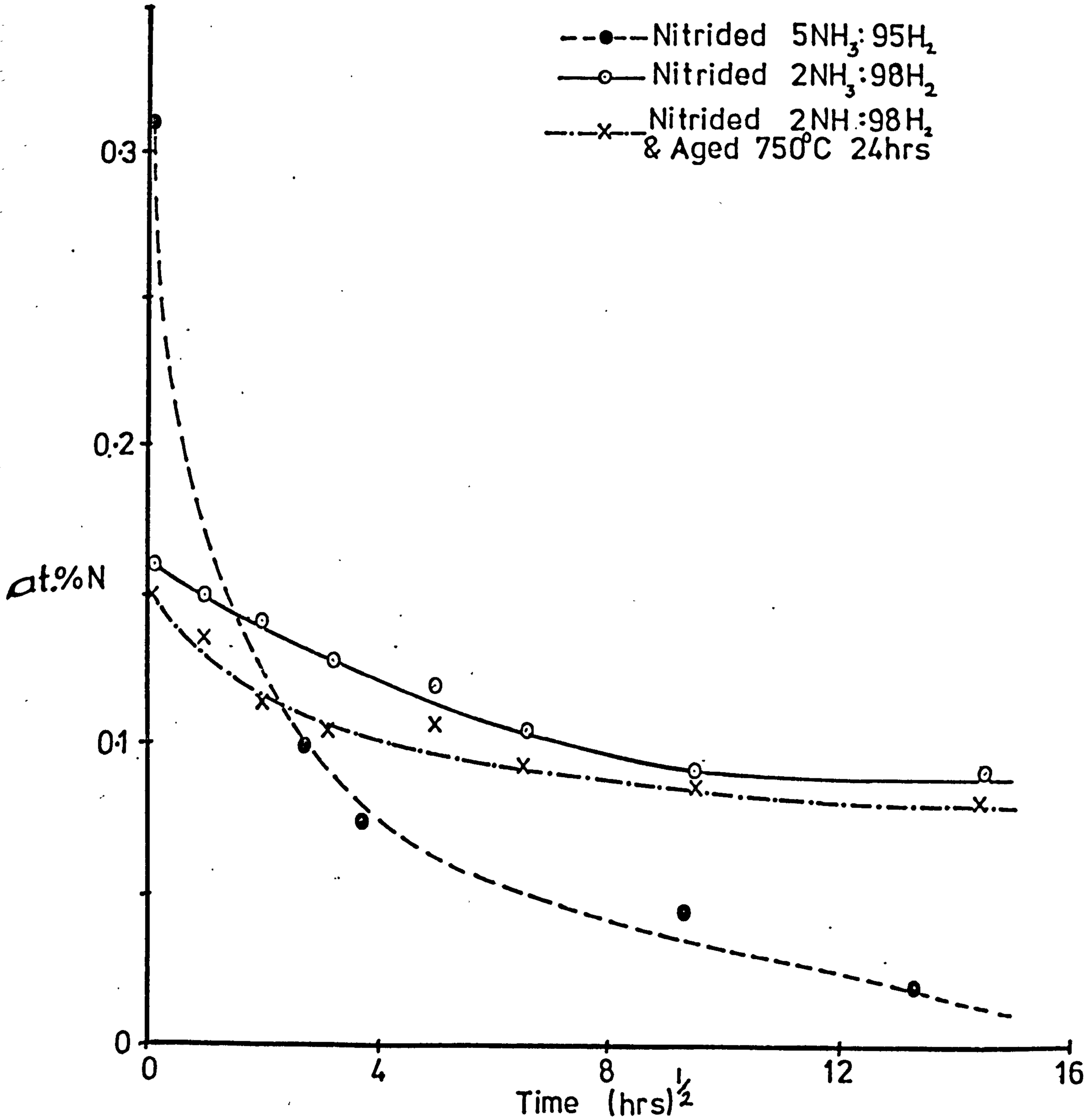
Whilst investigating the nitriding kinetics of the higher Fe - V alloys, Pope (1972) observed that internal nitriding theory was generally obeyed, although some deviation was evident in the lowest alloy (0.52at.%V). The Fe-0.15at.%V is found to nitride without the formation of a hard subscale and consequently, at this alloy content, internal nitriding theory is not obeyed. The behaviour can be explained in terms of the alloy content being so low that the reduced flux and low diffusivity of the substitutional atoms becomes rate controlling. Therefore, internal nitriding theory based upon nitrogen diffusion as the rate controlling factor, is no longer valid. Similar observations have been made in Fe-Cr alloys (Mortimer, 1971), when internal nitriding theory was no longer obeyed in a Fe-1.2at.%Cr alloy. It appears that the larger V-N interaction causes deviation from internal nitriding behaviour to occur at much lower substitutional solute contents than in Fe-Cr alloys.

VI.3 Hydrogen reduction of Fe-V alloys

The behaviour of nitrided alloys in hydrogen, i.e. in a denitriding environment, enables an assessment of the state of combination of nitrogen to be made. For example, Unthank et al (1972) have shown that hydrogen reduction treatment, at 580°C, of the initial clusters in a nitrided Fe-3at.%Mo alloy completely removes the nitrogen after 200 hrs., suggesting that the Mo-N or Fe-Mo-N clusters are less stable than MoN precipitates. Other nitrides, such as VN, might be expected to dissociate at a very slow rate and work by Pope (1972) on the high Fe-V alloys determined that hydrogen reduction treatment only reduced the N/V ratios to unity, i.e. to that expected for VN formation.

The effect of hydrogen reduction on the nitrided Fe-0.15 at.%V alloy is summarised in Fig. VI.4, and is observed to be markedly dependent upon the initial nitriding potential. After nitriding at 575°C in $5NH_3:95H_2$ gas mixtures, to produce 0.32at.%N and a microstructure similar to that shown in Fig. VI.2a hydrogen reduction treatment at 575°C removes all but a trace of the nitrogen after 176 hrs. Initially the rate of removal is rapid, but it continually decreases after about 20 hrs. Electron metallography of the reduced samples confirmed that the initial particles were completely dissolved. By contrast, the hydrogen reduction of the same alloy nitrided in $2NH_3:98H_2$ at 575°C does not remove all of the nitrogen. Although the nitrogen is removed fairly

Fig. VI. 4



Hydrogen reduction of Fe-0·15 at.%V at 575°C

rapidly at first, the rate of removal slows down and becomes insignificant after 40 hrs. Up to this time, the loss of nitrogen is the same as that which was in equilibrium with the ferrite matrix.

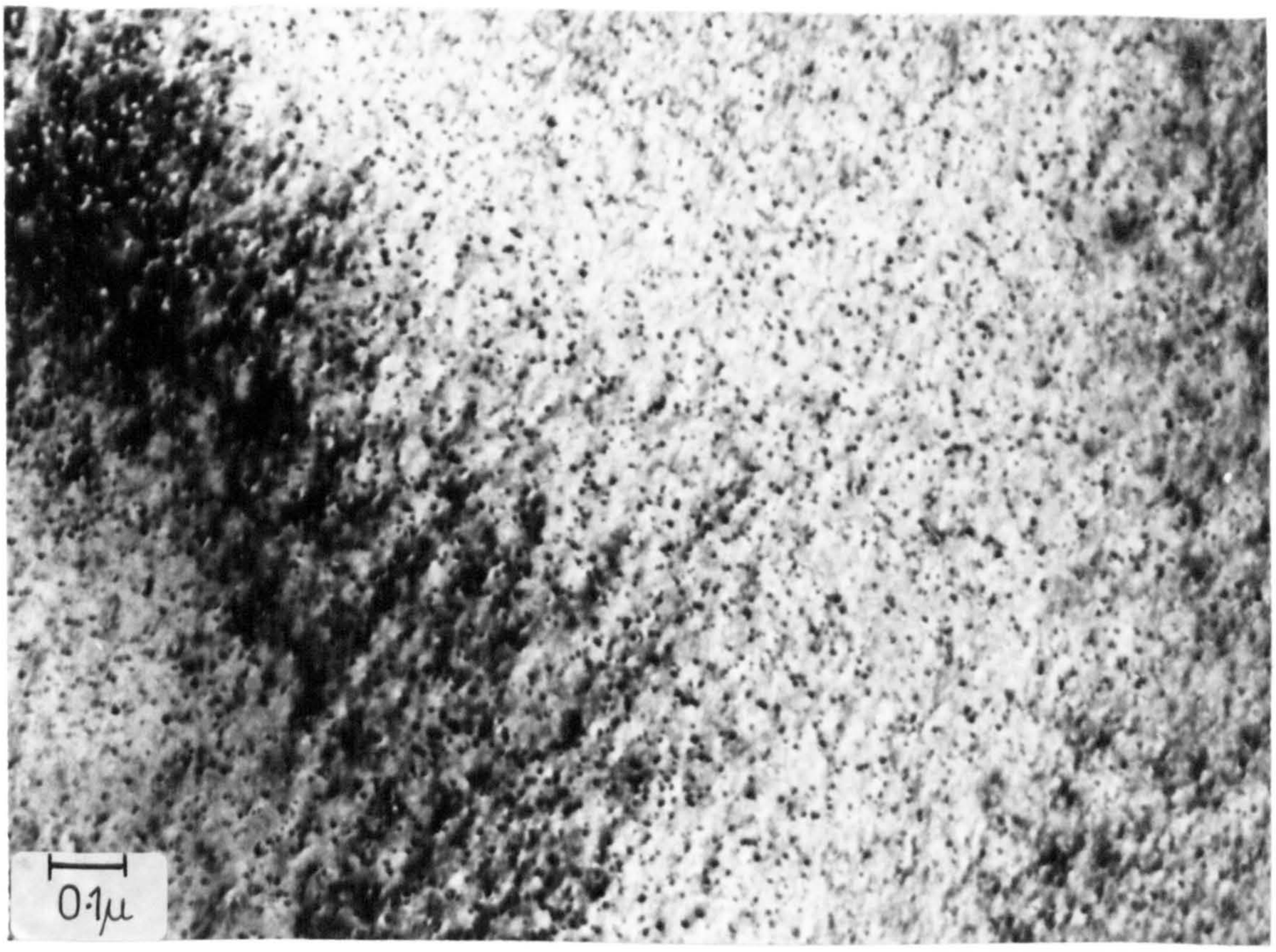
For the purpose of comparison, the behaviour of samples nitrided in $2NH_3$:$98H_2$ at 575°C and subsequently vacuum aged at 750°C for 24 hrs., to produce VN plates of 18nm diameter, is shown. The behaviour is observed to be similar to that of the as-nitrided alloy, suggesting that the initial particles of 5nm diameter are of the same stability as VN plates of 18nm diameter. After nitriding in $2NH_3$:$98H_2$ at 575°C there is 0.156at.%N present in the alloy, 0.046% of which is in equilibrium with the nitriding atmosphere. This leaves 0.11at.%N available for precipitation. After hydrogen reduction for 200 hrs., an average of 0.086at.%N remains in the samples. If one assumes that, initially, all the vanadium is not precipitated, which seems probable at low nitriding potentials, and that a N/V ratio of unity exists in the initial particles, then the N/V ratio decreases to 0.78 after prolonged reduction. This value is still within the range of stoichiometry of VN as calculated by Hahn (1949). Therefore, the particles formed at 575°C in $2NH_3$:$98H_2$ could be coherent VN plates. When all the particles were reduced, their initial size was about 3.5nm diameter. Therefore, these particles, either through their size or composition, are less stable than those of 5nm diameter.

Further experiments confirmed these observations, because after nitriding in $1NH_3:99H_2$ at both 575 and 640°C to precipitate larger particles, the particles were not reduced. Typical micrographs of specimens which have been hydrogen reduced after nitriding in these conditions are shown in Fig. VI.5. No appreciable differences in particle size are observed compared to the as-nitrided alloys.

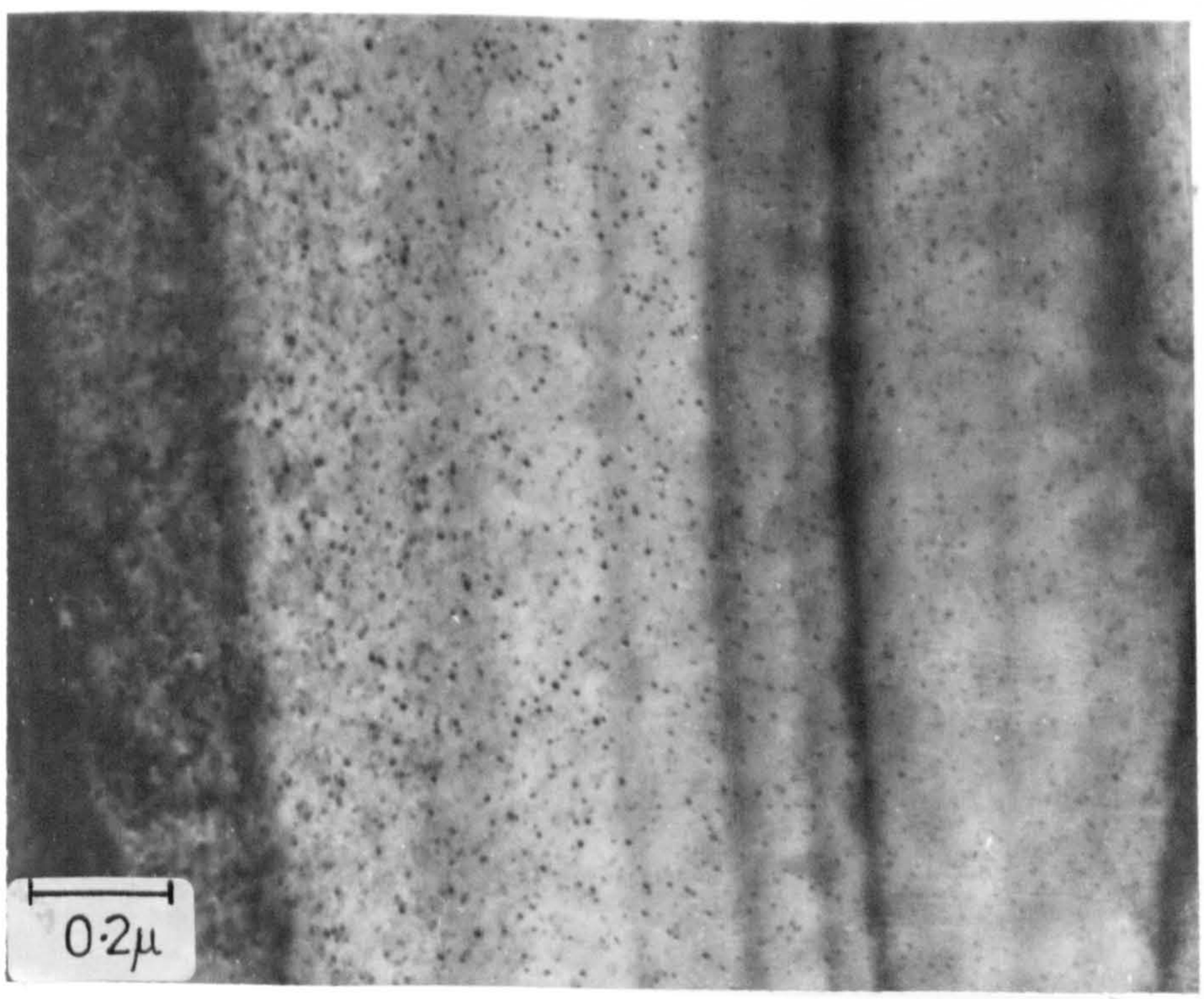
A qualitative explanation of the hydrogen reduction behaviour can be invoked using the observed N/V ratios. When the particles dissolve, they are unstable because the N/V ratio is >1. The higher nitrogen potential required to produce excess nitrogen makes more nitrogen available for precipitation and therefore, allows more to be chemically bound to vanadium. Consequently, smaller clusters are formed, richer in nitrogen, and so they are relatively unstable. At lower potentials, the structure is more stable as a result of each individual nitrogen atom being more tightly bound to vanadium. In fact, a ratio of 1:1 is observed and so the particles could be coherent VN plates, which would explain why they are not reduced at 575°C.

Although Unthank et al (1972) found that the initial zones in Fe-3at.%Mo were completely reduced at 580°C, leaving only molybdenum rich zones, Brenner and Goodman (1971) could only remove 0.4at.%N from a similar microstructure at 500°C. The difference in behaviour can be explained as being due to the lower stability of the zones at 580°C and the consequent increase in the rate of nitrogen removal. This

Fig. VI. 5



(a) Nitrided in $1NH_3:99H_2$ at 575°C + H_2 reduced for 6hrs at 575°C



(b) Nitrided in $1NH_3:99H_2$ at 640°C + H_2 reduced for 250hrs at 575°C

Electron micrographs of hydrogen reduced Fe-0·15at.%V

behaviour is comparable to that observed in the Fe-0.15 at.%V alloy, where the particles are unstable and are rapidly removed when they are less than 3.5nm in diameter.

VI.4 Homogeneous precipitation in Fe-Nb alloys

Three Fe-Nb alloys containing 0.1, 0.3| and 0.6 at.%Nb respectively, have been nitrided at various temperatures and nitrogen potentials. Nitriding at temperatures below 650°C results in the homogeneous precipitation of small, coherent particles. Fig. VI.6 shows the microstructures developed after nitriding the 0.1 and 0.6 at.%Nb alloys at 550°C in $1NH_3:99H_2$ and $2NH_3:98H_2$ gas mixtures respectively. In the low alloy easily resolvable, coherent particles of 3-6nm diameter are precipitated, whereas detail is obscured due to the high density of particles in the highest alloy. As in the Fe-V alloys continuous streaking is observed on electron diffraction patterns, despite the low volume fraction of solute, confirming the presence of thin zones or precipitates on the $\{100\}_\alpha$ planes.

Table VI.3 summarises the weight increases obtained after nitriding the three alloys in the various conditions. The higher niobium alloy nitrided in low potentials at 550°C is not fully nitrided even after 48 hrs. Prior to nitriding, the Fe-0.6at.%Nb alloy contains particles of Fe_2Nb which under these conditions, transform to δ-NbN (see Roberts, 1970). An estimated 0.3at.%Nb remains in solid solution to

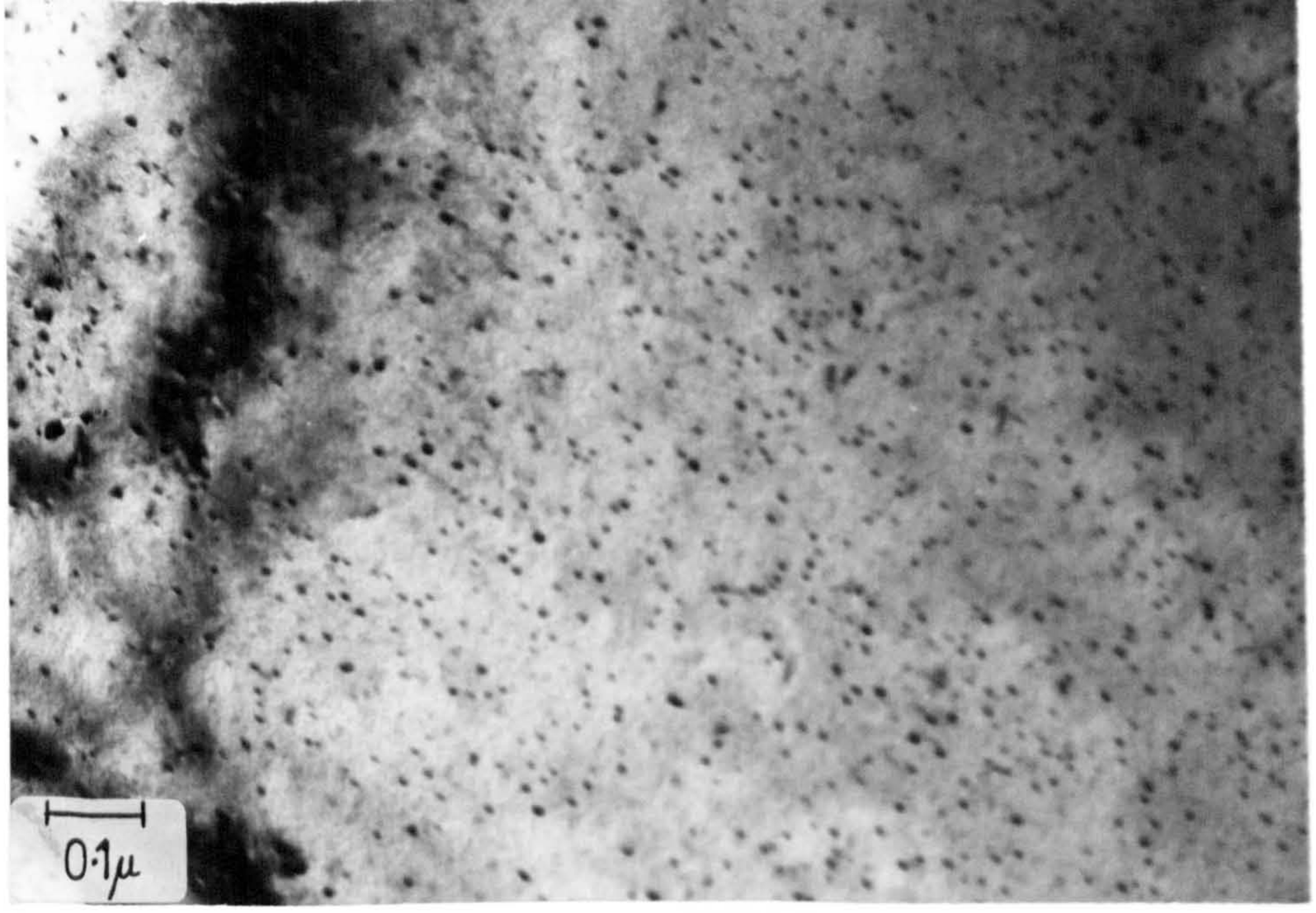
TABLE VI.3

WEIGHT INCREASES OF NIOBIUM ALLOYS AFTER NITRIDING (AT.%N)

nitriding conditions		$[N]_\alpha$	Niobium at.%		
$NH_3:H_2$	temp °C		0.10	0.31	0.60
0.5:99.5	550	0.008	0.06	0.10	0.32
1:99	550	0.016	0.068	0.21	0.46
2:98	550	0.034	0.09	0.212	0.69
2.7:97.3	550	0.046	0.126	-	-
2:98	575	0.046	0.12	0.312	-
0.9:991	650	0.046	0.14	0.352	0.72
0.6:99.4	700	0.046	0.132	0.325	0.67
5:95	575	0.122	0.312	-	-

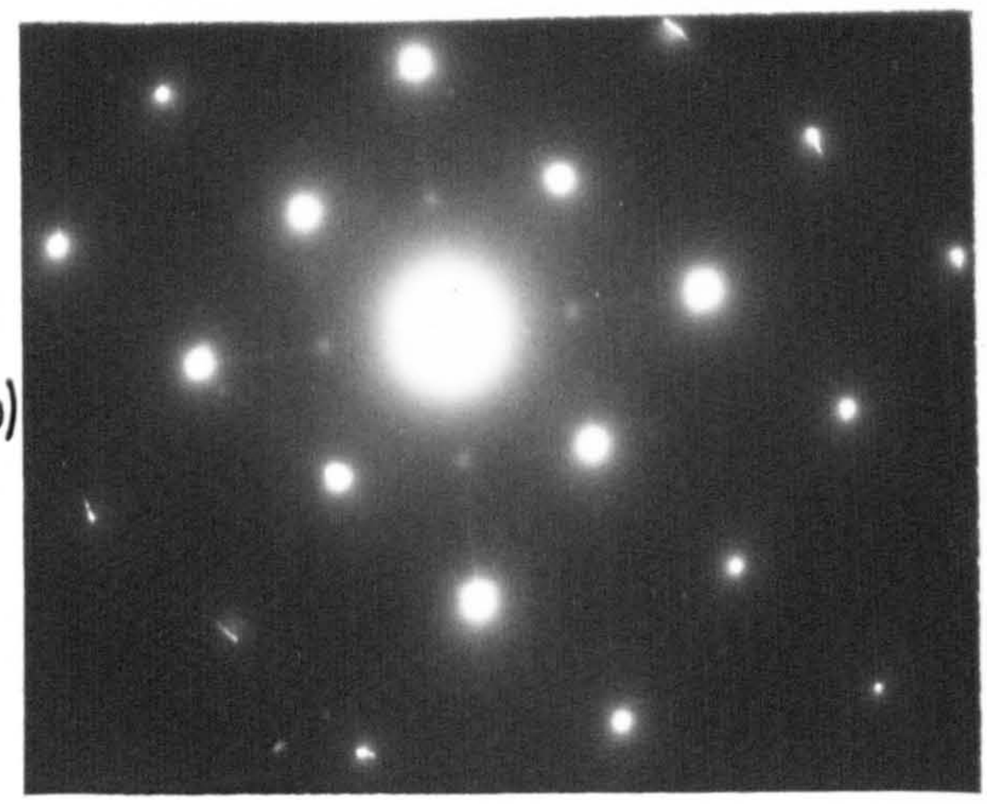
Fig. VI. 6

(a)



(a) Fe-0·1at%Nb nitrided at 550°C in $1NH_3:99H_2$ for 24hrs

(b)



(b) SADP of Fe-0·1at%Nb nitrided at 575°C in $2NH_3:98H_2$

(c)



(c) Fe-0·6at%Nb nitrided at 550°C in $2NH_3:98H_2$ for 48hrs

Electron microscopy of nitrided Fe-Nb alloys

be homogeneously precipitated. As with Fe-V-N alloys the N/Nb ratios vary considerably with nitriding potential. For example, after subtracting the nitrogen in equilibrium with the nitriding atmosphere, N/Nb ratios varying from 1:2 (in $1NH_3:99H_2$ at 550°C) to 2:1 (in $5NH_3:98H_2$ at 575°C) are obtained for the 0.1Cat.%Nb alloy. At the lower potentials it appears that all the niobium is not precipitated, whereas at the higher potential a large excess of nitrogen is accommodated in the strained matrix. Intermediate potentials give varying N/Nb ratios, the general trend being in accordance with a simple zone model, since the ratios increase with increasing nitriding potential. Nitriding at temperatures above 650°C yields ratios close to that expected for NbN formation.

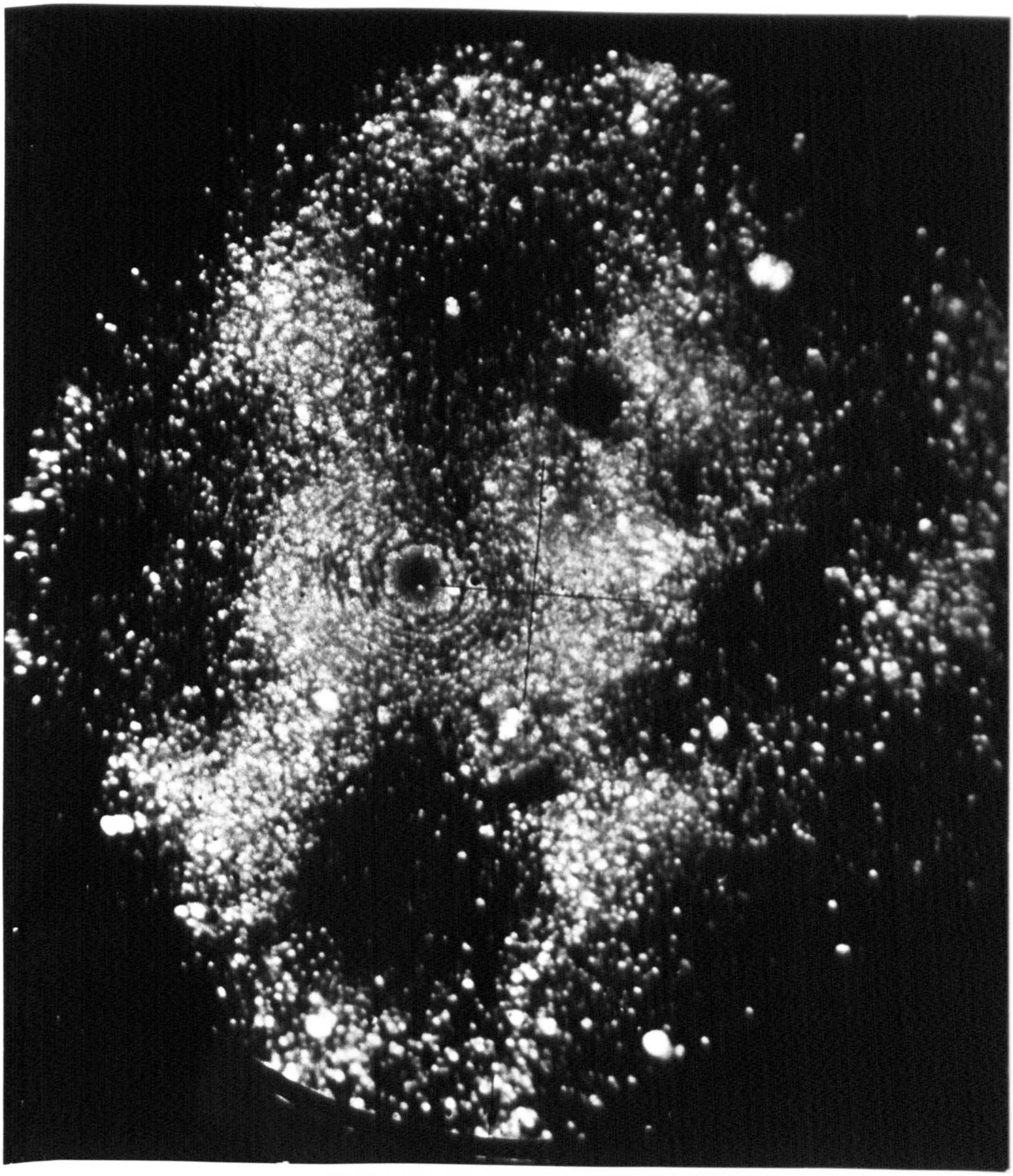
An alternative explanation of the variable N/Nb ratios is that the initial particles have a range of composition and contain an unknown amount of iron. For example, if all the niobium is precipitated at the lowest nitriding potential, then the initial particles must have a composition close to (Fe Nb)N.

In an attempt to obtain more detailed information about the nature of the initial particles, samples of the Fe-0.1 at.%Nb alloy nitrided at 550°C in $1NH_3:99H_2$ have been examined in the field ion microscope. In the field ion microscope, particles of refractory nitrides are observed as regions of bright contrast. This is due to the particles

having a higher evaporation field than the matrix and therefore, a lower radius of curvature at a given voltage. By adjusting the voltage, either the matrix or particles can be brought to the best imaging conditions. Fig. VI.7 shows a typical micrograph obtained after imaging with neon whilst ccoling the tip in liquid helium (20°K). The image diameter is about 100nm. The particles are fairly difficult to image because of the very low volume fraction and small size. However, zones of about 3 - 6nm diameter appear, in the form of bright arcs, as discs on $\{100\}_{\alpha}$. The zones are much smaller than those observed in the Fe-Mo-N system (see Fig. II.9) and are not as clearly imaged. Also, a relatively large number of bright spots are visible, which could be either individual or smaller aggregates of niobium atoms in solid solution. A rough estimate is that 50% of the niobium is in solid solution. The nitrogen content of the alloy, 0.068at.%, is such that the Nb/N ratio is 2:1. Therefore, as much as half of the niobium atoms could remain in solution after nitriding at low potentials. These tentative findings could be interpreted as being due to the formation of a zone of fixed composition, and would explain the relatively low density of zones ($\approx 1 \times 10^{16}/cm^3$) observed in the electron microscope after nitriding in low potentials (see Fig. VI.6(a)).

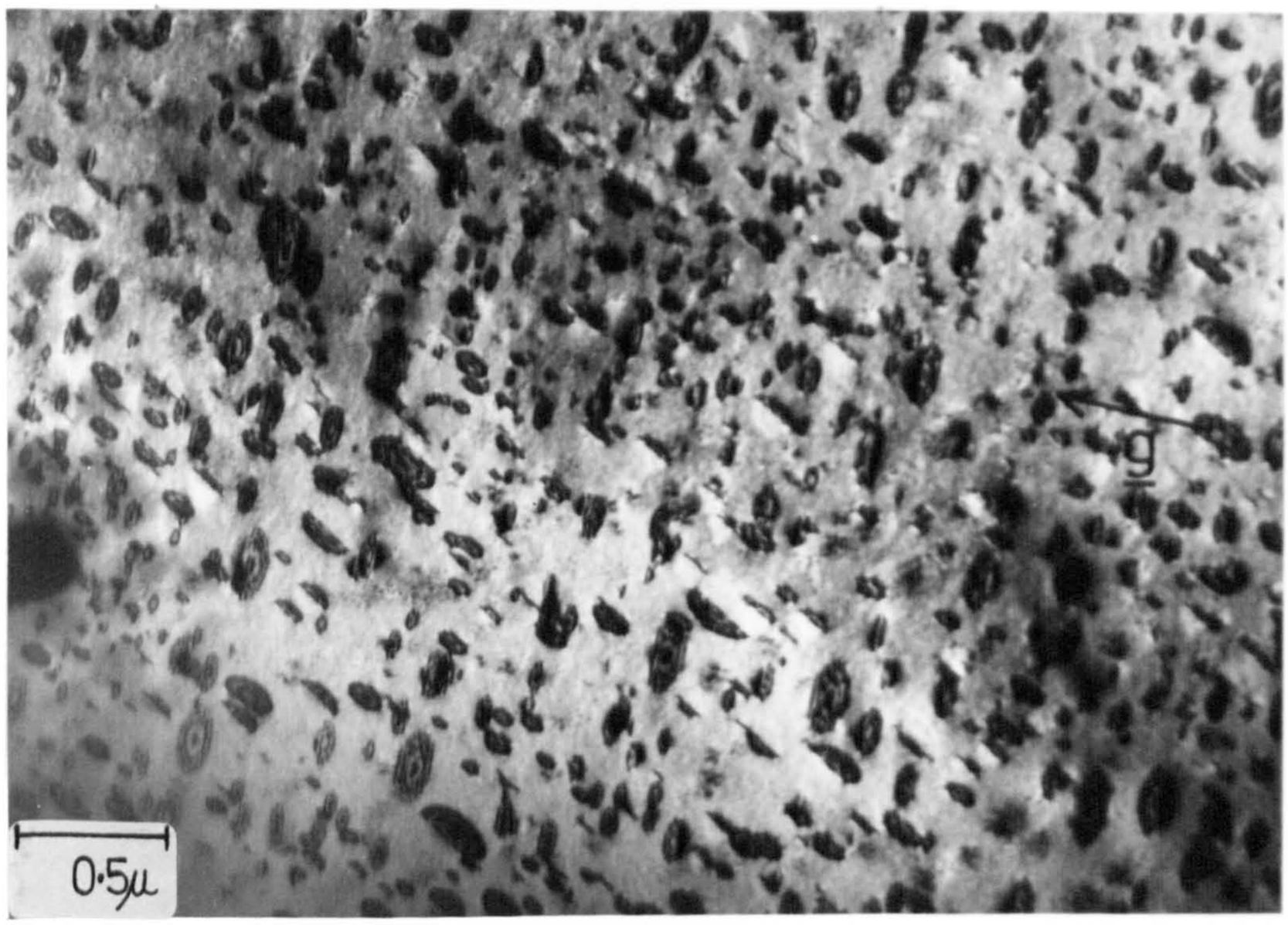
Nitriding Fe-Nb alloys at higher temperatures results in the rapid overageing of particles and precipitation of γ-NbN occurs. Fig. VI.8 shows the microstructures obtained

Fig. VI. 7



Field ion micrograph of Fe-0·1 at.%Nb nitrided at 550 °C in $1NH_3:99H_2$

Fig.VI. 8



(a) Fe-0·1at%Nb



(b) Fe-0·31at%Nb

Electron micrographs of Fe-Nb alloys nitrided at 700°C in 0·6NH_3:99·4H_2

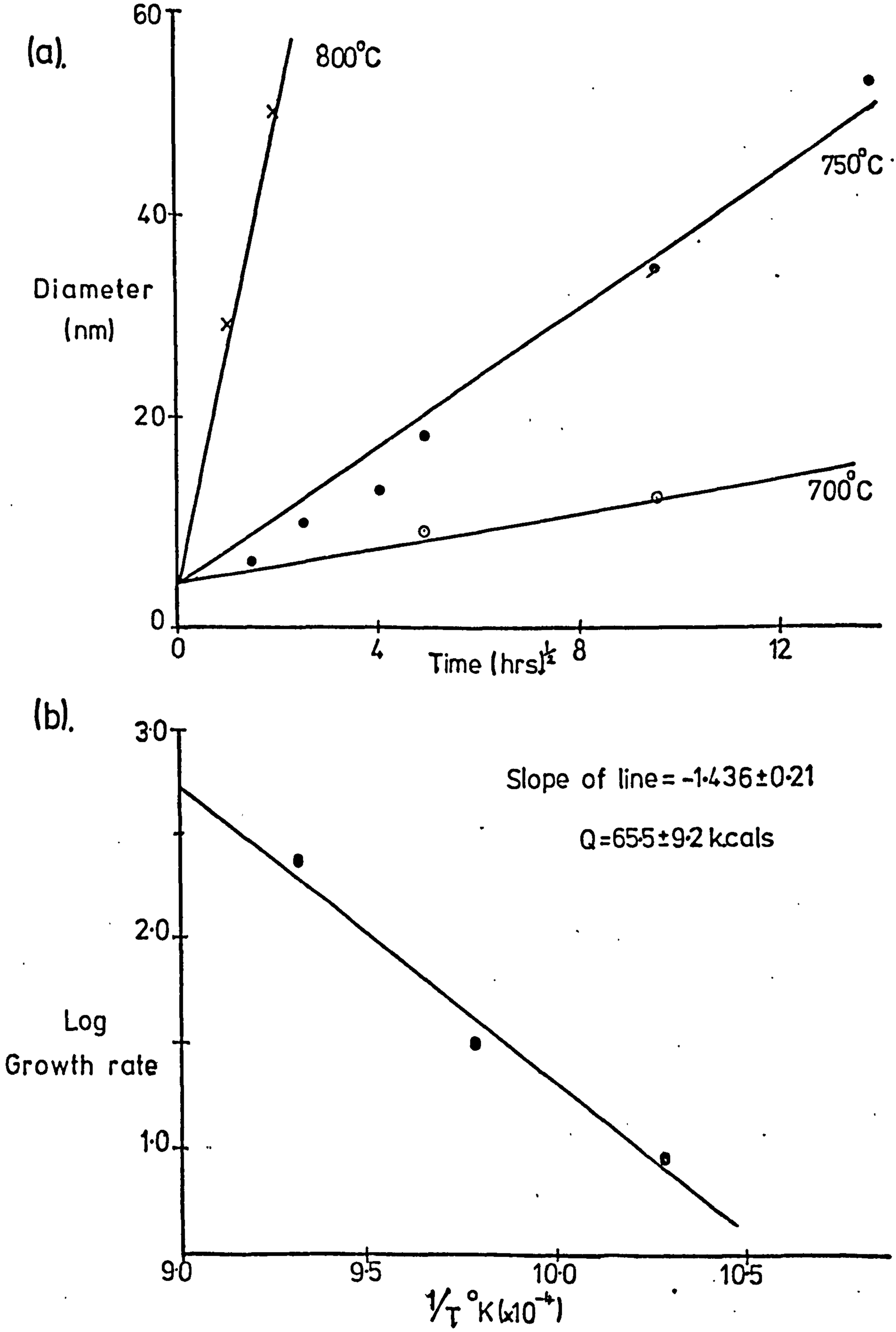
after nitriding the 0.1 and 0.31 at.%Nb alloys at 700°C in $0.6NH_3:99.4H_2$. In the low alloy, homogeneous nucleation of the equilibrium phase occurs, the particles showing displacement fringe contrast due to the foil orientation. Fig. VI.8(b) shows the effect of nitriding the higher alloy in the partially recovered state. Homogenecus precipitation occurs in parts of the matrix but noticeable precipitate free zones are observed near the dislocation sub-boundaries. This behaviour is typical of that expected during nitriding partially recovered alloys at high temperatures.

Heterogeneous precipitation of nitrides is observed on dislocations at high temperatures, since the elastically distorted regions of the dislocation act as preferential nucleation sites. Niobium atoms are large (15% greater than iron) and so segregation to a dislocation leads to a lowering of the elastic strain energy.

VI.5 High temperature ageing

Overageing of Fe-X-N alloys occurs extremely slowly at temperatures below 650°C and so high temperature ageing is necessary to coarsen the initial particles and obtain the equilibrium precipitate. The response to ageing of the Fe-0.15at.%V alloy is shown in Fig. VI.9(a). The data shows that ageing is slow even at 700°C. Prolonged ageing produces a coarser distribution of plates, the diameter of which grows as a function of the square root of ageing time. The particles can be identified as VN at about 12nm diameter and the

Fig. VI. 9



High temperature ageing of nitrided Fe-0·15at.%V

equlibrium phase precipitates with the Baker-Nutting (1959) orientation relationship:

$$(001)_{\alpha} // (001)_{VN} \quad ; \quad [100]_{\alpha} // [110]_{VN}$$

In this way, the misfit in the plane of the disc is small (≈2%), whereas there is a considerable expansion of the ferrite at the edge interface (≈40% misfit). Before discrete VN spots can be identified on electron diffraction patterns, streaking in $\langle 100 \rangle_{\alpha}$ is observed with intensity maxima close to the positions expected for VN reflections.

From the results of the high temperature ageing, it is possible to calculate an activation energy for the rate controlling process. The growth rate of particles follows a typical Arrhenius type equation:-

$$k = A \exp\left(\frac{-Q}{RT}\right) \qquad \ldots\ldots\ldots \quad (VI).1$$

therefore, plotting the logarithm of the growth rate against the reciprocal of ageing temperature leads to a straight line relationship, from which Q can be calculated. Fig. VI. 9(b) shows the results obtained from the high temperature ageing of the nitrided Fe-0.15at.%V alloy. From the slope of the graph, the activation energy for particle growth is found to be 66.5 ± 9.2k cals.

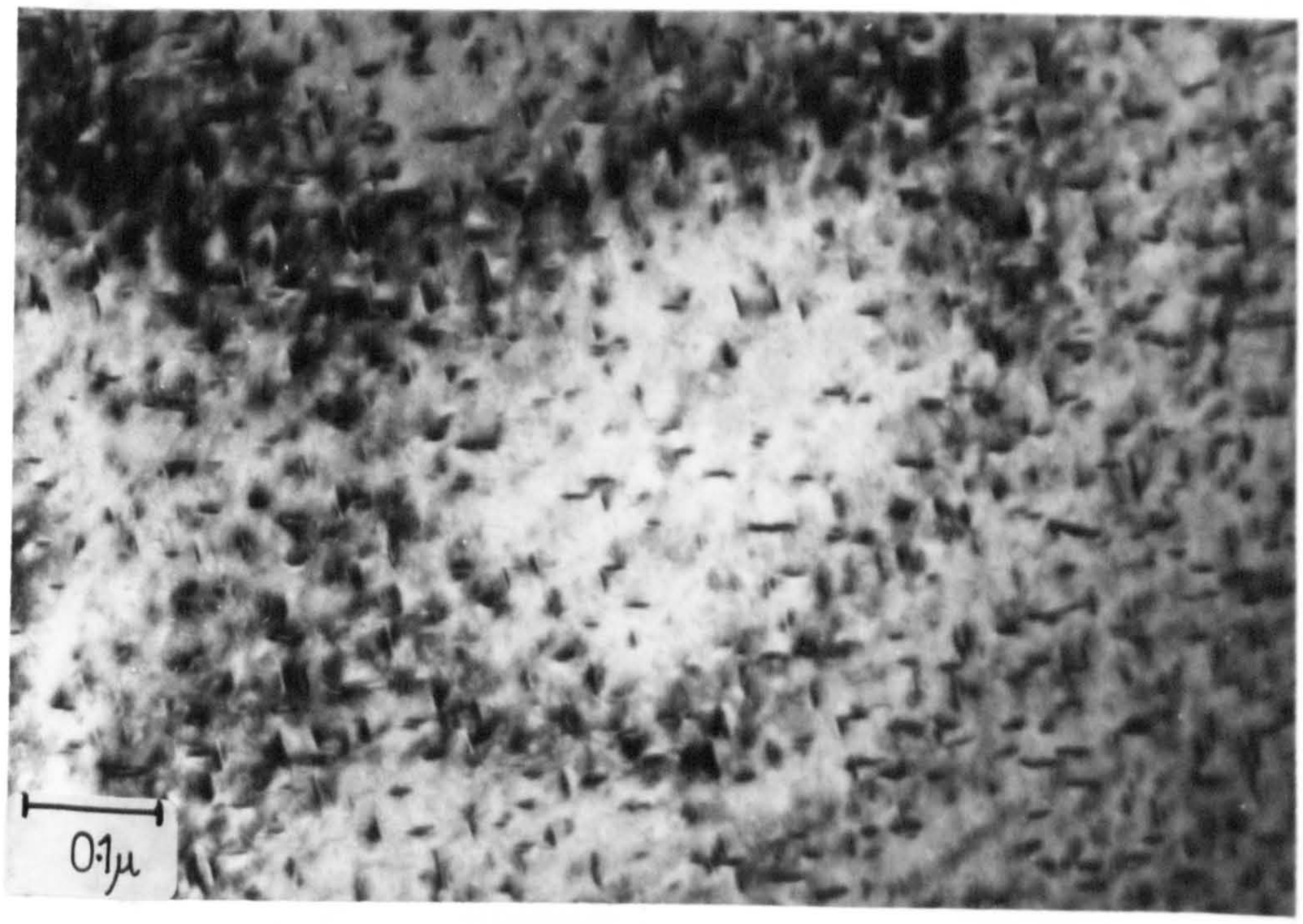
The activation energy for diffusion of vanadium in iron has been determined by Bowen and Leak (1970) using radiotracer

techniques. Values of from 56 to 58 k cals were obtained, depending upon the vanadium content, the energy increasing as the solute content decreased. From the trend of these results, slightly higher values would be expected for vanadium diffusion in a Fe-0.15at.%V alloy. Therefore, the activation energies for particle growth and for vanadium diffusion are similar, confirming that vanadium diffusion is the rate controlling process for particle growth.

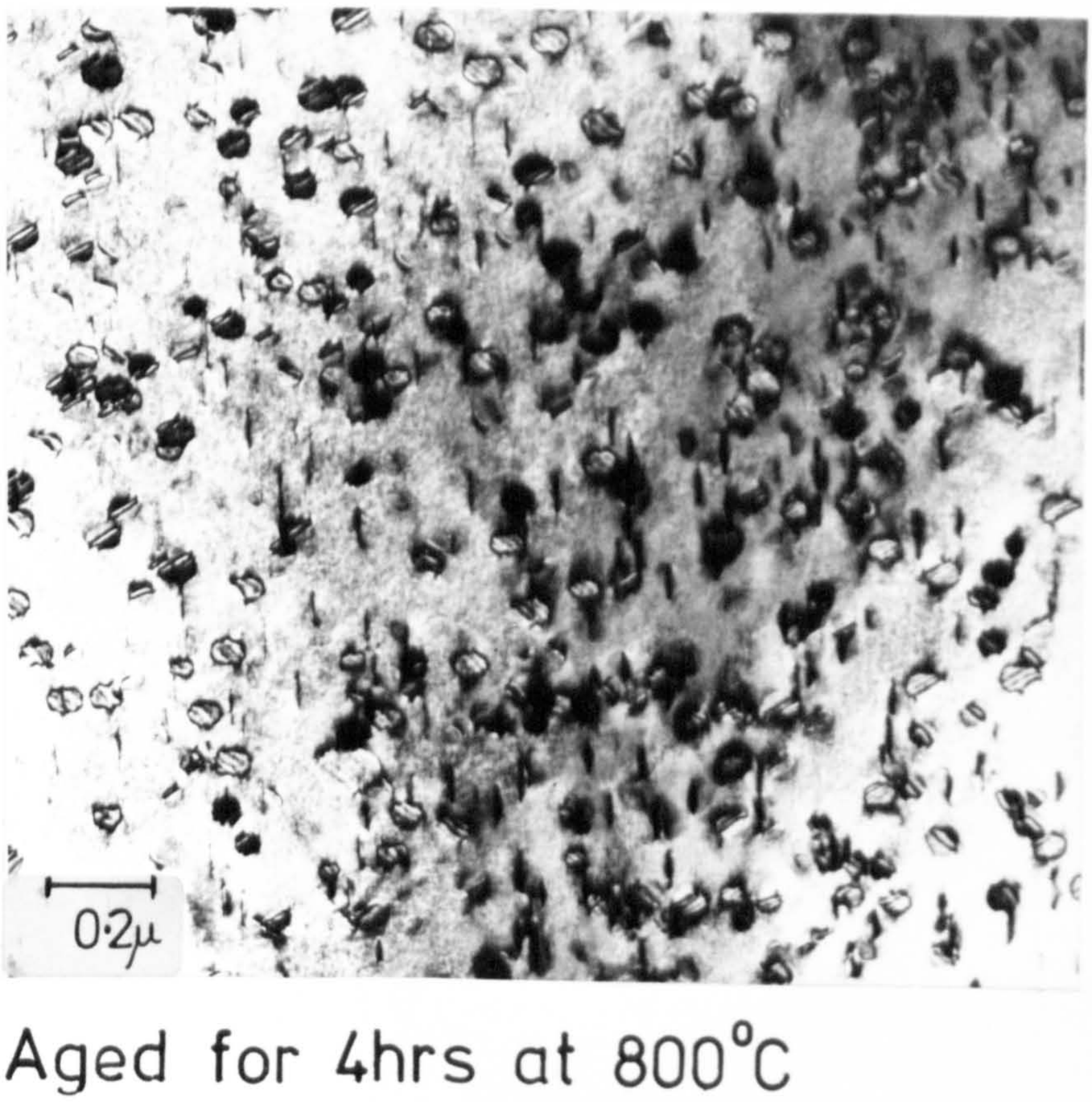
Electron micrographs of the structures observed at various stages of high temperature ageing are shown in Fig. VI.10. The particles in Fig. VI.10(a) are about 12.5nm diameter and are at the stage where they can be identified, from electron diffraction patterns, as VN. However, some of the smaller particles are still coherent at this stage. Raising the ageing temperature to 800°C results in rapid overageing of the particles; for example, after 4 hrs., incoherent VN plates of 50nm diameter are obtained. Interfacial dislocations, which form at the particle-matrix interface, can be seen around the plates which are favourably orientated (see Fig VI. IO (b)).

When particles of a second phase exist in saturated solid solution there is a tendancy for the smaller particles to dissolve, and larger ones grow, by the transfer of solute atoms through the solvent. The driving force for coarsening is derived from the consequent reduction in total interfacial energy. Whilst specimens of the Fe-0.15at.%V alloy were aged

Fig. VI. 10



(a) Aged for 96hrs at 700°C



(b) Aged for 4hrs at 800°C

Electron micrographs of Fe-0·15at.%V nitrided in $5NH_3:95H_2$ at 575°C and aged at high temperatures

at 750°C, studies of the variation of size, distribution and character of the second phase particles have been made (see Stephenson, 1974). Estimates of the particle-matrix misfit strain (ϵ) for the zones were made using the method of Ashby & Brown (1963); only symmetrical images at the exact Bragg condition were examined using $\{200\}$ reflections. A general trend was detectable (see Fig. VI.11), where the as-nitrided specimens, containing particles of 3-5nm diameter, give exceptionally high values of ϵ (20-40%). The strain decreases rapidly as the zones coarsen (5-10% for zones of 10nm diameter) and it is at sizes just beyond this that the equilibrium precipitate can be identified.

VI.6 Discussion

Previous research at Newcastle has established the general conditions under which a precipitation sequence of the form:

mixed clusters on $\{100\}_\alpha$ planes → one or more metastable intermediate precipitates → equilibrium precipitate

occurs in nitrided Fe-X alloys. These are:

i) the alloying element must reduce f^N in iron. This allows a high nitrogen concentration to be obtained after short times and therefore, enables rapid zone formation. By contrast, zone formation is never observed in Fe-Si alloys

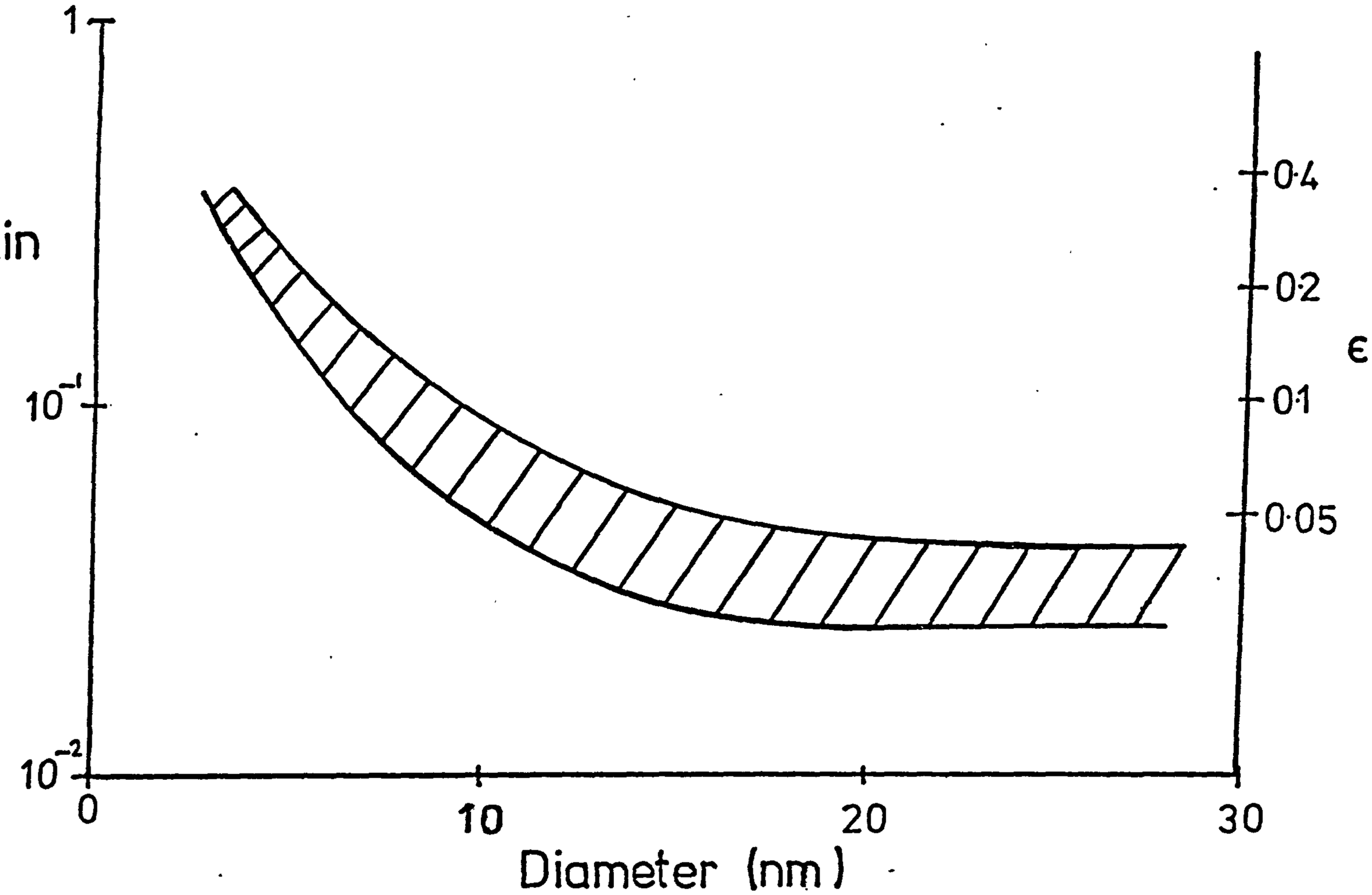


Fig. VI. 11

The variation of matrix strain (ϵ) with particle diameter during ageing of nitrided Fe-0·15at.%V

[after Stephenson, 1974.]

since silicon reduces the nitrogen solubility for a given nitrogen potential (Roberts, 1970).

ii) A critical nitrogen potential and substitutional solute activity must be exceeded, indicating the existance of a zone solvus.

iii) The interstitial solute atom supersaturation must be maintained by constant activity nitriding in the temperature range 450-650°C; for, although the clusters are less stable than the equilibrium precipitate, they form much more rapidly. This is because only very limited diffusion of the substitutional atoms is required.

Precipitation sequences of this type have been observed in Fe-Mo-N (Speirs, 1969), Fe-Nb-N (Roberts, 1970) and Fe-W-N (Stephenson, 1974) alloys. However, nitriding Fe-Cr-N (Mortimer, 1971) and Fe-Mn-N (Johnsson-Holmquist, 1971) alloys failed to give direct evidence of mixed clusters. Observations by Pope (1972) determined that the behaviour of Fe-V-N alloys fell in between these two extremes. Accurate lattice parameter measurements showed that the solute atoms occupied the same sites as in random ferrite. Excess nitrogen was observed during nitriding, although this could have been accommodated as easily in the strained matrix around coherent VN plates as around zones. Continuous ordering is thought to occur in most systems under appropriate conditions and the observation of intermediate precipitates in some systems and not others, is a direct consequence of this ageing process.

For example, in Fe-V-N, Fe-Cr-N and Fe-Ti-N alloys the equilibrium precipitate is f.c.c., and is related to ferrite by the Baker-Nutting (1959) orientation relationship, with a small misfit (≈2%) in the plane of the precipitate and a very large misfit (40% for VN) perpendicular to the disc. The matrix is expanded to accommodate the precipitate, and consequently, large coherency strains are generated. Such precipitates are expected to lose coherency when still very small, and indeed, Driver (1971) has shown by field ion microscopy that Mo_2N, a f.c.c. nitride of similar size to VN, has lost coherency in $[001]_\alpha$ when 1.5-2nm thick.

The formation of an equilibrium alloy nitride precipitate with the Baker-Nutting relationship in ferrite, is the result of complete ordering of the solutes on $\{200\}_\alpha$ planes. Consequently, identifiable equilibrium precipitates are not expected in Fe-V-N, Fe-Cr-N and Fe-Ti-N alloys. Roberts (1970) showed that the equilibrium precipitate in Fe-Nb-N alloys was γ-NbN. The unit cell dimensions (a=4.39Å) are appreciably greater than VN and so the lattice mismatch with ferrite is about 7.5% in the plane of the disc. The significance of this is indicated by the needle like morphology of large precipitates (≈ 300nm), and it is probable that the large misfit gives rise to the intermediate precipitate of body centred tetragonal structure.

Nitriding dilute Fe-V and Fe-Nb alloys enables several modifications to be made to the general principles of homo-

geneous precipitation in Fe-X-N alloys. It is evident that high nitrogen contents and substitutional levels are not essential to enable homogeneous precipitation to occur. Unlike in Fe-Mo alloys, precipitation occurs at low nitrogen potentials and can be attributed to the much larger substitutional-interstitial interactions. In Fe-Mo alloys the existence of a zone solvus was determined by Driver (1972). A similar solvus is found in the low Fe-V and Fe-Nb alloys, although it occurs at very low nitrogen potentials. It is also apparent that a range of nitriding potentials exists during which the amount of substitutional solute precipitated varies.

Electron metallography of the nitrided dilute alloys, reveals a homogeneous distribution of small, coherent particles. From the micrographs, images of the strain fields around coherent particles as small as 2nm diameter and 0.5nm thick can be resolved. Therefore, transmission electron metallography is more sensitive than would appear from the dynamical theory of Ashby & Brown (1963), who conclude that particles of less than 5nm diameter are invisible. A reason for this discrepancy could result from the high matrix strain (20-40%) produced by the particles. Electron diffraction patterns exhibit continuous streaking in $\langle 100 \rangle_{\alpha}$, despite the low volume fraction of solute, and consequently, confirm that the particles are very thin, possibly only two or three atom planes thick. These observations would support the theory that the initial particles are substitutional—interstitial solute atom clusters.

The simplest zone model is one in which the initial particles are considered to be a second phase of fixed composition. The weight increases obtained upon nitriding consist of nitrogen in zones plus the nitrogen in solution which is in equilibrium with the gas mixture. The effect of varying the nitrogen potential should be to increase the volume fraction of zones (because of the X-N solubility product) and to refine the structure (because of the effect on nucleation and coarsening). Both these phenomena are consistent with the observations made during the nitriding of dilute Fe-V and Fe-Nb alloys.

The structures produced are resolvable as discrete coherent particles after nitriding to saturation, although after very short times a type of modulated structure exists (see Fig. VI.3). With higher alloy contents, it would appear that some similarity in structure exists between what can be referred to as a 'modulated' structure and to one containing a high dispersion of very small coherent particles (see Fig.VI.6(c)). A similar structure is observed in a nitrided Fe-0.65at.%Ti alloy (see Fig. V.2).

A coherent interface has an atomic arrangement common to both crystal structures, regardless of the type of atoms in the interface. The lattice misfit strain is accommodated by long range stresses. As the interface grows, the total strain energy must be reduced by the introduction of a dis-

location, whereupon the long range stresses decrease. The loss of coherency occurs either as a result of a dislocation from the matrix being swept into the interface, or from the prismatic punching of dislocation loops by the precipitate.

The simplest geometric criterion for loss of coherency is that attributed to Brooks (1952). A particle of interface length Δt and misfit δ will be coherent if:

$$\Delta t . \delta < \underline{b} \qquad \ldots\ldots\ldots \qquad (VI)2$$

This is actually an underestimate of the critical size in most cases, because of the difficulty of nucleating interface dislocations. Values for the loss of coherency of VN in ferrite using this model are 0.6nm in the plane perpendicular to the disc (large misfit) and 12.5nm in the plane of the disc. An electron metallographic method to determine when an interface becomes incoherent, is to use matrix strain field contrast to obtain values of the matrix strain (ϵ). When an interface becomes incoherent, by the creation of n dislocations of Burgers vector, $\underline{b}$, the value of ϵ measured in a direction parallel to $\underline{b}$, will be reduced to ϵ', where

$$\epsilon' = \epsilon - \frac{n(\underline{b})}{r_o} \qquad \ldots\ldots\ldots \qquad (VI)3$$

and when the particles become incoherent

$$\epsilon' \longrightarrow 0.$$

Therefore, plots of ϵ against r_o should give a sharp drop when coherency is lost. However, since this assumes isotropic loss, which is extremely unlikely in the present instance, a more gradual decrease is expected. Values for the Fe-V-N system containing small, coherent particles have been made by Stephenson (1974), and are shown in Fig. VI.11. Possible sources of error in the measurements are numerous and include both the theoretical treatment, which assumes elastic isotropy and ignores the shear stresses at the particle-matrix interface, and the necessary estimation of the zone thickness when the particles are too small to measure accurately. Both these errors are most significant for small zones of 3-5nm diameter, yet despite this, a general trend is evident. The initial values are considerably in excess of those predicted by Weatherley (1968) for the energetically favourable production of prismatic loops ($\epsilon \geqslant$ 10%). However, the eventual stress relaxation process does not occur by matrix dislocation formation, but by internal loop formation (a lowering of the precipitate volume) and is similar to that observed in other systems having disc-shaped precipitates (Weatherley & Nicholson, 1968; Mitchell, 1971).

The rapid decrease in ϵ with small increases in zone diameter confirms the relative instability of high strains. The mechanism by which ϵ is lowered in the size range 5-10nm is not apparent, but no dislocations are observed in the matrix or in the particles (intrinsic loops). A possible reason would be a change in the zone composition during

coarsening at 750°C, involving either rejection of nitrogen, or by the introduction of vacancies (both of which would allow the zone to relax). When the particles grow to about 12nm diameter, electron diffraction patterns show discrete VN reflections and the particles begin to show evidence of internal vacancy loops. Therefore, the initially formed fully coherent zones grow to incoherent VN at sizes similar to those expected from the calculated method of Brooks (1952).

In the Fe-0.15at.%V and Fe-0.1at.%Nb alloys the N/X solubility product is low at low nitriding potentials, the N/X ratio being only 1:2. In higher potentials values of at least 1:1 are obtained. Therefore, at low nitriding potentials some of the substitutional solute remains in solid solution. For example, after nitriding the Fe-0.1at.%Nb alloy at 550°C in $1NH_3:99H_2$, as many as half of the niobium atoms could be left in solid solution, a fact which is substantiated by field ion metallography. Electron metallography shows a slight refinement in microstructure after nitriding at higher potentials and this is accompanied by an increased volume fraction of precipitated phase. Although the existance of a zone solvus is evident, it appears that the zone composition is fixed and there is a range of nitrogen potentials through which the volume fraction of precipitated phase increases.

The solute content of zones cannot be determined unambiguously by electron metallography because the proportion

of solute remaining in the matrix is unknown. Further difficulties arise because of the small particle sizes observed in Fe-X-N alloys (e.g. 3nm diameter by 1nm thick, see Figure VI.2). At such small sizes the representation of the initial particle depends upon a definition as to where it starts and finishes; a monolayer of VN could be described as a coherent Fe-V-N cluster if one slightly enlarges the boundaries of reference..

The shape of precipitated particles depends upon the ratio of atomic sizes of solute and solvent. If there is little mismatch, for example copper in iron, spheres are formed (Hornbogen, 1964); whereas if differences occur (e.g. f.c.c. nitrides in iron), plates are formed. The governing factor is that the interfacial energy is kept to a minimum. Therefore, in systems of the Fe-X-N type, the precipitation of discs is favoured in order to minimise the strain energy, despite them having a high surface area to volume ratio and being unfavourable from the surface energy viewpoint.

The influence of nitrogen potential on nucleation frequency is characterised in the present low alloys. The particle size increases with temperature and decreases with increasing solute concentration at constant temperature, due to the greater supersaturation leading to a finer critical nucleus size. At higher temperatures diffusion rates are faster and the nucleation of more stable, larger precipitates occurs.

Although there have been numerous investigations into precipitate formation in alloy steels, the exact nature of the initial precipitation stage is poorly defined. This is partly due to the difficulties involved when studying precipitation in a complex matrix, where the driving force for precipitation is continually changing as the solute is depleted. Stephenson et al (1964) found that the strength increases in Mn-V-N steels were due to the precipitation of very fine VN platelets on $\{100\}_\alpha$ planes. The platelets were 10-40nm diameter by 2-9nm thick and some of them were coherent with the matrix. Phillips and Seybolt (1968) observed fine particle formation in a number of binary iron alloys containing 1% Al, Cr, Mn, Mo, Si, T or V as the substitutional solute. After ion nitriding at 550 - 600°C hardening was found in all excepi the molybdenum and manganese alloys. AlN, α-Si_3N_4 and CrN were identified as coarse nitrides, whilst in the vanadium and titanium alloys fine clusters, which could not be unequivocally identified, were observed.

The precipitation of small nitrides and carbides has been detected by numerous investigators in quenched and tempered steels. Tekin and Kelly (1965) observed that during the secondary hardening of pure Fe-V-C alloys, V_4C_3 precipitated either on dislocations or as coherent particles on $\{100\}_\alpha$ planes. From the experimental evidence, the exact mode of V_4C_3 precipitation was not apparent. Earlier work by Smith & Nutting

(1957), using electron metallography, showed that the initial particles were coherent and they proposed that the phase may have been preceeded by the formation of GP zones. Irani and Honeycombe (1963) have claimed that spherical zones, rich in vanadium, form initially; however, other investigators have noticed that in the early stages, the precipitate is 'cloud-like' or 'nebulous' (Pickering, 1957; Seal & Honeycombe, 1958). Subsequently, Smith (1966) observed that the peak hardness in a secondary hardened Fe-1wt.%V-0.2wt.%C alloy was associated with a coherent precipitate only a few unit cells thick and of 10nm diameter.

Objections to the possible formation of zones in secondary hardened Fe - V-C alloys have been made by Tekin & Kelly (1965) on the grounds that:-

(i) vanadium has a high solubility in iron (20% at 500°C), and therefore, in low alloys ($\approx$ 1%) there is no driving force to form zones.

(ii) if the carbon atoms are in solution and not precipitated, then, by virtue of their high mobility at the temperatures concerned and their strong interaction with vanadium, they would be expected to diffuse rapidly to an embryo zone and form V_4C_3.

Obviously such an argument could be applied to Fe-X-N alloys. However, the initial particles in nitrided Fe-X alloys can be very small and they are coherent with the matrix.

Although the zones could be coherent precipitates in Fe-V-N alloys, the presence of a pre-precipitation stage is apparent. In other alloy systems, where there is a lower X-N interaction, the existence of precipitation stages prior to the formation of the equilibrium alloy nitride are more evident.

Vanadium and niobium are two of the most common additions to high strength low alloy steels. After continuous cooling or controlled rolling of these materials, the precipitation of small particles is evident. Early work by Morrison (1963) using transmission electron microscopy, observed a fine precipitate in steels containing small niobium additions ($\approx$ 0.01%). The precipitate was thought to be coherent, a fact which would be substantiated by the fact that he could not extract any precipitate. More recently, Suzuki et al (1970) have observed coherent V_4C_3 in continuous cooled steels, whereas Lambert et al (1970) observed V(CN) precipitates of 3-10nm diameter and in densities of $10^{16}/cm^3$ in isothermally transformed steels.

During transformation, the precipitates form as sheets (interphase precipitation) parallel to the former α/γ boundary and under certain conditions, they can be small and coherent. Interphase precipitation has been studied by numerous investigators, (Davenport et al, 1968; Gray and Yeo, 1968; Tanino & Aoki, 1968; Woodhead & Webster, 1969; Freeman, 1971; Sutton & Whiteman, 1971; Baker, 1973(a)(b)). However, there is considerable debate as to the exact mechanism by

which the particles form and grow. Suzuki & Tanino (1972) claim that dislocation trails act as the nucleating site, whereas most investigators suggest that the particles nucleate heterogeneously at the α/γ interface during transformation, due to the lower solubility in α than in γ iron. An alternative explanation has been proposed by Baker (1973 b·), who advocates that the γ/α transformation causes a supersaturation of vanadium, carbon and nitrogen atoms at the interface, but nuclei are not formed until the interface has passed. In this way, homogeneous precipitation occurs and explains how a high density ($\approx 10^{16}/cm^3$) of coherent particles form, which give rise to diffraction streaking.

In many of these investigations, the particles which form are small (< 10nm diameter) and show the contrast effects expected from coherent particles. Although larger particles will nucleate heterogeneously, it is difficult to understand how high densities of small particles can do so.

Several aspects of the results obtained from homogeneous precipitation studies in Fe-V alloys are comparable to the effects observed in Fe-Ti alloys by Kirkwood et al (1974). The high hardness in nitrided Fe-Ti alloys was associated with the tetragonal distortion of the ferrite matrix produced by nitrogen and by the coherency strains between the matrix and thin plates precipitated on $\{100\}_\alpha$ planes. After annealing at 850°C, softening occurred and TiN plates were identified. From X-ray studies the matrix was observed to

be in great distortion and so it was impossible to determine if the initial plates were TiN or GP zones. More recent work by Kirkwood & Thomas (1976) using electron metallography to study the microstructure of a nitrided Fe-0.3at. %Ti alloy, could not detect any precipitate in as-nitrided alloys containing 3nm diameter particles. However, after ageing for 1 hr. at 800°C, diffraction streaks showed intensity maxima close to the positions where TiN spots would be expected. Measurements of the strain fields around coherent particles gave very large ϵ values (45%) which were interpreted as being due to the precipitation of coherent TiN.

Although X-ray measurements show lattice parameter increases and continuous streaking is observed on electron diffraction patterns, neither technique is sufficiently powerful to detect any precipitate at such small sizes, ($\approx$3nm diameter), as are obtained after nitriding Fe-X alloys. More detailed information about the initial structure of such small particles necessitates the use of atom probe field ion metallography.

A recent study by Dunlop & Turner (1975), using atom probe field ion metallography, of mixed V-Ti carbides in a low alloy steel showed that the initial particles contained some iron, which was rejected upon long term ageing. Particles of about 2nm diameter and four or five atom layers thick were imaged. However, the particles could be identified as precipitated carbides by using dark field electron

metallography. The field ion metallography of a Fe-3at,%Mo alloy (Driver and Papazian, 1973) has given evidence of mixed cluster formation in Fe-Mo-N alloys, the clusters possibly having a composition of $Fe_{10}Mo_6N_2$. Similar observations by Brenner & Goodman (1971) on the mechanism of nitride formation in Fe-3at.%Mo after nitriding at 480°C, have determined a composition of Fe_3Mo_3N from the atom probe spectrum.

Therefore, there is substantial evidence to suggest that mixed clusters are formed in Fe-X-N alloys during the initial stages of particle formation. Obviously, the composition of the initial clusters, the size when they become stable particles, and whether they form an intermediate precipitate on subsequent ageing, will depend on numerous variables, including:-

i) the interaction between the particular substitutional solute and nitrogen

ii) the substitutional solute content

iii) the nitriding time, temperature and potential

iv) the structure of the equilibrium precipitate.

More detailed information about the initial clustering process will necessitate the use of resistivity measurements and atom probe field ion metallography in any future investigations.

VI.7 Conclusions

a) In dilute Fe-V and Fe-Nb alloys, homogeneous precipitation of coherent particles occurs on the ferrite {100} planes. The first formed particles are thin discs of only

3nm diameter and two or three atom planes thickness.

b) Despite the low volume fraction of solute, a high density of particles forms (10^{16}-$2x10^{17}/cm^3$) which cause continuous streaking on electron diffraction patterns in <100>α.

c) The N/V and N/Nb ratios vary depending upon the nitriding potential and temperature. At low potentials it appears that some of the substitutional solute remains in solid solution, whereas at higher potentials excess nitrogen is accommodated in the strained matrix.

d) Field ion metallography of the Fe-0.1at.%Nb alloys confirms that some niobium is left in solid solution after nitriding at low potentials, and that the shape and size of the zones are the same as those determined by electron metallography.

e) The particles grow as a function of the square root of ageing time and lose coherency at about 12nm diameter. The rate controlling step for particle growth is diffusion of the substitutional solute.

f) Hydrogen reduction behaviour of the Fe-0.15at.%V alloy depends upon the initial particle size, particles of $\leq$3.5nm diameter being completely reduced.

Chapter VII

MECHANICAL PROPERTIES OF Fe-X-N ALLOYS

VII.1 Introduction

The mechanism of hardening steel by the precipitation of iron nitrides and carbides in a small dispersed form, has been used extensively in the quench and tempered and strain aged conditions. Recently, the combined additions of nitrogen and a substitutional solute, (often vanadium or niobium), have been found to improve the properties of a wide range of commercial steels in both the as rolled and the quench and tempered conditions. The strength increases are associated with fine scale precipitation of either nitrides, carbides or mixed carbo-nitride phases. However, the exact nature of the strengthening mechanism and the initial precipitation stages are not well defined, due to the problems of working in a complex matrix where the precipitate stability and size are continuously changing. These problems have been avoided in the present investigation by constant activity nitriding pure Fe-X alloys, under conditions where the structures are stable, and in a fully annealed matrix.

When alloy ferrites are nitrided to produce high volume fractions of zones or precipitates they become very hard and brittle, invariably fracturing before yielding. Such properties are of limited use, except in circumstances where the

high surface hardness give the requisite wear and abrasion resistance. To obtain potential strength increments in a wide range of steels by nitride precipitation, the study of dilute Fe-X-N alloys is advantageous, especially when strong interactions occur between the substitutional and interstitial solutes. The most suitable systems are those with either vanadium, niobium or titanium as the substitutional solute, since low nitrogen potentials, (e.g. $1NH_3:99H_2$ at 575^oC), enable the precipitation of a high dispersion of small ($\approx$ 3nm diameter) coherent, disc-shaped particles (see Chapter VI).

Previous work by Roberts (1970) has shown that a high hardness and yield strength are developed by the GP zone structure in a nitrided Fe-0.6at.%Nb alloy. The properties persisted after several hours overageing at temperatures approaching 700^oC, but decreased rapidly after ageing at 800^oC when the equilibrium precipitate, γ-NbN, formed. Despite the large strength increases obtained in alloys containing 0.5 - 1.0 at.% substitutional solute, the present investigation is primarily concerned with the mechanical properties of dilute iron alloys, where the substitutional solute content is similar to that used in many high strength low alloy steels ($\approx$ 0.1at.%).

VII.2 Experimental

Specimens for mechanical testing were prepared by hot

rolling to 2mm thick plate, followed by cold rolling to 0.75mm. Flat tensile specimens having a gauge length of 20mm were then stamped out from the rolled plate. Prior to nitriding, the specimens were degreased and annealed in purified hydrogen at 780 - 900°C in order to achieve a constant grain size of A.S.T.M. 7-8. Tensile tests were performed at a constant strain rate of $4.2 \times 10^{-4} sec^{-1}$, at both room and elevated temperatures, using an Instron testing machine (see Chapter III.10).

VII.3 Mechanical properties of Fe-V-N alloys

Fe-V alloys, with alloy contents varying from 0.15 - 1.1at.%V, have been nitrided at various nitrogen potentials from 550 - 700°C. After nitriding the 1.1at.%V alloy at 550 - 650°C, to produce a microstructure containing a high density of small coherent particles, microhardness increases of up to 700 kg/mm^2 are obtained. However, an evaluation of the mechanical properties is impossible, because the samples invariably fracture before yielding upon tensile testing. Suitable nitriding conditions which enable the yield strength of the higher alloys to be measured are obtained after nitriding at high temperatures and low potentials, thereby producing coarser precipitates of the equilibrium phase. For example, after nitriding the Fe-1.1at.%V alloy in $0.6NH_3$: $99.4H_2$ at 700°C to produce coarse VN precipitates of 40 - 120nm diameter (see Fig.VI.1), 0.1% Proof Stress (P.S.) values of 690 N/mm^2 are obtained. Under these conditions

1.10at.%N is present in the samples and consequently, they are still relatively brittle.

These initial results on Fe-V alloys showed that the precipitation of a high volume fraction of second phase particles strengthens the metal to such an extent that an interpretation of the mechanical properties is impossible in alloys containing above 0.5at.% substitutional solute. More informative results are obtained after nitriding the Fe-0.15at.%V alloy at temperatures in the range 550 to 650°C.

Some typical properties are given in Table VII.1. Strength increases of 345 - 675 N/mm^2 are obtained above that of the as-annealed alloy. The proof strength is seen to increase with increasing nitrogen potential at constant temperature, whereas increasing temperature at a constant potential lowers the strength. Despite the low solute content, most of the samples have a very poor ductility, and it is noticeable that fracture often occurs before the ultimate tensile strength is reached.

An interesting feature is observed after nitriding for various times at 575°C in $5NH_3:95H_2$. Nitriding to saturation (0.31at.%N) raises the strength to a very high level (755 N/mm^2) and fracture occurs immediately after yielding. However, nitriding for only 3 hours to produce 0.12at.%N, results in a lower yield strength together with appreciable ductility, enabling a higher fracture strength to be reached.

TABLE VII. 1

MECHANICAL PROPERTIES OF NITRIDED Fe-0.15 at % V

Nitriding conditions			at.%N	$[a_N]_{\alpha Fe}$	0.1%P.S. (N/mm^2)	U.T.S. (N/mm^2)	% El
temp °C	$\%NH_3$	time (hrs)					
As-annealed			-	-	80	240	35.5
575	1	24	0.08	0.02	425	565	13.0
575	2	24	0.16	0.046	630	595*	0.4
575	5	3	0.12	0.122	522	780*	10.4
575	5	24	0.31	0.122	755	755*	0.1
600	1.5	10	0.16	0.046	575	600*	0.9
650	0.9	6	0.17	0.046	445	560*	0.65

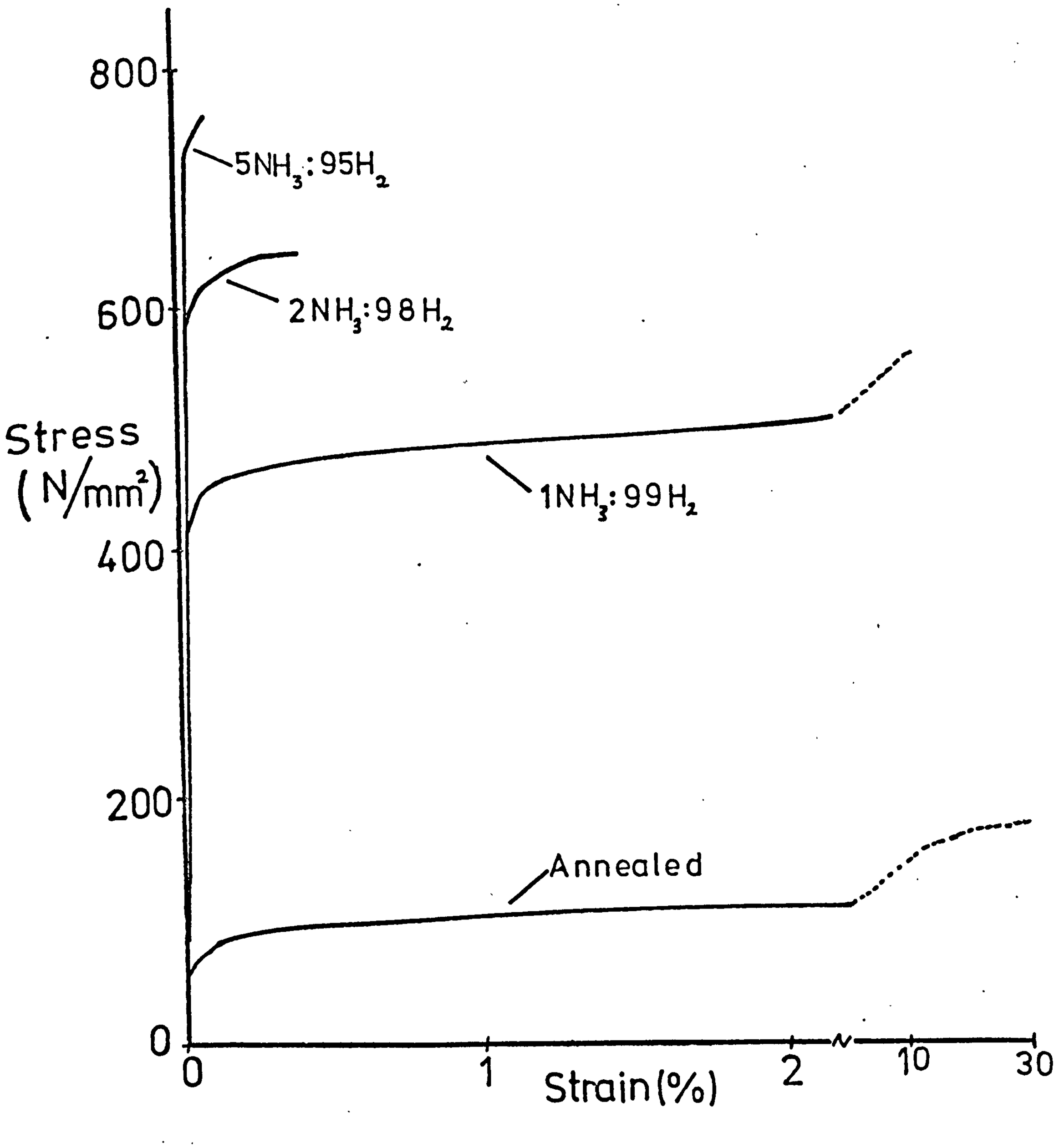
*Fracture occurs before reaching U.T.S.

After short nitriding times a fully developed GP zone structure is not perceptible (see Fig. VI.3(a)). The solute atoms are beginning to cluster together, and therefore, discrete particles are not observed. Consequently, the mechanical properties are appreciably different in this clustering stage. Continued nitriding produces a high density of zones which give a much higher strength.

Figure VII.1 shows the stress-strain curves for the Fe-0.15at.%V alloy after nitriding to saturation at 575°C in a range of nitrogen potentials. The curves have three regions; a linear portion representing the elastic extension of the specimen, a region of apparently rapid work hardening rate from the proportional limit up to or beyond the 0.1% P.S., and a region of varying work hardening rate which is dependent on the specimen condition. Nitriding the Fe-0.15 at.%V alloy at 575°C produces a homogeneous dispersion of fine, coherent, disc-shaped particles of 3 - 5nm diameter (see Fig. VI.2). The effect of increasing the nitrogen potential is to increase the volume fraction of precipitate and to refine the microstructure. From Fig. VII.1 it can be seen that the effect of increasing potential on the mechanical properties is dramatic, causing large strength increases with a consequent reduction in ductility.

The strength increments obtained are very large and approach an order of magnitude above the as-annealed strength. This represents an exceptionally high strengthening

Fig. VII.1



Stress-strain curves for Fe-0·15at.%V nitrided at 575°C

increment in an alloy with only 0.15at.% of solute. However, in association with the large yield strength increments, it is noticeable that fracture often occurs before the ultimate strength is reached. Therefore, the fine, coherent particles do not raise the ultimate strength and work hardening ability of the metal to the same extent as the yield strength. In fact, the work hardening rate is observed to be very similar to the as-annealed alloy, inferring that the particles are cut by dislocations during deformation. Because of the limited ductility of the samples nitrided in $2NH_3:98H_2$ and $5NH_3:95H_2$ at 575°C, it would appear that little dislocation interaction takes place and that the deformation is concentrated in local areas, which enables the fracture stress to be exceeded at these points.

VII.4 Mechanical properties of Fe-Nb-N alloys

Three niobium alloys containing 0.1, 0.3 and 0.6at.%Nb respectively, have been nitrided at various potentials in the range 550 - 700°C. Nitriding below 650°C results in the homogeneous precipitation of coherent particles, whilst above this temperature, coarser precipitates of the equilibrium phase are formed (see Chapter VI.4). Table VII.2 shows the properties obtained after nitriding Fe-Nb alloys to saturation at various temperatures and potentials. As in Fe-V-N alloys, high strength increments are obtained which are nearly an order of magnitude above the as-annealed alloy. It is evident that large strength increments are obtained in

TABLE VII. 2

MECHANICAL PROPERTIES OF Fe-Nb-N ALLOYS

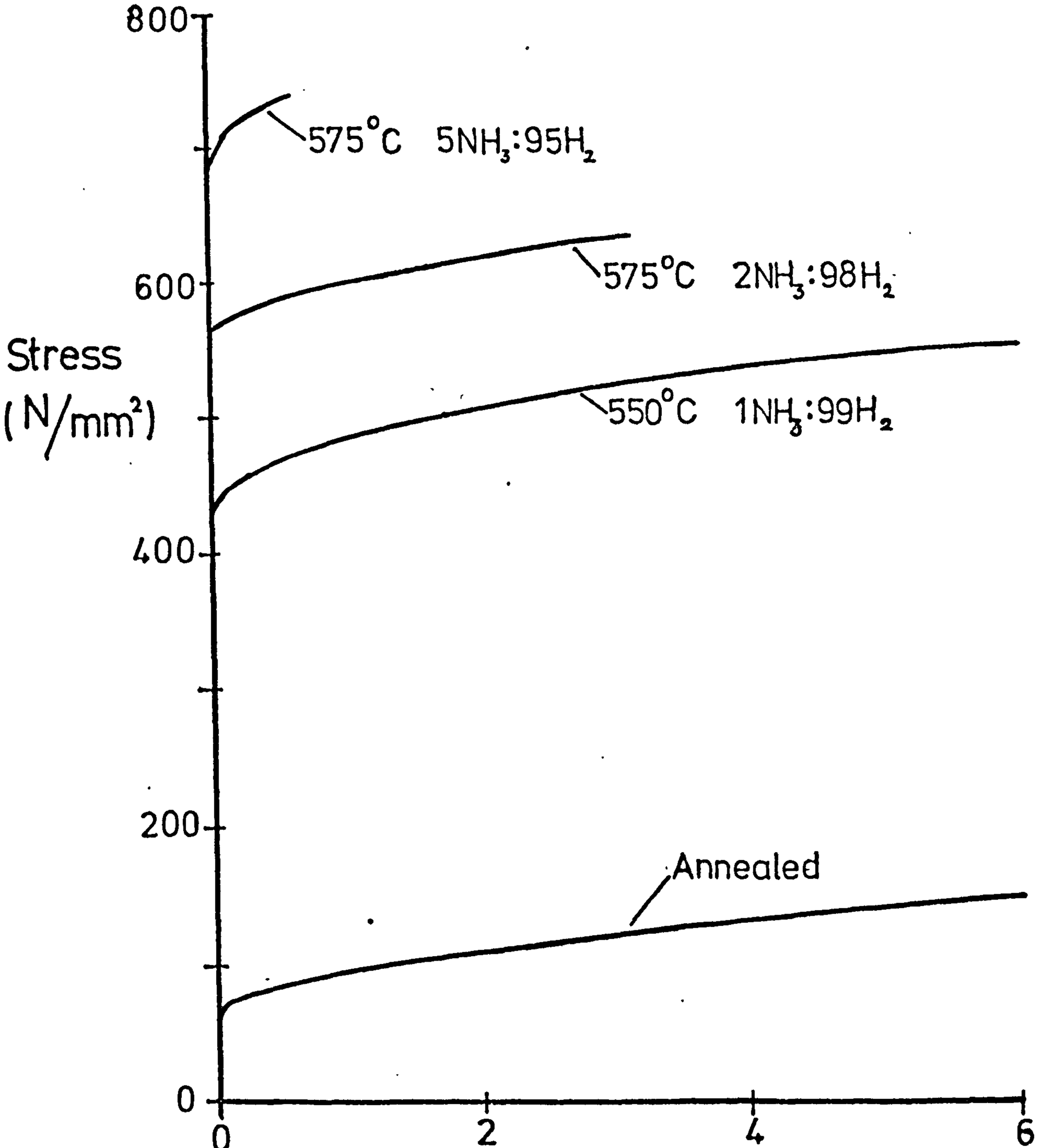
at % Nb	Nitriding conditions			at.%N	0.1% P.S. (N/mm^2)	U.T.S. (N/mm^2)	% El
	temp °C	$\%NH_3$	time (hrs)				
0.10	As - annealed			-	78	193	39.0
0.10	550	1	24	0.07	460	550	10.5
0.10	550	2	48	0.09	536	614*	4.9
0.10	575	5	24	0.31	700	740*	0.8
0.10	650	0.9	6	0.14	462	570	12.0
0.10	700	0.6	3	0.13	337	426	19.0
0.31	550	2	48	0.22	840	871*	0.7
0.60	550	2	48	0.72	995	1100*	4.5

* Fracture occurs before reaching U.T.S.

the lowest alloy, and although even larger increments occur in the higher alloys, they are not so proportionally high when one considers the solute content. From the results shown in Table VII.2, it is apparent that the strength increases with increasing nitriding potential and decreases with increasing temperature. With respect to the corresponding effect of nitriding conditions on the microstructure, it is apparent that the maximum strength is associated with the finest particle size.

Stress/strain curves of the Fe-0.1at.%Nb alloy exhibit low initial work hardening rates (solid solution behaviour) and are indicative of the initial particles being cut by dislocations during deformation (see Fig. VII.2). In the range of potentials used below 600°C, GP zones are produced of 3 - 6nm diameter, the effect of increasing potential being to refine the microstructure. The result of raising the nitrogen potential on the mechanical properties is to increase the strength and reduce the ductility, and after nitriding in $5NH_3:95H_2$ the samples are extremely brittle. Nitriding at this potential causes excess nitrogen to be present in the lattice and it seems inevitable that this will contribute to the deterioration in ductility. Nitriding at lower potentials, (e.g. $1NH_3:99H_2$), proceeds without any excess nitrogen being present, and indeed, there is insufficient to cause precipitation of all the substitutional solute. In these instances a more ductile structure is produced, together with substantial strength increases.

Fig. VII. 2

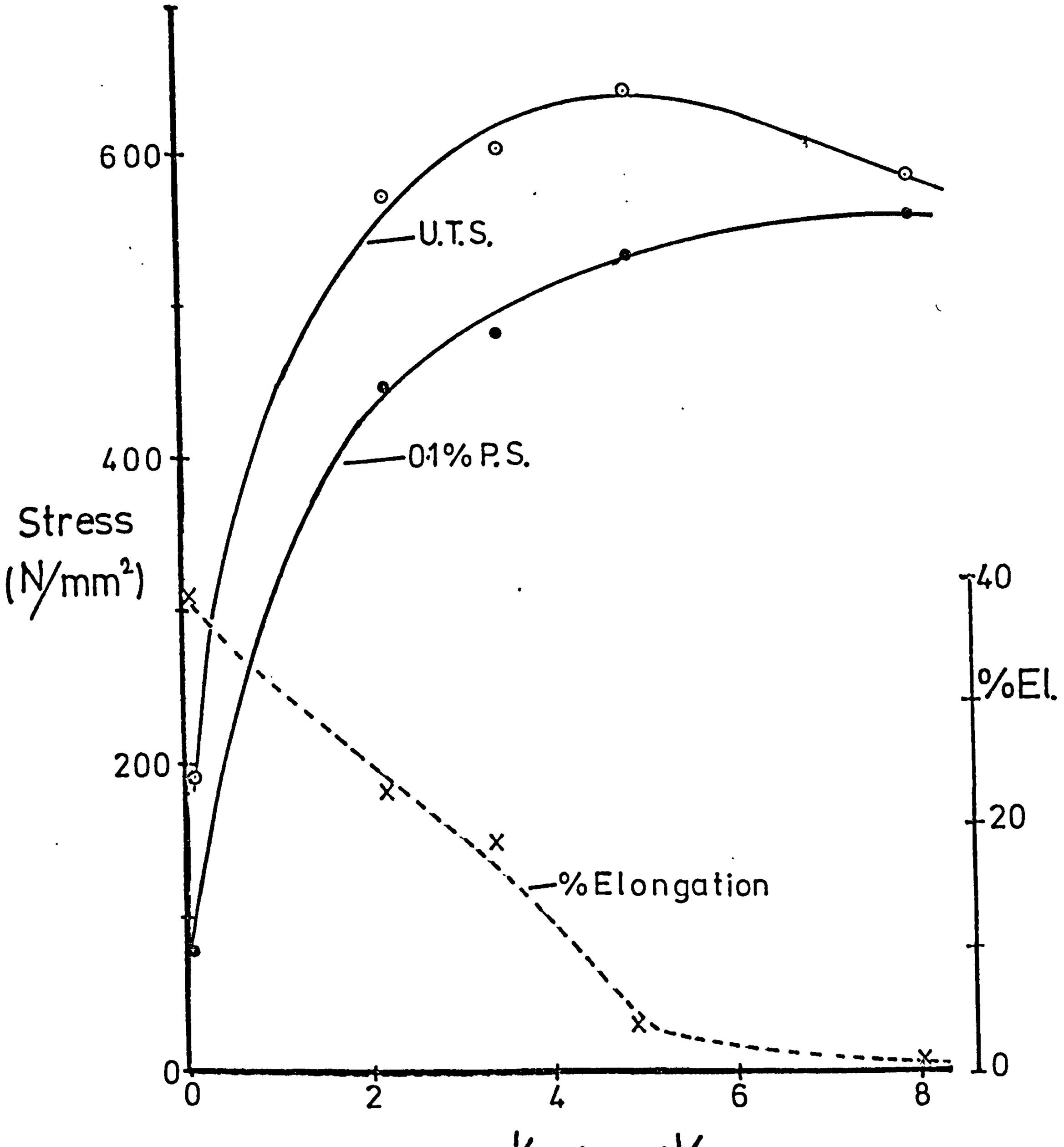


Stress-strain curves of Fe-0·1at.%Nb

To deduce a strengthening parameter to illustrate the exceptionally large increments obtained, the properties of the 0.1at.%Nb alloy after nitriding in $1NH_3:99H_2$ at 550°C can be used. Strength increments of 380 N/mm^2 are obtained for a total solute content of 0.17at.%. This is equal to an increase of 2235 N/mm^2 per at.% of solute, which is remarkably high. The solid solution strengthening produced by interstitial nitrogen in alpha-iron is regarded as one of the most effective methods of strengthening iron, yet this is only 575 N/mm^2 per at.%N (Baird & Jamieson, 1966; Bergstrom & Roberts, 1972). Consequently, the strength increments obtained by the coherent precipitation of very small discs represents a most effective method of strengthening iron base alloys.

Nitriding the Fe-0.10at.%Nb at 575°C results in the rapid formation of zones. The effect of nitriding time on the mechanical properties of the alloy after nitriding in $2NH_3:98H_2$ at 575°C is shown in Fig. VII.3. Large increases in the proof and ultimate strengths are obtained even after short times (5 hrs). Continued nitriding results in further strength increases, although the ductility is drastically reduced; eventually, after nitriding for 64 hrs., fracture occurs immediately after yielding and indeed, the breaking stress is lower than in alloys nitrided for shorter times. From these results it is evident that the optimum properties are obtained after very short times when there is insufficient nitrogen in the alloy to associate with all of the substitu-

Fig. VII. 3



Variation in properties with nitriding time for Fe-0·1at.% Nb nitrided at 575°C in $2NH_3:98H_2$

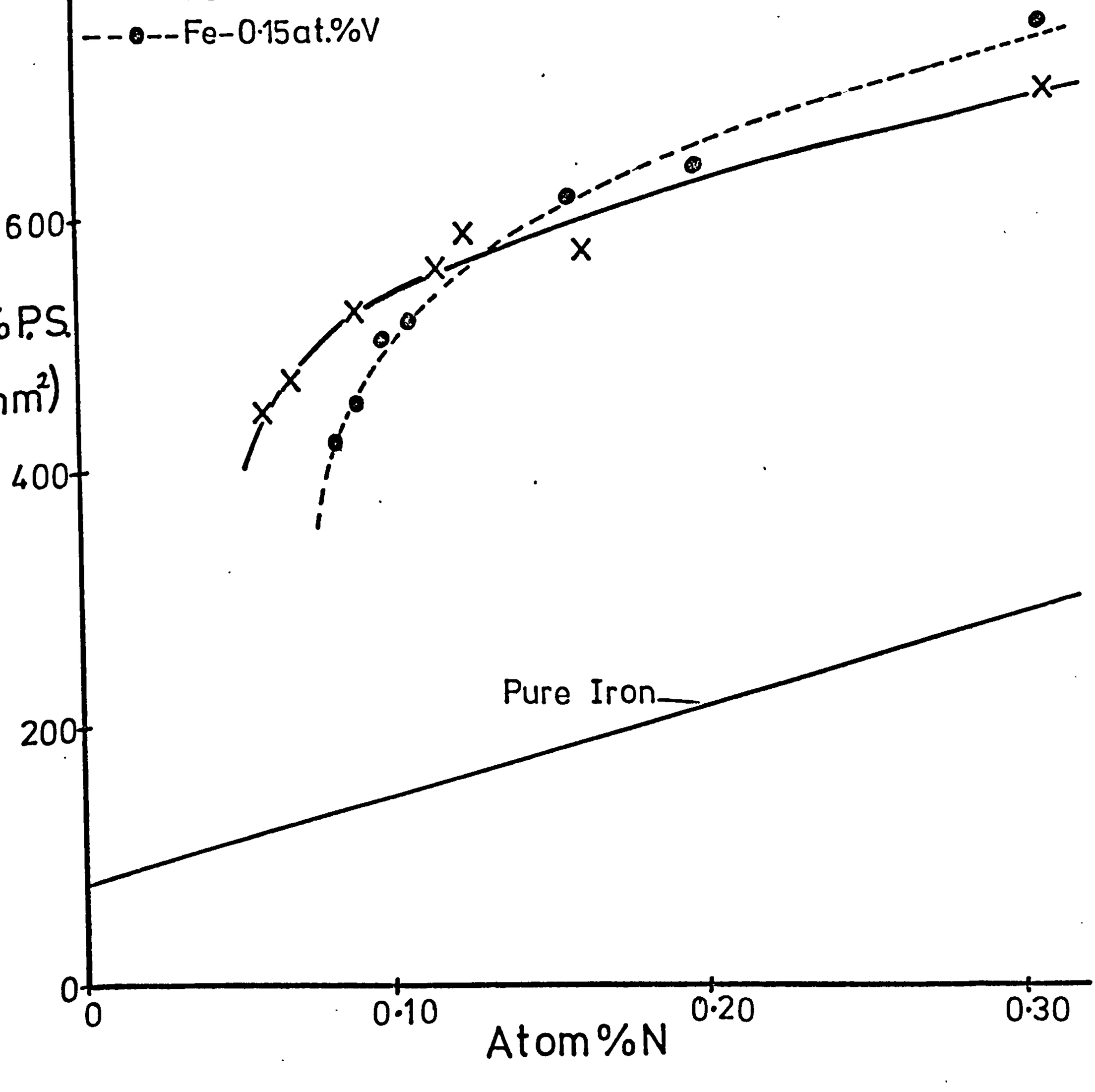
tional solute. After short times clustering of niobium and nitrogen atoms occurs, whereas nitriding the alloy to saturation results in the formation of discrete, coherent disc shaped zones. Once formed, the zones are stable at the nitriding temperature and it is necessary to age at higher temperatures to coarsen the particles. Upon ageing, the strength continuously decreases (see section VII.8). Therefore, the zone stage in Fe-Nb-N alloys represents the stage of highest attainable strength.

VII.5 The variation in yield strength with nitrogen content

Nitriding Fe-0.15at.%V and Fe-0.10at.%Nb alloys in a range of potentials varying from $0.5NH_3:99.5H_2$ to $5NH_3:95H_2$ at 550 - 600°C produces significant changes in nitrogen content, microstructure and hence, in properties. The variation in 0.1% P.S. with the total atom fraction of nitrogen is shown in Figure VII.4. The relationship for the solid solution strengthening of nitrogen in pure iron (after Bergstrom & Roberts, 1972) is included for comparative purposes. Under the prevailing nitriding conditions small coherent disc-shaped paricles of 3-6nm diameter are homogeneously precipitated (see Figs. VI.2,&6); the effect of increasing nitrogen potential being to increase the particle density and to refine the microstructure.

Similar trends in mechanical properties are observed for both alloys. Above some critical value in nitrogen content ($\approx$ 0.12 at.%), the strength increments become much smaller

Fig. VII. 4



Increase in 0·1%P.S. with at.%N for alloys nitrided at 550-600°C

than in the low nitrogen region. In fact, in the high nitrogen region the curves for the nitrided alloys are observed to be almost parallel to the solid solution strengthening behaviour of nitrogen in pure iron.

At low nitrogen contents, where the strength increases rapidly, the precipitate volume fraction increases. If, in these initial stages, all of the nitrogen is assumed to be precipitated as zones with an X:N ratio of 1:1, the strength increases can be related solely to the precipitated particles (see section VII.7). When excess nitrogen is present, the strength increments are in agreement with the additional nitrogen being in solid solution. Therefore, it is apparent that above some critical nitrogen potential, when all of the substitutional solute becomes precipitated, the zone structure remains substantially unaffected by increases in nitrogen potential; the only change is the slight refinement caused by the effect of increasing potential on the critical nucleus size.

At nitrogen contents below about 0.12at.% the strength increases are large, although all of the substitutional solute is not precipitated. At even lower nitrogen contents there is no hardening, since the nitriding potential is insufficient to exceed the zone solvus. It is noticeable from the region where the strength increases at low nitrogen contents, that the solvus for precipitation in the Fe-0.15at.%V alloy occurs at a higher potential than for the niobium alloy,

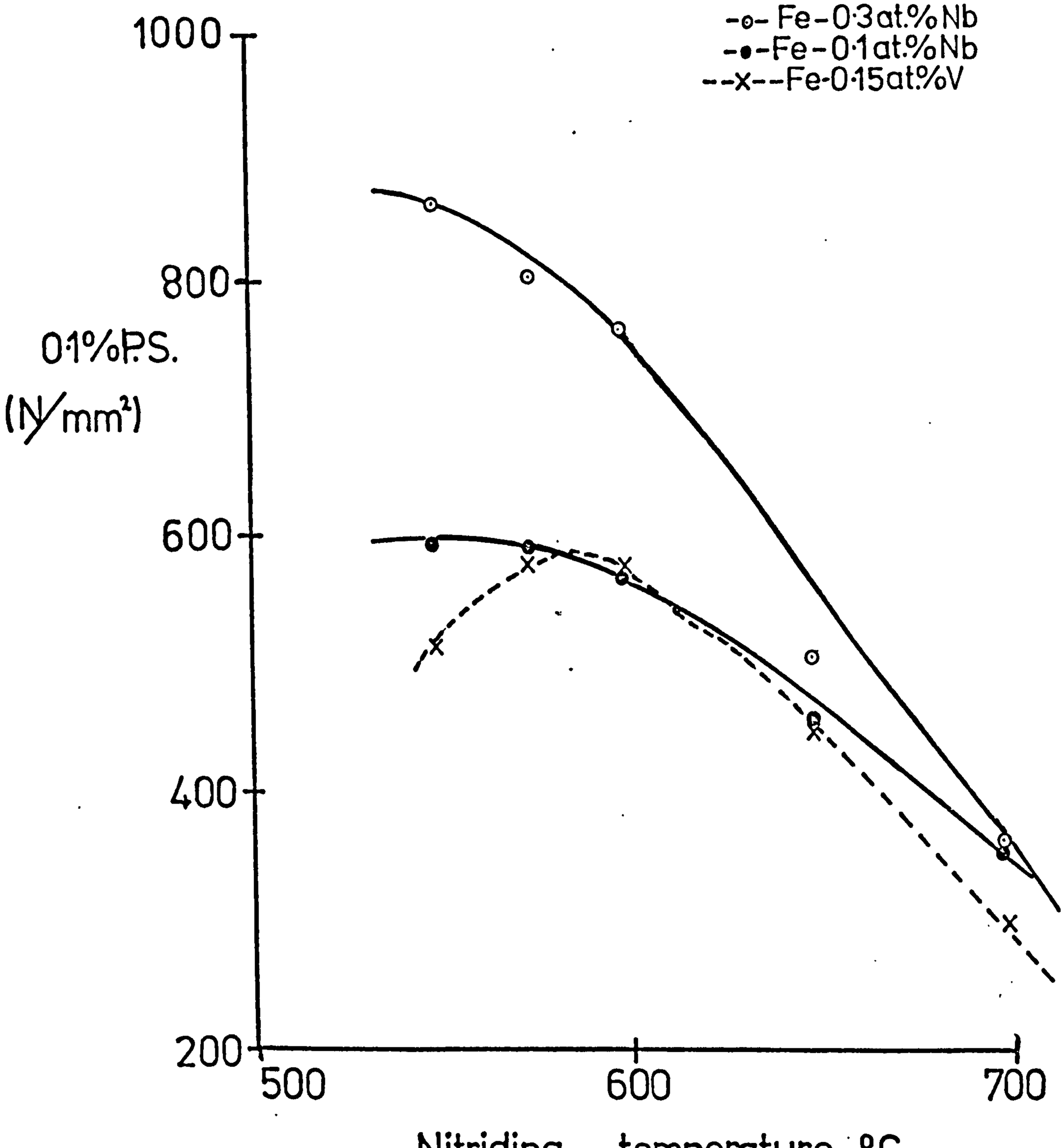
despite the higher solute content. This behaviour can be explained as being due to the greater niobium-nitrogen interaction.

VII.6 The effect of nitriding temperature on properties

The effect of nitriding at 550 - 700°C on the 0.1% P.S. of the Fe-0.15at.%V and Fe-0.1 & 0.3at.%Nb alloys is shown in Figure VII.5. In order to avoid any complications due to variability in nitrogen content, the samples were nitrided at a constant potential (a_N = 0.046at.%). The weight increases obtained confirmed that this was achieved, apart from one exception. This was the Fe-V alloy nitrided at 550°C, when only 0.11at.%N was introduced into the sample.

The strength is observed to increase continuously with decreasing nitriding temperature for both the niobium alloys, although below 600°C only slight increases are evident. This is due to the structures being stable at 550 - 600°C, whereas nitriding at higher temperatures results in larger particles being precipitated which continue to grow at the nitriding temperature. In this respect, the results in the high temperature range are time dependent, because prolonged holding at these temperatures will inevitably lead to decreases in strength. After nitriding the 0.1 and 0.3at.%Nb alloys, the nitrogen contents are 0.135 and 0.35at.% respectively; after subtracting the nitrogen in solid solution, this leaves 0.09 and 0.28at.% available for precipitation. Consequently, the Nb:N ratios are always $\approx$ 1:1. The effect of

Fig. VII. 5



Variation in 0·1% P.S. with nitriding temperature at a constant nitrogen potential ($a_N = 0{\cdot}045$ at.% N)

of increasing temperature on the microstructure is to cause coarsening of the particles. Therefore, the maximum strength for a constant volume fraction of precipitated phase is obtained at the finest particle size.

The behaviour of the Fe-0.15at.%V alloy is observed to differ after nitriding at 550°C, where a lower strength is obtained. This is due to the lower nitrogen content in the alloy (0.11at.%). At all other temperatures, 0.165at.%N is present. At the lower temperature it seems probable that all of the vanadium is not precipitated, and so a lower volume fraction of particles forms, resulting in a lower strength. This phenomenon illustrates the importance of nitriding temperature on the zone solvus for precipitation in Fe-V alloys.

After nitriding Fe-X-N alloys at 700°C, characteristic yield points are observed, whereas no such effects are obtained at the lower temperatures. Therefore, there must be nitrogen in random solid solution after nitriding at 700°C which causes dislocation locking. This can be explained by the larger interparticle spacing, and the consequent increase in unstrained ferrite, enabling nitrogen to occupy random sites. Nitriding at lower temperatures produces particles with extensive coherency strain fields around them, which act as sites where the nitrogen atoms become located. Consequently, the nitrogen is unable to diffuse to dislocations

and cause the characteristic yield points when small, coherent particles are precipitated.

VII.7 The influence of volume fraction on yield strength

Various precipitation strengthening models have been proposed, each model predicting that the yield strength is a function of the volume fraction of precipitated particles. Therefore, in order to assist the interpretation of the mechanical properties it would be advantageous to determine the relationship, if any, for the nitrided ferrites. This is not particularly easy in a system containing small particles because of the unknown volume fraction. However, it seems reasonable to assume that the volume fraction is proportional to the sum of the concentrations of solutes present as zones or precipitates.

In order to calculate the volume fraction of solutes it is necessary to assume that the nitrogen in excess of a X:N ratio of 1:1 is in solid solution. Also, when a deficit of nitrogen is present it must be assumed that it is all bound to the substitutional solute, leaving no nitrogen in random solid solution. These assumptions infer that the precipitated particles always have a X:N ratio of 1:1.

The strength increase due to the particles, $\Delta\sigma$, can be calculated from:-

$$\Delta\sigma = \sigma_{obs} - \sigma_{ann} - \sigma_{[N]_\alpha} \quad \ldots\ldots\ldots \quad (VII).1$$

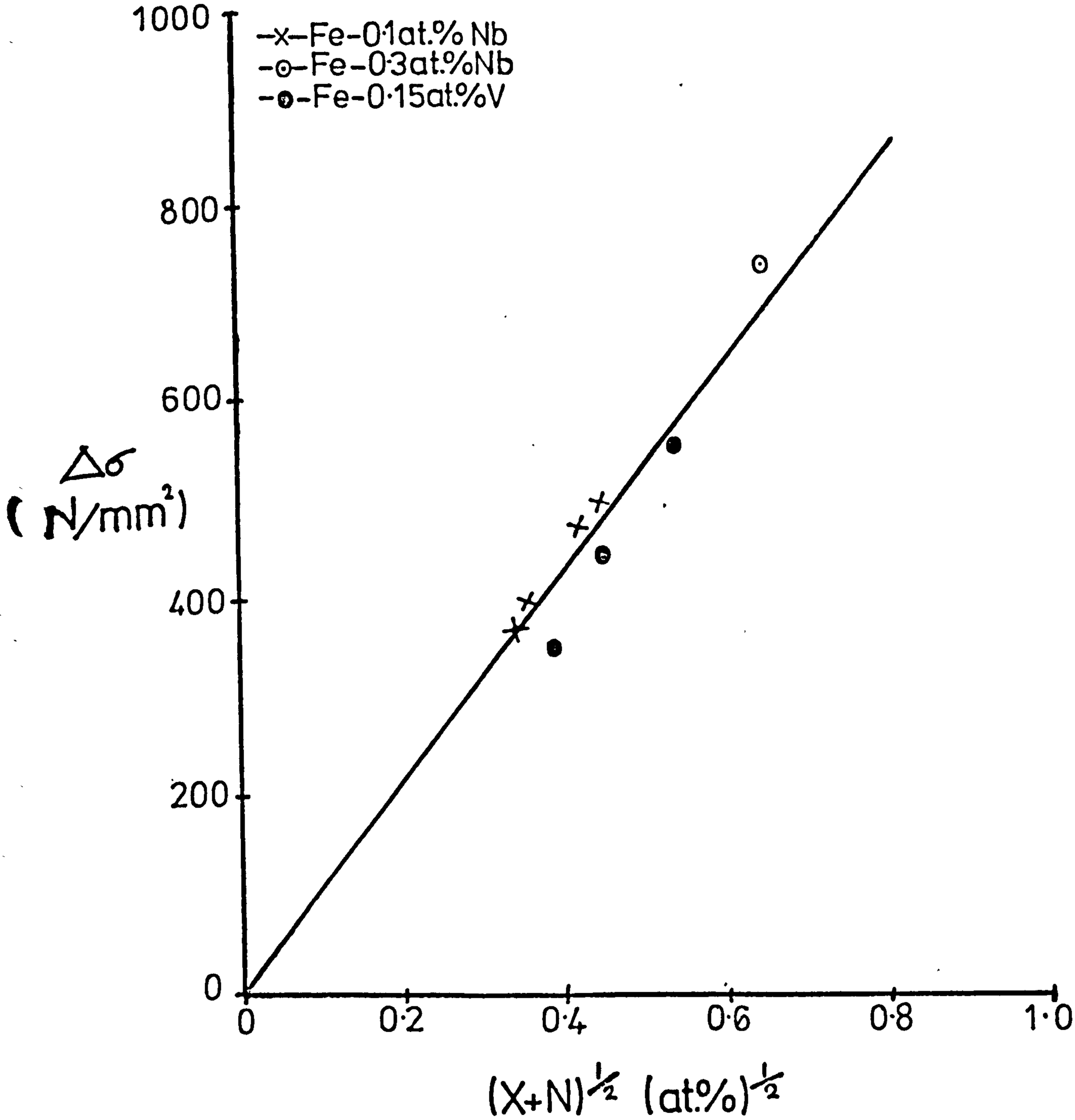
where σ_{obs} and σ_{ann} are the 0.1% P.S. values of the nitrided and annealed alloys respectively, and $\sigma_{[N]_\alpha}$ is the yield strength increment expected from the nitrogen in solid solution. The dependence of the strength increase with the volume fraction of precipitated phase is shown in Fig. VII.6. A linear relationship is obtained when the square root of the sum of the solute concentrations is plotted against strength, thus showing that the yield strength is proportional to the square root of the volume fraction of particles.

Table VII.3 shows the strength increments calculated using equation (VII).1 for the nitrided Fe-0.1at.%Nb alloy. The value taken for the solid solution strengthening of iron by nitrogen is 575N/mm^2 per at.%N (Baird & Jamieson, 1966; Bergstrom & Roberts, 1972). From these results it can be seen that the strength increases with nitrogen potential, due to the higher volume fraction of solute. However, when excess nitrogen is present, the strength increment is the same ($\approx$ 490N/mm^2), irrespective of the total nitrogen content. Therefore, the original supposition that the excess nitrogen is in solution seems justified.

VII.8 The variation in yield strength with ageing time at 750°C

Tensile specimens of the Fe-0.1at.%Nb and Fe-0.15at.%V alloys have been nitrided at 550°C in $1NH_3:99H_2$ and $3NH_3:97H_2$ gas mixtures respectively, and then aged for various

Fig. VII. 6



Increase in 0·1%P.S. with volume fraction for alloys nitrided at 550–600°C

TABLE VII. 3

YIELD STRENGTH INCREASES IN Fe-0.1 AT % Nb

nitriding conditions		Nitrogen at .%			yield ste ngth (N/mm^2)		
$\%NH_3$	temp ^oC	$[a_N]_\alpha$	$N_{total.}$	N_α	$\sigma_{Y.S.}$	$[\sigma_N]_\alpha Fe$	$\Delta\sigma$
0.5	550	0.008	0.06	-	444	-	366
1	550	0.016	0.07	-	460	-	382
2	550	0.033	0.092	-	530	-	452
2.7	550	0.046	0.128	0.028	589	16	495
5	575	0.122	0.312	0.212	700	122	500
1.5	600	0.046	0.128	0.020	570	11	479

times at 750°C in one atmosphere of argon. Fig. VII.7 shows the variation in 0.1% P.S. as a function of the square root of ageing time after these treatments.

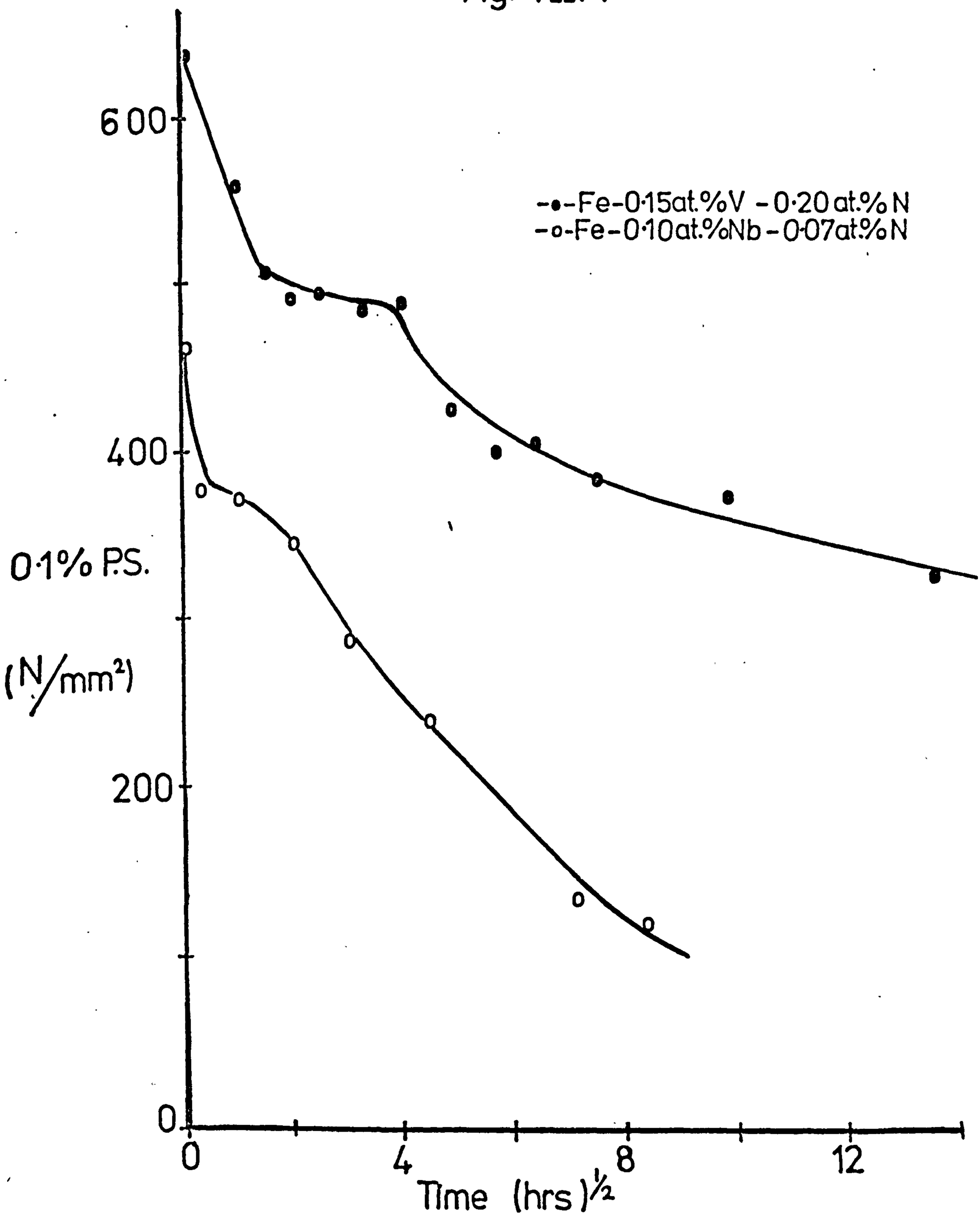
The behaviour of both alloys is similar. After short ageing times a considerable drop in strength is observed; this is followed by a period when the strength remains approximately constant, before it begins to continually decrease as the alloys overage.

The nitriding potentials produce 0.07at.%N in the Fe-Nb alloy and 0.20at.%N in the Fe-V alloy. The higher strength and slower ageing process of the Fe-V alloy can be related to the higher nitrogen concentration and the consequent higher volume. fraction of precipitated phase.

Electron metallography of both alloys shows that the initial homogeneous precipitation forms coherent discs of about 5nm diameter (aee Chapter VI), which grow linearly as a function of the square root of ageing time. At the point where the yield strength starts to decrease continuously, the particles have grown to about 15nm diameter and can be identificd as the equilibrium precipitate.
These results confirm that the maximum strength in Fe-X-N alloys occurs at the smallest particle size.

During the ageing of finely dispersed second phase particles, differences in work hardening rate often occur. Most

Fig. VII. 7

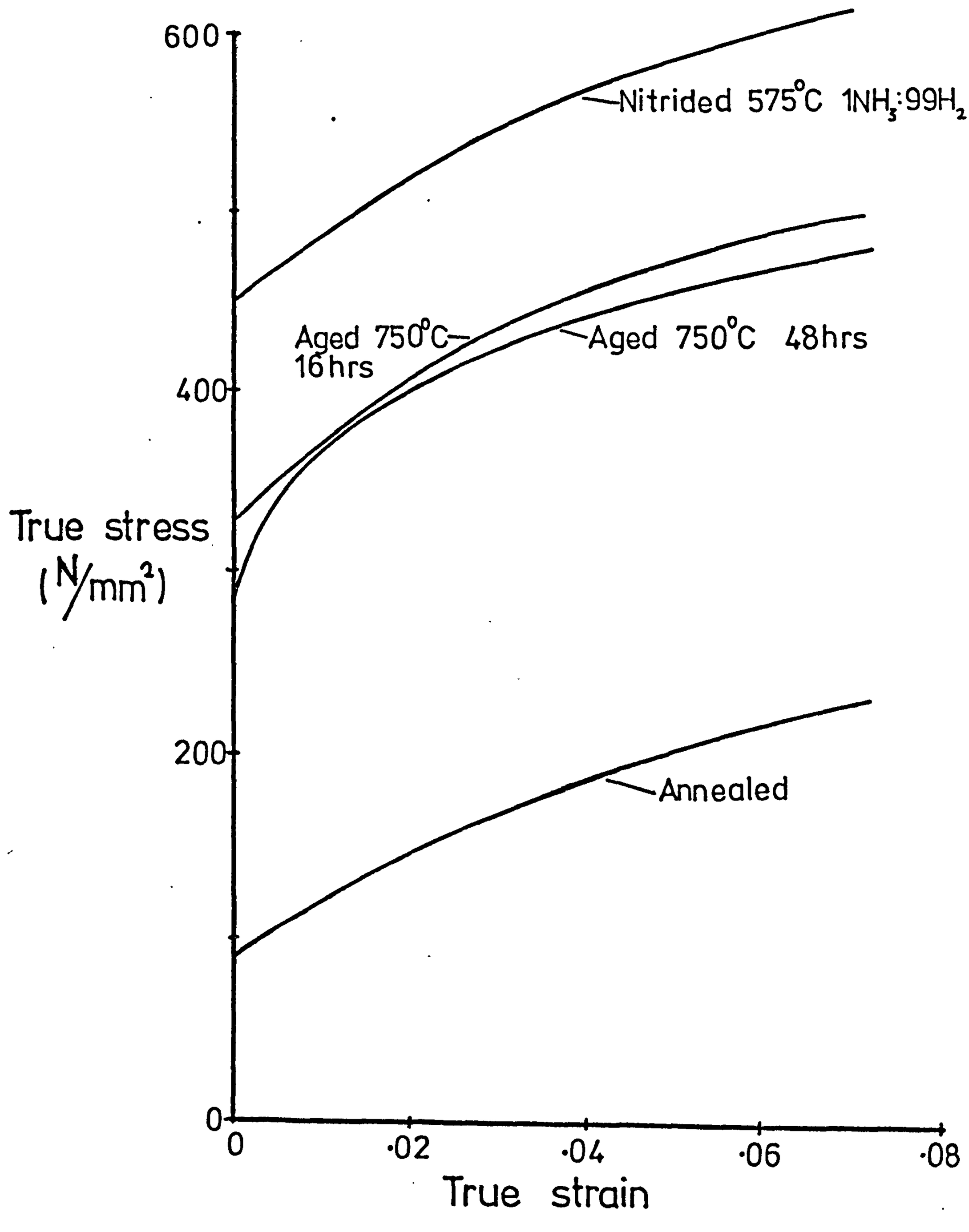


Variation in 0·1% P.S. with the square root of ageing time at 750°C

of the samples, nitrided to produce small, coherent particles, show low initial work hardening rates, similar to the as-annealed alloys. This is consistent with the mode of deformation occurring from particle cutting. After ageing classical age-hardening alloys, the work hardening rate usually increases as the alloys average, due to the dislocation particle interaction changing to a looping or by-pass mechanism.

In the nitrided ferritic alloys, the low volume fraction of solute makes it impossible for any large changes in work hardening rate to occur, only small changes being obtained. Further complications arise from the presence of nitrogen in solid solution, and so any changes in characteristics are most easily detected when little or no excess nitrogen is present in the matrix. This is possible after nitriding the Fe-0.15at.%V alloy in $1NH_3:99H_2$ at 575°C to produce 0.08at.%N. Typical stress-strain curves of the as-nitrided and aged samples are shown in Figure VII.8. The as-annealed alloy is also shown for comparative purposes. The curves obtained after nitriding, and after subsequent ageing for 16 hrs. at 750°C, are practically identical to the as-annealed alloy (solid solution behaviour). However, the initial work hardening rate increases after ageing for 48 hrs., when the precipitation of incoherent VN has evolved. At this stage, yielding occurs by dislocations by-passing or looping the particles. To obtain more substantial changes in work hardening behaviour necessitates the use of a higher volume fraction of precipitated phase (usually $>1\%$), but this is impos-

Fig. VII.8



True stress-true strain curves for
Fe-0·15at.%V-0·09at.%N

sible in nitrided ferrites because of the extreme brittleness of these materials when tested in tension.

VII.9 Hydrogen reduction of Fe-0.15at.%V

The effect of hydrogen reduction on the properties of the Fe-0.15at.%V alloy has been studied in two conditions:-

i) after nitriding in $2NH_3$:$98H_2$ at 575°C to produce a microstructure containing discs of about 5nm diameter.

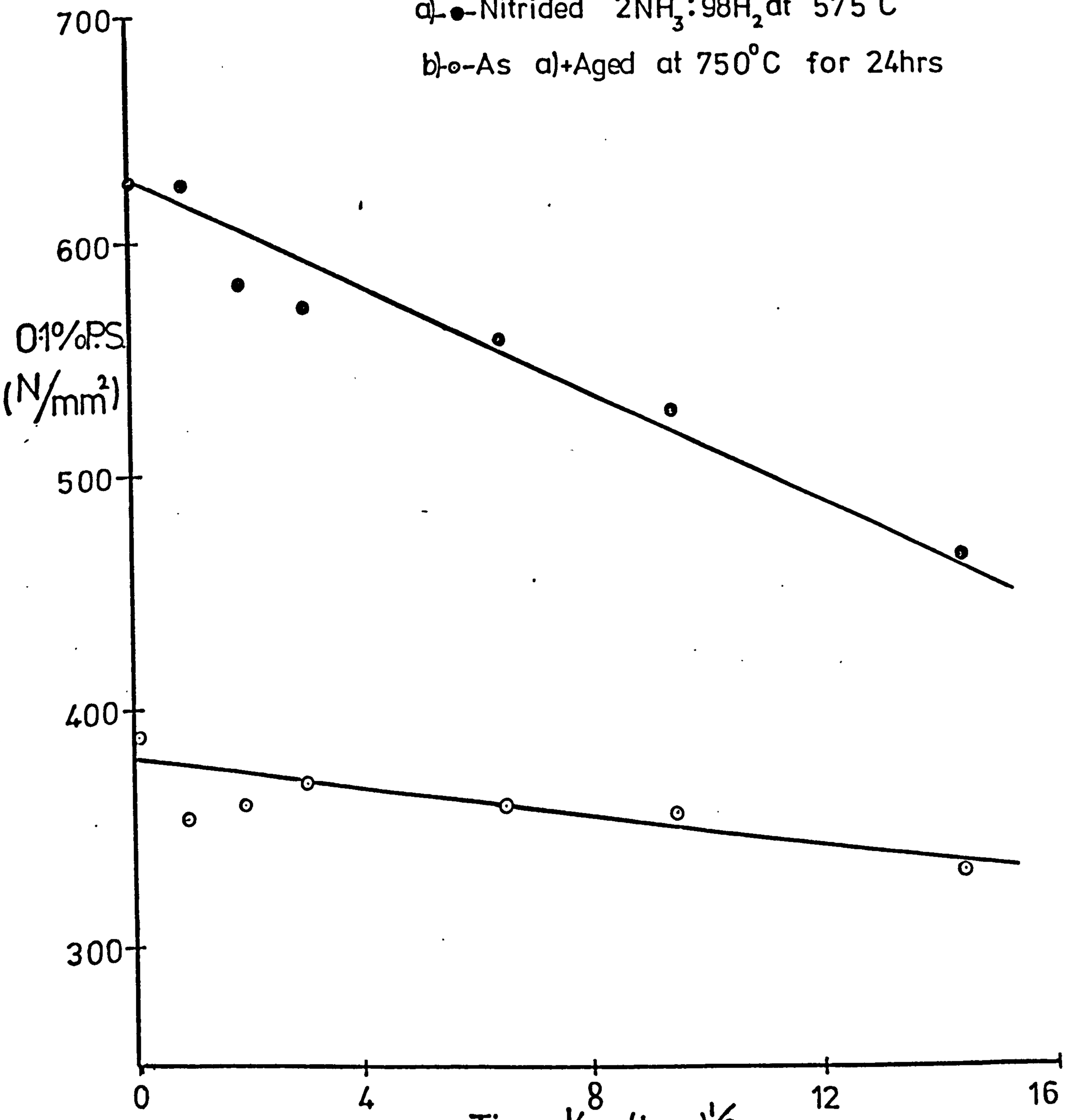
ii) after nitriding as in i) and subsequently ageing at 750°C for 24 hrs. in order to coarsen the particles to obtain incoherent VN plates of 15nm diameter.

Fig. VII.9 shows the decrease in strength for both microstructures for reduction times up to 210 hours. The strength of the aged alloy decreases at a slower rate than the as-nitrided alloy; this can be attributed to the presence of a more stable precipitate.

After reduction for 210 hours, the strength decreases of the as-nitrided and aged alloys are 165 and 45 N/mm^2 respectively. However, the weight decreases for both samples are identical (0.068at.%N). The strength decrease expected from the removal of 0.068 at.%N in solid solution is 40 N/mm^2. Consequently, the loss in strength of the aged alloy can be accounted for by the removal of the excess nitrogen from solid solution. However, the same explanation does not hold for the as-nitrided alloy.

The as-nitrided structure consists of a high volume frac-

Fig. VII. 9



Decrease in 0·1%P.S. during the Hydrogen reduction of Fe-0·15at.%V at 575°C

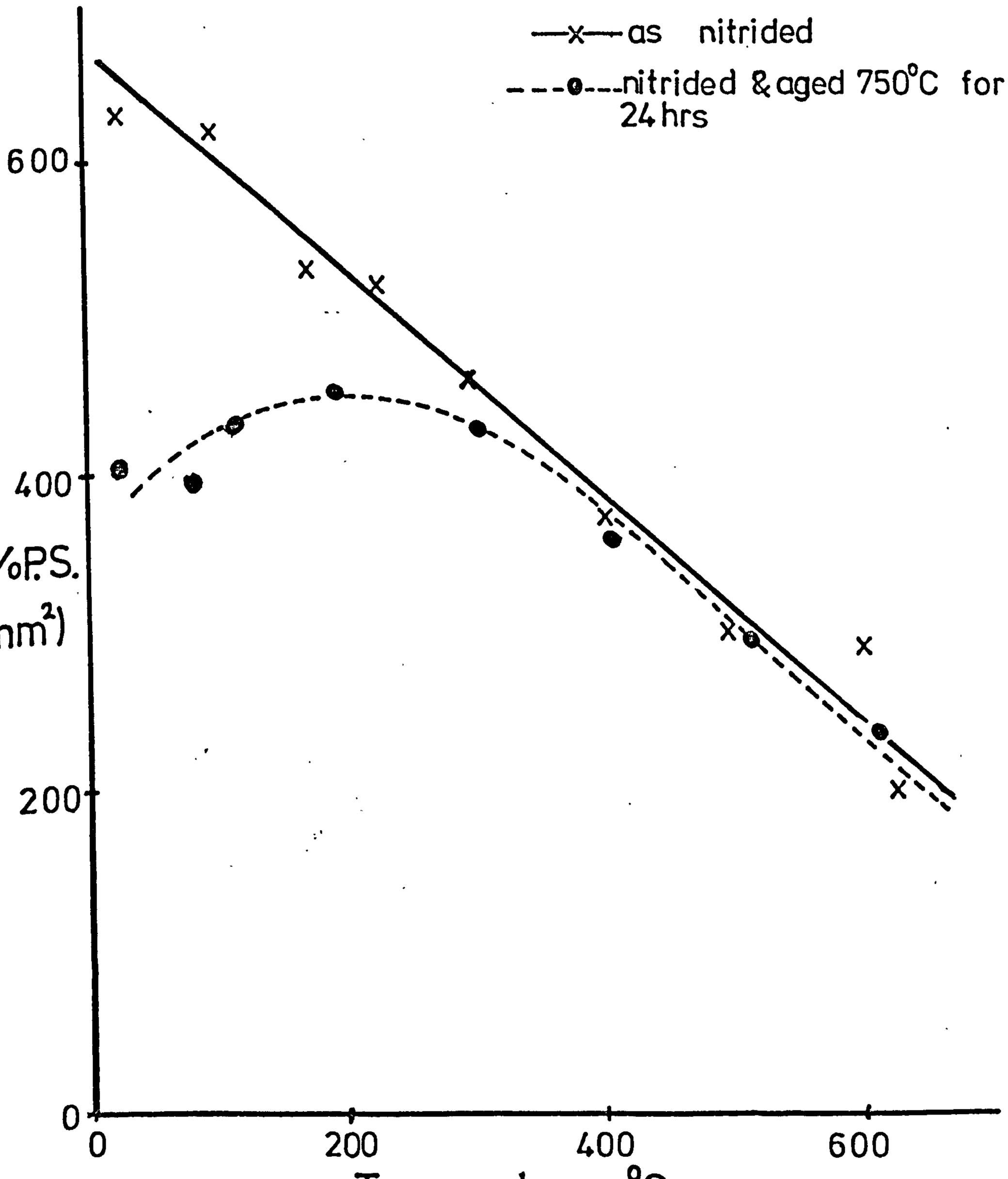
tion of small, disc-shaped particles, whose strength is markedly dependent on particle size and volume fraction. Therefore, any slight changes in either size or volume fraction during the prolonged reduction treatment would result in a noticeable strength decrease. Also, some contribution to the large decrease may be related to possible changes in the initial zone composition. A reduction in the nitrogen content of the particles is possible during prolonged reduction. The particles would consequently produce a lower matrix strain, which would lead to a further decrease in strength.

Hydrogen reduction treatment of the as-nitrided alloy for 210 hours reduces the nitrogen content to 0.09at.%N; the strength at this time is 465 N/mm^2. From the relationship between strength and nitrogen content (see Fig. VII.4), it can be seen that this value fits exactly onto the curve. Therefore, it appears that a decrease in the volume fraction of particles in itself would account for the loss in strength.

VII.10 High temperature properties

Fig. VII.10 shows the variation in yield strength with testing temperature for the Fe-0.15at.%V alloy containing 0.20at.%N in the as-nitrided and aged conditions. The strength of the as-nitrided alloy, containing coherent particles of 5nm diameter, is observed to decrease linearly with testing temperature. The aged alloy contains particles of incoherent VN of about 15nm diameter. At temperatures above

Fig. VII. 10



Temperature dependence of the yield strength in Fe-0·15at.%V-0·16at.% N

200°C the strength is observed to be similar to that of the as-nitrided alloy. However, the strength is observed to increase slightly in the serrated flow region (100 - 200°C), the highest strength being obtained at 200°C. The slight increase can be associated with an increase in friction stress caused by the nitrogen in solid solution (dynamic strain ageing). The absence of this phenomenon in the as-nitrided alloy infers that there is no nitrogen free to lock dislocations. In the nitrided alloy, the nitrogen is probably located in the strained matrix around the coherent particles and cannot cause dynamic strain ageing.

VII.11 Discussion

The strength increases obtained in dilute Fe-Nb-N and Fe-V-N alloys are extremely large when consideration is made of the low volume fraction of solute. The associated microstructures contain a high density of small, coherent disc shaped zones which are only two or three atom planes thick. It is the combination of the shape, size, structure and density of the particles which makes such large increments possible.

In order to compare the strength increments in Fe-X-N alloys to other precipitation hardening alloy systems, an expression developed by Borland & Segall (1972) can be used:-

$$S = V_H - V_S \Big/ \{(1+f)V_S\} \qquad \ldots\ldots\ldots \qquad (VII).2$$

The parameter, s, is a measure of the strength produced by a given volume fraction, f, of solute, whilst V_H and V_S are the Vickers hardness (or 0.1% P.S.) values of the precipitation hardened and solution treated alloys respectively. Some typical values of s for various precipitation hardening alloys are given in Table VII.4, together with the values calculated for Fe-Nb-N and Fe-V-N alloys. The exceptional nature of the strengthening produced in the nitrided ferrites is clearly apparent, the parameter being five times greater than in any other alloy system.

The high strength of the nitrided ferrites is associated with the homogeneous precipitation. From the results it is obvious that the maximum strength is obtained when the particles are at the smallest possible size. At this stage, the particles are very thin in one dimension (0.5 to 1nm) and are fully coherent with the matrix. The shape of the particles will strongly influence the properties since Kelly (1972) has shown that thin plates can cause strengthening up to three times that obtained from the same volume fraction of spherical particles.

When such large strength increases are obtained it is inevitable that some decrease in ductility will occur. However, the reduction of ductility, even in the dilute Fe-X-N alloys, is often drastic with fracture occurring immediately after yielding. Two possible reasons for the loss in ductility are:

i) the deformation mechanism associated with the homo-

TABLE VII.4

STRENGTHENING PARAMETER,S, FOR PRECIPITATION HARDENED ALLOYS

alloy system	Cu-Cr	Cu-Co	Al-Cu	Cu-Be	Fe-Nb-N	Fe-V-N
atom %. solute	0.55	2.81	4.95	18.2	0.2	0.3
S	1.06	0.41	0.16	0.23	4.95	4.8

geneous nucleation of fine particles; and

ii) the excess nitrogen which is present in the alloys after nitriding at high nitrogen potentials.

The development of a high strength in ferrous materials is based upon increasing the resistance to the motion of dislocations. This is produced in Fe-X-N alloys by the homogeneous nucleation of fine particles. However, Hornbogen (1971) has claimed that the degree to which useful strength increases can be obtained is limited by the occurence of particle shearing; the liklihood of this is enhanced when small coherent particles are precipitated. Shearing of the particles can result in a coarse slip distribution, producing dangerous stress concentrations and plastic instability in local areas, although the macroscopic strain is low.

The consequence of this is a drastic reduction of ductility. Therefore, it would appear that particle shearing could occur in dilute Fe-X-N alloys containing small particles because fracture often occurs immediately after yielding. The inability of the metal to work harden and attain the ultimate tensile strength is a consequence of this deformation mode. Overageing the particles to form the incoherent, equilibrium precipitate improves the ductility with a consequent reduction in strength.

The extremely poor ductility of nitrided ferrites is not an isolated example of embrittlement in precipitation hardened ferrous materials. Watson & Brown (1974) observed poor ductility in age-hardened Fe-Si-Ti alloys containing

fine coherent particles, whilst the embrittlement at 475°C in age-hardened Fe-Cr alloys has been observed by numerous investigators (Lagneborg, 1967; Williams & Baxton, 1957; Courtnall & Pickering, 1976). In the Fe-Cr system the embrittlement is caused by the precipitation of chromium rich b.c.c. α' - phase which forms as zones on {100} ferrite planes. The precipitation causes large strength increases together with a drastic reduction in ductility. Therefore, it appears that embrittlement of ferrous materials is a common feature when high strength increments are developed due to the precipitation of fine, coherent particles.

The presence of excess nitrogen in the matrix is another reason why embrittlement can occur in ferrous materials. Nitriding Fe-X alloys at low nitrogen potentials, when there is a deficit of nitrogen, results in improved ductility, although it is difficult to evaluate the effect because of the lower density of precipitated particles. It is relevant to note that high strength increments (up to 1000N/mm^2) can be achieved in isothermally transformed steels without such detriment to ductility. In these steels precipitation occurs during transformation and there is a deficit of interstitial atoms compared to the substitutional solutes.

Despite the presence of excess nitrogen in many of the nitrided samples, there is no evidence of any yield points when small, coherent particles are precipitated. The significance of this phenomenon and the fact that hydrogen

reduction treatment, to remove the excess nitrogen, only slightly improves the ductility of Fe-X-N alloys, suggests that the major cause of the poor ductility is the deformation mechansim associated with the fine, coherent particles.

The strengthening produced in nitrided steels has been the subject of numerous investigations. Chen (1965) found that hydrogen reduction treatment improved the ductility of dispersion strengthened Fe-Ti-N alloys. The stress-strain curves of the nitrided structures were found to have a high initial work hardening rate, which was dependent upon the volume fraction of particles. This behaviour was taken as being indicative of the particles being looped during deformation, which would be expected since the alloys were nitrided at high temperatures (700 - 800^{o}C). Chen claimed that particles below 40nm diameter were coherent with the matrix. However, in view of the present investigation it is impossible to comprehend how such large particles are coherent, and the results of Chen's work can be explained as being due to the production of large, undeformable particles of the equilibrium phase. By producing smaller particles in Fe-Ti-N alloys, Kirkwood et al (1974) found that the strength increased continuously down to the smallest particle size and was proportional to the square root of the volume fraction of precipitated phase. This behaviour is typical of that observed in Fe-Nb-N and Fe-V-N alloys containing small, coherent particles.

Other research by Melkumov et al (1973) associated the high strength of the nitrided layer with the formation of finely dispersed nitrides which were either completely or partially coherent with the matrix, the maximum hardness being found in the initial stages of nitride formation. From hardness measurements on the nitrided layer of a Cr-Mo steel, L'vosky & Gerasimov (1973) determined that the hardness decreased to half its initial value in the temperature range 400 - 500°C. The findings of the present work confirms the observations made in these investigations and establishes conclusively that the maximum strength in nitrided ferritic alloys is associated with the production of a homogeneous dispersion of coherent discs of 3 - 5nm diameter and 0.5 - 1nm thick on the ferrite cube planes.

The observation that the maximum strength is associated with the formation of coherent particles is comparable to other precipitation hardening systems. In either the random solid solution or overaged condition, the strength is lower due to the easier dislocation movement. However, one of the main differences in the nitrided ferrites is the very small particle size associated with the maximum strength. The only other age-hardening system studied in any detail in b.c.c. iron is the Fe-Cu system, where Hornbogen (1964) found similar stages of ageing to those observed in the nitrided ferrites. The maximum strength was observed at the stage where the first formed f.c.c. particles appeared

(5 - 15nm diameter), which were coherent with the matrix. In either the clustered solid solution or with overaged, incoherent particles, lower strengths were obtained. Evaluation of the properties in this particular system is facilitated by the copper rich particles precipitating as spheres.

Significant strength increases have been observed by numerous investigators in high strength low alloy steels containing vanadium or niobium additions. Frequently, the strengths are associated with the precipitation of fine, coherent particles. In semi-killed low C-Mn steels to which single and combined additions of vanadium and nitrogen were made, Stephenson et al (1964) found that the combined additions increased the yield strength of the hot rolled steel by 110 N/mm^2. The strength increase was significantly above that obtained from the single additions and was related to the precipitation of VN platelets on $\{100\}_\alpha$ planes. Suzuki et al (1970) observed what was claimed to be a remarkably high strength level in 0.05%C, 0.05%V steels containing coherent V_4C_3 particles of 8-10nm diameter, whereas Gray (1973) found that the strength increased down to the smallest particle size (1.5nm diameter) in niobium containing steels. Whilst investigating the effects of niobium, vanadium and titanium on the processing of fine grained steels, Irvine et al (1967) found that small precipitates of 3nm diameter formed in the titanium steel which produced

very high strength increases (310 N/mm^2). Smaller increases of 45 - 155 N/mm^2 were found in the niobium and vanadium steels. Despite the fact that most investigators have found that the maximum strength is obtained at the smallest particle size, Lamberigts & Greday (1974) claim that the maximum strength in niobium and vanadium containing dispersion hardened steels occurs at a critical particle diameter of 7nm.

The strengthening due to small particles is not restricted to low carbon steels. Steiner et al (1975) observed fine plate or rod shaped particles (10 - 40nm diameter) within the ferrite of the pearlite in 0.5%C steels containing 0.1%V and 0.01%N. The precipitation caused strength increases of 110 - 150 N/mm^2 upon air cooling. During investigations into the secondary hardening of steels, the peak hardness has been associated with the homogeneous precipitation of coherent V_4C_3 or VN precipitates (Tekin & Kelly, 1965; Smith, 1966; Baker, 1973(b)); whereas Simcoe et al (1968) observed large strength increases associated with low work hardening rates in a tempered Mo-W-N steel and concluded that particle cutting took place during deformation.

From the majority of the research on the precipitation of second phase particles in steels, it is evident that the particles must be both small and coherent to produce large strength increases. Nevertheless, the strength increases

are low in comparison to those found in the present work. For example, Gladman et al (1971) obtained maximum strength increases of 150 N/mm^2 in a 0.15at.%V steel containing 3nm diameter particles. It is evident from the present investigation that all of the substitutional solute cannot be homogeneously precipitated in this steel since increases of 400 - 500 N/mm^2 would be obtained. A possible reason for the large difference is that some of the interstitials are precipitated with other alloy elements (e.g. aluminium) which cause grain refinement. Therefore, a smaller amount of interstitial solute is available for homogeneous precipitation. Also, some larger particles will probably precipitate on dislocations during cooling, rendering a proportion of the alloy additions ineffective for precipitation at the lower temperatures where small, coherent particles form.

The present investigation has shown that the yield strength is strongly temperature dependent when small particles are precipitated (see Fig. VII.7). However, during the elevated temperature testing of steels, the yield stress is normally expected to increase at about 200°C due to the free nitrogen causing dynamic strain ageing. The absence of this behaviour in the as-nitrided alloy, despite the high nitrogen content, can be explained in one of two ways:-

i) there is no nitrogen in suitable sites to cause dislocation locking, i.e. it is trapped in higher energy sites; or

ii) the controlling deformation mechanism requires a higher strength level than that necessary to free nitrogen from dislocations.

Ageing the alloy to precipitate the equilibrium phase permits dynamic strain ageing in the range 150 - 250°C. Consequently, there is now nitrogen present in random ferrite sites. These sites are in the undistorted matrix region between the precipitates.

The behaviour at testing temperatures above 300°C is anamolous because of the continual strength decrease and the accompanying poor ductility. In a study of the high temperature properties of iron containing molybdenum or chromium in the absence of any interstitials, Baird & Jamieson (1972) found that the strength was fairly temperature insensitive in the range 20 - 700°C. Therefore, the strong temperature dependence of the nitrided alloys must be associated with the precipitated particles, presumably as a result of the prevalent strengthening mechanism.

The role of precipitates in determining the mechanical properties is obviously important in Fe-X-N alloys. The strength increases obtained are very much greater than those obtained in f.c.c. materials for comparable volume fractions of solutes. Therefore, it seems that the strengthening is unique due to the size, shape, density and com-

position of the particles formed after nitriding dilute Fe-X alloys in the range 550 - 600°C. The attainment of similar strength increases in commercial steels is difficult due to the liklihood of precipitation on dislocations at high temperatures, and because the homogeneous precipitates form over a range of temperatures.

From the thermodynamics and solubility data of numerous substitutional and interstitial solutions in α and γ iron, the relative usefulness of alloy additions in commercial steels can be predicted. Calculations of the free energies of formation of VN and VC in α and γ iron have been made (Chino & Wada, 1965; Fountain & Chipman, 1958), which show that there is a greater tendancy to form VN in α and γ iron than VC. If both are present, the carbide will dissolve first as the temperature is raised. This is confirmed by the work of Stephenson et al (1964) who claimed that only VN is present in steels heated up to 780°C. In steels there is a tendancy for vanadium to form nitrides whilst niobium preferentially forms carbides, though many of the particles formed in commercial steels are mixed carbo-nitride phases. Of the solutes which have a strong interaction with nitrogen, vanadium is likely to be of the most benefit in commercial steels. This is because VN becomes soluble at about 950°C, and therefore, can be taken into solution and be re-precipitated on cooling. Both niobium and titanium carbides or nitrides are less suitable because of their low solubility in austenite.

Consequently, high soaking temperatures are required to dissolve these phases. Due to the lower soaking temperatures necessary to dissolve VN or VC precipitates, it is anticipated that the practice of controlled rolling will be much easier in vanadium containing steels. Upon retransformation it is necessary to precipitate particles of a size which enables the maximum strength increase to be obtained. From the results of the present investigation it is evident that in order to attain the highest strength, precipitation should occur within the range 550 - 600°C.

VII.12 Conclusions

a) High strength increments are obtained in nitrided dilute Fe-X alloys when small, coherent disc-shaped particles are precipitated on the {100} ferrite planes. In the Fe-0.1at.%Nb and Fe-0.15at.%V alloys small additions of nitrogen (0.1at.%) increase the strength by about 400 N/mm^2. Increasing the nitrogen content above this level results in a further strength increase which can be explained as being due to the presence of nitrogen in solid solution.

b) The maximum strength increase is obtained at the finest possible particle size.

c) The yield strength is proportional to the square root of the sum of the substitutional and interstitial solutes available for precipitation.

d) The high strength increases are associated with very poor ductility, fracture often occurring immediately after

yielding. Ageing the particles to reduce the strength results in a simultaneous increase in ductility. The reason for the poor ductility is believed to be caused by the mode of deformation occurring when small, coherent particles are precipitated.

e) The yield strength decreases continuously as the testing temperature is increased in the range 20 - 600°C when zones are precipitated. A similar dependence is found in aged alloys containing equilibrium precipitates at temperatures above 250°C. The ductility remains low at higher temperatures despite the reduction in strength.

f) No yield points are obtained upon tensile testing nitrided Fe-X alloys containing small, coherent particles.

Chapter VIII

ELECTRON METALLOGRAPHY OF DEFORMED ALLOYS

VIII.1 Introduction

A study of the interaction between dispersed second-phase particles and dislocations during deformation was instigated in order to obtain a more thorough understanding of the strengthening mechanism in Fe-X-N alloys. The strength of any metal is governed by the particular type of dislocation interaction taking place, and theories of particle strengthening necessitate the assumption of the pertinent dislocation-particle interaction. Therefore, if the mechanism by which the particles deform can be determined, the relevant strengthening model can be applied more confidently.

Transmission electron microscopy enables the interaction, distribution and orientation of dislocations to be directly examined. Nitrided ferritic alloys containing zones and overaged particles of the equilibrium phase have been studied in order to determine the dislocation-particle interactions associated with the various stages of ageing. During the course of the investigation it became apparent that the deformed microstructures are a feature of the distribution of second phase particles and so the structures obtained for one particular Fe-X-N system are comparable to other alloy systems containing a similar distribution of

particles.

VIII.2 Experimental

Thin foils for transmission electron microscopy were prepared from deformed 0.75mm thick tensile samples. The samples were thinned to about 0.05mm, by chemically polishing in a $H_2O_2/HF/H_2O$ solution, and were then electropolished using the window technique.

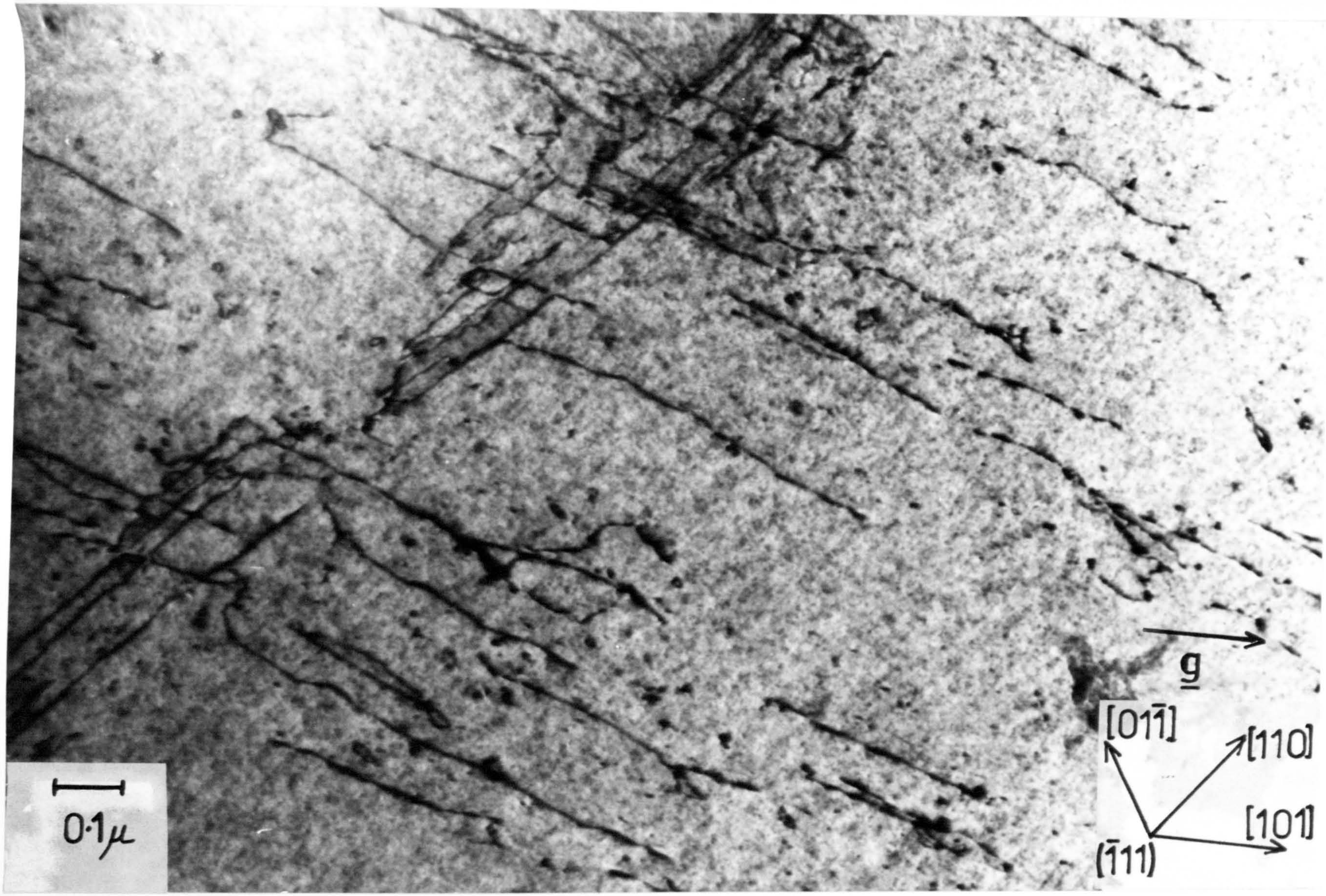
A factor which governs the metallography of deformed microstructures is their reproducibility, any anomolous structures being a consequence of mishandling. Therefore, every precaution was taken to prevent bending or working the foils during preparation.

VIII.3 Fe-X-N alloys prior to peak strength

Nitriding dilute Fe-X alloys to saturation in the range 550 - 600°C precipitates discrete disc-shaped zones which are associated with peak strength. After short nitriding times, lower strengths are associated with the clustering of substitutional and interstitial solutes. Fig. VIII.1 shows the dislocation distribution obtained after nitriding the Fe-0.15at.%V alloy in $5NH_3:95H_2$ at 575°C for 3 hrs. and straining in tension by 1%.

The dislocation structure is similar in many respects

Fig. VIII. 1



Dislocation substructure in nitrided Fe-0·15at.%V prior to peak strength

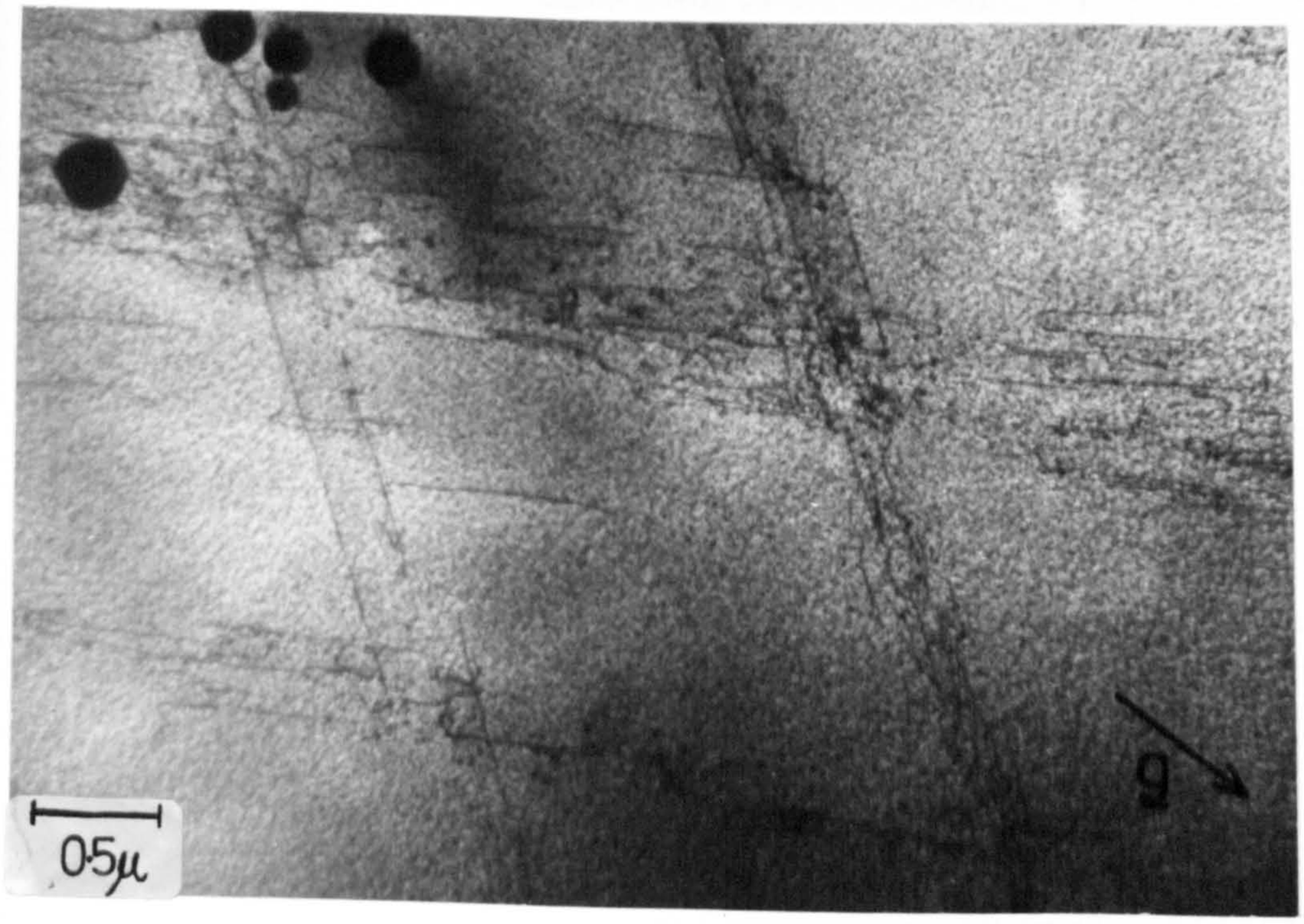
to that observed by Turkalo & Low (1962) in single crystals of Fe-3%Si alloys. Numerous long, fairly straight, screw dislocations are visible which appear to be predominantly on two slip planes. On closer inspection, the dislocations are observed to contain several jogs. There is also some dislocation debris present in the form of equiaxed and elongated loops. The jogs are indicative of drag on screw dislocations. Under the applied stress, which causes the screw dislocations to move, the jogs are immobile. As the screw dislocations continue to move, a trail forms behind them and it is from the pinching off of these extended jogs that the debris is formed. The fact that the dislocation structure in the clustered Fe-V-N alloy is similar to those in homogeneous solid solutions of pure iron or Fe-X alloys (Turkalo & Low, 1962; Hornbogen, 1964) infers that the deformation mechanism is also the same.

VIII.4 Fe-X-N alloys containing zones

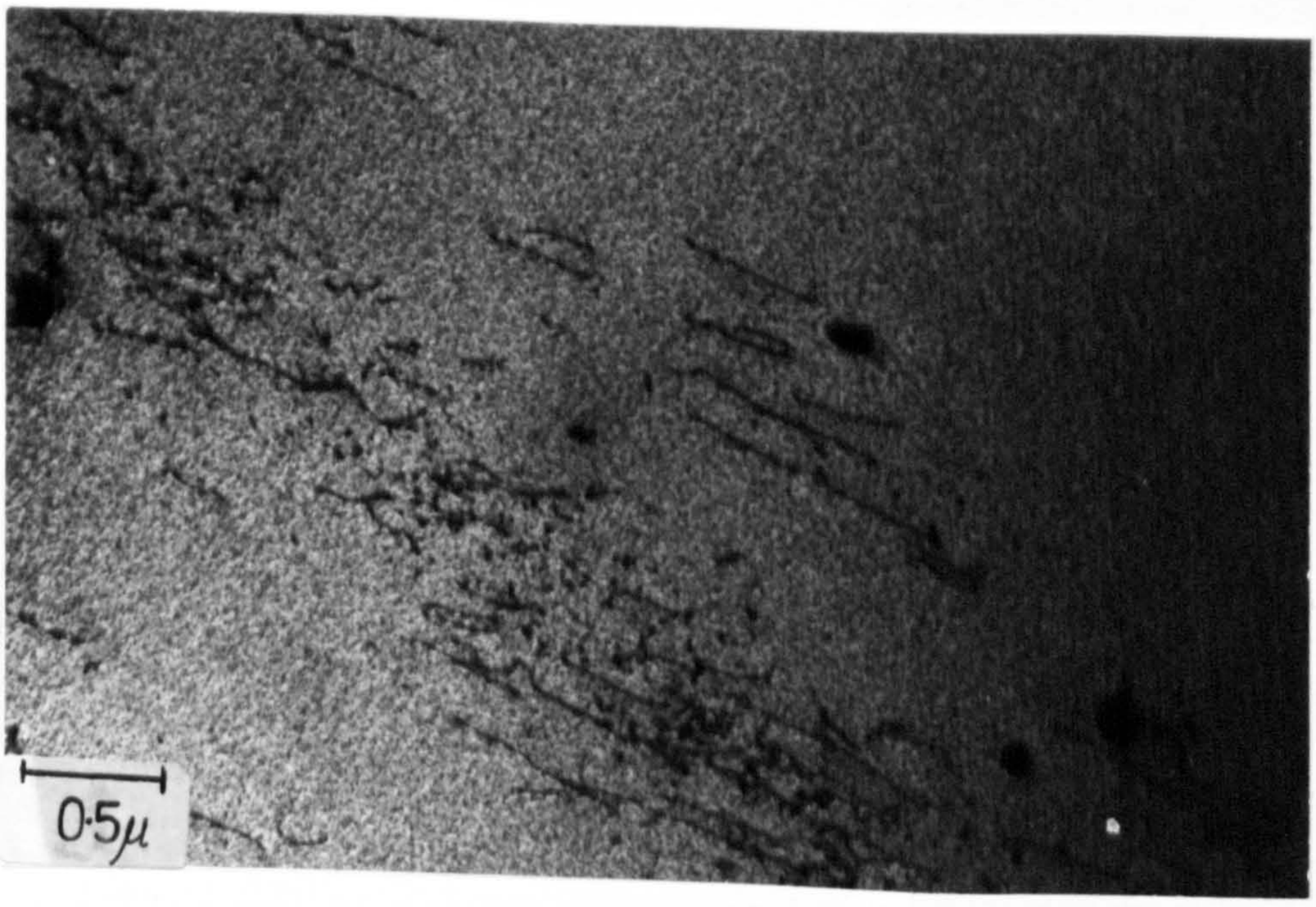
Nitriding Fe-Nb and Fe-V alloys to saturation below 600°C produces a homogeneous dispersion of small, coherent disc-shaped zones. It is at the smallest possible size (3 - 5nm diameter) that the highest strength is obtained. The dislocation substructures produced after deforming both alloys are very similar. Figs. VIII.2&3 show some typical dislocation networks obtained after deforming a microstructure containing the coherent zones.

Fig. VIII. 2

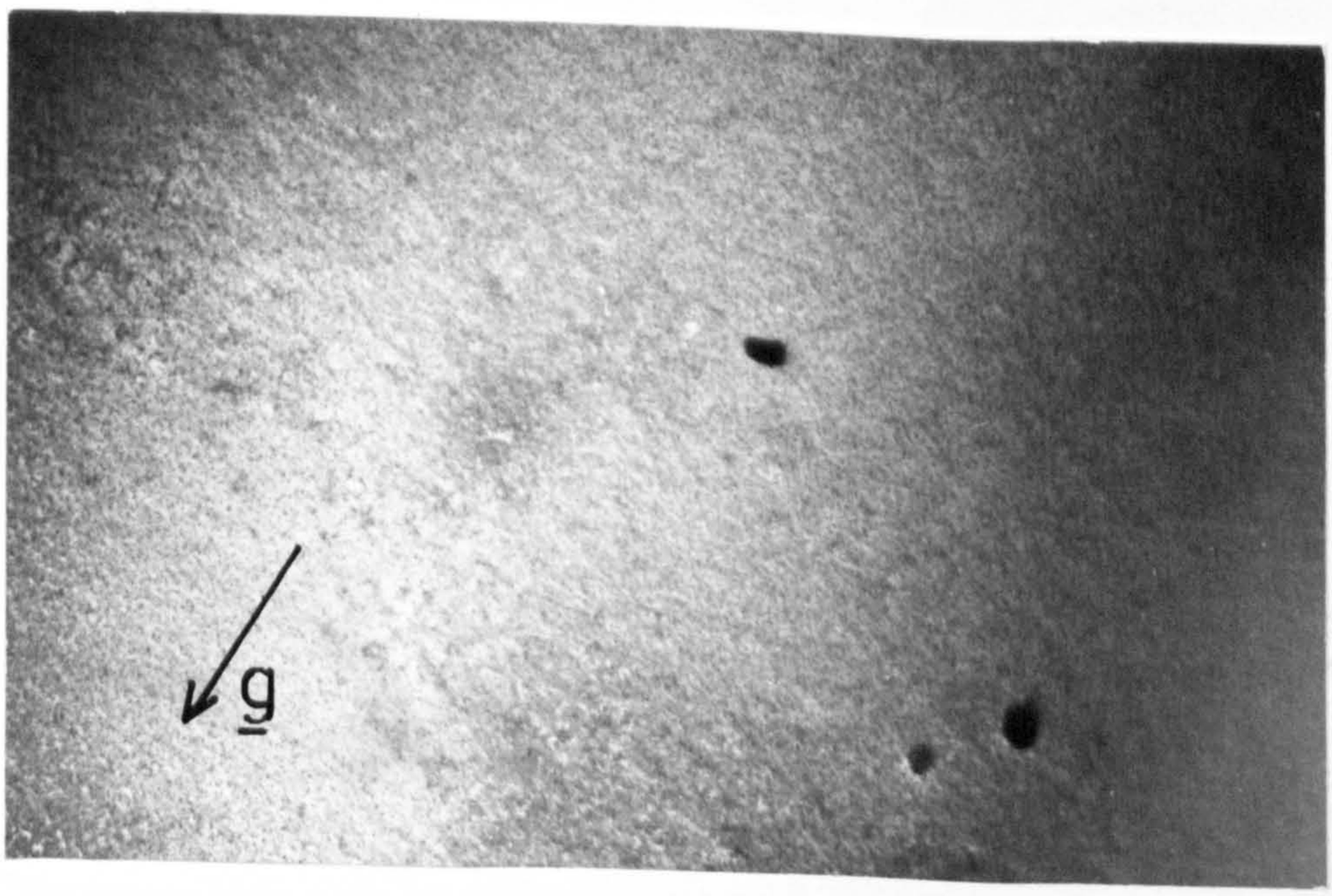
(a)



(b)



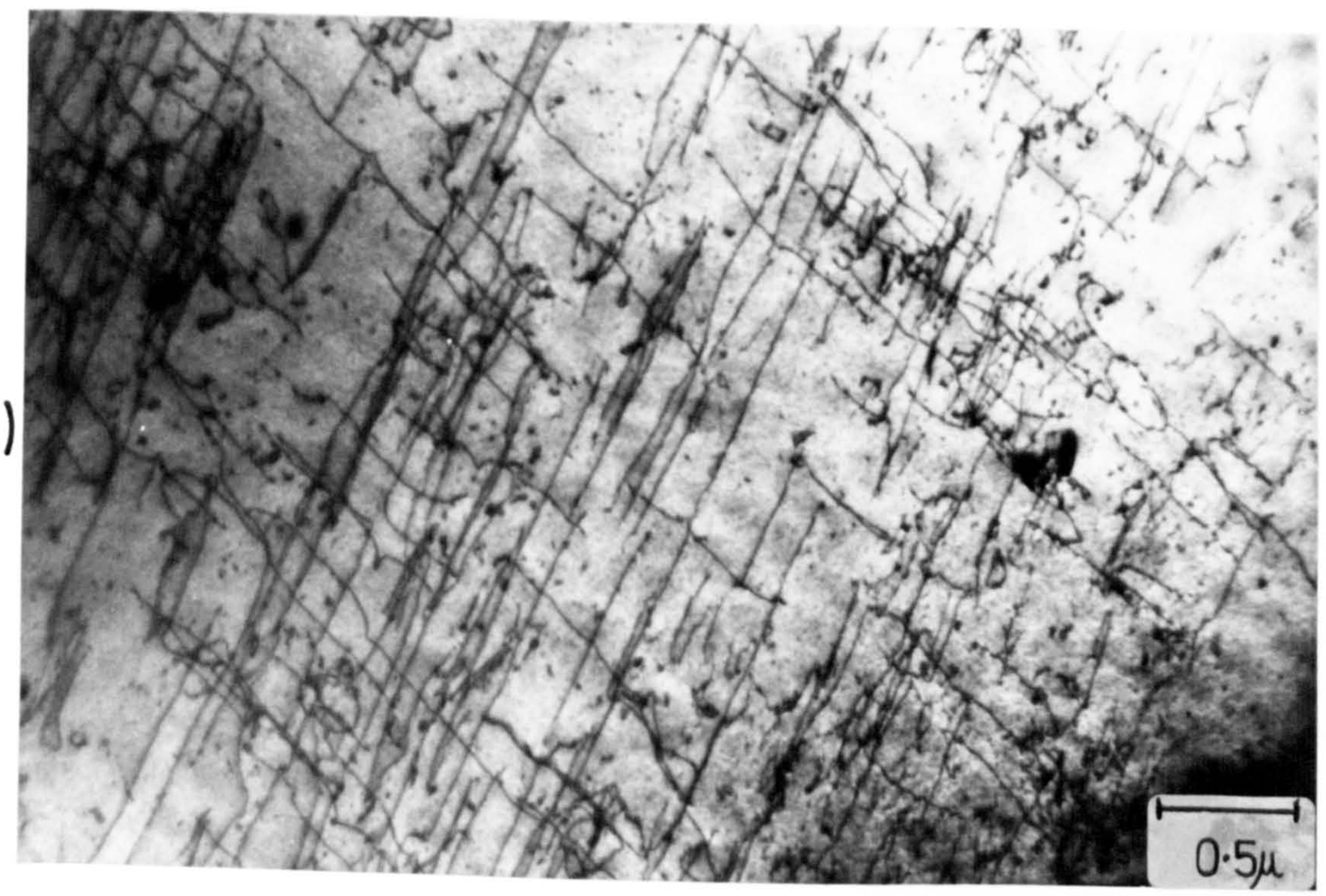
(c)



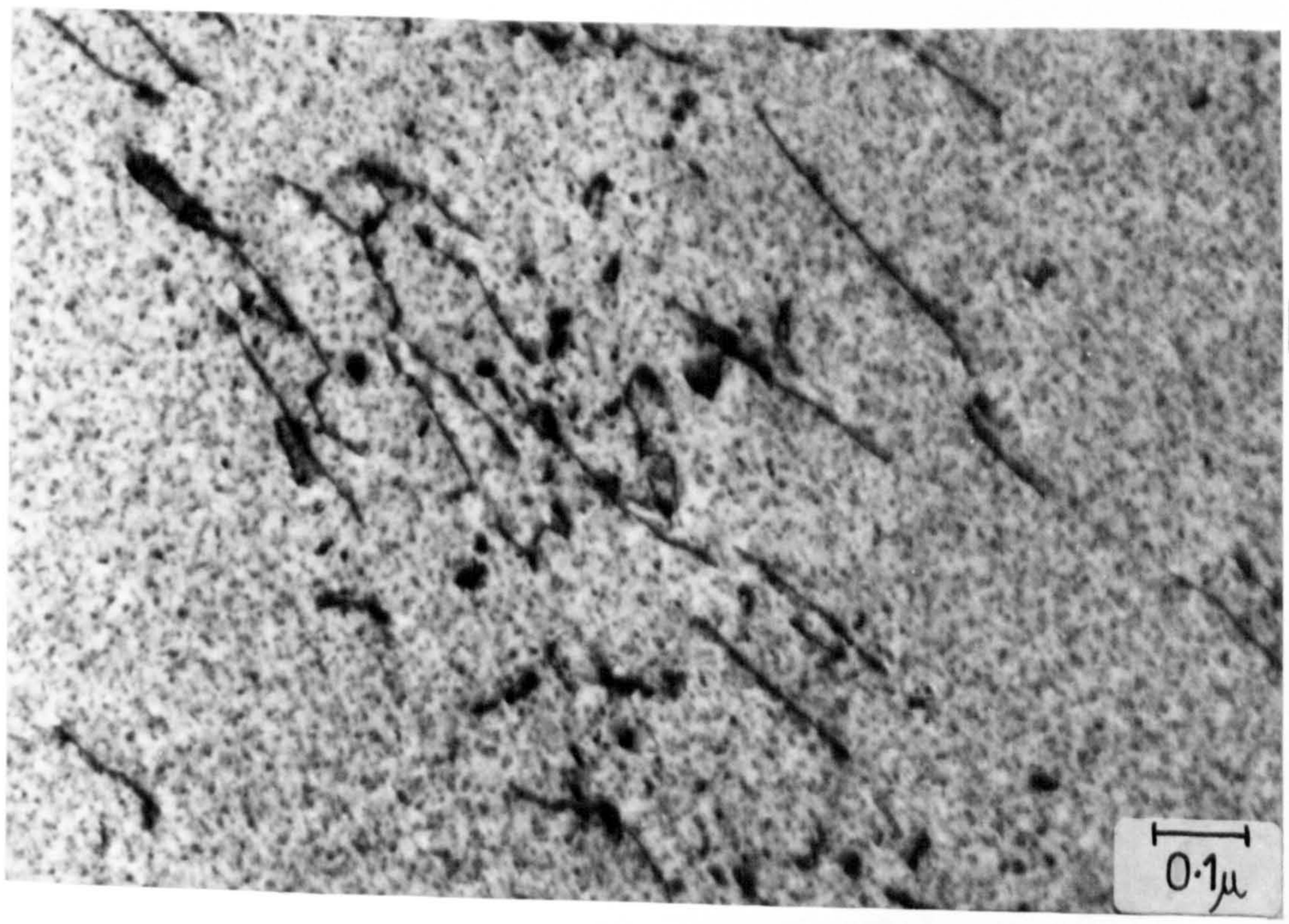
Dislocation substructures in nitrided Fe-0·1at.%Nb

Fig. VIII. 3

(a)



(b)



Dislocation-particle interactions in Fe-0·1at.%Nb nitrided at 550°C in 1NH 99H to precipitate coherent disc-shaped zones

The structure shown in Fig. VIII.2(a) is obtained after nitriding the Fe-0.1at.%Nb in $0.5NH_3$:$99.5H_2$ at 550°C for 48 hrs. and straining by 1%. A heterogeneous dislocation distribution is observed, slip occurring on several adjacent planes grouped together within about 0.3 μ of each other and each group being separated from the next by about 1.5 μ. The areas between the bands are comparatively free from dislocations. The configuration consists primarily of long lengths of straight dislocations which are apparently confined to their slip planes, and at the low level of strain introduced into the sample there is no development of any sub-cells or tangles.

Fig. VIII.2(b) shows a similar band of dislocations, but the foil is parallel to (011), the primary slip plane of b.c.c. iron. From the observation of discrete slip bands being present it seems that slip is restricted to certain planes. If this is true, then all of the dislocations within a given band will have the same Burgers vector, except for changes of sign. Therefore, all of the dislocations should disappear when the correct imaging reflection is used (see Section VIII.6). This phenomenon is observed in Fig. VIII.2(c) when the slip band structure disappears using the $(2\bar{1}\bar{1})$ reflection. This confirms that the Burgers vector $\underline{b}$ is $a/2\,\langle 111\rangle$ and consequently, that the dislocations are screw in character ($\underline{b}$ is parallel to the line of the dislocation).

The individual particles are only just discernable in the micrographs shown in Fig. VIII.2 and so it is impossible to tell the exact nature of the dislocation-particle interaction. However, no dislocation loops are present and the general character of the dislocations and the type of slip observed are consistent with the particles having been sheared during deformation.

The restriction of slip in certain bands (coarse or planitary slip) is a feature generally associated with particle cutting. This has been explained by Gleiter & Hornbogen (1965) as arising because of the shearing of precipitates in one glide plane lowering the resistance to further dislocations, resulting in paths of easy deformation and therefore, inhomogeneity of slip. A consequence of this type of deformation is poor ductility, which is frequently observed in the nitrided ferrites.

Fig. VIII.3(a) shows the deformed microstructure after nitriding the Fe-0.1at.%Nb alloy in $1NH_3:99H_2$ at 550°C, associated with a higher strain (2%). A predominance of long, straight, screw dislocations is observed and many of them appear to be pinned. In between the long dislocations there is a considerable amount of debris. The larger dislocation debris consists of elongated and equiaxed loops, which are thought to originate from the points where the dislocations appear to be pinned. In places, the process of forming these pinched off loops can be seen to be nearly

completed.

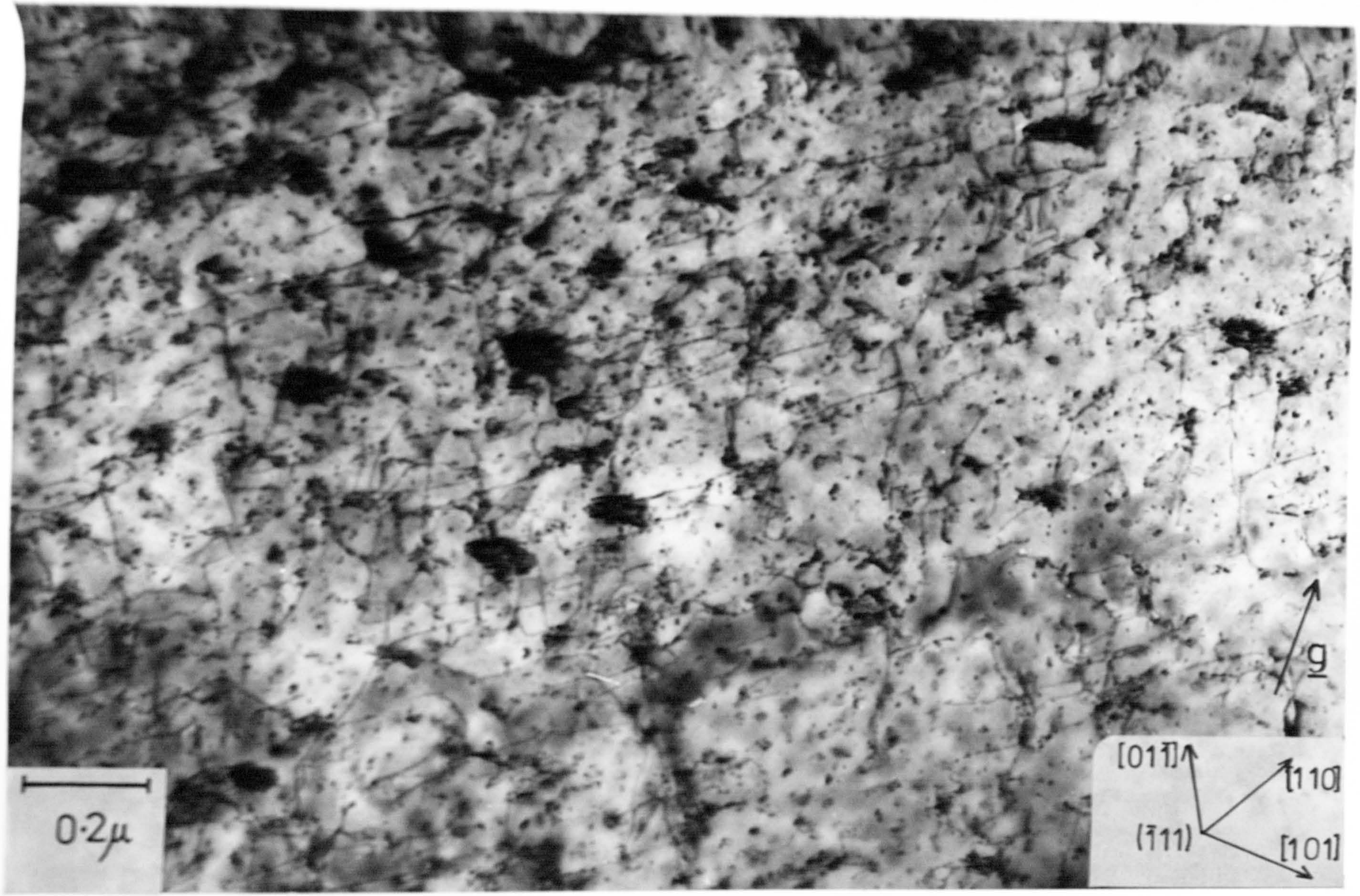
Fig. VIII.3(b) is of a similar area taken with the foil orientated on (011), the primary slip plane, and at a higher magnification. The longer lengths of dislocations are observed to be in <111> . The individual particles are also resolved in this micrograph and appear as coherent discs of about 5nm diameter. Many dislocations appear to pass through the particles, therefore providing substantial evidence that the first formed particles (GP zones) in nitrided Fe-X alloys are sheared during deformation.

Most samples of nitrided Fe-X alloys cannot be deformed to high strains due to their extreme brittleness. Only by nitriding at low potentials to produce a lower particle density, which is due to the incomplete precipitation of the substitutional solute, can tensile samples be more extensively deformed. For example, nitriding the Fe-0.15 at.%V alloy in $1NH_3:99H_2$ at 575°C only introduces 0.08at.%N. Consequently, a lower volume fraction of zones forms, which enables the microstructure to be deformed to a higher strain. Fig. VIII.4 shows the dislocation arrangement in this alloy after 10% strain. Due to the greater work hardening, dislocation tangles and cells start to form and individual dislocations are observed to inter-connect these tangles.

VIII.5 Fe-X-N alloys containing precipitates

Either nitriding at temperatures above 650°C or ageing

Fig. VIII. 4



Dislocation structure in Fe-0·15at.%V nitrided at 575°C in $1NH_3:99H_2$
(ϵ=10%)

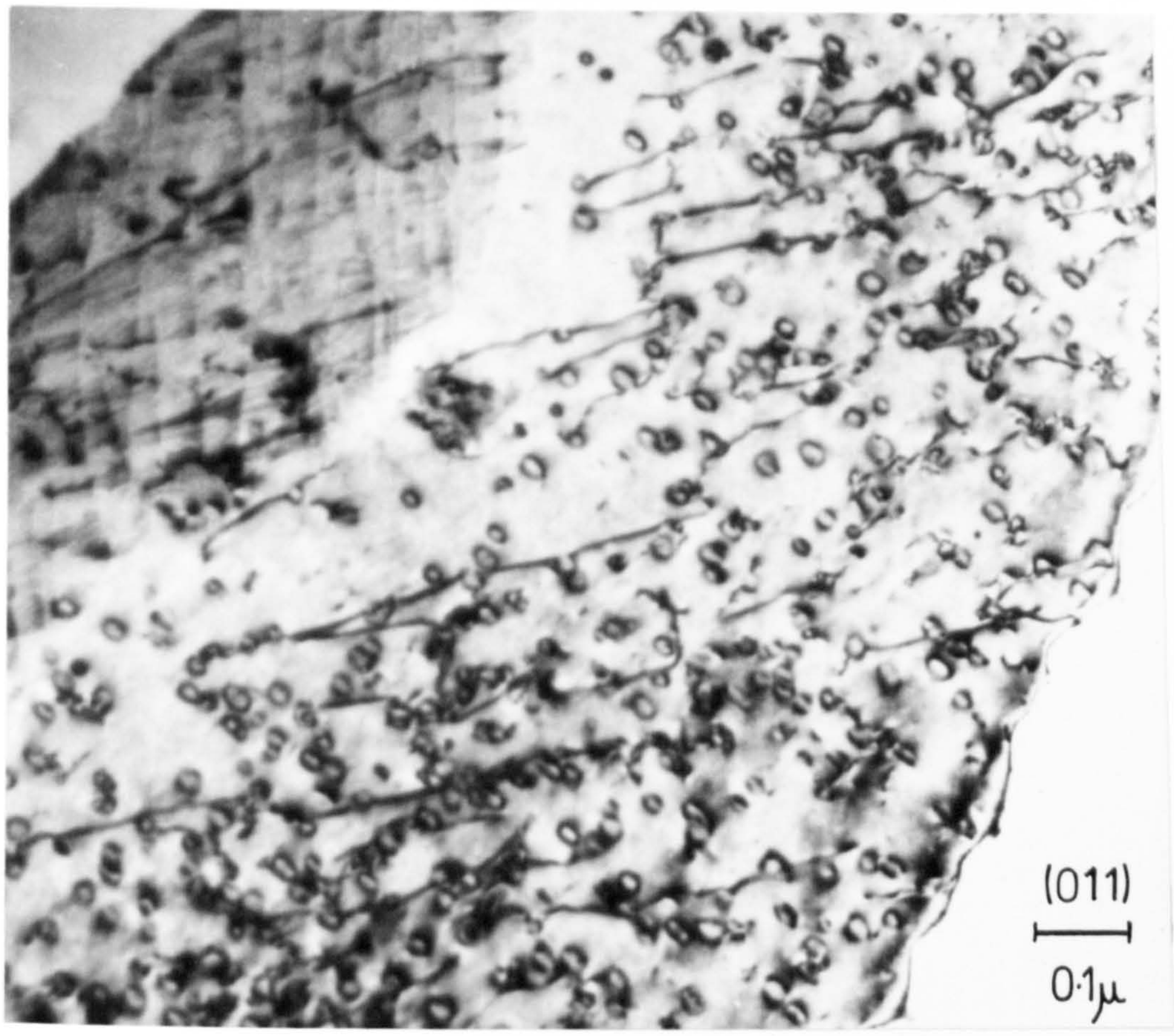
the zones formed at low temperatures results in the precipitation of the equilibrium alloy nitride. Figs. VIII. 5 & 6 show the dislocation interactions associated with the incoherent precipitates.

Fig. VIII.5 is of the Fe-0.15at.%V alloy nitrided at 575°C in $3NH_3:97H_2$, to form zones, and subsequently aged for various times at 750°C to precipitate incoherent VN. After ageing for 24 hrs., particles of ≈ 18nm diameter are present. The dislocation network shows dislocations which are apparently looping some of the particles. Continued ageing for 60 hrs. (see Fig. VIII.5(b)) forms particles which show displacement fringe contrast. The rectangular appearance of some of the particles is caused by their intersection with the top or bottom surfaces of the foil. The dislocations appear to surround or go across the precipitates. Although no individual loops are visible, it is evident that the particles have been by-passed.

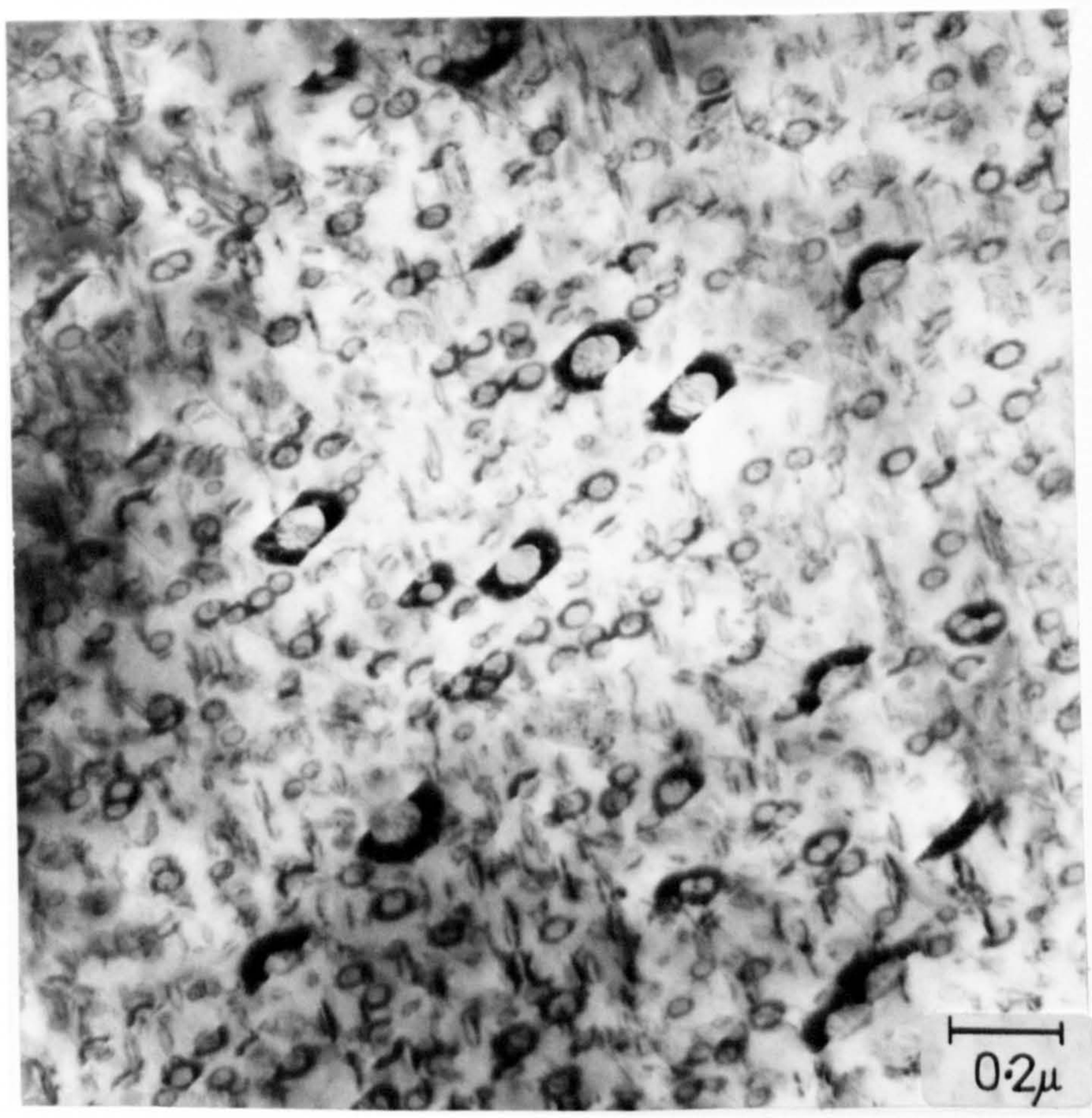
Similar types of interactions are observed after nitriding at high temperatures to precipitate the equilibrium alloy nitride. Fig. VIII.6 shows the dislocation interactions with NbN precipitates in the Fe-0.10at.%Nb alloy in two different foil orientations. Dislocations appear to be tangled around the particles and some interconnect the particles, although the exact mechanism of deformation cannot be identified. The more random orientation of dislocations in the presence of precipitates is indicative of easier dislocation movement. This explains why the alloys

Fig. VIII. 5

(a)

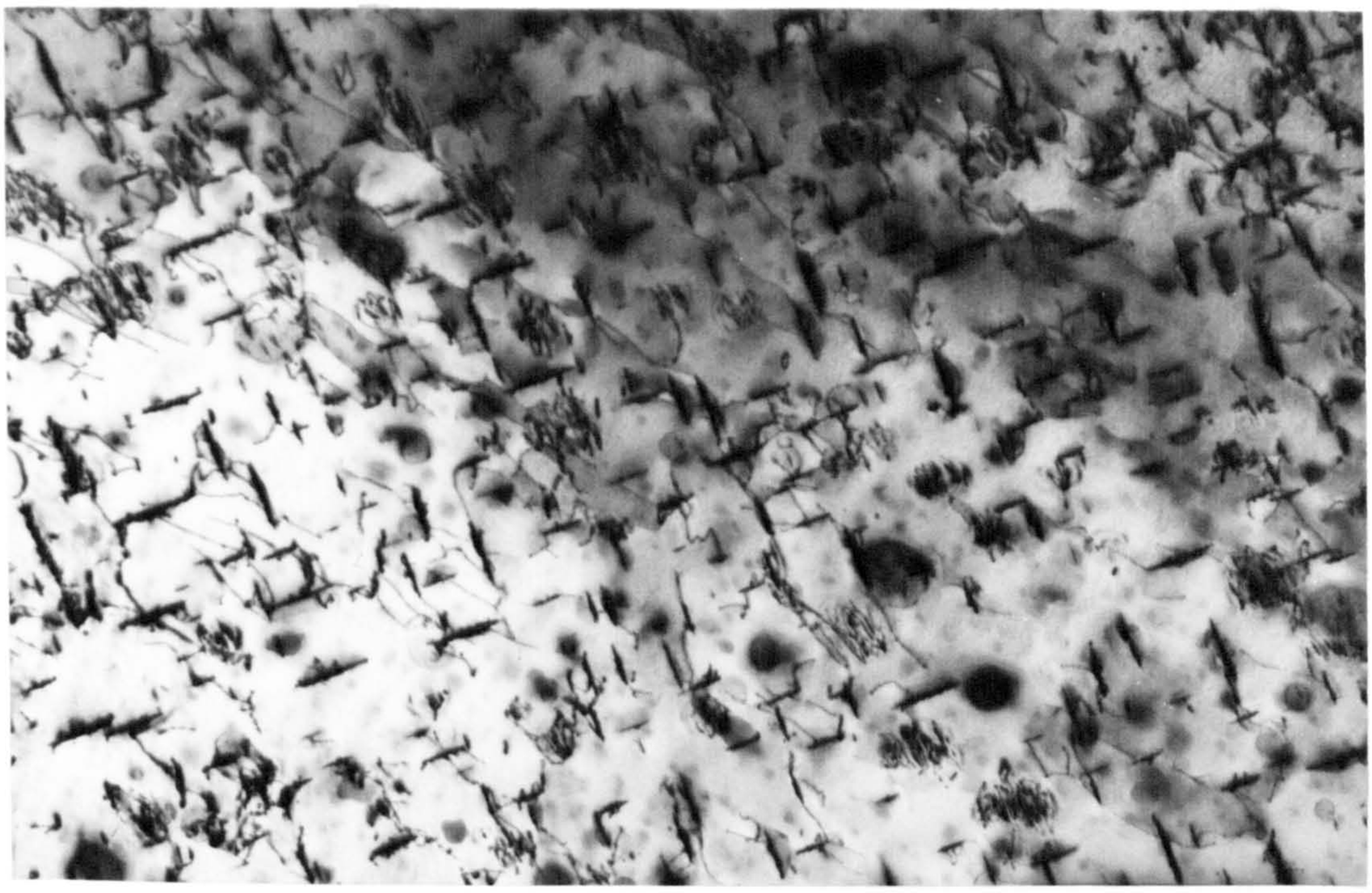


(b)



Dislocation-particle interactions in Fe-0·15 at.%V nitrided at 575°C in 3NH 97H and aged at 750°C for (a) 24hrs and (b) 60hrs to produce VN

Fig. VIII. 6



(001)



($\bar{1}$11)

Dislocation-particle interactions associated with NbN precipitates produced by nitriding Fe-0·1at.%Nb at 700°C in 0·6NH_3:99·4H_2

are capable of allowing more work hardening, and consequently, why they are more ductile. Many dislocations probably originate at the particle-matrix interface due to the necessity of maintaining continuity; this is because the particles remain undeformed as the surrounding matrix deforms.

VIII.6 Burgers vector analysis

Dislocations become invisible in the electron microscope when the correct imaging reflection is used. If g is the reciprocal lattice vector, the condition for no contrast is:-

$$\underline{g}.\underline{b} = 0 \qquad \ldots\ldots\ldots \qquad (VIII)_1$$

The criterion is not strictly applicable for edge dislocations due to the presence of some minor atomic displacements perpendicular to $\underline{b}$. However, contrast is weak for edge dislocations, and screw dislocations become invisible. In order to identify $\underline{b}$, a series of micrographs is taken using different $\underline{g}$ vectors. From one or more of the vanishing conditions $\underline{b}$ can be calculated. In Figs. VIII.2(b) & (c), the dislocations within the localised slip bands were shown to go out of contrast using a $(2\bar{1}\bar{1})$ reflection, confirming that the dislocations have a Burgers vector of the type $a/2\ \langle 111\rangle$ i.e. they are screw dislocations.

When dislocations in more than one orientation are present, only one set will disappear for a particular g. The principle is shown in Fig. VIII.7 for dislocations in the Fe-0.1 at.%Nb alloy containing zones. The foil is parallel to (O11), the primary slip plane of b.c.c. iron. Fig VIII.7 (a) shows the general dislocation structure without a strong g vector. A primary set of long, straight dislocations are visible together with some shorter lengths in a different slip system. By tilting and rotating the foil, images of the dislocation structure can be obtained using different g vectors. For example, using the $(2\bar{1}1)$ reflection the primary dislocations are still visible and only by using the $(\bar{2}\bar{1}1)$ reflection do the dislocations disappear (see Fig. VIII.7(c)). Therefore, applying VIII.1 they must have a b of either $^{a}/_{2}\ [\bar{1}1\bar{1}]$ or $^{a}/_{2}\ [1\bar{1}1]$. Consequently, the dislocations can be identified as screw dislocations with a Burgers vector of the type $^{a}/_{2}\ \langle 111\rangle$.

VIII. 7 Discussion

There are two ways in which dislocation structures observed in thin foils may be unrepresentative of bulk material:-

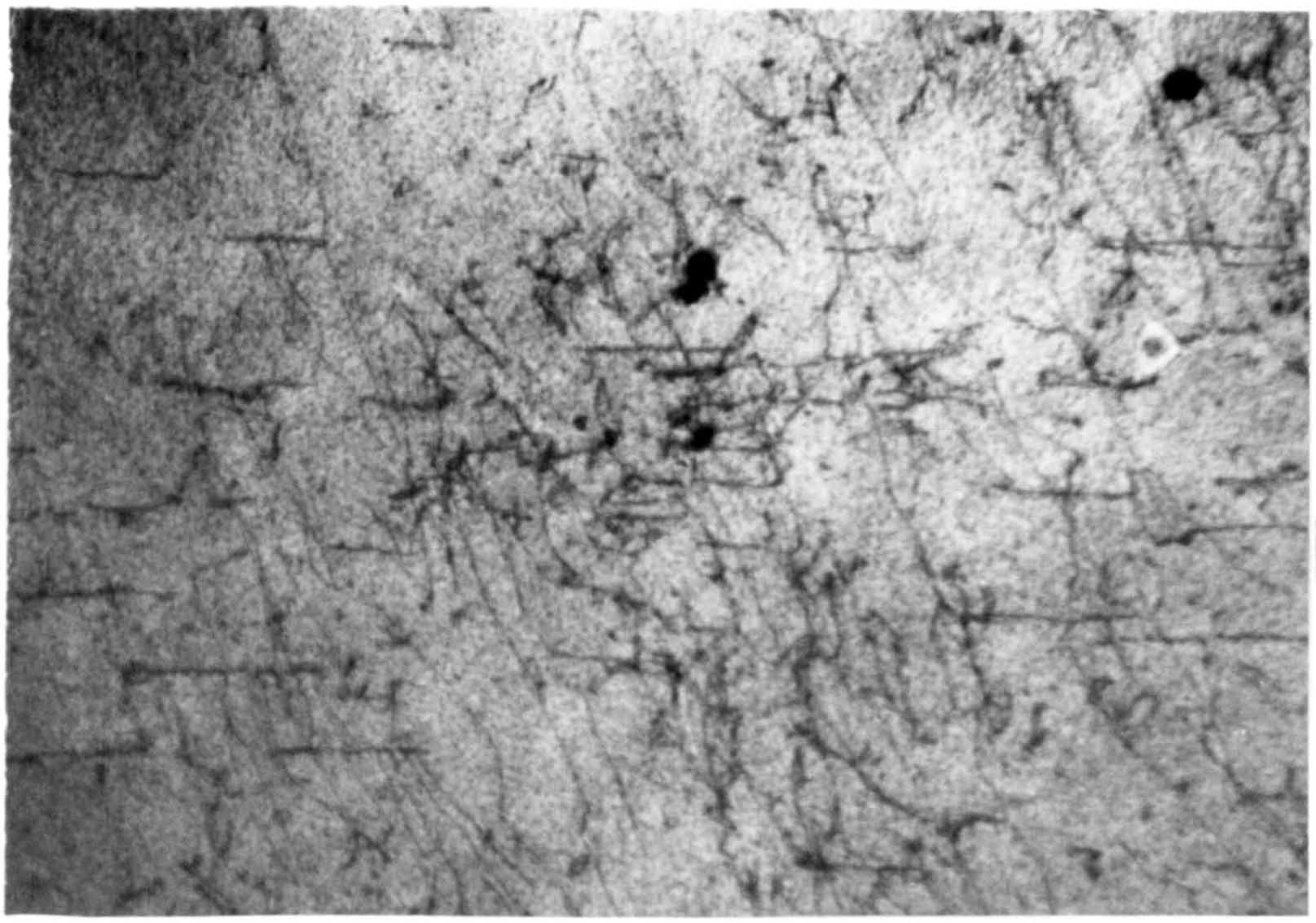
i) Dislocations may be lost or re-arrange themselves on thinning due to relaxation of long range stresses.

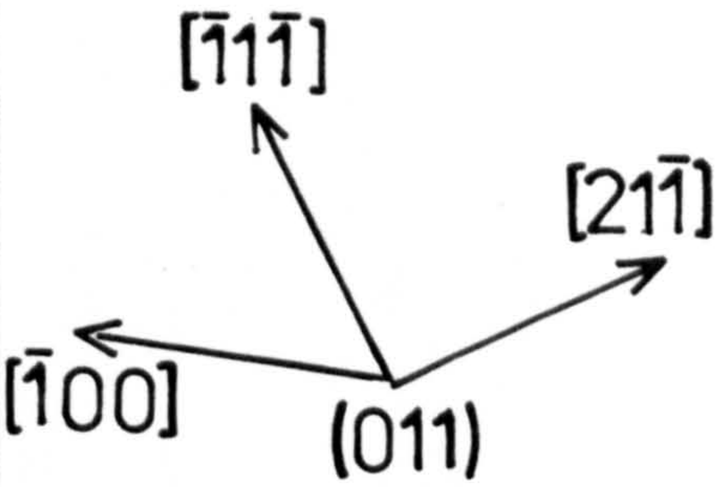
ii) Some dislocations may be introduced by mechanical deformation during the foil preparation.

However, it is generally accepted that the reproducibility

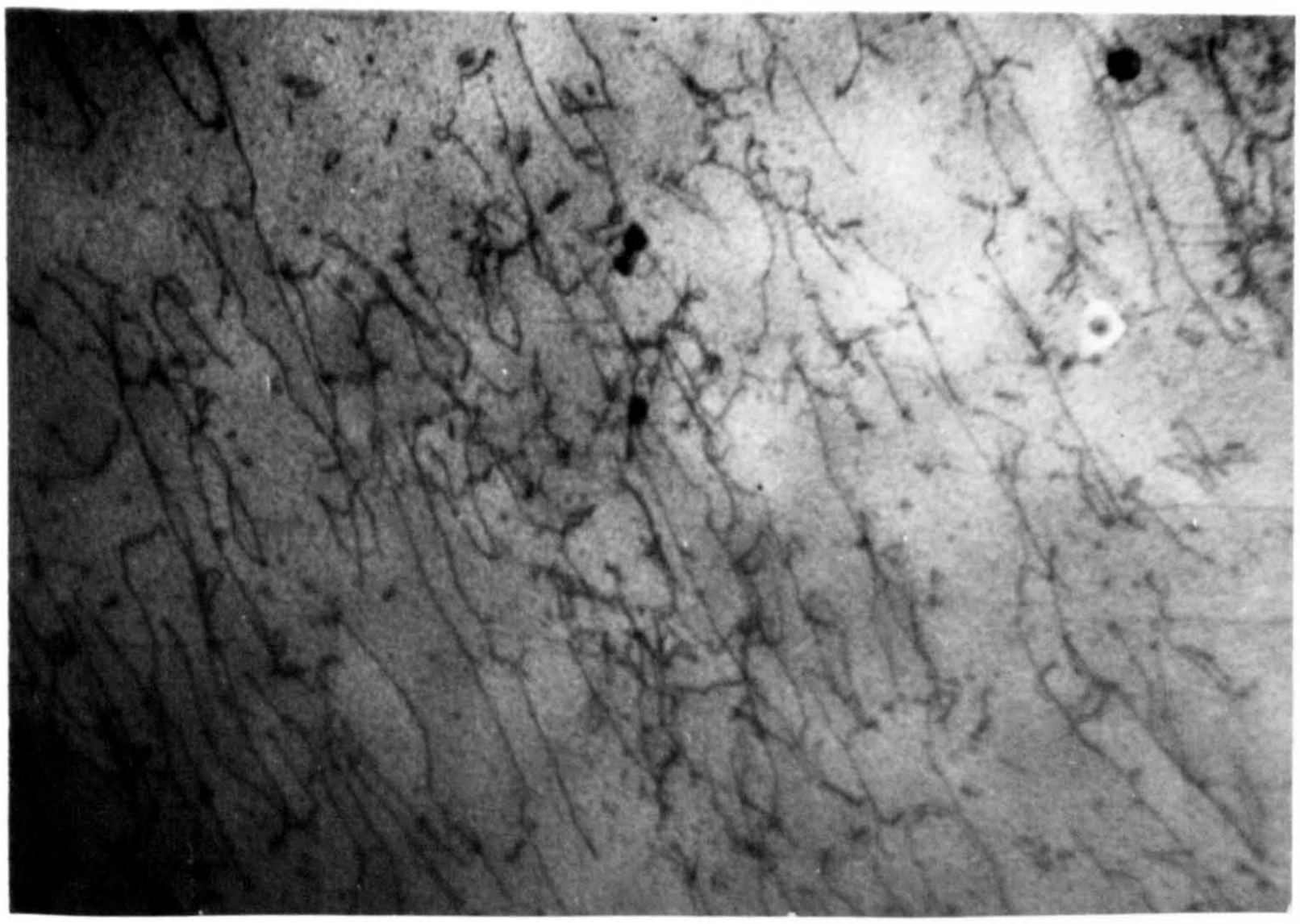
Fig. VIII. 7

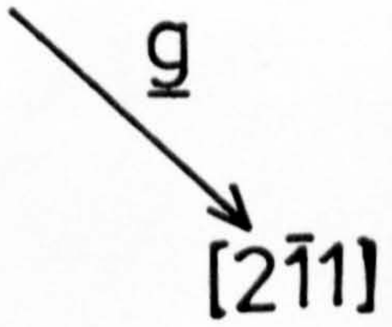
(a)



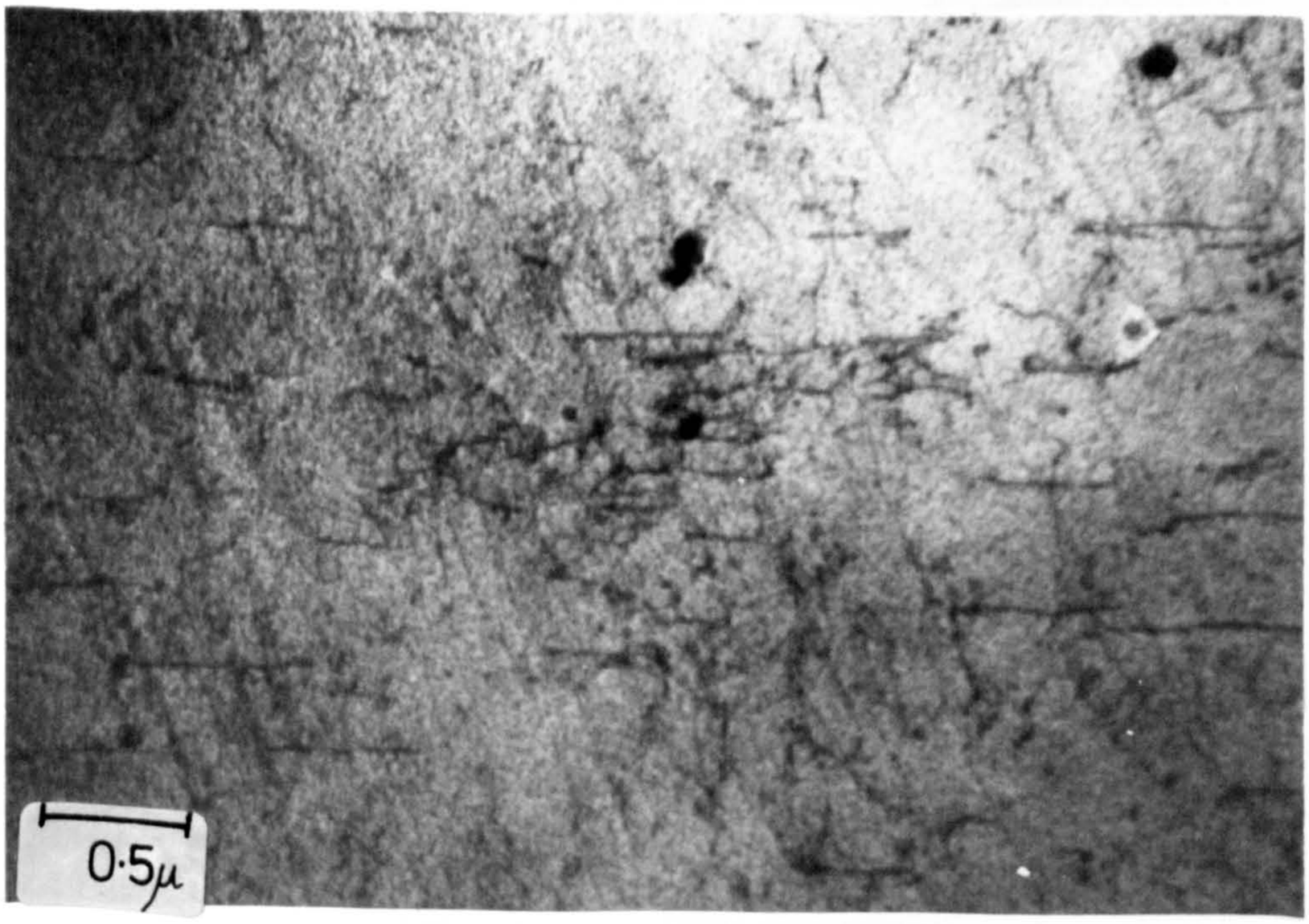


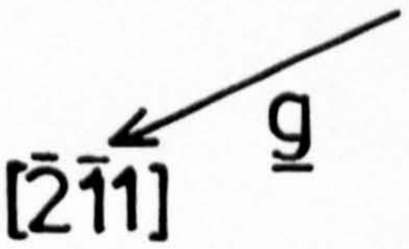
(b)





(c)





of dislocation arrays gives a true indication of the actual structure, any peculiar or anomolous observations probably being artefacts. The structures observed in deformed Fe-X-N alloys are reproducible and any misinterpretation or anomolies due to foil preparation are considered to be unlikely because the nitrided ferrites are hard, stable structures at room temperature.

An examination of dislocation configurations and interactions with dispersed particles assists in obtaining an understanding of the prevalent deformation mechanism, since the most fundamental aspect of second phase particles is the way in which they behave during deformation. Transmission electron metallography enables these interactions to be directly examined.

It is generally accepted that small; coherent particles are cut by dislocations during deformation; partially coherent particles are sometimes cut, whilst incoherent particles remain unchanged. However, full coherency in itself is not a sufficient criterion to establish particle cutting; the binding energy, size and spacing of the particles are also important parameters. Kelly & Nicholson (1963) concluded that generally, coherent particles up to 20nm diameter are cut and larger particles, which initially resist shearing, may deform at higher strains. Some shearing of smaller particles is even possible when the flow stress is controlled by the looping or by-passing of particles. Most

of these conclusions are based on studies of dislocation interactions in Al-Cu alloys (Nicholson et al 1960) and other f.c.c. age hardened alloys.

Particle cutting is often characterised by a low dislocation density, and the occurrence of dislocation pairing or banding. These observations have been noted in many age-hardening systems prior to and at peak hardness. Overaged precipitates are generally associated with higher dislocation densities, with the precipitates being surrounded by dislocation loops or tangles.

From the present investigation it appears that the small, coherent disc-shaped zones are sheared during deformation. Continued deformation, when possible, results in the formation of dislocation tangles and cells. Overageing the particles to a size where the equilibrium precipitate can be identified results in dislocationslooping or bypassing the particles. Complex tangles form around the larger incoherent precipitates as a result of the particle-matrix interface providing further dislocation sources and anchoring points for the multiplication of dislocations.

When the particles are sheared, bands of high dislocation density form on $\{110\}_\alpha$ planes. The dislocations within the band are screw in character and have a Burgers vector of the type $a/2\ \langle 111 \rangle$.

The dislocation substructures associated with the zones provide substantial evidence for particle shearing. The planarity of slip is considered to be evidence for cutting and this feature would explain the extreme brittleness of Fe-X-N alloys at peak strength. Gleiter & Hornbogen (1965) proposed that the reduction in ductility arises from crack initiation where slip bands intersect with one another and with grain boundaries.

The exact nature of the dislocation-particle interaction is difficult to identify in the presence of zones. The width of the dislocation images varies from 4-10nm, whereas the particles are only 5nm diameter and two or three atom planes thick. Nevertheless, it would appear that the dislocations pass through some of the zones shown in Fig. VIII. 3(b). The general character of the type, distribution and orientation of dislocations supports this deformation mechanism.

Similar dislocation structures to those observed in Fe-X-N alloys containing zones have been observed in the low temperature deformation of iron (Keh & Weissmann, 1963) and in single crystals of pure Fe-3%Si alloys (Low & Turkalo, 1962). As in the present investigation, Low & Turkalo observed jogs on screw dislocations. The jogs acted as pinning points for single ended sources of new dislocations and, depending on their separation, the edge dislocation trails pinched off to form debris of small loops in

the slip plane. Because of the absence of second phase particles in the Fe-Si alloys, the jogs were explained as being due to the plane of maximum shear stress not being precisely aligned to the crystallographic glide plane.

Jogs can form when particles are sheared because the slip planes in the matrix and particle are not parallel, the energy of formation depending upon the particle size. The preferred direction of jogs is perpendicular to the screw dislocations, i.e. in $\langle 211 \rangle$ and so they cause drag. This is a common feature in the deformation of all b.c.c. metals. The similarity in the dislocation structures in Fe-X-N alloys containing zones, is indicative of the same deformation mechanism occurring as in pure iron alloys. The only difference in Fe-X-N alloys is the much higher stress required to cause dislocation movement.

Several other investigators have either observed or postulated that cutting of coherent precipitates occurs in iron base alloys. Smith (1966) observed that the dislocation network appeared to be held by coherent precipitates in secondary hardened Fe-1%V - 0.2%C alloys at peak hardness. Some particles were apparently lined up with dislocations passing through them. Baker (1973b) thought that particle cutting contributed to the strength of tempered, control rolled low C-V-N steels, whilst Greday & Lamberigts (1974) assumed that particles of less than 7nm diameter were sheared by couples of dislocations in disper-

sion hardened vanadium and niobium containing steels. Also, there is some evidence for particle cutting in the simpler quench-aged binary Fe-C and Fe-N alloys (Hale & McLean, 1963; Keh, 1963).

Considerable attention has been given to the age-hardening of Fe-Si-Ti alloys (Papaleo & Whiteman, 1971; Watson & Brown, 1974; Jack & Guiu, 1975). This system is similar to the nitrided ferrites in that peak strength is observed at a small particle size. There is substantial evidence to suggest that the particles are sheared at peak strength, since both planarity of slip and dislocation pairing have been observed.

The transition from particle cutting to a by-pass mechanism takes place at a specific particle size, but the uniformity of change is gradual due to the range of particle sizes and spacings. There is evidence for such a change in Hornbogen's (1964) work on Fe-Cu alloys, although the particle size at which this occurs is not apparent. In Fe-X-N alloys, it is difficult to decide exactly when a change in mechanism actually occurs, although from the microstructures observed, it would appear to be within the particle size range of 10-15nm diameter.

Therefore, from the results of the present investigation and numerous other investigations it is apparent that particle cutting occurs in alpha-iron containing small, coherent particles and is associated with the maximum strength

increases. Indeed, the feature is not restricted to alpha-iron but is a common occurrence in all b.c.c. metals. Other investigators have observed similar dislocation structures in age hardened Ti-Mo alloys (Gysler et al, 1974) and in irradiated niobium (Ohr et al, 1970). In the latter investigation the behaviour was ascribed to the migration of interstitial impurities to defect clusters, which strengthened them as effective barriers to slip dislocations.

VIII.8 Conclusions

a) The dislocations associated with zones are similar to those observed in iron alloys, without any second phase particles, and to pure iron deformed at sub-zero temperatures.

b) Bands of dislocations on $\{110\}_\alpha$ are observed at peak strength. They are a consequence of the high yield strength and are a feature associated with particle shearing. This type of deformation favours crack nucleation at low macrostrains and explains the extreme brittleness of Fe-X-N alloys at peak strength.

c) The dislocations are screw in character with a Burgers vector of the type $a/2\langle 111\rangle$.

d) Numerous jogs form on the screw dislocations which are pinched off to form dislocation debris. The debris is often visible as elongated or equiaxed loops.

e) A change in deformation mechanism from particle shearing to looping or by-passing occurs when the zones are

from 10-15nm diameter.

f) Overaged, incoherent precipitates are associated with dislocation tangles at and around the particle-matrix interface.

Chapter IX

STRENGTHENING MECHANISMS IN Fe-X-N ALLOYS

IX.1 Introduction

The yield strength of a metal containing dispersed second phase particles is determined by the interactions which occur between moving dislocations and particles. There are two main ways in which the strength can be increased:

i) The particles act as impenetrable barriers to dislocation movement, forcing the dislocations to by-pass or bow out between them (Orowan hardening).

ii) The particles are sheared before the Orowan stress is reached, the strength deriving from the additional work required for the dislocation to shear the particle.

When coherent particles are precipitated it is usually easier for slip dislocations to shear particles than to by-pass them. However, full coherency in itself is not a sufficient criterion for particle shearing because the size, spacing and binding energy of the particles are relevant parameters.

Recent reviews of precipitation hardening include those of Kelly & Nicholson (1963), Gleiter & Hornbogen (1967), Brown & Ham (1971) and Kelly (1973). For simplification, the notation used in these reviews for the various strengthening mechanisms has been standardised and is shown in Table IX.1.

TABLE IX.1

G	-	shear modulus of matrix
ν	-	poissons ratio
b	-	Burgers vector
T	-	line tension of dislocation line
R	-	mean partide radius (sphere)
D	-	disc diameter
t	-	disc thickness
f	-	volume fraction of dispersed phase
τ	-	shear yield stress
$\Delta\sigma$	-	increment of tensile yield stress due to particles ($=2\tau$)
N_v	-	number of particles/unit volume
N_A	-	number of particles/unit area
L	-	mean centre-centre planar spacing
λ	-	effective interparticle spacing
ro	-	dislocation core radius ($\approx 2b$)
r_s	-	mean planar radius intersecting slip plane (sphere)
$\bar{A}$	-	mean area of intersection of slip plane
$\bar{l}$	-	mean intercept length
ϵ	-	particle-matrix mismatch
γ_p	-	internal interface or anti-phase boundary energy
γ_s	-	surface energy

Most strengthening models are derived for spheres, and therefore, suitable modifications to a system containing thin discs must be made whenever possible. The strengthening produced by discs is greater than that produced by the same volume fraction of spherical particles due to the greater number of particles intersecting the slip plane. From the observations of the mechanical properties and deformed microstructures of Fe-X-N alloys, it would appear that strengthening due to both deformable and non-deformable particles occurs at some stage during ageing. Therefore, the models for these strengthening mechanisms are explained in greater detail in the following sections.

IX.2 Strengthening by non-deformable particles

Most precipitation hardening models predict that dislocations can by-pass particles without shearing them beyond a critical obstacle spacing. In this way, the particles remain undeformed and so no terms are necessary to describe the inherent properties of the particle. The initial relationship predicting the yield stress was proposed by Orowan (1948):

$$\tau = \frac{2T}{bL} \qquad \ldots\ldots\ldots \quad (IX).1$$

Numerous modifications have been made to this relationship by incorporating more refined estimates of the dislocation line tension, by allowing for the effect of particle size on the mean planar interparticle spacing and by

taking into account the interaction of bowing segments. The combined additions give the currently accepted version of the Orowan equation for spherical particles (see Kelly, 1973):

$$\tau = \frac{0{\cdot}83Gb}{2\pi(1-\nu)^{\frac{1}{2}}} \frac{\ln\,(2R/r_o)}{(L-2R)} \quad \ldots\ldots\ldots \quad (IX)2$$

The equivalent expression for disc-shaped particles will be:

$$\tau = \frac{0{\cdot}83\ Gb}{2\pi(1-\nu)^{\frac{1}{2}}\lambda} \frac{\ln\,(\bar{x}/r_o)}{} \quad \ldots\ldots\ldots \quad (IX)3$$

where $\bar{x}$ is a measure of the particle diameter intersecting the slip plane and λ is the effective interparticle spacing.. For aligned discs, Kelly (1972) has shown that:

$$\bar{x} \approx \frac{2D}{\pi} \quad \ldots\ldots\ldots \quad (IX)4$$

Therefore the increase in yield strength produced by disc-shaped particles due to an Orowan type deformation mechanism is:

$$\Delta\sigma \approx \frac{1{\cdot}477 \times 10^{-2} \log\,(D/\pi b)}{\lambda} \ {}^{N}/_{mm} \quad \ldots\ldots \quad (IX)5$$

An additional theoretical expression of the Orowan equation for alloy systems containing elongated plate or rod shaped particles of length, l, and width, t, has been derived by Hirsch & Humphreys (1969):

$$\tau = \frac{0{\cdot}83\ Gb}{2\pi(1-\nu)^{\frac{1}{2}}} \cdot \frac{1 + {}^{l}/_{L}}{L} \ln({}^{t}/_{r_o}) \quad \ldots\ldots\ldots \quad (IX)6$$

However, L is the mean centre to centre planar spacing and

not the effective interparticle spacing, λ. For disc-shaped particles it is probable that the minimum end to end spacing will control the strength, and to allow for this Kelly (1972) has developed an expression to calculate λ:

$$\lambda = \frac{L}{1 + P/L} - \frac{\pi t}{2} \qquad \ldots\ldots\ldots \quad (IX).7$$

where $P = \frac{2D}{\pi} - t/2$

Using this expression in (IX).6, Kelly has shown that an aligned array of thin plates can cause strengthening up to three times that produced by the same volume fraction of spheres.

IX.3 Strengthening by deformable particles

For small, coherent particles it is likely that the energy required to force dislocations through the particle will control the flow stress. However, there is no single equation which combines all the strengthening mechanisms and so the contribution from the various interactions occurring between dislocations and particles have to be evaluated.

The resistance to shearing is controlled by numerous factors (see Kelly & Nicholson, 1963) which include:

i) The interaction between moving dislocations and the coherency stress fields around the particles (coherency hardening).

ii) The particle may be ordered internally and so the Burgers vector of the moving dislocation does not equal the repeat distance of the ordered structure. Therefore, work is required to create a disordered interface across the slip plane, which raises the energy of the system. This contribution to strengthening is called chemical or order hardening and the new interface has an energy, γ_p.

iii) The lattice parameters of the matrix and particle may be different, so that extra work is required to form misfit dislocations at the interface (surface hardening). If the slip plane of the particle is tilted with respect to the matrix, additional energy will be required to form jogs as the dislocations pass through the particle.

It is apparent form transmission electron metallography that the zones in nitrided Fe-X alloys are associated with large coherency strain fields. Therefore, coherency hardening may make a marked contribution to the yield strength. A quantitative estimate of the strength increases produced by spherical particles has been made by Gerold & Haberkorn (1966):

$$\tau = G (\epsilon)^{3/2} \left(\frac{R}{b}\right)^{\frac{1}{2}} f^{\frac{1}{2}} \qquad \ldots\ldots\ldots \quad (IX),8$$

The maximum interaction occurs at small distances from the particle. The equation is derived for spheres and its application to thin discs is restricted in view of the varying degrees of strain at the plate interfaces.

An alternative method of calculating the stress field of thin disc-shaped particles has been made by Kelly & Nicholson (1963). The stress necessary to force dislocations through particles intersecting the slip plane is found by regarding the stress field as being equivalent to a loop of edge dislocation, and applying a calculation made by Saada (1960). The force required to move a dislocation through the particle is then equivalent to that required to move it through a forest of dislocations intersecting the slip plane. The applied stress, τ, is given by:

$$\tau = \frac{Gb_p}{5L} \qquad \ldots\ldots\ldots \text{(IX).9}$$

where L is the average separation of fixed dislocations and b_p their Burgers vector. In applying this result to particles (of separation L on the slip plane), b_p is taken as the discontinuity in elastic displacement obtained when a Burgers circuit is made through the particle and matrix.

Numerous estimates have been made for determining the stress required to force dislocations through particles. However, the process in itself consists of several individual components. Kelly & Nicholson (1963) estimated the contribution to the yield stress by equating the work done in moving a dislocation forward a distance $\underline{b}$ to the individual short range interactions. The particles are of average separation L, and of average length $\bar{l}$ on the slip plane. The individual components are:

i) The work done in disordering = $\gamma_p \bar{l} b$

ii) The energy of the new surface interface = $(\underline{b}.\underline{n})b\gamma_s$ where n is a unit vector normal to the interface.

iii) The energy required to increase the length of the dipole of edge dislocation arising from the production of jogs when the dislocation enters the particle $\approx \frac{Gb^3 \cos^2\alpha}{2}$

where α is the angle between the moving dislocation line and its $\underline{b}$.

Therefore,

$$\tau b^2 L = \gamma_p \bar{l} b + (b.n)b\gamma_s + \frac{Gb^3}{2}\cos^2\alpha \ldots\ldots\ldots \quad (IX).10$$

Applying this relationship for thin disc-shaped particles (see Fullman, 1953):

$$L = \left(\frac{Dt}{f}\right)^{\frac{1}{2}} \text{ and } \bar{l} = 2t$$

Putting these values in (IX).10:

$$\Delta\sigma = \frac{4\gamma_p}{b}\left(\frac{ft}{D}\right)^{\frac{1}{2}} + 2\left(\frac{f}{Dt}\right)^{\frac{1}{2}}\left(\frac{b.n}{b}\gamma_s + \frac{Gb}{2}\cos^2\alpha\right) \ldots\ldots\ldots \quad (IX).11$$

More accurate determinations of the individual components have been made. Ham (1968) calculated the average particle breaking strength for finite, ordered spherical particles to be:

$$\tau = \left(\frac{2}{\pi\Gamma}\right)^{\frac{1}{2}} \frac{\gamma_p^{\frac{3}{2}}}{b} (r_s f)^{\frac{1}{2}} \quad \ldots\ldots\ldots \quad (IX).12$$

Ham's model is derived for spheres and so it is necessary to modify the equation to estimate the strength increases produced by discs. In order to do this, the same approach as Ham used for spheres is adapted:

The Friedel relationship may be stated as,

$$S.N = 1 \qquad \ldots\ldots\ldots \quad (IX).13$$

Where S is the area swept out by the dislocation when released from the obstacle and N is the number of particles per unit area.

For spheres, Ham obtains:

$$S = 2\left(\frac{T}{\tau b}\right)^2 \left(\frac{\gamma_p r_s}{T}\right)^3 \left(1 - \frac{2r_s}{L}\right) \qquad \ldots\ldots\ldots \quad (IX).14$$

An equivalent term for r_s is required, the mean planar radius of the sphere intersecting the slip plane. The mean intercept length of a thin disc is 2t (Fullman, 1953). Therefore, the distance t will be comparable to r_s Substituting t for r_s in (IX).14 and putting $N = f/Dt$ equation (IX).13 becomes:

$$\tau \approx \frac{\sqrt{2}\, t}{bT^{\frac{1}{2}}} \left(\frac{f}{D}\right)^{\frac{1}{2}} \gamma_p^{\frac{3}{2}} \qquad \ldots\ldots\ldots \quad (IX).15$$

Substituting $T = \dfrac{G.b^2}{4\pi(1-\nu)^{\frac{1}{2}}} \ln D/\pi b$

the strength increment due to shearing is:

$$\Delta\sigma \approx \frac{9.236\, t\, (\gamma_p)^{\frac{3}{2}}}{G^{\frac{1}{2}}\, b^2 \ln\left(D/\pi b\right)^{\frac{1}{2}}} \left(\frac{f}{D}\right)^{\frac{1}{2}} \qquad \ldots\ldots\ldots \quad (IX).16$$

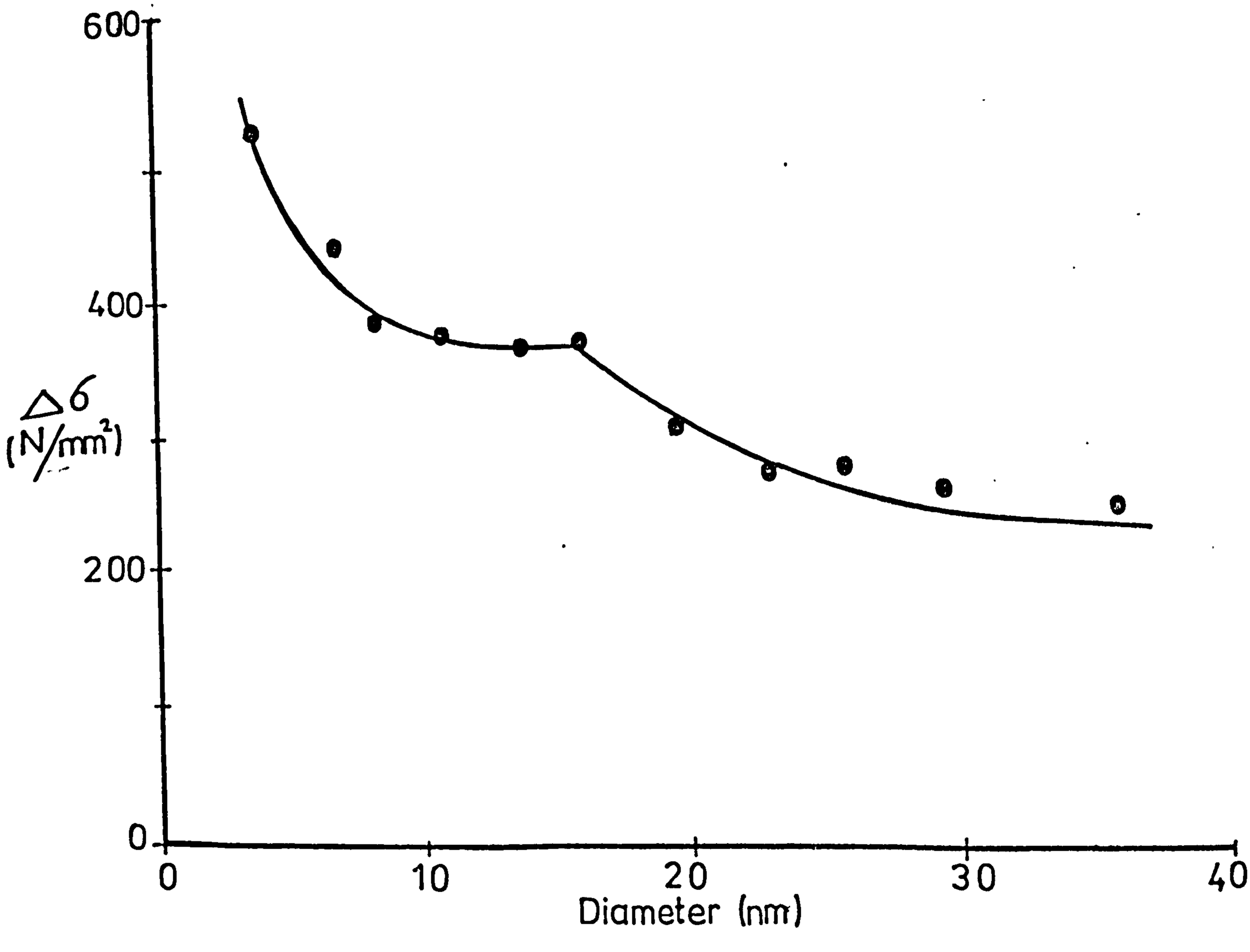
Obviously, in view of the numerous expressions available it is difficult to identify which particular process predominates when particles are deformed. Also, there may be some doubt as to the validity of the expressions due to the very thin nature of the particles.

IX.4 Application of theories to Fe-X-N alloys

The most informative results of the variation in yield strength with particle diameter have been obtained in the nitrided Fe-0.15at.%V alloy (see Fig. IX.1). After nitriding in $3NH_3:97H_2$ at 575°C the alloy contains 0.20at.%N and zones of $\approx$4nm diameter. The zones were subsequently aged in argon at 750°C for various times to produce the range of particle sizes. The strength increases, which exclude the contributions made by nitrogen in solid solution and the as-annealed strength, can be attributed solely to the precipitated particles. From the general shape of the curve it would appear that more than one strengthening mechanism is prevalent over the full range of particle sizes. The observations made from the deformed microstructures suggest that a change in deformation mechanism occurs when the particles become incoherent (10-15nm diameter), and it is at sizes above this that the strength continuously decreases as the alloys overage.

In order to demonstrate if a change in the deformation mechanism occurs it is necessary to plot the yield strength

Fig. IX. 1



Variation in yield strength with particle diameter for Fe-0·15at.%V-0·20at.%N

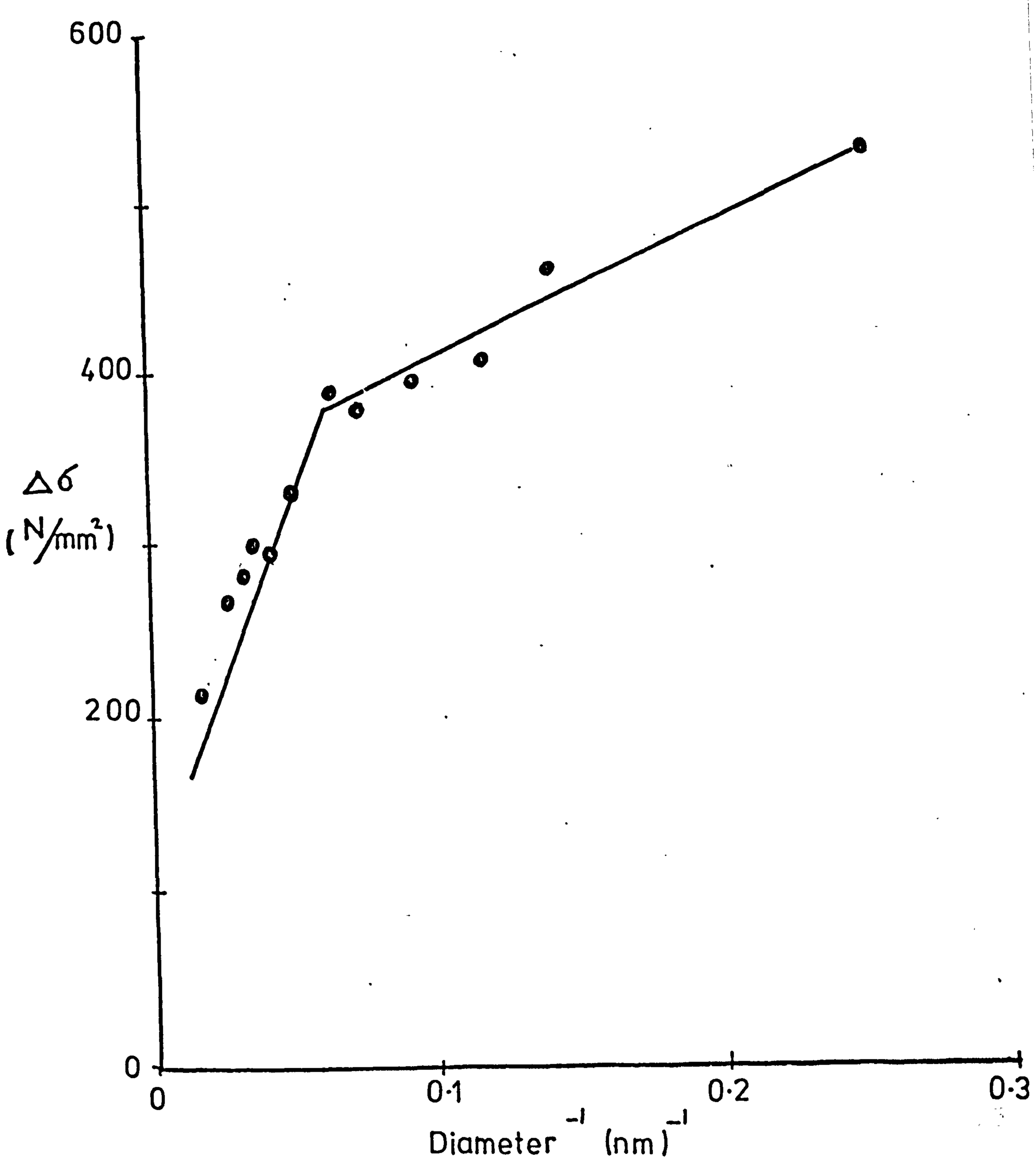
against a relevant parameter. The Orowan mechanism, which will control the strength of overaged particles, is proportional to $^1/_L$. For thin discs:

$$L = \left(\frac{Dt}{f}\right)^{\frac{1}{2}} \qquad \ldots\ldots\ldots \quad (IX).17$$

Therefore, the Orowan stress will be proportional to the reciprocal of the disc diameter if the disc aspect ratio is assumed to remain approximately constant. Most strengthening mechanisms for deformable particles predict a different dependence on particle diameter. Consequently, if a change in mechanism occurs the strength should not be proportional to D^{-1} for the entire range of particle sizes. Fig.(IX)2 shows the results for the Fe-V-N alloy. A discontinuity in the graph occurs at a diameter of about 15nm, inferring that a different mechanism controls the strength below this particle size. The change in slope is substantial and an inspection of the results shows that it is not due to the approximation made in predicting a D^{-1} relationship. Any discrepancy could stem from the fact that the disc aspect ratio is less at small diameters.

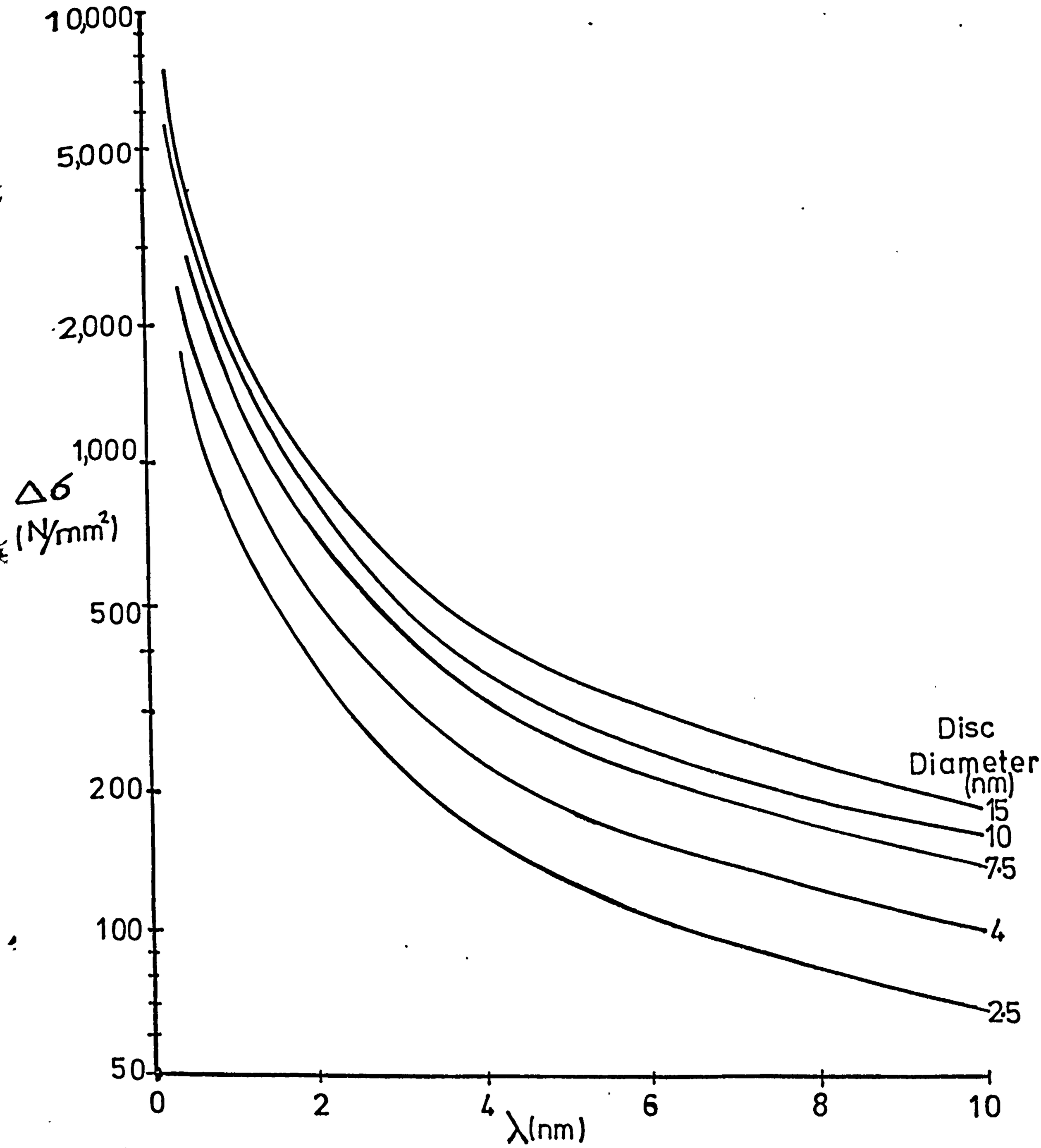
Accurate determinations of the Orowan stress for disc shaped particles are complicated due to the necessity of calculating the effective interparticle spacing, which is dependent on the disc dimensions and volume fraction of precipitated phase. Fig. IX.3 shows the relationship between the yield strength and the effective spacing using equation

Fig. IX. 2



Variation in yield strength increment with the reciprocal of disc diameter for Fe-0·15at.%V-0·20at.% N

Fig. IX. 3



Orowan relationship using equation (IX).5

(IX).5 for particles having different disc diameters. In order to predict the strength for a particular Fe-X-N alloy it is necessary to assume that all of the substitutional solute is precipitated as particles with an X:N ratio of 1:1. To calculate λ , the mean centre to centre spacing is obtained from (IX).17 and then this value is used in (IX).7. For the Fe-0.15at.%V alloy at peak strength, λ is found to be about 25nm, predicting an Orowan stress of 450 N/mm^2. This is below the observed strength increment (530 N/mm^2), a result which is unexpected since the Orowan stress should be higher.

Possible reasons for the low value could arise from the inadequacy of the equation or from an underestimate of λ . The initial discs are so small that many of the particles are only just discernable in the electron microscope and therefore, the particle size is probably overestimated, resulting in λ also being an overestimate.

The initial zones become incoherent at 12-15nm diameter and at sizes beyond this the Orowan mechanism can be expected to be prevalent. At a disc diameter of 15nm the observed strength increment is $380N/mm^2$ whereas the predicted Orowan stress from Fig. (IX)3 is in the range $250-300N/mm^2$ (i.e. an underestimate of at least 20%).

Therefore, it is apparent that the Orowan equation (IX).5 underestimates the strength produced by thin discs. Calculation of the Orowan stress using (IX).6 gives even lower

values. Strength increments varying from 120-440N/mm^2 are obtained for the initial zones depending upon the log term used; very low results are obtained when the disc thickness is used.

The difficulty of using an Orowan relationship for such very small particles as are observed in the nitrided ferrites is that small changes in the particle size markedly effect the interparticle spacing, causing large differences in the predicted values. However, the equations even predict low strengths for overaged particles. This could partly be explained as being due to the log term representing an overcorrection of the dislocation line tension (see Kelly, 1973).

An evaluation of the strength increases produced by deformable particles cannot be accurately made because of the unknown energy values. An alternative method of using the equations is to equate the terms to the observed strengths and calculate the pertinent energy necessary to cause the strengthening. Further complications arise from the unknown contribution form each individual mechanism, making it necessary to assume that a single process contributes to all the strength increase. Also, the values can only be approximations because the equations are of doubtful validity in view of the very thin nature of the particles.

Assuming that all the terms in (IX).11 are zero except for γ_p, then the energy required to predict the observed

yield strength of the as-nitrided Fe-0.15at.%V at peak strength is 1,350 ergs/cm^2. Using equation (IX).16 a similar value of 1,520 ergs/cm^2 is obtained for γ_p. Alternatively, if all the strength derives from surface hardening, then γ_s (as calculated from (IX).11) would be about 17,000 ergs/cm^2.

The values are those necessary to predict the strength from a single deformation mechanism. If, more than one mechanism prevails the energy will be lower; therefore, the values represent an upper limit of the energy for the individual process.

Estimates of the strength produced by coherency stresses using (IX).18 range from 70N/mm^2 (2%misfit) to 3,000N/mm^2 (40 % misfit). The values are calculated using the disc diameter for the 2% misfit and the disc thickness for the large misfit region. Despite the uncertainty arising from the varying strain at the plate interfaces, it is evident that some contribution to the strength can be expected.

The Kelly & Nicholson (1963) approach for the stress field of thin discs (eqn.(IX).9) predicts strength increments of 130N/mm^2 using b_p=0.1nm. A detailed estimate of the strength arising from this method is impossible to attain in view of the uncertainty of the value of b_p.

The most informative results on the size and structure of the initial zones have been observed in the Fe-Mo-N system. From field ion metallography (see Fig. II.9) the zones are clearly imaged as discs of about 12nm diameter by 1.5nm thick. The effective end to end spacings are observed to be as low as possibly 4nm. These observations enable many of the theories developed for strengthening by discs to be evaluated. From (IX).17 the mean centre spacing is 17nm, so that using (IX).7 the effective spacing becomes 10nm; this is observed to be an overestimate. From Fig. (IX).3 the Orowan strength for the nitrided Fe-3.0at.%Mo alloy at peak hardness will be from 2,000 - 5,000 N/mm^2 depending upon whether the calculated or observed spacing is used. The increase in microhardness (V.P.N.) is 750 kg/mm^2, so the yield strength can be expected to be about 2,250 N/mm^2. Using this value in the equations for chemical hardening predicts that a γ_p value of about 1,600 $ergs/cm^2$ would be necessary to produce this strength increase. The value is very similar to that obtained for shearing the zones in the Fe-0.15at.%V alloy.

IX.5 Temperature dependence of the yield strength

The yield strength of the nitrided Fe-0.15at.%V containing coherent particles has been shown to be very temperature dependent (see Fig. VII.10). It is thought that this arises due to the prevalent deformation mechanism. Orowan hardening is not expected to produce a large temperature dependence, whereas when short range interactions control the yield

strength thermal activation is expected to facilitate the process of shearing.

The temperature dependence of the yield strength has been analysed following the model of Kelly & Nicholson (1963). For a dislocation to overcome the resistance of a barrier (e.g. a GP zone) in the absence of an applied stress, the energy of the system is increased by U_o . The stress required to reduce U_o to zero is τ_o. If the dislocation moves under an applied stress, τ, the variation of the energy of the dislocation with distance is given by:

$$U(x) = U_o \left\{ 1 - \frac{1}{1+\exp x/x_o} \right\} - bl_o \tau x \quad \ldots\ldots (IX).\ 18$$

where l_o is the separation of particles on the slip plane.

The potential to be overcome is reduced to

$$U = U(x_2) - U(x_1)$$

where x_2 and x_1 are the roots of the equation

$$\frac{d\,U(x)}{dx} = 0$$

Solving this equation, U is given by:

$$U = U_o\,(1-\tfrac{\tau}{\tau_o}) - bl_o x_o \tau \ln\left\{ \frac{1 + \frac{(1-\tau/\tau_o)^{\frac{1}{2}}}{1-\frac{1}{2}\tau/\tau_o}}{1 - \frac{(1-\tau/\tau_o)^{\frac{1}{2}}}{1-\frac{1}{2}\tau/\tau_o}} \right\} \ldots\ (IX).19$$

where x_o is the width of the barrier to be surmounted and

$$\tau_o = \frac{U_o}{4bl_o x_o}$$

If the temperature dependence of the flow stress is large ($\tau \ll \tau_o$) then (IX).19 reduces to:

$$U = U_o - 4bl_o x_o \tau \qquad \ldots\ (IX).20$$

The measured flow stress, which is related to the energy required for a dislocation to shear an obstacle, is found by using the strain rate equation:

$$\dot{\epsilon} = \dot{\epsilon}_o \exp - \frac{U(\tau)}{KT} \qquad \ldots\ (IX).21$$

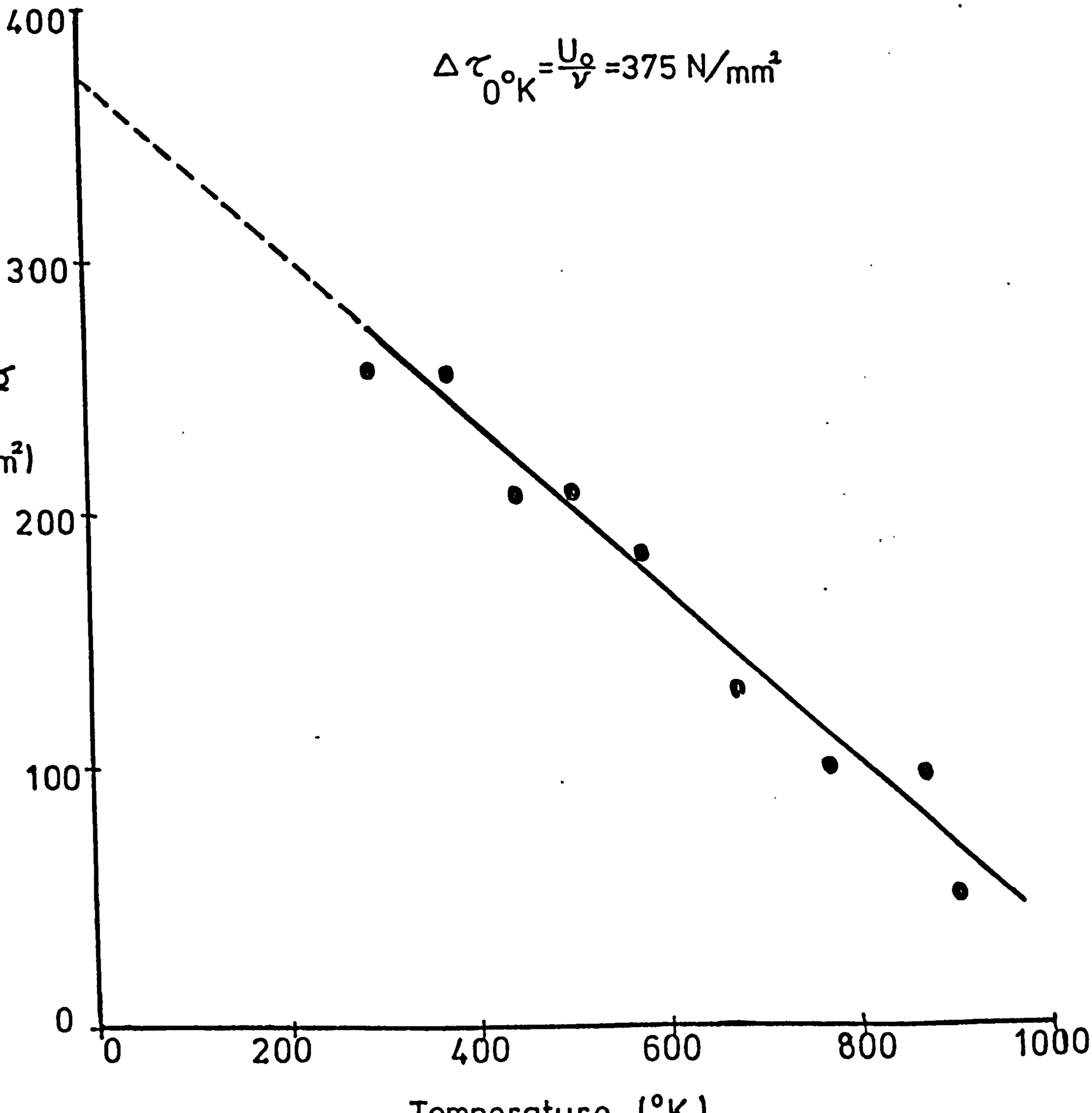
Substituting (IX).20 in (IX).21 and putting $\nu = 4bl_o x_o$

$$\tau = \frac{U_o}{\nu} - \frac{kT}{\nu} \ln \frac{\dot{\epsilon}_o}{\dot{\epsilon}} \qquad \ldots\ (IX).22$$

where ν is called the activation volume and $\dot{\epsilon}_o$ is a material constant. Therefore, when the temperature dependence of the yield stress is large a plot of τ against T should be linear, with an intercept of U_o/ν.

Fig. (IX)4 shows the results obtained for the zones in the nitrided Fe-0.15at.%V alloy. The back extrapolation is artificial since it neglects the effect of temperature on the lattice friction stress; however, this should be unimportant as it is the value for the shearing process above room temperature which is of interest (each thermally activated process will have its own U_o value). From Fig. (IX)4

Fig. IX. 4



Temperature dependence of the shear stress in Fe-0·15at.%V-0·16at.%N containing 5nm diameter GP zones

the value of U_o/γ is 375N/mm^2. It is possible to estimate ν from the zone size and distribution. For spherical zones it is given by 2 rbl_o, i.e. $x_o = r/2$ where r is the zone radius. For thin discs the value of x_o should be related to the zone thickness and not its diameter.

Putting $\nu = 2\ tbl_o$ for the initial coherent zones gives ν values from 8.34×10^{-21} (for t = 0.6nm) to $1.82 \times 10^{-20}/cm^3$ (for t = 1nm) using a constant zone diameter of 4nm. Therefore, U_o is in the range 3.13×10^{-11} - 6.79×10^{-11} ergs.

If U_o is the energy required to shear a zone by one interatomic distance, the value of γ is:

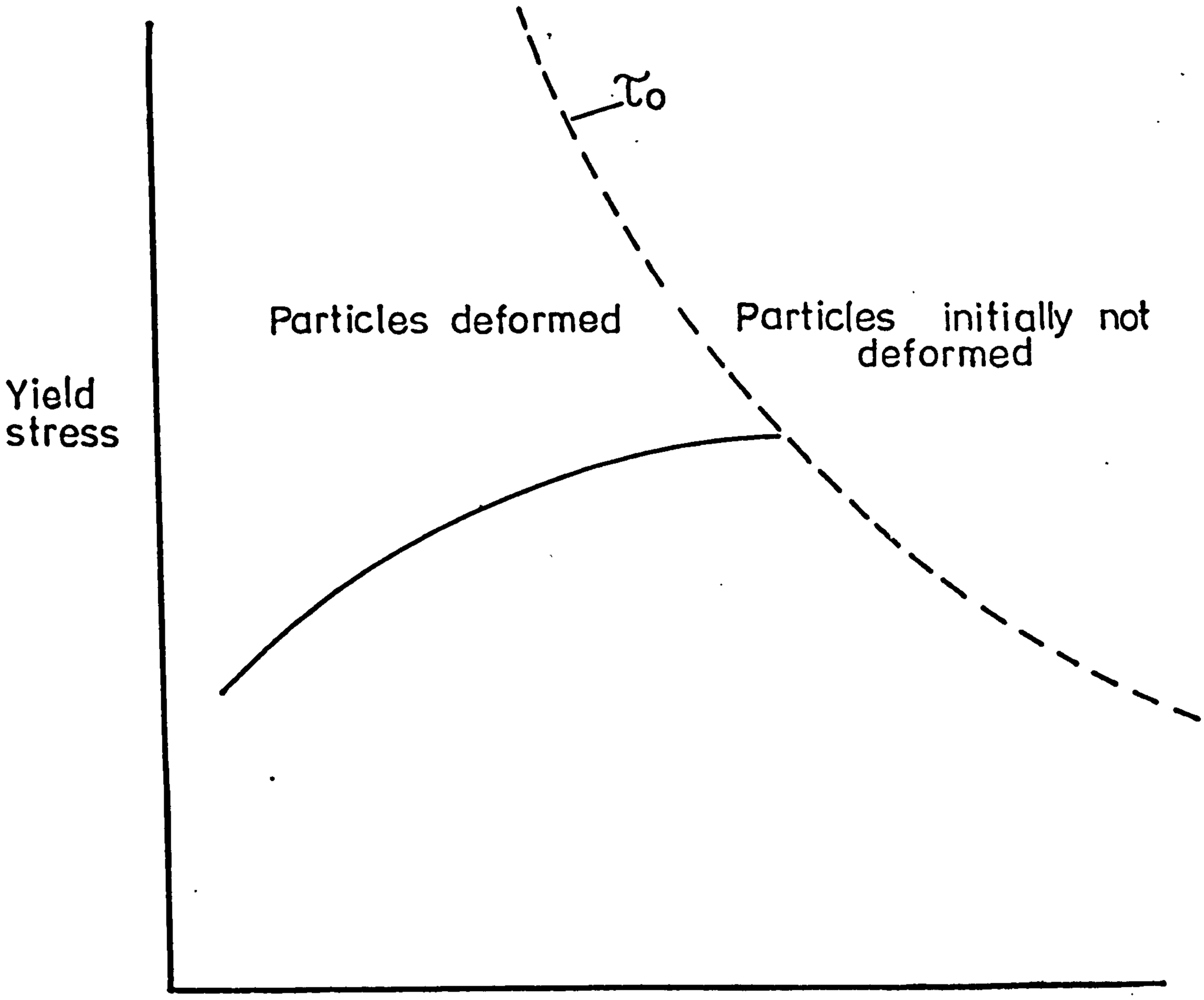
$$\gamma = \frac{U_o}{Dt} \qquad \ldots\ (IX).23$$

Therefore, γ is from 1300 - 1700 ergs/cm^2, which agrees favourably with the value calculated for shearing the zones using (IX).11 & (IX).16.

IX.6 Discussion

The variation in yield strength with ageing time (or particle diameter) for a typical age-hardening alloy is shown schematically in Fig. IX.5. The strength increases until a maximum is reached, remains approximately constant, and then decreases as the alloy overages. Generally, a change in deformation mechanism from particle cutting to looping occurs

Fig. IX. 5



Schematic variation of the yield stress with ageing time (or particle size) for a typical age-hardening alloy system. τ_o is the stress necessary to force dislocations between precipitates.

[after Kelly & Nicholson, 1963]

at, or just beyond, the peak strength. The behaviour of the nitrided Fe-X alloys is different (see Fig. IX.1), since the maximum strength is observed at the smallest particle size. Upon ageing, the strength decreases rapidly at first and then remains approximately constant before decreasing as the alloy overages.

Calculations of the Orowan stress for the fine, coherent platelets predict strengths below the observed strength increases. However, when the particles become undeformable and an Orowan type deformation mode almost certainly predominates, the predicted strengths are at least 20% too low. Therefore, the Orowan stress for the initial zones is probably a considerable underestimate.

A possible explanation for the low values is the log term in the Orowan expression, which approaches zero for very small particles. The term originates from calculations of the the dislocation line tension as $\ln \lambda/r_o$ and is replaced by the smaller value $\ln \bar{x}/r_o$ in order to allow for the mutual interaction of bowing segments. However, this has been shown to represent an over correction for these interactions (see Kelly, 1973) and consequently, low values are predicted.

Although Gladman et al (1971) showed that the strengths of finely dispersed second-phase particles in steels obeyed the Orowan-Ashby (1964) equation, Baker (1973 b) found that the relationship did not account for the strength increases

produced by the precipitation of similar particles in tempered, control-rolled steels. The application of the equation to commercial steels is difficult in view of the wider ranges of particle sizes and morphologies, and because of the unknown volume fraction of particles precipitated in a finely dispersed form, Further errors may arise from the exact value of $\bar{x}$ used in (IX).3. This term should describe the average particle diameter intersecting the slip plane, which is not the same as the actual particle diameter. In view of these considerations it is thought that any agreement to an Orowan equation for finely dispersed, coherent particles is coincidental.

When particles precipitate as a coherent second-phase they are usually deformable, whereas the Orowan relationship is developed for incoherent particles which remain undeformed at least initially, during deformation. From the results of the present investigation it is apparent that the coherent platelets in nitrided Fe-X alloys are deformable and that a change in deformation mechanism occurs at a similar particle diameter as when coherency is lost (12-15nm diameter).

There is no single equation which combines all the strengthening mechanisms for deformable particles. However, Nicholson (1971) has advocated that the yield strength of deformable, spherical paticles is represented by a relationship of the form:

$$\sigma = K R^{a} f^{b} \Delta E^{c} \qquad \ldots\ldots\ldots \text{(IX).24}$$

where $0 < a < \frac{1}{2}$, $\frac{1}{3} < b < \frac{2}{3}$, $1 < c < \frac{3}{2}$ and K is a material constant. Therefore, the strength is strongly dependent on ΔE, the irreversible energy change occurring when particles are cut, and will be maximised when ΔE is large (i.e. when the forces of interaction between dislocations and particles are as large as possible). Expressions for coherency hardening are similar to (IX).23 with ΔE replaced by ϵ, the misfit strain. The exact role of coherency hardening is difficult to evaluate for thin discs in view of the varying strains at the disc interfaces. Nevertheless, the strain is observed to decrease rapidly as the particles grow (see Fig. VI.11), and therefore could partly explain the initial strength decrease.

Although equation (IX).24 infers that the strength increases with increasing diameter it has been suggested that the maximum strength occurs at the finest possible size when chemical strengthening predominates (Brown & Ham, 1971). When the expressions are modified to a system containing thin disc-shaped particles it is apparent why this may occur since the strength is proportional to $(t/D)^{\frac{1}{2}}$ or $t/D^{\frac{1}{2}}$. Therefore, if the disc aspect ratio increases during particle growth and the other parameters remain constant, the strength will decrease.

For example, if the γ_p value calculated for the initial zones (1350 ergs/cm^2) is used in (IX).11 for the same volume fraction of 10nm diameter by 1nm thick particles the expected strength increase is 375N/mm^2. This is very close to

the observed strength of particles of this diameter. Similar calculations using a constant surface energy term predict an even larger strength decrease during particle growth and therefore, if either of the mechanisms predominates in Fe-X-N alloys, an initial strength decrease will occur as the zones coarsen.

An additional reason for the initial strength decrease could arise from a change in the volume fraction of particles. In classical age-hardening alloys (see Fig. IX.5) the initial strength increase is partly due to increases in the volume fraction of particles. However, in Fe-X-N alloys the volume fraction is probably at a maximum as soon as the zones are formed and could actually decrease on ageing, due to the rejection of iron and/or nitrogen.

In view of these considerations, possible reasons for the apparently anomolous feature of the maximum strength occurring at the minimum particle size are:

i) The disc aspect ratio increases on ageing,

ii) The volume fraction of particles decreases, and

iii) The rapid decrease in coherency strains during the initial stages of particle growth.

An exact evaluation of the short range interactions cannot be made due to the number of possible contributary mechanisms. The problem arises in how to combine more than one strengthening mechanism for deformable particles, or whether the strength should be considered to derive solely from the

strongest obstacle. However, this is an area of research which has received little attention. The results of the present investigation suggest that the strength of the zones derives from chemical, surface and coherency hardening mechanisms, the net effect being that the maximum strength increase is obtained at the minimum particle size. Although the contribution from each mechanism is unknown, all of these mechanisms predict that the strength is proportional to the square root of the volume fraction of precipitated particles, which is observed for Fe-X-N alloys containing coherent particles (see Fig. VII.6).

The poor ductility of nitrided ferritic alloys at peak strength can be attributed to the presence of deformable particles. Lütjering & Hornbogen (1968) have proposed that the precipitation of very fine nitrides or carbides will strongly influence the properties of iron alloys. They postulated that shearing of the particles in one glide plane lowers its resistance to further dislocation movement compared to parallel planes, leading to paths of easy deformation, strain inhomogeneity and increased tendancy to fracture. This tendancy is expected to increase with increasing volume fraction of precipitated phase, which satisfactorily explains why Fe-X-N alloys containing higher volume fractions of particles are extremely brittle. When particle shearing is the operative deformation mechanism other age-hardened b.c.c. metals are observed to be extremely brittle. For example, this occurs in age-hardened titanium alloys (Blackburn & Williams,

1969; Gysler et al, 1974) and in Fe-Si-Ti alloys (Papaleo & Whiteman, 1971; Watson & Brown, 1974; Jack & Guiu, 1975). Therefore, the feature appears to be common to b.c.c metals containing finely dispersed, coherent second-phase particles.

The high initial strength of Fe-X-N alloys containing coherent particles can be explained if energy values of 1,500 ergs/cm^2 are used in the modified chemical strengthening equations. Specific interfacial energies have been measured calorimetrically by Boyd & Nicholson (1971) for the Al-Cu system. The mean interfacial energies were 530(max) ergs/cm^2 for θ'' and 1,530 ergs/cm^2 for θ^1, although the peripheral energy of θ' was expected to be about 21,500 ergs/cm^2. These values were much higher than expected, but were believed to be a true indication of the real value. In age-hardened Fe-Si-Ti alloys energy values ranging from 500 ergs/cm^2 (Schwarz & Ralph, 1969) to 1280 ergs/cm^2 (Brown & Whiteman, 1969) have been assumed to explain the high strengths, whereas other calculations by Papaleo & Whiteman (1971) claimed that 900 ergs/cm^2 is an underestimate of the actual value. In view of these findings it does not seem unreasonable to assume that the zones in the nitrided ferrites have an interfacial energy of 1,500 ergs/cm^2.

The energy required to shear the zones in Fe-0.15at.%V calculated from the temperature dependence of the yield strength is also of a similar value. Therefore, it is considered that the major part of the strengthening is of a chemical nature, deriving from the creation of a new interface

as the particles are sheared.

Upon consideration of the strengthening mechanisms, deformed microstructures and general properties of Fe-X-N alloys at peak strength, the following observations give support to the supposition that the zones are sheared during deformation:

i) The maximum strength occurs at the minimum particle size;

ii) The strong temperature dependence of the yield strength;

iii) The extreme brittleness of the alloys at peak strength;

iv) The discontinuity in the yield strength obtained for particles in the size range 4-12nm (coherent) when plotted as a function of D^{-1}; and

v) From the electron metallography of deformed microstructures planar slip bands, low dislocation densities, jog formation and a predominance of long, straight screw dislocations on $\{110\}_{\alpha}$ with a Burgers vector of $a/2\langle 111\rangle$ are observed.

The zones in nitrided Fe-V and Fe-Nb alloys become incoherent at $\approx$ 12nm diameter and it is below this size that the particles are believed to be deformable. Numerous other investigators have assumed that particle cutting occurs in ferrous alloys. Baker (1973 b) proposed that the initial particles are cut in tempered low C-V-N steels because the Orowan equation does not explain all of the observed strengths; whereas Greday & Lamberigts (1974) claimed that particles of less than 7nm diameter in dispersion hardened vanadium and niobium containing steels are sheared by couples of dislocations. Gray (1973) observed that the strength increased down to the smallest particle size (2nm) in precipitation hardened niobium steels. A plot of strength against D^{-1} showed a discontinuity at $\approx$12nm diameter (similar to Fig. IX. 2) although it was thought that this was too large a size for particle cutting to be predominant. Other researchers have either obtained tentative evidence (Smith, 1966) or postulated (Simcoe et al 1968) that coherent particles are sheared in secondary hardened steels.

Qualitative interpretation of the yield strength from structural observations often presents difficulties, but they are enhanced in precipitation hardened ferrous alloys because of the morphology, size, distribution and unknown volume fraction of second-phase particles. Nevertheless, the results of the present investigation provide substantial evidence to suggest that the coherent particles in the nitrided ferrites are sheared during deformation.

In Brown & Ham's (1971) review of strengthening mechanisms, it was concluded that when chemical strengthening arising from the breaking of chemical bonds and the creation of a new interface was dominant for thin plate-like zones, such as GP zones in Al/Cu or Cu/Be, coherency hardening was minor. A similar explanation would account for numerous features observed in the deformation of zones in Fe-X-N alloys, even though this necessitates the use of high energy values. Nevertheless, in view of the strong nature of the substitutional interstitial bond strength it seems probable that the values will be higher than in most other age-hardening alloys. Consequently, the high initial strengths of the nitrided ferrites can be explained if the interfacial energy of the zones is 1,500 ergs/cm^2.

IX.7 Conclusions

a) The Orowan relationship underestimates the strength of Fe-X-N alloys containing both overaged and small coherent particles.

b) The yield strength shows a sharp discontinuity when plotted against the reciprocal of disc diameter at a diameter of 12nm, inferring that a change in deformation mechanism occurs at this particle size.

c) An extension of the chemical and surface hardening equations to an alloy system containing thin discs explains why the maximum strength can occur at the minimum particle size.

d) The initial strength decrease occurring as the zones coarsen can be attributed to changes in the disc aspect ratio, coherency strains or in the volume fraction of particles.

e) The major part of the high initial strengthening is of a chemical nature, deriving from the creation of a new interface as the particles are sheared.

f) The strong temperature dependence of the yield strength arises from the energy required for dislocations to shear the thin disc-shaped zones.

g) The energy values obtained from the chemical strengthening equations and temperature dependence of the yield stress are about 1,500 ergs/cm^2. The high value is indicative of the presence of very strong particles being precipitated.

h) The poor ductility of the nitrided ferrites is a consequence of the particles being sheared during deformation.

Chapter X

GENERAL CONCLUSIONS

Constant activity nitriding binary iron alloys containing strong nitride forming elements as the substitutional solute produces a homogeneous dispersion of fine, coherent disc-shaped particles on the ferrite cube planes. The first formed particles are analagous to GP zones in Al-Cu alloys and overage to the equilibrium precipitate through a precipitation sequence which may involve intermediate stages.

Anomolous internal friction characteristics are associated with the homogeneous precipitation. When small particles are precipitated both the Snoek and substitutional-interstitial interaction peaks are negligible. However, an abnormal internal friction peak occurs in the range 150 - 230°C, the peak moving to higher temperatures as the structure coarsens. The high temperature peak is broad and assymmetric and is believed to be due to the movement of the less firmly held nitrogen atoms in the strain fields around the precipitated particles. During the initial stages of precipitation additional damping is observed, which can partly be explained as arising from the movement of nitrogen atoms in the vicinity of the substitiutional solute.

The precipitation of stable GP zones in alpha-iron produces a new method of strengthening ferrous alloys. Large strength increases are observed even in dilute Fe-X-N alloys

because a uniform distribution of small, coherent particles is precipitated. The coherent particles are thought to be sheared during deformation.and a change to an Orowan type deformation mechanism occurs when the particles become incoherent. The yield strength is proportional to the square root of the volume fraction of particles, is strongly dependent on temperature, and the maximum strength is achieved at the smallest particle size.

Electron metallography of deformed alloys containing zones shows that slip is predominantly on $\{100\}_{\alpha}$ and dislocations (mainly screw in character) have a Burgers vector of $a/2\ \langle 111 \rangle$. The dislocation substructure is similar to pure iron deformed at low temperatures and the occurrence of dislocation banding is indicative of the particles being sheared during deformation.

Interpretation of the structure-property relationships, although to some extent speculative, gives some agreement between theory and practice. The major part of the high initial strengthening is thought to be of a chemical nature, deriving from the creation of a new interface as the particles are sheared. The energy values of the interface dislocations and the chemical bonds are probably the most important parameters determining the properties and an energy of 1,500 ergs/cm^2 satisfactorily explains the strength. The relatively high value is indicative of the presence of strong particles which maximise the forces of interaction

between dislocations and particles, resulting in high strengths. It is the shearing of strong particles which results in a restriction of slip and explains the consequent poor ductility of Fe-X-N alloys at peak strength.

Application of the present work to high strength low alloy steels, where vanadium, niobium and nitrogen are common additions, shows that in order to attain the highest strength increases the particles must be both fine and coherent. The principle of producing a fine dispersion of coherent particles by constant activity nitriding is not restricted to ferrous alloys, but can be applied to a wide range of alloys where the resultant homogeneous precipitation will lead to a most effective method of metal strengthening.

REFERENCES

Ashby, M.F. 1964, Z. Metallkunde 55, 5.

Ashby, M.F. & Brown, L.M. 1963, Phil. Mag. 8, 1649.

Baird, J.D. & Jamieson, A. 1966, J.I.S.I. 204, 793.

Baird, J.D. & Jamieson, A. 1972, J.I.S.I. 210, 842.

Baker, T.N. 1973a, J.I.S.I. 211, 502.

Baker, T.N. 1973b, I.S.I. Special Report 163, 13.

Baker, R.G. & Nutting, J. 1959, I.S.I. Special Report 64, 1.

Baldi, G. & Buzzichelli, G. 1973, Scripta Met. 7, 711.

Bergstrom, T. & Roberts, W. 1972, Scand. J. Met. 1, 265.

Beshers, D.N. 1965, J. App. Physics 36, 290.

Blackburn, M.J. & Williams, J.C. 1969, Trans A.S.M. 62, 398.

Booker, G.R., Norbury, J. & Sutton, A.L. 1957, J.I.S.I. 187, 205.

Borland, D.W. & Segall, R.L. 1972, Scripta Met. 6, 1201.

Bowen, A.W. & Leak, G.M. 1970, Met. Trans. 1, 2767.

Boyd, J.D. & Nicholson, R.B. 1971, Acta Met. 19, 1971.

Brenner, S.S. & Goodman, S.R. 1971, Scripta Met. 5, 865.

Brooks, H. 1952, "Metal Interfaces" (Trans A.S.M.) 20.

Brown, L.M. & Ham, R.K. 1971, "Strengthening Mechanisms in Crystals" Elsevier Pub. Co.

Brown, G.G. & Whiteman, J.A. 1969, J. Aust. Inst. Metals 14, 217.

Brunhauer, S., Jefferson, M.E., Emmett, P.H. & Hendricks, S.B. 1931, J. Am. Chem. Soc. 53, 1778.

Chen, F.P.H. 1965, Ph.D. Thesis, Reneselaer Polytechnic Institute New York, U.S.A.

Chino, H. & Wada, K. 1965, Yawata Tech. Report 251, 75.

Couper, G.J. & Kennedy, R. 1967, J.I.S.I. 205, 462.

Courtnall, M. & Pickering, F.B. 1976, Metal Sci.J. 10, 273.

Davenport, A.T., Berry, F.G. & Honeycombe, R.W.K. 1968, Metal Sci.J. 2, 104.

Dijkstra, L.J. 1949, Trans.A.I.M.E, 185, 252.

Dijkstra, L.J. & Slakek, R.J. 1953, Trans A.I.M.E. 197, 69.

Driver, J.H. 1972, Unpublished work, University of Newcastle upon Tyne.

Driver, J.H. & Papazian, J.M. 1973, Acta Met. 21, 1139.

Dunlop, G.L. & Turner, P.J. 1975, Metal Sci.J. 9, 370.

Enrietto, J.F. 1962, Trans A.I.M.E. 224, 1119.

Epstein, S., Cuther, H.J. & Frame, J.W. 1950, J. Metals 2, 830.

Fast, J.D. 1961, Met. Corr. Ind. 36, 431.

Fast J.D. 1971, "Interactions of Metals and Gases". Macmillan.

Fast, J.D. & Meijering, J.L. 1953, Philips Res. Rep. 8, 1.

Fast, J.D. & Verrijp, M.B. 1954, J.I.S.I. 176, 24.

Fast, J.D. & Verrijp, M.B. 1955, J.I.S.I. 180, 337.

Forrest, P.B. & Hopkin, L.M.T. 1963, N.P.L. Symposium 15.

Fountain, R. & Chipman, J. 1958, Trans A.I.M.E. 212, 737.

Freeman, S. 1971, I.S.I. Spec. Report 145, 151.

Frohberg, M.G, & Graf, H. 1960, Stahl und Eisen, 8, 539.

Fullman, R.L. 1953, Journal of Metals 5, 447.

Gerold, V. & Haberkorn, H. 1966, Physica Status Solidi 16, 675.

Gladman, T., Holmes, B. & McIvor, I.D. 1971, I.S.I. Spec. Report I45, 68.

Gleiter, H. & Hornbogen, E. 1965, Physica Status Solidi 12, 251.

Gleiter, H. & Hornbogen, E. 1967, Mater. Sci. Eng. 2, 284.

Gray, J.M. 1973, I.S.I. Spec Report 163, 19.

Gray, J.M. Webster, D. & Woodhead, J.H. 1965, J.I.S.I. 203, 812.

Gray, J.M. & Yeo, R.B.G. 1968, Trans. A.S.M. 61, 255.

Greday, T. & Lamberigts, M. 1972, "Processing and Properties of low Carbon Steel" A.I.M.E.

Guinier, A. 1938, Nature 142, 569.

Guinier, A. 1959, Solid State Physics 9, 293.

Gysler, A., Lutjering, G. & Gerold, V. 1974, Acta Met. 22, 901.

Hahn, H. 1949, Z. Anorg. Chem. 258, 58.

Hale, K.F. & McLean, D. 1963, J.I.S.I. 201, 337.

Ham, R.K. 1968, Trans. Japan Inst. Metals 9, Supplement 52.

Hansen, M. 1958, "Constitution of Binary Alloys". McGraw-Hill.

Harkness, 3.D. & Hren, J.J. 1970, Met. Trans. 1, 43.

Hayes, P. & Grieveson, P. 1975, Scripta Met. 9, 39.

Henderson, S. 1974, Unpublished work, University of Newcastle upon Tyne.

Hirsch, P.B., Howie, A., Nicholson, R.B., Pashley, D.W. & Whelan, M.J. 1965, "Electron Microscopy of Thin Crystals", Butterworths.

Hopkin, L.M.J. 1965, J.I.S.I. 203, 583.

Hornbogen, E. 1964, Trans A.S.M. 57, 120.

Hornbogen, E. 1971, Proceedings I.C.S.T.I.S. Trans I.S.I. Japan II, 997.

Irani, J.J. & Honeycombe, R.W.K. 1963, I.S.I. Special Report 86, 1.

Irvine, K.J., Pickering, F.B. & Gladman, T. 1967, J.I.S.I. 205, 161.

Ishida, Y. & McLean, D. 1967, J.I.S.I. 205, 88.

Jack, D.H. & Guiu, F. 1975, J. Mat. Sci. 10, 1161.

Jack, K.H. 1951a, Proc. Roy. Soc. (A) 208, 200.

Jack, K.H. 1951b, Proc. Roy. Soc. (A) 208, 216.

Jack, K.H. 1973, I.S.I. Special Report 163, 39.

Jack, K.H. & Maxwell, D. 1952, J.I.S.I. 170, 254.

Jamieson, R.M. & Kennedy, R. I966, J.I.S.I. 204, I208.

Johnsson-Holmquist, B. 1971, Unpublished work, University of Newcastle upon Tyne.

Jones, W.R.D. & Coombes, G. 1953, J.I.S.I. 174, 9.

Ke, T.S. I948, Phys. Rev. 74, 9

Keefer, D.W. & Wert, C.A. I963, Acta Met. II, 489

Keh, A.S. 1963, "Precipitation from Iron-Base Alloys" Gordon & Breach.

Keh, A.S. & Weissmann, S. 1963, "Electron Metallography and Strength of Crystals". Interscience.

Keh, A.S. & Wreidt, H.A. 1962, Trans. A.I.M.E. 224, 560.

Kelly, A. & Fine, M.E. 1957, Acta Met. 5, 365.

Kelly, A. & Nicholson, R.B. 1963, "Progress in Materials Science". 10, 151.

Kelly, P.M. 1972, Scripta Met. 6, 647.

Kelly, P.M. 1973, International Met. Reviews 18, 31.

Kirkwood, D.H. Atasoy, O.E. & Keown, S.R. Metal Science J. 8, 49

Kirkwood, D.H. & Thomas, G. 1976, Met. Trans. 7A, 764.

Koster, V.N. & Horn, W. 1966, Arch. Eisenhutten. 37, 245.

Krawitz, A. & Sinclair, R. 1975, Phil. Mag. 31, 697.

Kuo, K. 1956, J.I.S.I. 184, 258.

Lagneborg, R. 1967, Trans. A.S.M. 60, 67.

Lambert, N., Crustin, J. & Greday, T. 1970, Proceedings I.C.S.T.I.S. 1040.

Lamberigts, M. & Greday, T. 1974, C.R.M. 38, 25.

Leak, D.A., Thomas, W.R. & Leak, G.M. 1955, Acta Met. 3, 501.

Lehrer, E. 1930, Z. Electrochem. 36, 460.

Low, J.R. & Turkalo, A.M. 1962, Acta Met. 10, 215.

Lucas, W.R. & Fishel, W.R. 1954, Trans. A.S.M. 46, 277.

Lutjering, G. & Hornbogen, E. 1968, Z. Metallkunde 58, 29.

L'vovsky, A.Y. & Gerasimov, L.P. 1973, Metallovedenie i. Term 3, 64.

Masteurs, H. & Duwez, P. 1952, Trans. A.S.M. 46, 277.

Mehl R.F., Barret, C.S. & Jerabek, H.S. 1934, Trans. A.I.M.E. 113, 211.

Meiklejohn, W.H. & Skoda, R.E. 1960, Acta Met. 8, 773.

Melkumov, I.N., Klyuev, M.M. & Pirovarora, L.I. 1973, Steel in the U.S.S.R. 3, 687.

Middleton, P. 1974, Unpublished work, University of Newcastle upon Tyne.

Mitchell, J.B. 1971, Acta Met. 19, 1063.

Morrison, W.B. 1963, J.I.S.I. 201, 317.

Morrison, W.B. & Leslie, W.C. 1973, J.I.S.I. 211, 129.

Mortimer, B. 1971, Ph.D. thesis, University of Newcastle upon Tyne.

Mura, T., Tamura, I. & Brittain, J.D. 1961, J. Appl. Physics 32, 92.

Nacken, V.M. & Kuhlman, U. 1966, Archiv Eisenhutten. 37, 235.

Nicholson, R.B. & Nutting, J. 1958, Phil. Mag. 3, 531.

Nicholson, R.B., Thomas, G. & Nutting, J. 1960, Acta Met. 8, 172.

Nicholson, R.B. 1971, I.S.I. Special Rep. 145, 1.

Nowick, A.S. & Berry, B.S. 1961, I.B.M. Journal 297.

Ohr, S.M., Wechsler, M.S., Chen, C.W. & Hinke, N.E. 1970, "Proceedings 2nd Int. Conf. on Strength of Metals & Alloys" A.S.M.

Papaleo, P. & Whiteman, J.A. 1971, I.S.I. Special Report 145, 23.

Paranjpe, V.G., Cohen, M., Bevers, M.B. & Floe, C.F. 1950, Trans A.I.M.E. 188, 261.

Perry, A.J., Malone, M. & Boon, M.H. 1966, J. Appl. Physics 37, 4705.

Petarra, D.P. & Beshers, D.N. 1967, Acta Met 15, 791.

Phillips, V.A. & Livingstone, D. 1962, Phil. Mag. 7, 969.

Phillips, V.A. & Seybolt, A.U. 1968, Trans. A.I.M.E. 242, 2415.

Pickering, F.B. 1957, I.S.I. Special Report. 64, 23.

Pipkin, N.J. 1967, Ph.D. Thesis, University of Newcastle upon Tyne.

Podgurski, H. & Knechtal, H.E. 1969, Trans. A.I.M.E. 245, 1595.

Pope, M. 1972, Ph.D. Thesis, University of Newcastle upon Tyne.

Powers, R.W. & Doyle, M.V. 1956, Acta. Met. 4, 233.

Powers, R.W. & Doyle, M.V. 1959, Trans. A.I.M.E. 215, 655.

Preston, G.D. 1938, Proc. Roy. Soc. A. 167, 526.

Rashid, M.S. 1976, Met. Trans. 7A, 497.

Rawlings, R. & Robinson, P.M. 1961, J.I.S.I. 197, 211.

Rawlings, R. & Tambini, D. 1956, J.I.S.I. 184, 302.

Ritchie, I.G. & Rawlings, R. 1967, Acta Met. 15, 491.

Roberts, W. 1970, Ph.D. Thesis, University of Newcastle upon Tyne.

Saada, G. 1960, Acta Met. 8, 200.

Saguez, A.A. & Gibala, R. 1974, Acta Met. 22, 1423.

Schiller, A.J. & Duren, C. 1971, Trans A.S.M.E. 93, 1169.

Schwartz, D.M. & Ralph, B. 1969, Metal Science J. 3, 216.

Seal, A.K. & Honeycombe, R.W.K. 1958, J.I.S.I. 188, 343.

Seybolt, A.U. 1969, Trans A.I.M.E. 245, 769.

Simcoe, C.R., Nehrenberg, A.E., Bis, V. & Cohen, A.P. 1968, Trans A.S.M. 61, 834.

Smith E. 1966, Acta Met 14 , 538.

Smith E. & Nutting, J. 1957, J.I.S.I. 187, 314.

Snoek, J.L. 1948, Physica 8 , 711.

Speirs, D. 1969, Ph.D. Thesis, University of Newcastle upon Tyne.

Speirs, D.L., Roberts, W.,Grieveson, P. & Jack, K.H. 1970, "Proceedings 2nd International Conference on Strength of Metals" A.S.M.

Stark, P.,Averbach, B.L. & Cohen, M. 1956, Acta Met 4 , 91.

Steiner, A., Horn, E. & Preis, G. 1975, Stahl und Eisen 95 , 209.

Stephenson, A. 1973, Ph.D. Thesis, University of Newcastle upon Tyne.

Stephenson, A. 1974, Unpublished work, University of Newcastle upon Tyne.

Stephenson, E.T. 1965, Trans A.I.M.E. 233, 1183.

Stephenson, E.T., Karcher, G.H. & Stark P. 1964, Trans A.S.M. 57, 208.

Sutton, H.G. & Whiteman, J.A. 1971, J.I.S.I. 209, 220.

Suziki, H.G., Sato, T & Tanino, M. 1970, Proceedings I.C.S.T.I.S. I08I.

Suzuki, H.G. & Tanino, M. 1972, Trans I.S.I. Japan 12, 217.

Szabó-Miszenti, G. 1970, Acto Met. 18, 477.

Tanino, M. & Aoki,K1968, Trans I.S.I. Japan 8, 377.

Tekin R. & Kelly, P.M. 1965, J.I.S.I. 203, 715.

Unthank, D., Driver, J.H. & Jack, K.H. 1972, Nature Phys. Sci. 238, I36.

Watson, J.D. & Brown, G.G. 1974, Metal Science.J. 8, 9.

Weatherley, G.C. 1968, Phil. Mag 17, 791.

Weatherley, G.C. & Nicholson, R.B. 1968, PHil Mag. 17, 801.

Welch, W.D. & Carpenter, S.H. 1973, Acta Met. 21, 1169.

Wert, C.A. & Marx, J. 1953, Acta Met 1, 113.

Wever, F. & Jellinghaus, W. 1930. Mih Kaiser Wilhelm Inst. Dussledorf I3, 93.

Williams, R.O. Baxton, H.W. 1957, J.I.S.I. 185, 358.

Woodhead, J.H. & Webster, D. 1969, J.I.S.I. 207, 51.

Wreidt, H.A. & Zwell, L. 1962, Trans A.I.M.E. 224 1242.

Yeo, R.B.G. & Gray, J.M. 1968, Trans A.S.M. 6I, 255.

Zener, C. 1948, Phys. Rev. 74, 639.